Cellular Models for Characterisation of MINA53, a 2-Oxoglutarate-Dependent Dioxygenase

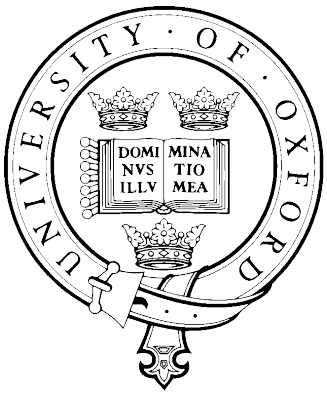

A thesis submitted for the degree of Doctor of Philosophy

Trinity Term 2012

Adam Zayer

St Anne's College

Supervisors:

Professor Peter Ratcliffe and Dr Mathew Coleman

Cellular Models for Characterisation of MINA53, a 2-Oxoglutarate-Dependent Dioxygenase

Adam Zayer, St Annes College
Thesis submitted for the degree of Doctor of Philosophy
Nuffield Department of Clinical Medicine, University of Oxford
Trinity Term 2012

2-Oxoglutarate/Fe(II)-dependent dioxygenases (2OG Oxygenases) are a relatively poorly characterised enzyme family that hydroxylate biological macromolecules to regulate a variety of essential cellular processes in mammals, including; chromatin remodeling, extra-cellular matrix formation and oxygen sensing.

The work in this thesis focuses on a 2OG Oxygenase termed Myc-Induced Nuclear Antigen (MINA53). This enzyme has been implicated in ribosome biogenesis and cell proliferation, and observed overexpressed in several tumour types, yet the identity of its substrate(s) and their role in cancer is unknown.

The aims of the research that has resulted in this thesis were to; (i) develop a cell model of MINA53 enzyme activity, (ii) apply this model to study the role of MINA53 activity in cell transformation and cancer, and (iii) discover novel cellular processes regulated by MINA53 activity. As such, I have created an isogenic cell model consisting of K-Ras-transformed MINA53 knockout mouse embryonic fibroblasts (MEFs) reconstituted with either wildtype or enzyme-inactive MINA53. Using this model I have shown that MINA53 activity maintains normal levels of the large ribosomal subunit (60S), and suppresses anchorage-independent growth, autophagy and gene expression. These observations suggest the existence and involvement of one or more substrates. Indeed, proteomic and biochemical analyses in collaboration with the Schofield laboratory (Chemistry, Oxford) confirmed the identity of a MINA53 substrate, the 60S ribosomal protein Rpl27a. Together we have shown that Rpl27a is abundantly hydroxylated, and that MINA53 is a histidinyl hydroxylase; this represents the first discovery of a ribosomal oxygenase.

The model developed here did not support a positive role for MINA53 in the transformation of MEFs. Rather it suggested that MINA53 can suppress transformation in some contexts. This prompted a wider investigation that demonstrated underexpression of MINA53 in several tumour types, and the presence of inactivating mutations in breast, ovarian and colon cancer. This thesis provides data supporting further research to understand the role of Rpl27a hydroxylation in the regulation of 60S biogenesis, autophagy and cancer.

Declaration

The thesis that I am submitting is wholly my own work, with the exception of the following experiments:

Figure 4.1 (Dr Nicolas Granatino and Dr Matthew Cockman)

Figure 4.2 (Dr Wei Gee), Professior Christopher Schofield.

Figure 4.10 (Rok Serkinik), Professior Christopher Schofield.

All WP-MS analysis was done by Rok Sekirnik (Schofield lab, University of Oxford).

Microarray done in collaboration with Dilair Baban and Dr Christine Blancher, Core facility, The Wellcome Trust Centre for Human Genetics, University of Oxford

Xenograft done in collaboration with Professor Adrian Harris, Ji-Liang Li and Esther Bridges.

Table of contents

Chapter 1: Introduction

Chapter 2: Role of MINA53 in proliferation

Chapter 3: An isogenic MEF model for studying the enzymatic activity of MINA53

Chapter 4: Ribosomal protein Rpl27a is a MINA53 substrate

Chapter 7: Discussion

List of figures and legends

Figures

Tables

Abbreviation list

2-OG	2-oxoglutarate
4E-BP1	4E-Binding Protein 1
5'TOP	5 ' Terminal Oligopyrimidine Tract
5-FU	5-Fluorouracil
Ac	Acethylation
AlkB	Alpha-ketoglutarate-dependent dioxygenase
ARD	Ankyrin Repeat Domain
ASBH	Asparaginyl Beta (egf) Hydroxylase
Atg	Autophagy Gene
ATR	Ataxia Telangiectasia and Rad3-related
BTG	B-cell translocation gene
Cdknc1	Cyclin-dependent kinase inhibitor 1c
COX-4	Cytochrome c oxidase
CRTAP	Cartilage-Associated Protein
CypB	cyclophilin B
DAPI	4',6-diamidino-2-phenylindole
DFC	Dense Fibrillar Compartment
DSBH	Double-Stranded Beta-Helix
E. Coli	*Escherichia coli*
EGF	Epidermal Growth Factor
EGFH	Epidermal Growth Factor Hydroxylase
EGFR	Epidermal Growth Factor Receptor
eIFs	eukaryotic Initiation Factors
FC	Fibrillar Centre
Fgf13	Fibroblast growth factor 13
FIH	Factor inhibiting HIF
FTO	Fat mass and obesity associated
GAIT	IFN-Gamma Activating Inhibitor of Translation
Gap43	Growth associated protein 43
GC	Granular Compartment
hABH2/3	AlkB homologs 2 and 3
HDM	Histone Demethylase
HIF	Hypoxia Inducible Factor
HPLC	High-throughput Liquid Chromatography
Hsp27	Heat-shock protein 27kda
Hspbap1	Heat shock 27kda associated protein 1
Igfbp5	Insulin-like growth factor binding protein 5
LC3	Microtubule-associated protein light chain 3
LH	Lysyl Hydroxylase
MALDI-TOF MS	Matrix-Assisted Laser Deporption/Ionization- Time Of Flight Mass Spectrometry
MAPK	Mitogen-activated protein kinase
Me	Methylation
MEF	Mouse Embryonic Fibroblast

MINA53	Myc-Induced Nuclear Antigen of 53 kda
mTOR	mammalian Target Of Rapamycin
MTS	3-(4,5-dimethylthiazol-2-yl)-5-(3-carboxymethoxyphenyl)-2-(4-sulfophenyl)-2H-tetrazolium
MTT	3-(4,5-Dimethylthiazol-2-yl)-2,5-diphenylteatrazolium bromide
NFATC1	Nuclear Factor of Activated T-cells, Cytoplasmic 1
NO66	Nucleolar protein of 66 kda
Nog	n-oxalylglycine
P	Phosphorylation
P3H	Prolyl-3-Hydroxylase
P4H	Prolyl-4-Hydroxylase
PHD	Prolyl Hydroxylase
PHD	Plant Homebox
PhyH/PAHX	Phytanoyl-CoA hydroxylase
PI3K	Phosphatidylinositol-3-kinase
Pla2g4b	cytosolic phospholipase a2beta gene
Pip5k1a	Phosphatidylinositol-4-phosphate 5-kinase type-1 alpha
PTDSR	Phosphatidylserine Receptor
Rb	Retinoblastoma
rDNA	ribosomal DNA
RISC	RNA-Induced Silencing Complex
RP-HPLC	Reverse-Phased High-throughput Liquid Chromatography
Rpl	Ribosomal protein, large subunit
SDS-PAGE	Sodium Dodecyl Sulfate Polyacrylamide Gel Electrophoresis
shRNA	short-hairpin RNA
SILAC	Stable-Isotope labeling by/with Amino acids in Cell culture
siRNA	small-interfering RNA
SKP1	S-phase Kinase-associated Protein 1A
Tpr	Ubiquitously transcribed tetratricopeptide repeat
Ub	Ubiquitylation
ULK	Unc-51-like kinase
UTX	Ubiquitously Transcribed tetratricopeptide repeat, X chromosome
VHL	Von-Hippel-Lindau factor
Vps34	Vacuolar Protein Sorting 34
Wp-ms	Whole-protein mass spectrometry
XLMR	X-Linked Mental Retardation

Chapter 1
Introduction

1.1 Overview

This thesis describes my studies of Myc-Induced Nuclear Antigen (MINA53), an Fe(II)- and 2-oxoglutatate (2OG)-dependent dioxygenase (2OG oxygenase). As such, this Introduction will first begin by providing a structural and mechanistic overview of the 2OG Oxygenase enzyme family, before discussing known roles of 2OG Oxygenases in cell biology, physiology and disease. The Introduction will then end on a detailed assessment of what is currently known about MINA53 and closely related enzymes.

1.2 2OG Oxygenases

2OG Oxygenases are a class of enzyme that catalyses diverse oxidative reactions involved a wide range of important biological functions. The first 2OG Oxygenase was identified in 1967 and subsequently shown to be a collagen prolyl hydroxylase (Hutton et al., 1967). Bioinformatic analyses have since identified 2OG enzymes in most organisms, including animals, bacteria and plants. In humans more than 60 different 2OG Oxygenases have been identified thus far (Figure 1.1). Whereas prokaryotic and plant 2OG Oxygenases catalyse diverse types of oxidative modifications, their eukaryotic counterparts catalyse modifications limited to hydroxylation and demethylation in protein, nucleic acid and lipid. In order to catalyse these modifications 2OG Oxygenases utilize molecular oxygen, Fe(II), 2OG, and in some cases ascorbate, with oxidation being coupled to the decarboxylation of 2OG to yield succinate and carbon dioxide (Hewitson et al., 2005) (see below).

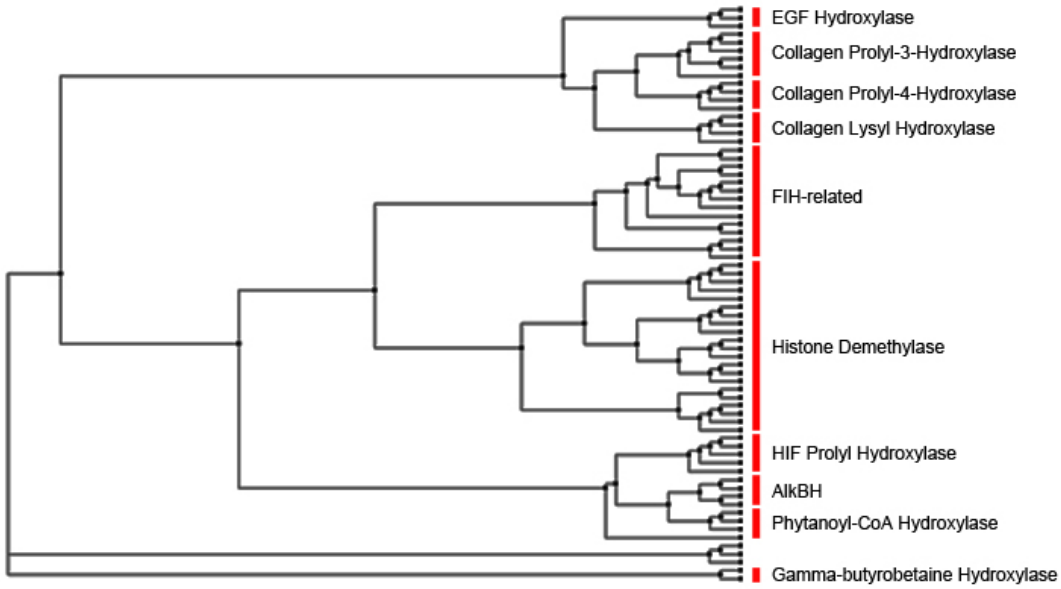

Figure 1.1. Human 2OG Oxygenase gene family. Phylogenetic tree based on sequence similarity within the catalytic domains of known and predicted human 2OG Oxygenases, showing several sub-families of related enzymes. This figure was adapted from analyses performed by Dr Nicolas Granatino (Schofield laboratory, Oxford).

1.3 Structure and Catalytic Mechanism of 2OG Oxygenases

1.3.1 Structure

2OG Oxygenases share a common structural fold known as the Double-Stranded Beta-Helix (DSBH). This domain consists of eight anti-parallel β-strands that together form a 'barrel'-like structure also known as a 'jelly-roll' motif (Hausinger, 2004). Positioned at the more open end of this motif lies the active site (Figure 1.2). However, unlike other oxygenases (e.g. cytochrome P450s) that utilize a heme-bound iron at the active site, 2OG Oxygenases coordinate Fe(II) directly *via* a '2-His, 1-Carboxylate' facial triad (HXD/E…H motif; see Fig 1.2) (McDonough et al., 2010). In addition to arranging ligands involved in coordinating Fe(II), the DSBH also positions residues involved in binding 2OG; These residues are typically Threonine/Serine, Phenylalanine, Tyrosine, and Lysine, although variants are possible (Klose et al., 2006).

Aside from the catalytic DSBH domain, many (but not all, see below) 2OG oxygenases contain other structural motifs involved in their function. For example, 2OG oxygenases that catalyse histone demethylation also contain DNA- and methylated-histone- binding domains, and protein:protein interaction motifs (Klose et al., 2006).

1.3.2 Catalytic Mechanism

The catalytic mechanism of 2OG Oxygenases is characterised by the incorporation of molecular oxygen into the prime substrate and co-substrate (2OG) in an Fe(II)-dependent manner. The active site of 2OG Oxygenases forms a quaternary complex with Fe(II), 2OG and the substrate together with oxygen. The order in which

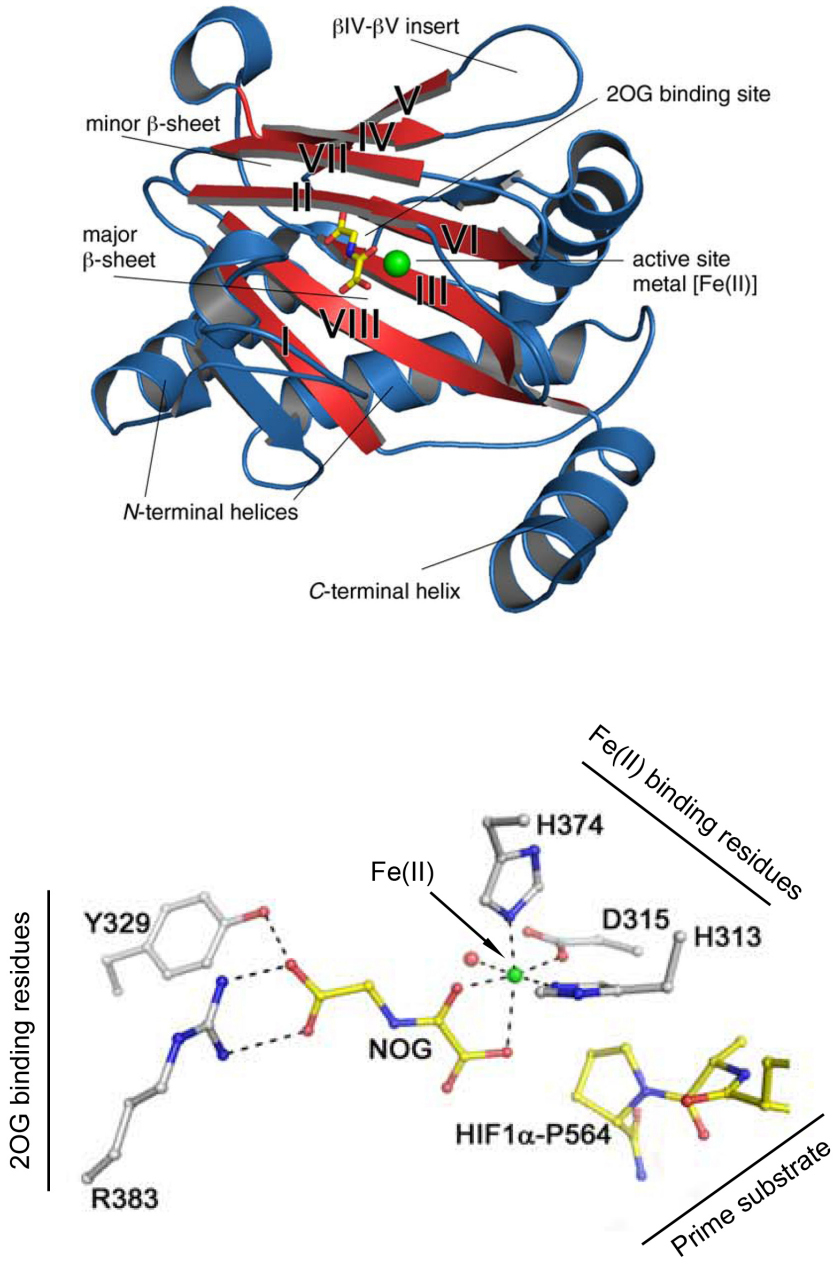

Figure 1.2. Structure of the 2OG Oxygenase catalytic domain. A. The catalytic domain of 2OG Oxygenases consists of a double-stranded β-helix that brings together amino acid side chains involved in Fe(II) and 2OG binding. This figure depicts the catalytic domain of the HIF prolyl hydroxylase PHD2 with core strands (I-VIII) of the double-stranded β-helix coloured in Red. 2OG is shown in yellow, and Fe(II) in green**. B.** Minimal representation of the catalytic domain of PHD2 in complex with the HIF1α substrate. 2OG and Fe(II) binding residues are shown in Grey, Fe(II) in Green (additional metals are Red), and the 2OG mimic N-Oxalylglycine (NOG) in Yellow. This figure was adapted from (McDonough et al., 2010). Reprinted by permission from Elsevier, copyright 2010.

these components bind is not fully clear but is thought to proceed from 2OG binding to the Fe(II) centre first, followed by the substrate and then oxygen. 2OG binding is proposed to weaken the interaction of a water molecule bound to the iron, thereby facilitating its displacement by oxygen (Rose et al., 2011). The catalytic reaction initiates with oxygen attacking the 2OG through an electron transfer from Fe(II), resulting in the formation of a covalent bond between Fe centre and 2OG is via O_2 (Figure 1.3). The 2OG is subsequently decarboxylated generating succinate, CO_2 and an 'Fe(IV)-oxo' intermediate. The substrate becomes hydroxylated in the next step of the cycle by reduction of the ferryl intermediate (IV) through abstraction of a hydrogen atom from the substrate, followed by rebound of the oxygen onto the substrate to generate the hydroxylated product, with coincidental reversion of the iron centre to the active Fe(II) form (Hewitson et al., 2005), (Schofield and Zhang, 1999). In summary, this reaction results in the transfer of one oxygen atom to the succinate by-product and one to the protein substrate, with the release of carbon dioxide. Ascorbate is required for the full activity of some 2OG oxygenases in order to maintain the ferrous state of the iron. 2OG Oxygenases apply this mechanism in order to catalyse a wide range of oxidative modifications. In the next sections I describe specific 2OG oxygenase sub-families and their biological roles in more detail.

1.4 Extracellular protein hydroxylation by 2OG Oxygenases

1.4.1 Collagen Hydroxylases

The collagen family, of which there are 28 members (type 1 – XXVIII), are one of the best characterised targets of 2OG Oxygenases. Collagen forms part of the extracellular matrix, providing vital functions in structural support for organs and

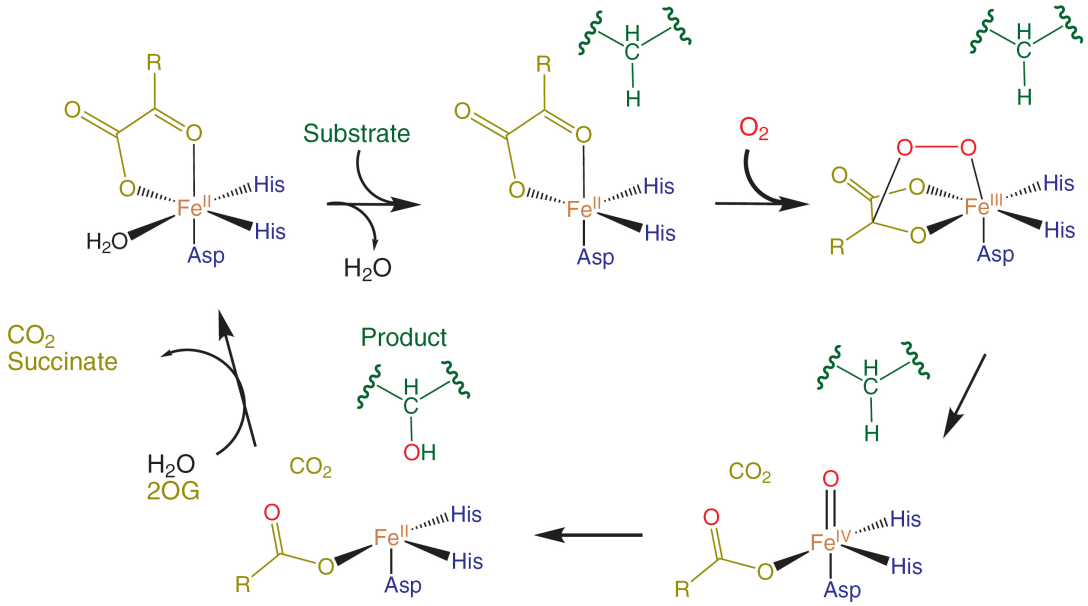

Figure 1.3. Catalytic Cycle of 2OG Oxygenases. Example of the catalytic cycle of a 2OG oxygenase catalysing hydroxylation of a C-H bond (note that related enzymes catalyse demethylation *via* hydroxylation, see Figure 4). Fe(II) in the active site is coordinate by a HXD/E-H 'facial triad' (Blue) and 2OG (Gold). Oxygen (red) binding occurs following displacement of water by the substrate (Green), thereby producing a highly reactive Fe(IV)=O ferryl intermediate that drives the hydroxylation reaction. Oxidative decarboxylation of 2OG occurs in parallel, with the production of succinate and CO_2. This figure was reproduced from (Loenarz and Schofield, 2008). Reprinted by permission from Nature Publishing Group, copyright 2008.

tissues and in the formation of basement membrane. Collagen types I, II, III, V, XI, XXIV and XXVII are built up of large tri-helical structures, fibrils, which are stabilised by crosslinking of parallel collagens (Myllyharju and Kivirikko, 2004). The fibril-associated collagens consisting of types IX, XII, XIV, XVI, XIX, XX, XXI, XXII and XXVI, are not directly involved in fibril formation, but rather bind to the surface of pre-existing collagens. Collagen IV forms part of the basement membrane that surrounds epithelial and endothelial cells to provide structural support (Myllyharju and Kivirikko, 2004). Collagen VII and X provides structural integrity by hexagonal networks found between the stroma of the eye and the endothelial layers that surrounds the eye (van der Rest and Garrone, 1991).

1.4.2 Collagen-4-hydroxylation

Prolyl-4-hydroxylase (P4H) catalyses essential and irreversible hydroxylation of proline residues (-X-Pro-Gly) in collagen (Figure 1.4). These modifications are important for stabilisation of the collagen tri-helix chains (Myllyharju, 2008), (Gorres and Raines, 2010), (Myllyharju, 2003). In vertebrates PH4 consists of $alpha_2beta_2$ tetramers, where the alpha subunit possesses the catalytic activity. Two main forms of the alpha subunit exist; Alpha(I) is the most prevalent, expressed in most cells and tissues (Annunen et al., 1997), while Alpha II expression is restricted to chondrocytes, osteoblasts and endothelial cells (Nissi et al., 2001). Interestingly, Collagen prolyl-4-hydroxylases may also target other substrates; Recent work suggests that P4H1 hydroxylates P700 of Argonaute2, an essential component of the RNA-induced silencing complex (RISC) involved in gene-silencing (Qi et al., 2008). Although Argonaute2 does not contain any tri-helical collagen-like structures it is hydroxylated at a X-Pro-Gly sequence. It is

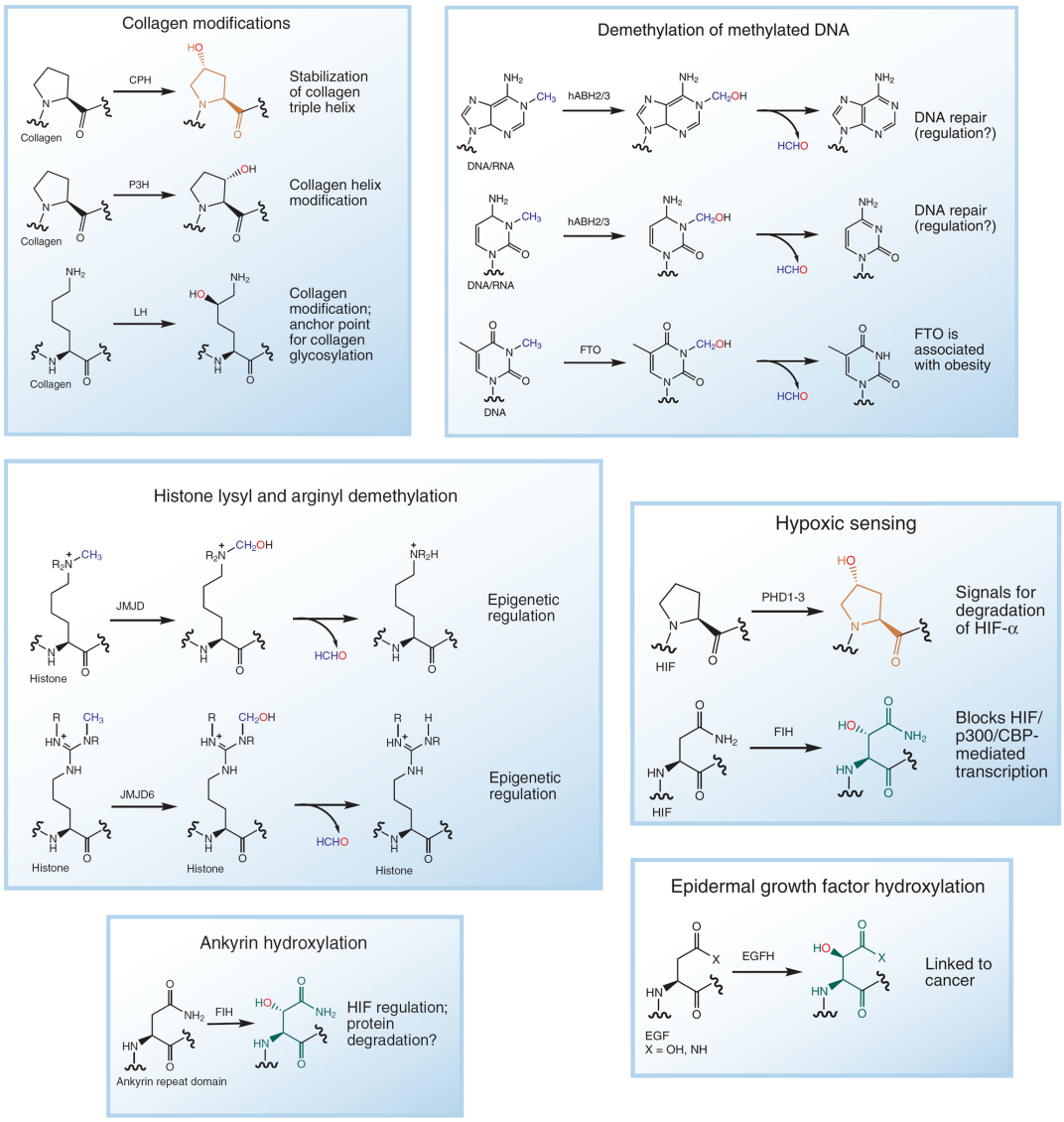

Figure 1.4. Reactions catalysed by 2OG Oxygenases. *Collagen Hydroxylases* – Collagen is highly modified by hydroxylation, which is catalysed by prolyl hydroxylases, (P4H and P3H) and lysyl hydroxylases (LH). Together they play an important role in collagen function and extracellular matrix formation. *Histone Demethylases* – These enzymes catalyse demethylation via a hydroxylation reaction which produces a highly unstable intermediate that decomposes to the unmethylated residue + formaldehyde (HCHO). Histone demethylases of the 2OG Oxygenase family regulate chromatin conformation, gene expression and development and are implicated in cancer. It is likely that an Arginine Histone Demethylase has not yet been discovered. *DNA repair* – 2OG enzymes have also been implicated in DNA repair. In a process similar to the proposed histone demethylase mechanism, Alpha-ketoglutarate-dependent

dioxygenase (AlkB) enzyme in *Escherichia Coli* catalyses the repair of N-alkylated single-stranded DNA caused by alkylating agents. In human eight AlkB homologues (hABH) have so far been identified, of which two have been shown to exhibit DNA demethylation activity (ABH2 and ABH3). *Metabolism and obesity* – recently an unexpected link between DNA demtehylation and obestity has been described. In mouse, the Fat mass- and obesity associated gene (FTO), involved in demethylation of N-methylated DNA, has been shown to be regulated at the mRNA level in the brain by feeding, suggesting a role for this enzyme in regulation of feeding or metabolism. *Hypoxic Sensing* – HIF expression and activity is regulated by Prolyl hydroxylases (PHD1-3) and an Asparaginyl hydroxylase (FIH). These modifications are central to a conserved oxygen sensing pathway in animals. Note that FIH has a large number of other substrates, all of which are modified at one or more specific Asparagine residues within *Ankyrin Repeat Domains* (ARD). The function of ARD hydroxylation is likely to be structural. *JMJD6* – This enzyme is a lysyl-5-hydroxylase (same as LH) that modifies splicing factors such as U2AF65 to regulate splicing and gene expression. *Epidermal Growth Factor Hydroxylase (EGFH)* – EGFH catalyses aspartyl (X=OH) and asparaginyl (X=NH) hydroxylation of EGF repeats in the extracellular domain of plasma membrane proteins. The exact function is unknown, but this enzyme has been implicated in cancer. This figure was adapted from (Loenarz and Schofield, 2008).

thought that hydroxylation of Argonaute2 P700 is important for Argonaute2 stability since mutants that cannot be hydroxylated exhibit reduced protein half-life. Likewise, suppression of P4H1 also reduces Argonaute2 protein (Qi et al., 2008).

1.4.3 Collagen-3-hydroxylation

Although Prolyl-3-hydroxylase (P3H) is known to target a single proline in type I, II and III collagens, the function of this modification is still not fully understood. P3H was identified over 30-years ago (Risteli et al., 1977), (Tryggvason et al., 1976) but was only recently cloned from embryonic chicks (Vranka et al., 2004). The P3H family consists of three members; P3H1, P3H2 and P3H3. Northern blot analysis have revealed that P3H1 mRNA is expressed in a wide range of human tissues including heart and muscle (Kaul et al., 2000) while P3H2 and P3H3 mRNA is expressed in mouse kidney, heart and liver (Vranka et al., 2009) P3H1 is known to interact with cartilage-associated protein (CRTAP) and cyclophilin B (CypB) to form a complex with chaperone activity towards collagen (Ishikawa et al., 2009). Lastly, mutation studies implicate P3H in a recessive bone disease in humans, consistent with important roles in bone formation and collagen helix synthesis (Cabral et al., 2008).

1.4.4 Collagen lysyl hydroxylation

Collagen lysyl hydroxylases (LH) target specific lysine residues of collagenous- X-Lys-Gly sequences to perform two important functions. Firstly, the modification stabilises collagen by forming inter-molecular crosslinks (following the action of lysyl oxidase), and secondly, it serves as attachment site for galactose and

glucosylgalactose (Myllyla et al., 2007). The hydroxylation status of the lysine residues on collagen varies with collagen type and tissue type. In collagen IV lysine is highly hydroxylated and glycosylated whereas only one third of the residues are hydroxylated in Collagen I (Khoshnoodi et al., 2008). The LHs consist of three family members, LH 1-3. In humans LH1 mRNA is expressed in several tissue types, including brain, kidney, pancreas and lung, with the highest expression in skeletal muscle and liver (Yeowell et al., 1994). LH2 is mostly found in skin, heart, kidney and spleen (Yeowell et al., 1994), while LH3 is most highly expressed in placenta, spinal cord, heart and pancreas (Valtavaara et al., 1998). Although all three of the LH isoforms exert lysyl hydroxylase activity, only LH3 have been shown to possess galactosyltransferase activity (Wang et al., 2002).

1.4.5 Aspartyl (asparaginyl)-beta-(EGF) hydroxylases.

Epidermal growth factor (EGF) stimulates cell proliferation and differentiation by binding to the epidermal growth factor receptor (EGFR) (Carpenter and Cohen, 1990). The EGF is formed from release of EGF domains in the C-terminal part of the large EGF precursor protein (Stenflo et al., 1987). Several proteins that contains EGF-like domains, including factors VII, IX and X are known to be hydroxylated on aspartate and asparagine residues by the aspartyl (asparaginyl)-beta-(EGF) hydroxylases.(ASBH or BAH) (Figure 1.4), (McMullen et al., 1983), (Stenflo et al., 1989). The function of these modifications are not yet clear although loss of hydroxylation of EGF domains in mice caused developmental defects and increased incidence of neoplasia (Dinchuk et al., 2002). Inhibition of ASBH led to decreased migration in cholangiocarcinoma cells (Maeda et al., 2003)(Maeda et al.,

2003). Furthermore overexpression of ASBH in hepatocellular carcinoma was associated with metastasis and tumour progression (Lavaissiere et al., 1996).

1.5 Intracellular protein hydroxylation by 2OG Oxygenases

1.5.1 Histone Demethylases

Histone methylation is important in the regulation of gene expression and forms part of the epigenetic memory system that regulates cell fate and identity. The basic unit of chromatin (the 'nucleosome') consists of 147 bp of DNA wrapped around two copies of each of the four histones: H2A, H2B, H3 and H4 (Figure 1.5). Protruding from the globular core of the nucleosome are the histone tails, which are subject to extensive post-translational modifications, including; arginine and lysine methylation, lysine acetylation, serine/threonine phosphorylation, and lysine ubiquitination/sumoylation (Kouzarides, 2007), (Bannister and Kouzarides, 2011). Together these modifications are thought to contribute to a histone 'code', which is read by a variety of transcriptional regulators to modulate chromatin architecture and gene expression. Histone methylation/demethylation plays an important role in this histone code; Lysine methylation at H3K9, H3K27, and H4K20 is associated with regions of transcriptionally silenced chromatin, whereas methylation at H3K4, H3K36 and H3K79 is associated with transcriptionally active regions (Kouzarides, 2007), (Bannister and Kouzarides, 2011). Several 2OG Oxygenases have been implicated in the demethylation of such marks and the chromatin conformation at these sites. 2OG Oxygenases are able to catalyse demethylation reactions because hydroxylation of the methyl group produces a highly unstable hydroxyl-methyl group. This spontaneously decomposes to release

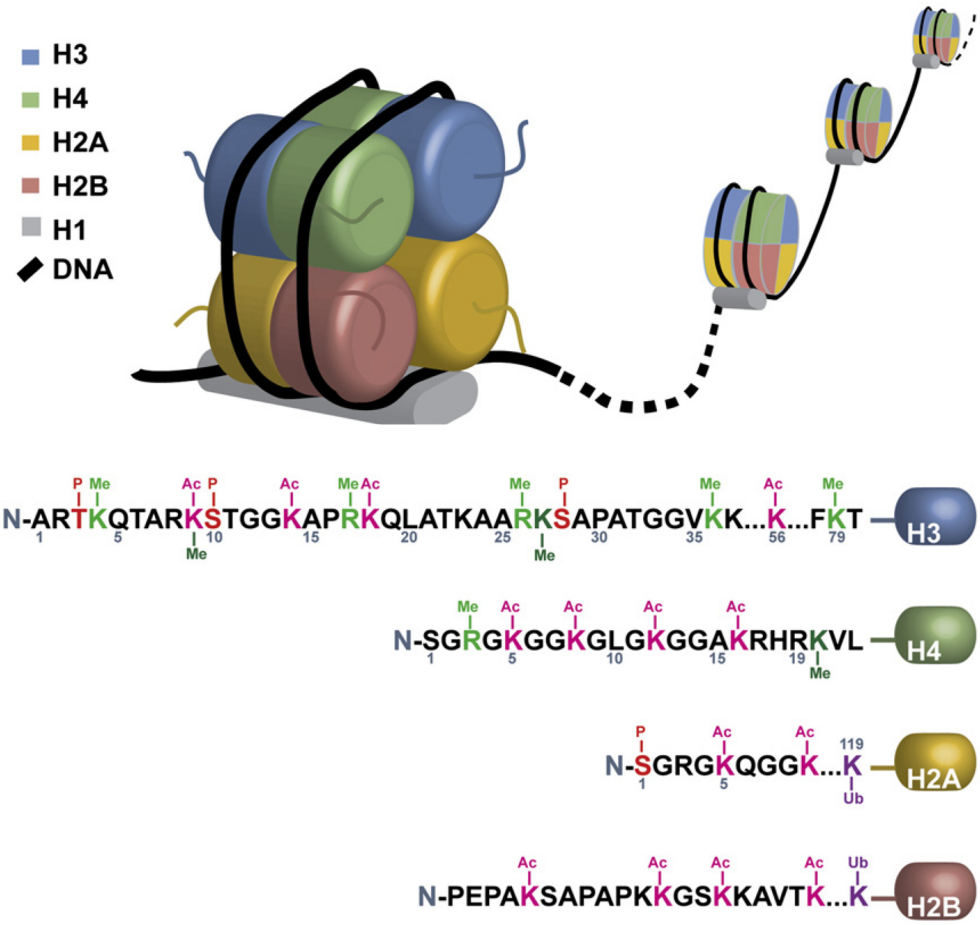

Figure 1.5. Nucleosome organisation and the Histone Code. Chromatin is organised into nucleosomes, which consist of 147bp of DNA wrapped around an octamer of histone proteins (two each of H2A, H2B, H3 and H4). The N-terminus of each histone is exposed and subject to a plethora of post-translational modifications that together are thought to act as a 'code' read by chromatin modifying enzymes and transcriptional regulators. Histone modifications include; Phosphorylation (P), Methylation (Me), Acetylation (Ac), and Ubiquitylation (Ub). Some methylations are reversible by 2OG oxygenases *via* a hydroxylation reaction. This figure was reproduced from (Hamon and Cossart, 2008). Reprinted by permission from Elsevier, copyright 2008.

formaldehyde and the demethylated residue (Figure 1.5). These histone demethylases represent the largest subfamily of 2OG Oxygenases (Figure 1.1), and can be further subdivided based on function and structural similarity.

JHDM1 Histone Demethylases. The JHDM1 histone demethylase family is conserved from budding yeast to humans and all members share leucine-rich repeats, and F-box and CXXC zinc-finger domains (Klose et al., 2006). These enzymes have been assigned as H3K36 demethylases; Overexpression of the enzyme reduces the levels of H3K36 methylation *in vivo*, although the biological function of this modification is not clear (Tsukada et al., 2006). The F-box is known to interact with S-phase kinase-associated protein 1A (SKP1) to form a ubiquitin ligase complex (Bai et al., 1996), perhaps linking histone methylation to protein ubiquitylation. The DNA-binding CXXC zinc-finger domain has also been implicated in epigenetic regulation, further supporting a role for this family in chromatin remodelling (Ayton et al., 2004), (Jorgensen et al., 2004).

JHDM2 Histone Demethylase. Found from flies to humans JHDM2 is a H3K9 demethylases that associates with the androgen receptor in response to hormone treatment and contributes to AR-mediated gene activation (Yamane et al., 2006). Mutation of another member of this family (Hairless) results in congenital hereditary alopecia (Ahmad et al., 1998). Although Hairless is thought to function as corepressor of the thyroid hormone receptor (Potter et al., 2001) the precise mechanism is unknown since it is unlikely to exhibit functional 2OG oxygenase activity (the HXD/E…H motif is not conserved) (Klose et al., 2006).

JHDM3/JMJD2 Histone Demethylases. Conserved from yeast to humans, the JHDM3/JMJD2 family members contain JmjN (Jumonji N domain, co-occurs with JmjC domain, important for enzymatic activity and protein stability), plant homebox domain (PHD, implicated in chromatin regulation) and Tudor domains (mediate protein-nucleotide and protein-protein interactions), (Klose et al., 2006). These enzymes are known to stimulate Retinoblastoma (Rb) protein activity by direct binding (Gray et al., 2005). Furthermore, several groups have reported that JHDM3/JHDM2 enzymes function as trimethyl-H3K9 and -H3K36 histone demethylases (Whetstine et al., 2006), (Klose et al., 2006). Overexpression of the enzyme suppresses trimethylation of these histone marks in cultured cells. The modification was activity-dependent since the inactive mutant did not display any reduction in trimethylated H3-K9/K36 (Whetstine et al., 2006).

JARID1/JARID2 Histone Demethylases. The JARID family is divided into two subgroups; JARDI1 and JARID2. JARID1 contains JmjN, AT-rich interactive, C5HC2-zinc-finger and PHD-finger domains, whereas the JARID2 family lacks PHD domains (Klose et al., 2006). JARID1A (KDM5A) is a H3K4 histone demethylase (Secombe et al., 2007) that interacts with Rb to repress Rb-activated genes (Blair et al., 2011). JARID1A was also shown to interact with C-Myc *in vitro* (Secombe et al., 2007). JARID2 has been implicated in organogenesis, functioning as a repressor for several cardiac genes and controlling cell proliferation through interaction with transcription factors (Takeuchi et al., 1999), (Jung et al., 2005), (Kim et al., 2005). Inhibition of JARID1 and JARID2 enzymes reduces tumour growth in preclinical studies suggesting that targeting these enzymes with inhibitors may be a useful anti-cancer strategy (Blair et al., 2011).

PHF2/PHF8 Histone Demethylases. Members of this family all share a PHD domain besides the catalytic domain and have been identified in worms, mice, and humans (Klose et al., 2006). These enzymes are involved in demethylation of H3K9 and H3K27 (Fortschegger and Shiekhattar, 2011), (Yokoyama et al., 2010), PHF8 have been implicated in regulation of the cytoskeleton (Asensio-Juan et al., 2012). Mutations in human PHF8 cause inherited X-linked mental retardation (XLMR). PHF8 is regulating cell migration and invasion in early prostate cancer (Crea et al., 2012).

UTX/UTY Histone Demethylases. The ubiquitously transcribed tetratricopeptide repeat (TPR) UTX/UTY group of proteins have orthologues from worms to humans, and contain a tetratricopeptide repeat (that mediates protein-protein interaction). UTX is a H3K27 histone demethylase involved in regulation of HOX gene regulation (Agger et al., 2007). UTX has also been found to be mutated in several cancers and is though to be a tumour suppressor (Dalgliesh et al., 2010), (van Haaften et al., 2009) Recently the *Caenorhabditis elegans* homologue of mammalian UTX was found to be an essential gene that is required for correct embryonic and postembryonic development, but surprisingly it was found not to require its enzymatic activity (Vandamme et al., 2012).

1.5.2 HIF hydroxylases and Oxygen Sensing

The maintenance of cellular oxygen homeostasis is a critical process as either excess (hyperoxia), or limiting (hypoxia), oxygen levels can be harmful to the cell, resulting in excessive oxidative damage of biomolecules or cessation of ATP production by oxidative phosphorylation, respectively. Because of oxygen's vital

importance its homeostasis is tightly controlled by a highly conserved oxygen sensing pathway that regulates an extensive array of genes in response to cellular hypoxia. The master regulator of this pathway is a transcription factor termed hypoxia-inducible factor (HIF), which is a heterodimer consisting of a constitutively expressed HIF-β subunit, and a HIF-α subunit whose expression and activity is induced by hypoxia (Lee et al., 2004). HIF activation in response to hypoxia induces the transcription of a wide range of genes involved in cellular and systemic adaptation to hypoxia, including genes involved in; cell migration, energy metabolism, angiogenic signalling, transcriptional regulation, growth and apoptosis (Schofield and Ratcliffe, 2004). HIF is involved in many cancers and known to stimulate tumour growth and angiogenesis (Mabjeesh and Amir, 2007).

HIF prolyl hydroxylases, PHD1-3. The inducible expression of HIF-α is mediated by a family of prolyl-4-hydroxylases that together target two conserved Proline residues in HIF1-α (P402 and P564), (Masson and Ratcliffe, 2003). Hydroxylation of these residues by PHD1-3 under normoxic conditions creates a high affinity binding site for pVHL, the targeting subunit of an E3 ubiquitin ligase (Figure 1.6). Subsequent ubiquitylation of HIF-α targets it for proteasomal degradation, rendering the protein highly unstable. Because the HIF PHDs have a relatively low affinity for oxygen (Hirsila et al., 2003) their enzymatic activity is impaired during hypoxia, thereby preventing HIF-α hydroxylation and degradation (Schofield and Ratcliffe, 2004).

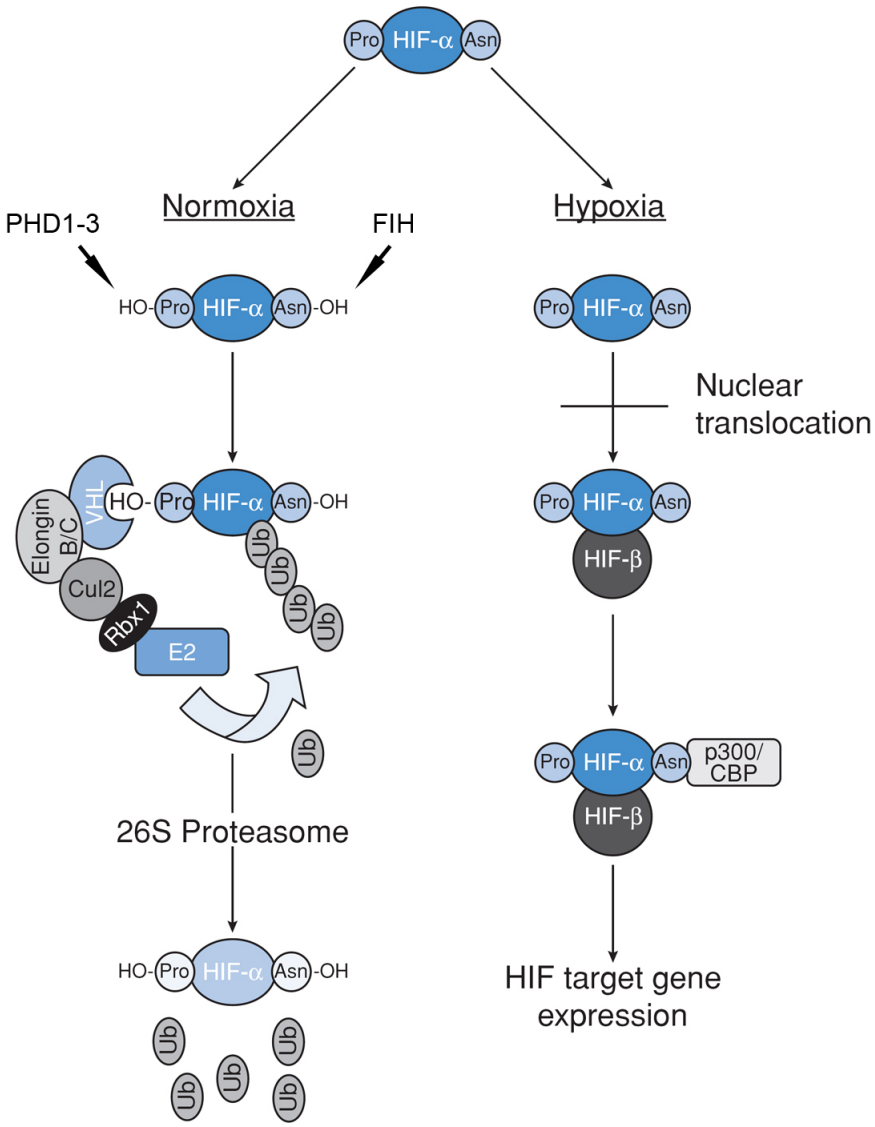

Figure 1.6. HIF regulation by hydroxylation. In the presence of Oxygen (Normoxia, left column), HIF is inactive due to (i) prolyl hydroxylation by PHD1-3, which creates a binding site for the VHL E3 ubiquitin ligase complex (VHL, Elongin B/C, Cul2, Rbx1, E2) and subsequent ubiquitylation (Ub) and proteasomal degradation, and (ii) asparaginyl hydroxylation by FIH, which prevents binding of the transcriptional co-activators p300/CBP. Under conditions of low oxygen (Hypoxia, right column), these hydroxylations are prevented, leading to HIF-a stabilisation, nuclear translocation, binding to the HIF-b subunit and recruitment of p300/CBP. The active HIF complex then transactivates a large number of genes involved in cellular and systemic adaption to hypoxia. This figure was adapted from (Coleman and Ratcliffe, 2007). Reprinted by permission from Portland Press, copyright 2007.

HIF asparaginyl hydroxylase, FIH. HIF-α is subject to a second tier of oxygen-dependent regulation; A 2OG Oxygenase termed Factor inhibiting hypoxia inducible factor (FIH) targets HIF-α asparagine residue 851. This modification prevents binding of the coactivator p300, thereby limiting HIF activity (Lando et al., 2002), (McNeill et al., 2002). Under hypoxic conditions FIH activity is inhibited, thereby preventing N803 hydroxylation and allowing p300 recruitment and HIF activation. Unlike the PHDs, which shows a high affinity for oxygen (Hirsila et al., 2003) FIH exhibits a low affinity for oxygen (Koivunen et al., 2004), (Stolze et al., 2004) making it less sensitive as oxygen sensor. Besides HIF, FIH is known to hydroxylate ankyrin repeat domains asparagine (ARD) on asparagine residues (Cockman et al., 2009), (Yang et al., 2011). ARDs are found on around 6% of the eukaryotic proteins sequenced (Barrick et al., 2008) and are involved in many biological processes including embryogenesis (Krebs et al., 2012), (Krebs et al., 2012) and cell migration (Tachibana et al., 2009). The first ARDs shown to be hydroxylated by FIH was p105 (NFKB1) and IkappaBalpha (Cockman et al., 2006). The role of these modifications is not yet clear but most likely they are involved in influencing stability and function of the ARDs (Hardy et al., 2009), (Kelly et al., 2009).

1.5.3 FIH-related 2OG Oxygenases

The HIF-α asparaginyl hydroxylase belongs to a 2OG Oxygenase subfamily consisting of several other members, all of which lack any other recognisable structural motifs. This subfamily is poorly characterised compared to other 2OG Oxygenases, but what is know is summarised below:

***JMJD5*.** Although this 2OG Oxygenase was originally suggested to be a H3K36 demethylase that regulates Cyclin A1 transcription (Hsia et al., 2010), recent structural data questions its assignment as a histone demethylase (Del Rizzo et al., 2012). JMJD5 appears overexpressed in several cancer types; Consistent with this observation, JMJD5 loss-of-function in the breast cancer cell line MCF-7 induced cell cycle arrest (Hsia et al., 2010). JMJD5 has also recently been reported to function as an osteoclastogenic repressor by destabilisation of the major osteoclast transcription factor, NFATc1 (Youn et al., 2012). Although the proposed mechanism was suggested to involve direct hydroxylation and targeting to pVHL for proteasomal degradation, no evidence of hydroxylation by mass spectrometry was provided. Therefore, the exact nature of the JMJD5 substrate(s) remains elusive.

JMJD7. The function of JMJD7 is unknown**.** Most tissues express read-through transcripts from the JMJD7 gene into the downstream cytosolic phospholipase A2β (PLA2G4B) gene, which contains a calcium sensing domain and a phospholipase domain. Besides its ability to hydrolyse phospolipids containing arachidonic acid, little is known about the JMJD7-PLA2G4B product (Klose et al., 2006).

HSPBAP1. Heat shock 27kDa associated protein 1 (HSPBAP1) is a widely expressed cytoplasmic enzyme conserved from fly to humans. As its name suggests, this 2OG Oxygenase was discovered following its interaction with heat shock protein 27kDa (HSP27). Overexpression of HSPBAP1 was found to inhibit the capacity of HSP27 to protect cells against sublethal heat shock (Liu et al., 2000). Interestingly, HSPBAP1 has been described in two other contexts. It is

targeted by a chromosomal translocation in renal cell carcinoma producing a fusion with the DIRC3 gene (Bodmer et al., 2003), and is overexpressed in the anterior temporal neocortex of patients with intractable epilepsy (Xi et al., 2007). How these observations relate to the predicted 2OG Oxygenase activity of HSPBAP1 is unknown.

JMJD6. This 2OG Oxygenase was originally known as the phosphatidylserine receptor (PTDSR). By binding to phosphatidylserine, which is found on the outer plasma membrane of cells undergoing apoptosis, it was proposed to play a role in the clearance of apoptotic cells (Li et al., 2003). However, more recent studies have cast doubt on this since JMJD6/PTDSR is mostly localised to the nucleus (Bose et al., 2004). JMJD6/PTDSR knockout mice exhibit perinatal lethality, growth retardation and disturbances in the differentiation of the kidney, intestine, liver and lungs during embryogenesis (Bose et al., 2004) perhaps consistent with a fundamental biological role. Although JMJD6 has been suggested to possess histone arginine demethylase activity (Chang et al., 2007), this has also been called into question; Recent evidence indicates that JMJD6 is in fact a lysyl hydroxylase, regulating splicing *via* hydroxylation of splicing factors such as U2AF65 (Hahn et al., 2010), (Webby et al., 2009). In breast cancer JMJD6 promotes tumour growth and is associated with a poor prognosis (Lee et al., 2012).

NO66. Nucleolar protein of 66 KDa (NO66, also known as MAPJD) is a nucleolar-localised 2OG Oxygenase implicated in ribosome biogenesis; Sucrose gradient fractionation of *Xenopus* oocyte nuclei indicates that NO66 is enriched in fractions containing precursors of the large ribosomal subunit and various forms of the 90S

preribosomal particle (Eilbracht et al., 2004), NO66 is upregulated in non-small cell lung cancer and its knockdown by siRNA suppresses the growth of non-small cell lung cancer cells (Suzuki et al., 2007); the authors propose the role of NO66 in the growth of these cells relates to its interaction with Myc. Others suggest that NO66 is a H3K4 and H3K36 histone demethylase involved in regulation of osteoblast differentiation *via* the osteoblast-specific transcription factor Osterix (Sinha et al., 2010). However, work from our laboratory in collaboration with Christopher Schofield has failed to detect any demethylase activity of NO66 either *in vitro* or *in vivo*.

NO66 shares significant sequence homology (36% overall, 57% within the catalytic domain) with another predicted 2OG Oxygenase, termed Myc-Induced Nuclear Antigen, which is the subject of this thesis, and described in more detail in the section that follows.

1.6 Myc-Induced Nuclear Antigen (MINA53)

1.6.1 Identification

MINA53 was originally identified in a screen for Myc target genes in glioblastoma cells (Tsuneoka et al., 2002). The MINA53 gene was shown to encode a 53 KDa protein consisting of a single recognisable structural motif, the 2OG Oxygenase domain. Whilst it is highly conserved in mammals, the evolutionary conserved form found in lower organisms more closely resemble NO66. Bioinformatic alignment of MINA53 from several organisms indicates that Fe(II) and 2OG binding residues are conserved, suggesting that the enzyme is functionally active (Figure 1.7).

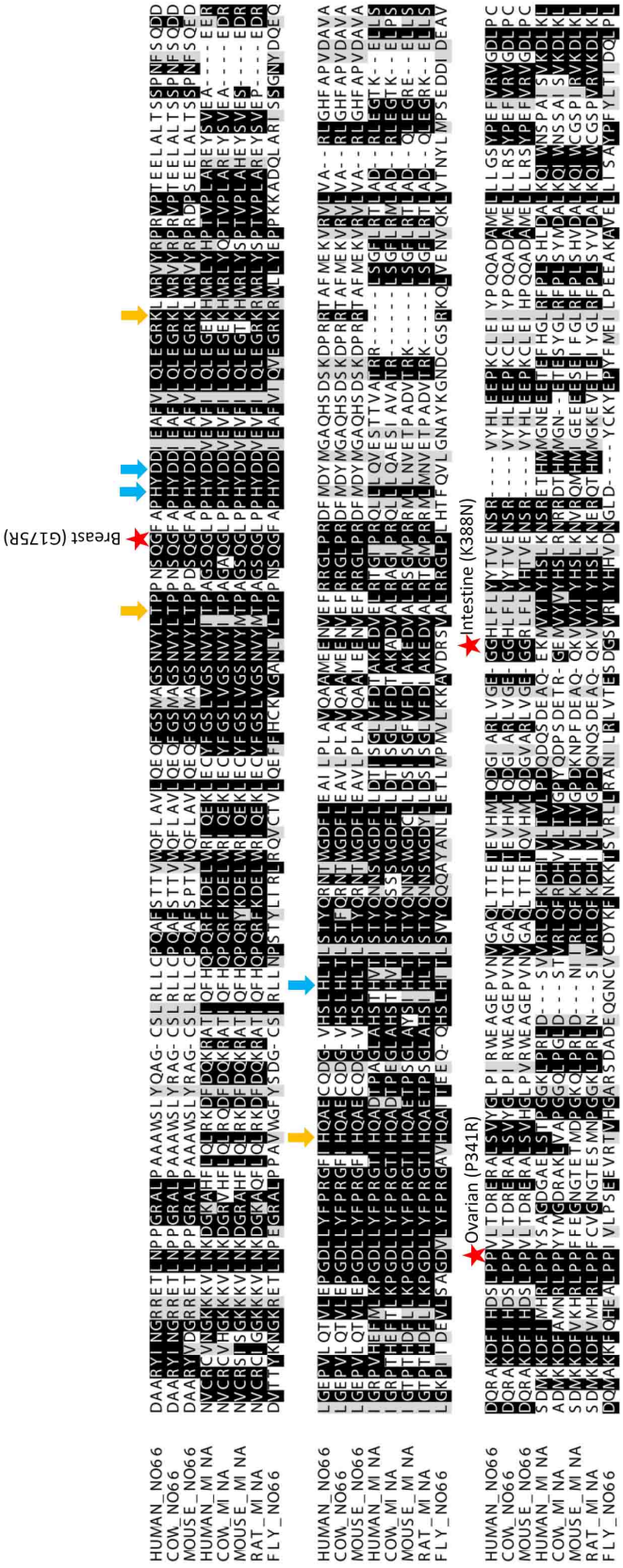

Figure 1.7. Conservation of MINA53 and NO66. Bio-informatic alignment showing conserved sequence similarity between MINA53 and NO66 in the indicated organisms. Note that in lower organisms such as Drosophila there is a single ortholog which is most similar to NO66. 2OG (Orange) and Fe(II) (Blue) binding residues are conserved. The position of recently described MINA53 cancer mutations are indicated by a red star, along with the corresponding tumour type in which the mutation was detected (see Chapter 6). Alignment was performed using ClustalW and shading by BoxShade.

1.6.2 Localisation of MINA53

MINA53 is mainly localised to the nucleolus, albeit with a low level of nuclear staining as demonstrated by immunoflourescence (Tsuneoka et al., 2002), (Eilbracht et al., 2005). Immunoelectron microscopy using an antibody raised against MINA53 confirmed its localisation to the nucleolus and specifically to the granular component of this organelle, similar to NO66 (Eilbracht et al., 2005), (Eilbracht et al., 2004). Interestingly, the granular component of the nucleolus is implicated in the later processing stages of ribosome biogenesis (see below and Chapter 7).

1.6.3 MINA53 is implicated in ribosome biogenesis

As outlined above, immunofluorescence and electron microscopy have shown that MINA53 localizes to the nucleolus. Interestingly, RNAse treatment abolishes this localization (Tsuneoka et al., 2002), (Eilbracht et al., 2005). Likewise, treatment with low doses (0.04ug/ml) of Actinomycin-D known to specifically inhibit RNA polymerase I, or prolonged serum starvation, also results in depletion of MINA53 from the nucleolus (Eilbracht et al., 2005). These results suggest that the localisation of MINA53 to the nucleolus requires ongoing transcription of ribosomal RNA (rRNA), perhaps consistent with an interaction with rRNA and/or a role in ribosome biogenesis. Biochemical characterisation has also suggested a role for MINA53 in ribosome biogenesis. Large-scale immunoprecipitations using lysates from human A431 cells showed co-precipitation of MINA53 with nucleolar protein nucleophosmin and ribosomal proteins from both large and small ribosomal subunit (Eilbracht et al., 2005). Furthermore, gradient fractionation of

Xenopus oocyte detected MINA53 in a fraction known to be enriched in preribosomes (Eilbracht et al., 2005).

1.6.4 Role in immunology: MINA53 is an IL4 repressor

In a recent publication MINA53 was specifically found to bind and repress the *Il4* promoter in CD4+ T cells through an unknown mechanism. MINA53 overexpression in transgenic mice impaired *Il4* expression, while its knockdown in primary $CD4^+$ T cells led to *Il4* derepression. Together, these findings suggest a possible involvement of MINA53 in an *Il4* pathway regulating T_H differentiation and genetic variation in T_H2-bias (Okamoto et al., 2009). Presumably, the role of MINA53 as a transcriptional repressor of IL4 relates to its nuclear, as opposed to nucleolar, localisation. Whether MINA53 mediates the repression of other gene transcription is unclear.

1.6.5 Expression of MINA53 in cancer

MINA53 has been found to be upregulated in a wide range of tumours and in some cases is associated with poor prognosis (Ogasawara et al., 2010), (Teye et al., 2004), (Teye et al., 2007), (Ishizaki et al., 2007). In one study of gastric carcinoma (Zhang et al., 2008), increased expression of MINA53 was observed in most of the tumours (91.1%) but negatively expressed in all normal mucosa tissues. Elevated expression of MINA53 was found to be coupled with a poor prognosis in renal cell carcinoma (Ishizaki et al., 2007), and overexpressed in most oesophageal squamous cell carcinomas tumours (83%) where it is associated with shorter survival (Tsuneoka et al., 2004). MINA53 expression was correlated with tumour proliferation but not prognosis in gingival squamous cell carcinoma (Kuratomi et

al., 2006), and was found frequently expressed in aggressive types of B cell lymphoma (Teye et al., 2007). Furthermore, increased levels of MINA53 were associated with poor prognosis in neuroblastoma (Fukahori et al., 2007), and associated with poorly undifferentiated tumours and tumours with larger diameter in hepatocellular carcinoma (Ogasawara et al., 2010). The majority of these reports on MINA53 overexpression in cancer derive from the same collaborator network based in Japan, who clearly make a strong case for MINA53 as a novel prognostic marker and/or novel cancer target. However, one study from this network indicates that lung cancer patients with a negative staining for MINA53 had a significantly worse prognosis than patients with a positive staining (Komiya et al., 2010a). Therefore, the role of MINA53 in cancer may be tissue specific.

1.6.6 Cellular phenotypes of MINA53 associated with cancer

In vitro tissue culture models have recently begun to investigate the role of MINA53 in tumourigenesis. siRNA targeting MINA53 may suppress the growth of several human cancer cell lines including; cervical carcinoma HeLa cells, lung adenocarcinoma A549 cells, and human colon carcinoma SW620 cells (Teye et al., 2004), (Zhang et al., 2005), (Tsuneoka et al., 2002). This may be consistent with observations that MINA53 overexpression correlates with staining of the proliferation marker Ki67 in some human tumours (Kuratomi et al., 2006), (Teye et al., 2004). Overexpression of MINA53 can induce the transformation of NIH/3T3 cells in soft-agar growth assays (an assay of anchorage-independent growth) and injection of these cells into nude mice produces tumours (Komiya et al., 2010b). cDNA microarray analysis of overexpressing MINA53 NIH/3T3 cells indicated that

MINA53 regulates genes involved in cell proliferation, metastasis, cell migration and metabolic process (Komiya et al., 2010b).

The observation that MINA53 overexpression in lung cancer may be associated with a favourable prognosis (Komiya et al., 2010a) prompted the authors to investigate the mechanisms involved. Overexpression of MINA53 in the squamous lung cancer cell line H226B inhibited cancer cell invasion, whilst it induced apoptosis in A549 cells (Komiya et al., 2010a). Furthermore, transfection of MINA53 shRNA into H226B cells increased their invasion. These data further support the possibility that the role of MINA53 in tumourigenesis is cell and/or tissue specific.

1.6.7 Enzyme Activity and substrates of MINA53

Although MINA53 is recognised as a 2OG Oxygenase and has been implicated in multiple cellular processes and cancer, the role and identity of its substrates are not yet clear. However, similar to NO66, it has been suggested that MINA53 is a histone demethylase. Lu *et al* propose that MINA53 is a histone demethylase that targets H3K9 at the ribosomal RNA promoter, thereby inducing promoter activity (Lu et al., 2009). siRNA treatment of MINA53 increased the levels of H3K9me3 at the ribosomal DNA promoter while overexpression enhanced the expression of 28S and 18S rRNA. However, direct evidence of MINA53 histone demethylase activity (i.e. mass spectrometry) was not presented. In line with this, local attempts have failed to detect histone demethylase activity of MINA53 in *vivo* or *in vitro* (personal communication Professor Christopher Schofield and Dr Mathew

Coleman). The enzymatic activity of MINA53 involved in rRNA transcription, ribosome biogenesis, cell proliferation and cancer remains elusive.

1.7 Aims and scope of this thesis

The aim of my thesis is to expand our knowledge of MINA53 and specifically to explore the role its enzymatic activity in cellular processes associated with tumourigenesis. In order to achieve this I have created cellular models that allow the role of enzyme activity to be dissected. Chapter 2 describes my work investigating the role of MINA53 in proliferation using both acute and chronic gene silencing to reduce the levels of MINA53. In chapter 3 I develop an isogenic MINA53 knockout cell model for studying the role of MINA53 activity in various biological processes, including *suppression* of K-Ras transformation. In Chapter 4 I describe our identification and characterisation of a MINA53 substrate, providing proof that MINA53 is a ribosomal hydroxylase. In chapter 5 I examine the role of MINA53 in ribosome biogenesis and autophagy, and in the final results chapter I provide additional genetic evidence supporting a negative role of MINA53 enzyme activity in tumourigenesis. Chapter 7 discusses the results in my thesis in a wider context and outlines further directions for the work presented.

Chapter 2
Role of MINA53 in proliferation

2.1 Introduction

MINA53 is reported to play an important role in tumour cell growth. Knockdown of MINA53 by siRNA inhibited the growth of HeLa cervical carcinoma, rat 3Y1MycB, SW620 human colon carcinoma, and A549 lung adenocarcinoma cell lines (Teye et al., 2004), (Zhang et al., 2005), (Tsuneoka et al., 2002) In contrast, MINA53 may promote anti tumourigenic phenotypes under some conditions: MINA53 shRNA in the lung squamous cell carcinoma cell line, H226B, increases cell invasion. Furthermore, overexpression of MINA53 in A549 cells induces apoptosis (Komiya et al., 2010a). Therefore, the role of MINA53 in tumour cell proliferation and survival is currently unclear. A role for the potential 2OG oxygenase activity of MINA53 in the phenotypes described above has not yet been explored.

2.2.1 Effect of MINA53 siRNA on cell growth in A549 and HeLa cell lines

In order to identify a suitable system for investigating the role of MINA53 enzyme activity in tumour cell proliferation, I first began by attempting to replicate some of the published observations described above. A549 and HeLa cell lines were transfected with MINA53 (2 different siRNA, #2 published sequence, (Zhang et al., 2005)) or control (dHIF) siRNA, or treated with transfection reagent alone (oligofectamine), before monitoring MINA53 knock-down efficiency by western blot (Figure 2.1A and 2.2A). In parallel, cell proliferation was monitored for four days using the 3-(4,5-imethylthiazol-2-yl)-2,5-diphenyl-tetrazolium bromide (MTT) mitochondrial cell viability assay. This assay requires the activity of mitochondrial reductase enzymes to convert the added tetrazolium salt into a purple formazan product whose absorbance can be detected using a spectro-photometer (Mosmann, 1983), (Cory et al., 1991).

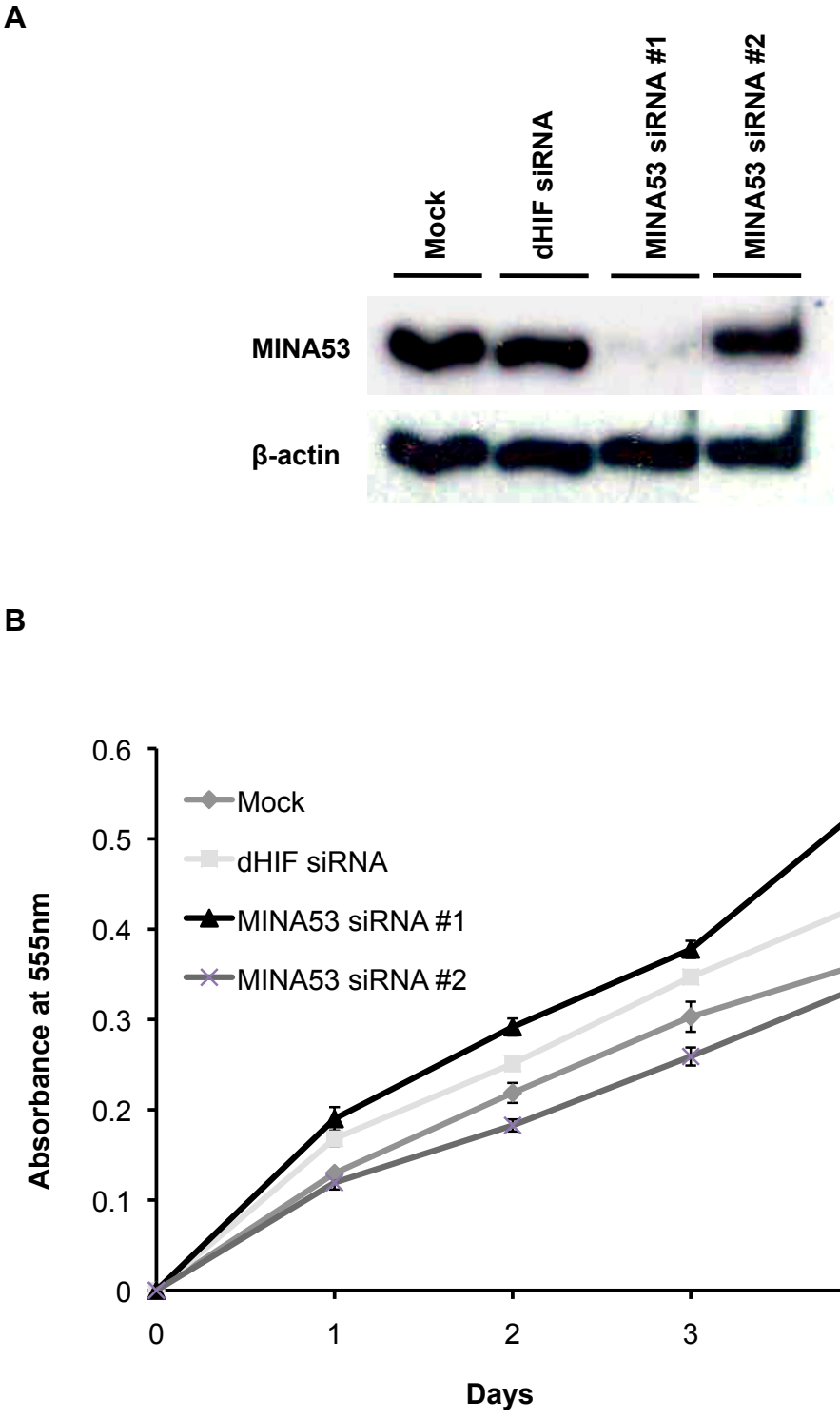

Figure 2.1. Effect of MINA53 siRNA on cell growth in HeLa cells. A. Western blot of control (Mock (oligofectamine alone) or dHIF siRNA) and MINA53 siRNA in HeLa cells. **B.** Cell growth of transfected siRNA MINA53 HeLa cells measured by 3-(4,5-Dimethylthiazol-2-yl)-2,5-diphenyltetrazolium bromide (MTT) assay.

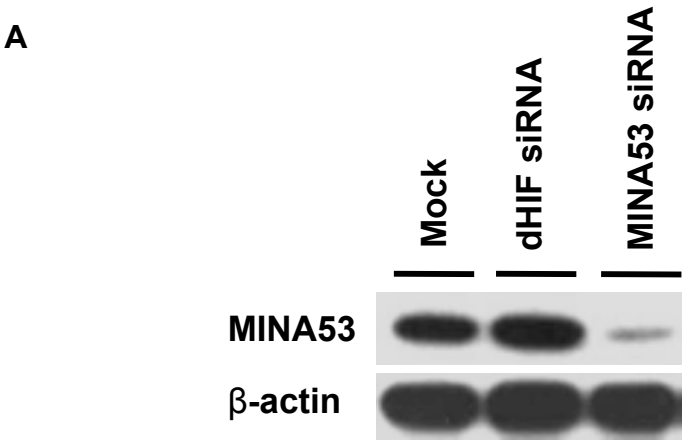

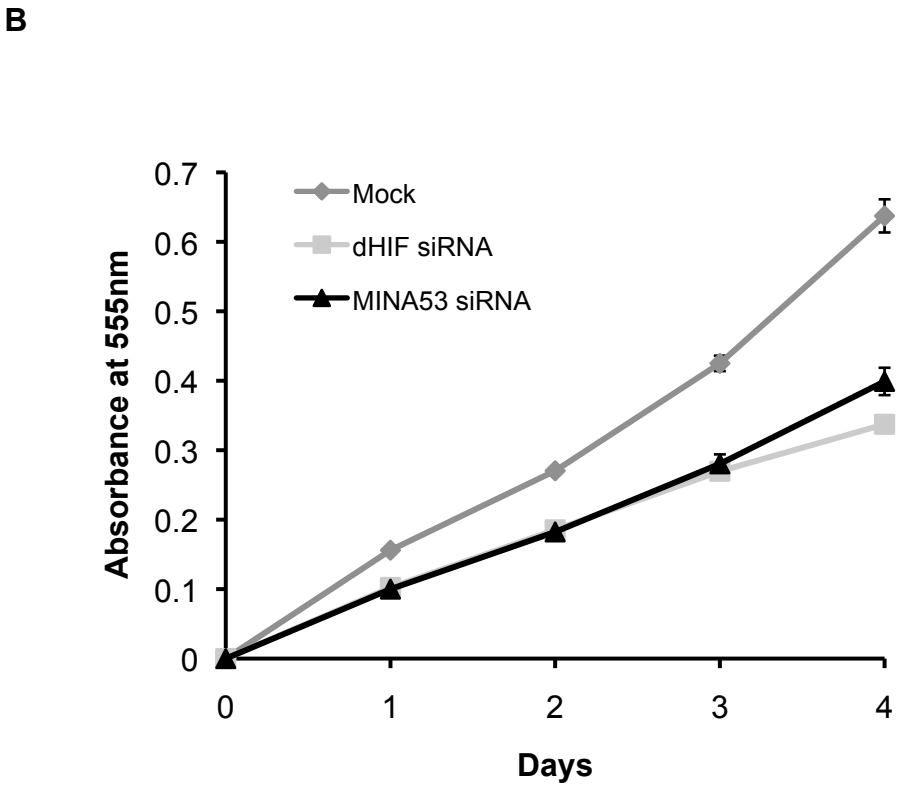

Figure 2.2. Effect of MINA53 siRNA on cell growth in A549 cells. A. Western blot of control (mock (oligofectamine alone) and dHIF siRNA) and MINA53 siRNA in A549 cells. **B.** Cell growth of A549 cells transfected with control (Mock (oligofectamine alone) or dHIF siRNA) and MINA53 siRNA, evaluated by MTT assay.

Surprisingly, although effective knockdown of MINA53 (using siRNA #1) was achieved in both cell lines, no negative effect on proliferation was observed (Figure 2.1B and 2.2B). I therefore conclude that a transient reduction of MINA53 using siRNA does not significantly affect the proliferation of these cells, at least under the examined conditions here.

2.2.2 Effect of MINA53 shRNA on cell growth in A549 and HEK293T cell lines

I next sought to determine whether more chronic enzyme knockdown was required to elicit reduced growth rates. I established A549 and HEK293T cells stably expressing either a MINA53 or control shRNA sequence (Figure 2.3A and 2.4A). I had to isolate clones from the pool of MINA53 shRNA A549 cells in order to obtain a satisfactory knockdown of MINA53. Therefore, for comparative analyses we compared three independent clones for each shRNA (Figure 2.3A). Cell growth was monitored for 5 days by either MTT assay for A549 clones, or MTS assay for 293T cells. The MTS assay is a simpler 'next generation' MTT reagent and was therefore used for much of the subsequent analyses. In line with the findings described in section 2.2.1, there was no consistent MINA53-dependent effect on cell proliferation in either cell background (Figure 2.3B and 2.4B). Although, selected MINA53 shRNA A549 clones exhibited reduced growth rate compared to some controls clones, no clear correlation was found between the level of MINA53 expression (Figure 2.3A) and cellular proliferation (Figure 2.3B). In conclusion, despite efficient and chronic knockdown of MINA53, I was unable to observe any significant or consistent affect on cell proliferation in either of two independent cell lines. However, I cannot rule out the possibility that a low level of residual

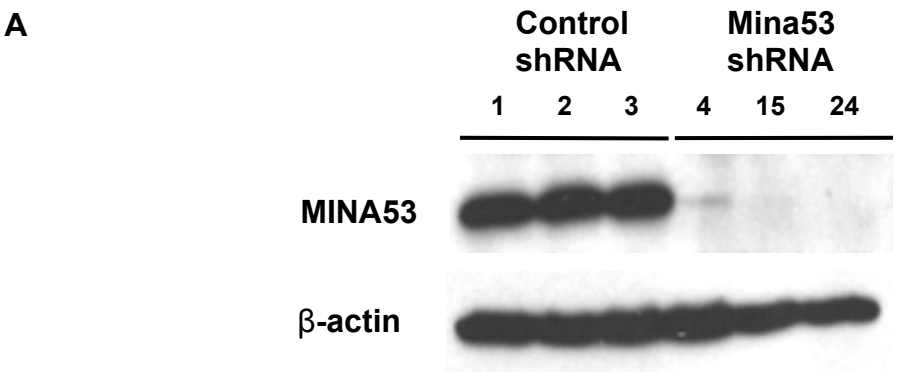

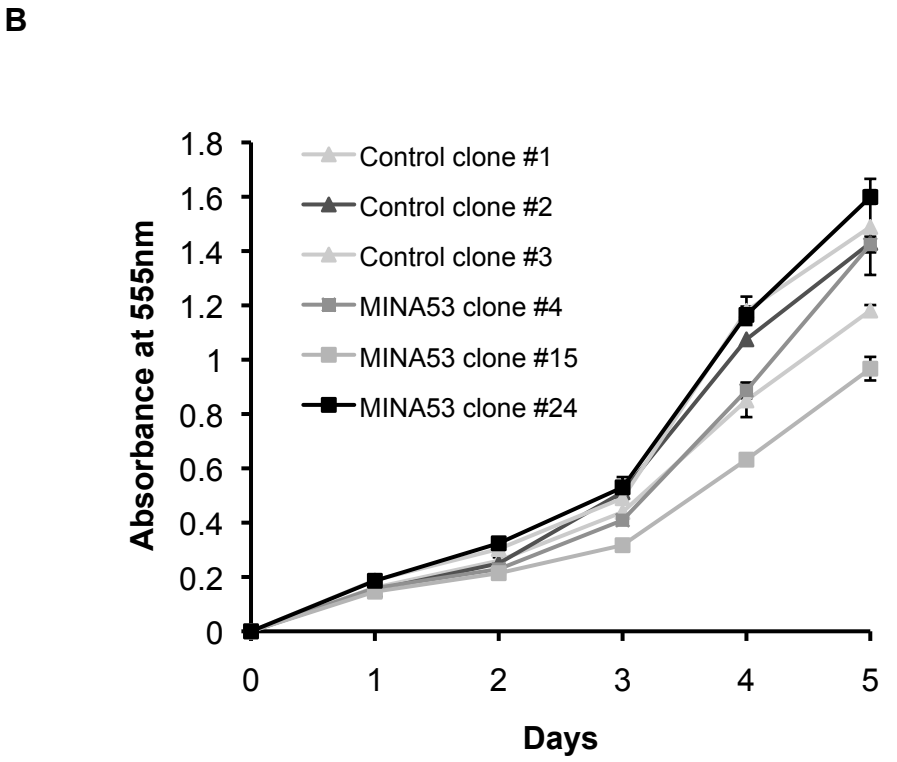

Figure 2.3. Effect of MINA53 shRNA on cell growth in A549 cells. A. Western blot of control shRNA and MINA53 shRNA in A549 clones. **B.** Effect of shRNA against MINA53 on cell growth in A549 cell lines compared to controls examined using an MTT assay.

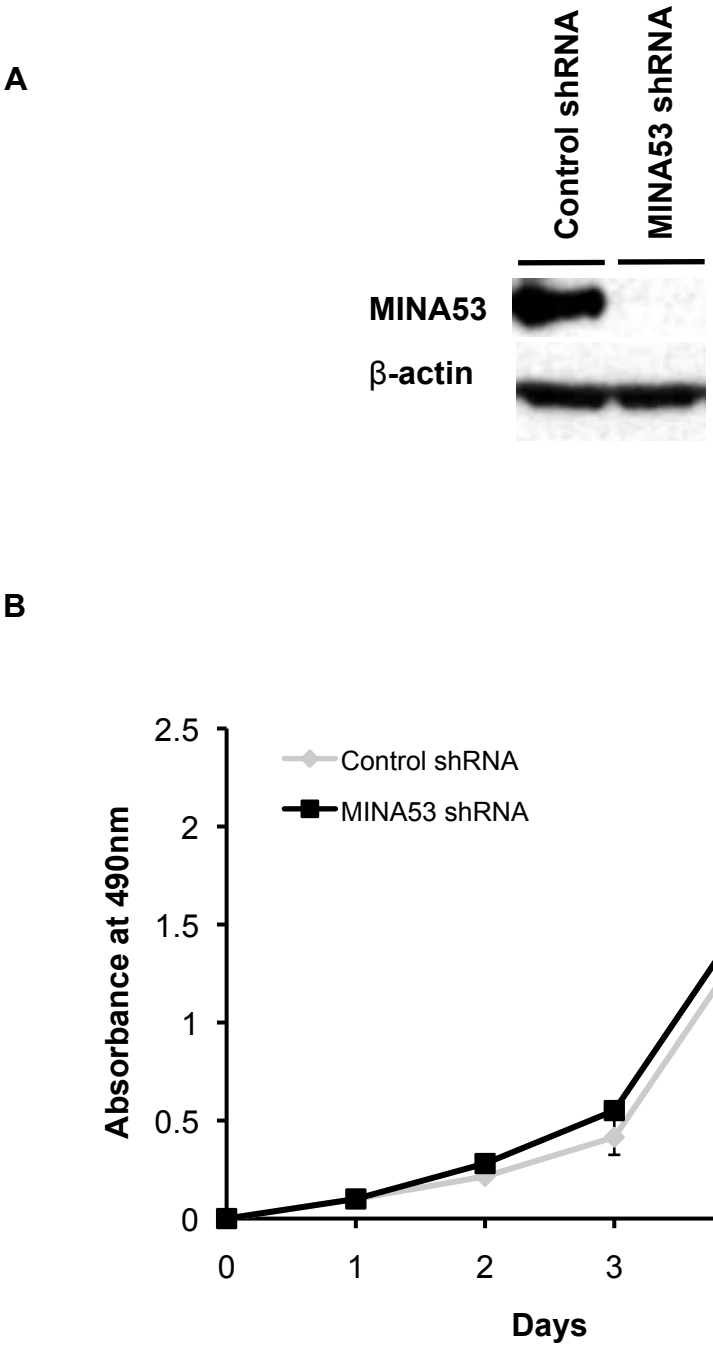

Figure 2.4. Effect of MINA53 shRNA on cell growth in HEK293T cells. A. Western blot of control shRNA and MINA53 shRNA expressing HEK293T cells. **B.** Effect of shRNA against MINA53 on cell growth in HEK293T cells. Cell proliferation examined using a 3-(4,5-dimethylthiazol-2-yl)-5-(3-carboxymethoxyphenyl)-2-(4-sulfophenyl)-2H-tetrazolium) (in the presence of phenazine methosulfate (PMS)) MTS assay.

MINA53 in knockdown cells was sufficient to maintain normal cell growth under these conditions.

2.3.1 A MINA53 gene knockout cell model

To study the consequence of complete loss of MINA53 expression on cell proliferation (and other cellular processes) I generated Mouse Embryonic Fibroblasts (MEFs) from MINA53 wildtype (WT), heterozygous (HET), and homozygous knockout (KO) mouse embryos (Figure 2.5). Others in our laboratory previously established the conditional knockout MINA53 mice. The targeting vector used to create this transgenic line contained LoxP sites flanking MINA53 exons 3 and 4 (encoding the catalytic JmjC domain) to allow Cre recombinase-mediated inactivation of MINA53 *in vivo*. Timed mating of MINA53 heterozygous KO mice was used to isolate 11 littermate embryos at E13.5, from which fibroblasts were then cultured *in vitro*. In parallel, genomic DNA was isolated from a limb tip from each embryo and genotyped by PCR using specific primers (Figure 2.5A). PCR products of expected sizes for WT (260 bp) and KO (439 bp) MINA53 alleles identified 3 WT, 5 HET, and 3 KO embryos in the litter (Figure 2.5B). Primary MEFs were obtained from three embryos of each genotype, which I then immortalised using a retrovirus expressing the SV40 Large-T antigen (Figure 2.6A).

2.3.2 Effect of MINA53 gene knockout on cell growth in immortalised MEFs

To study the effect of MINA53 gene loss in MEFs, the proliferation of immortalised WT, HET and MINA53 KO cells was monitored using the MTT assay for 5 days.

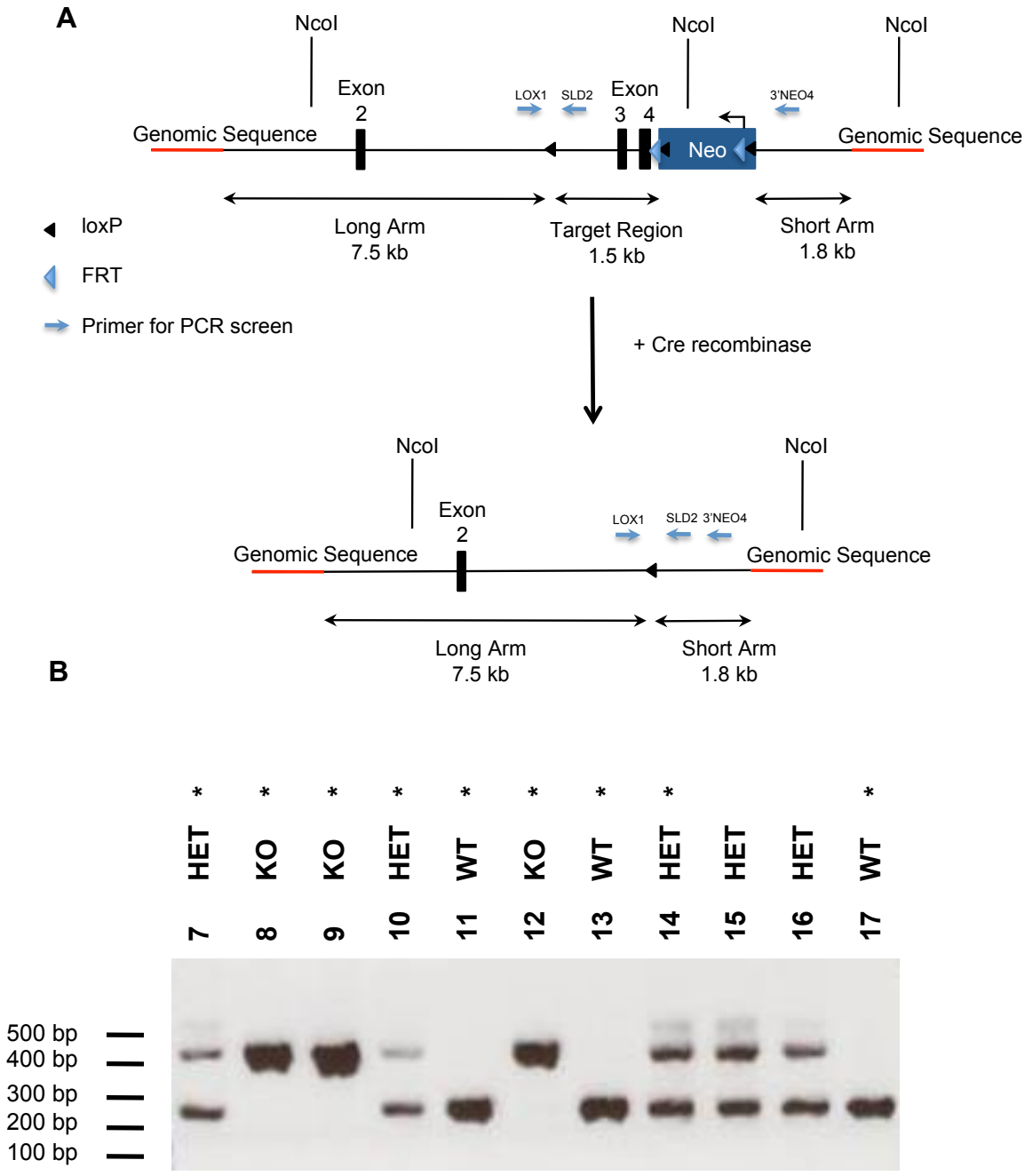

Figure 2.5. **Establishment of MINA53 gene knockout MEFs. A.** Targeting vector for MINA53 outlining loxP sites, sequencing primer binding sites, and neo cassette. Lower figure shows MINA53 after removal of floxed exon 3 and 4 by Cre recombines. **B.** DNA blot of genotyping PCR of WT, HET and KO MINA53 primary MEFs, using primers detecting LoxP sites and Neo-casette. (*) denotes primary MEF cell lines that were subsequently immortalised and assayed for cellular proliferation.

A

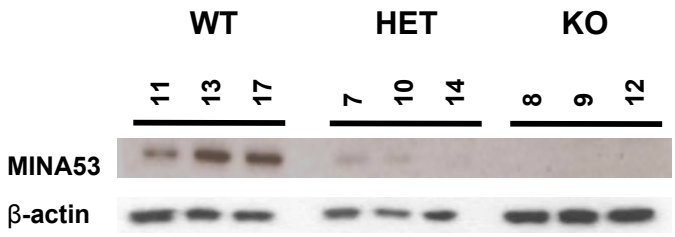

B

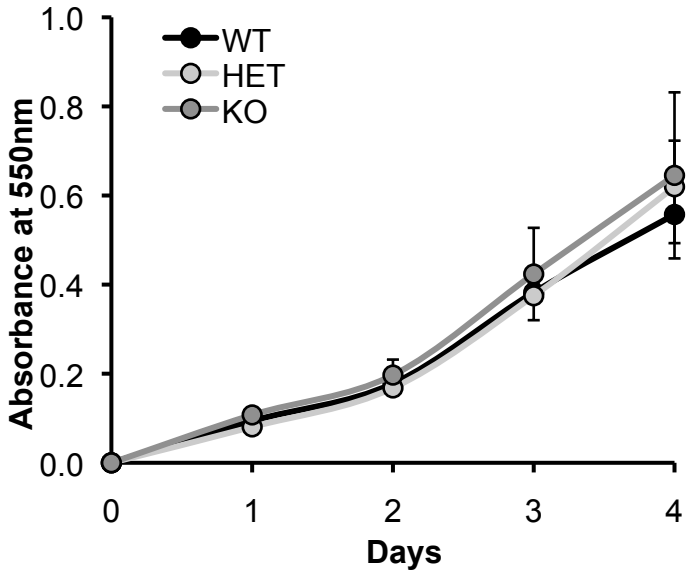

Figure 2.6. Effect on growth using immortalised WT, HET and KO MINA53 MEFs. A. Western blot of SV40 Large T immortalised wild-type (WT), heterozygous (HET) and knockout (KO) MINA53 MEFs. Primary MEFs were immortalised by a retrovirus expressing SV40 LargeT antigen. Number denotes identification number for each cell line. **B.** Cell proliferation of immortalised WT, HET and KO MEFs monitored using a MTT assay.

Consistent with my previous findings, no significant MINA53-dependent effect on cell growth was observed (Figure 2.6B).

2.3.3 Effect of MINA53 gene knockout on cell growth in K-Ras transformed MEFs

Since published observations of MINA53 in cell growth relate to the transformed cell state I next sought to test whether transformation of immortalised MINA53 MEFs would elicit a growth phenotype. Therefore, I transformed WT and KO MINA53 MEFs with a retrovirus expressing oncogenic K-Ras (a G12V mutation that renders it GTPase deficient): K-Ras-transformed WT and KO MEFs exhibited several hallmarks of transformed cells, including spindle-shaped morphology (Figure 2.7A), and enhanced growth rate compared to their immortalised counterparts (Figure 2.7B). However, despite enhanced proliferative drive in the transformed MEFs, we still did not observe any MINA53 dependent effect on cellular proliferation (Figure 2.7B). We therefore conclude that neither immortalised nor transformed MEFs have any specific requirement for MINA53 expression for cell proliferation. Taken together, my findings thus far suggest that MINA53 is not required for the proliferation of several cell types, at least under the conditions of two-dimensional (2D) growth assayed here.

2.3.4 MINA53 KO transformed MEFs show enhanced anchorage-independent growth

To test whether MINA53 is required for the growth of transformed cells in a model which more closely resembles 3D growth within a tumour, I compared the

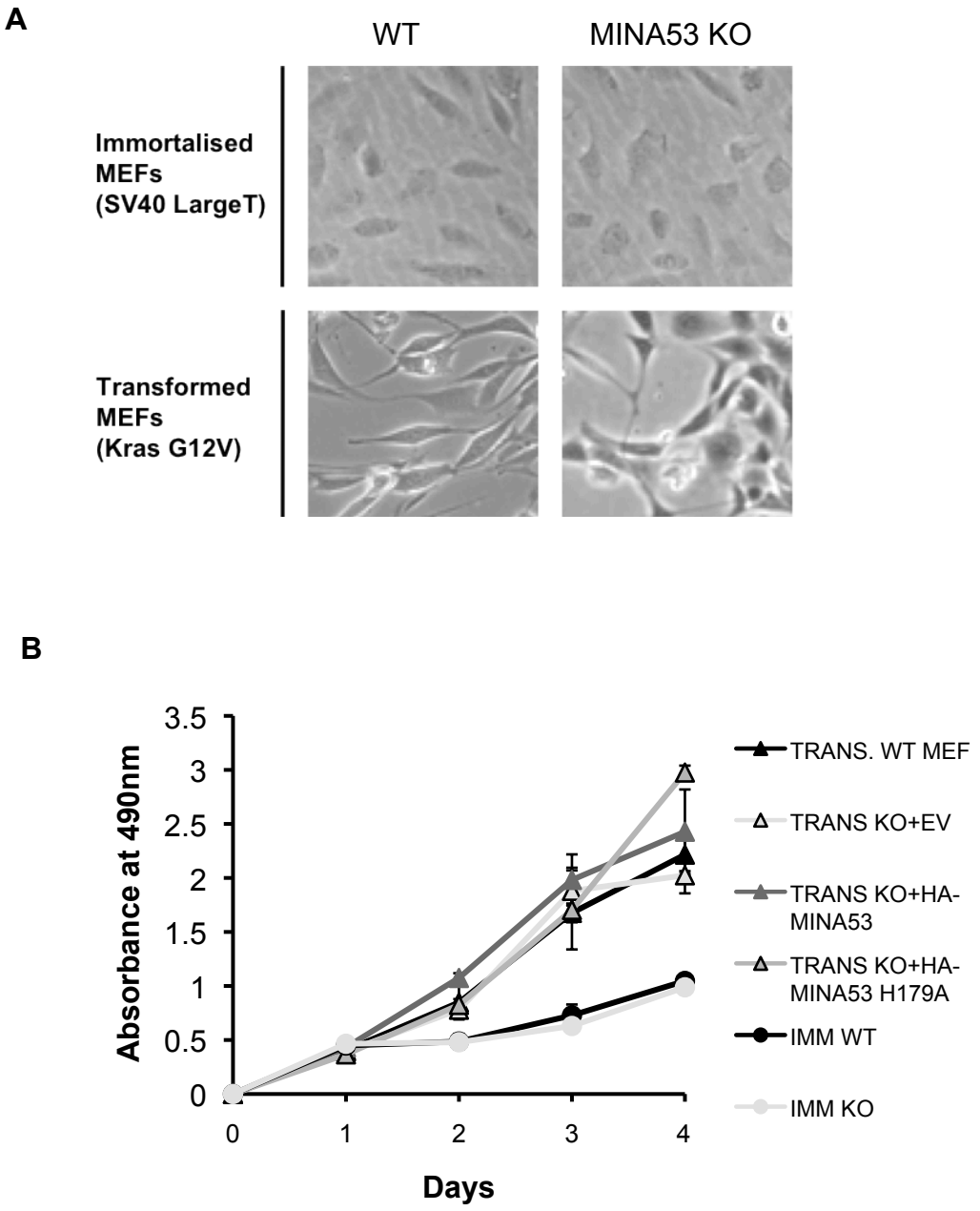

Figure 2.7. Morphology and growth of immortalized MEFs compared to transformed MEFs A. Phase contrast images of SV40 LargeT immortalized and K-Ras G12V transformed WT and MINA53 KO MEFs. **B.** Cell growth of Immortalised MEFs compared to transformed MEFs evaluated using a MTS assay.

anchorage-independent growth of WT and KO MEFs *in vitro*. Fibroblasts must be attached to a solid surface in order to survive and proliferate: Suspension in a viscous fluid or gel causes cells to undergo apoptosis in a process called *anoikis* (Frisch and Screaton, 2001). However, when fibroblasts are transformed using a potent oncogene they become anchorage-independent and grow without the need for attachment. Anchorage-independent growth can be monitored *in vitro* using a 'soft agar' assay in which cells are seeded in semi-solid agar, before suspending on a layer of higher percentage agar, and culturing for 3-4 weeks. Colonies are stained using crystal violet dye and counted to assess a cell lines tumourigenic potential. Using this assay I measured the anchorage-independent growth potential of K-Ras-transformed MINA53 WT and KO MEFs. In contrast to a pro-tumour role for MINA53, KO transformed MEFs formed significantly more colonies than MINA53 WT MEFs (Figure 2.8). Therefore, MINA53 negatively regulates the anchorage-independent growth of K-Ras transformed MEFs.

2.3.5 Effect of MINA53 on clonogenic survival

To determine whether the observed effect of MINA53 on anchorage independent growth was due to inherent differences in clonogenic viability I measured survival of MINA53 wildtype and knockout cells using a 2D colony formation assay. In this assay cells are seeded out at several different densities and left for three weeks to form colonies from single cells, after which the colonies were stained with crystal violet and counted. Although I observed slight differences in the survival of each cell line, there was no clear genotypical correlation (Figure 2.9).

A

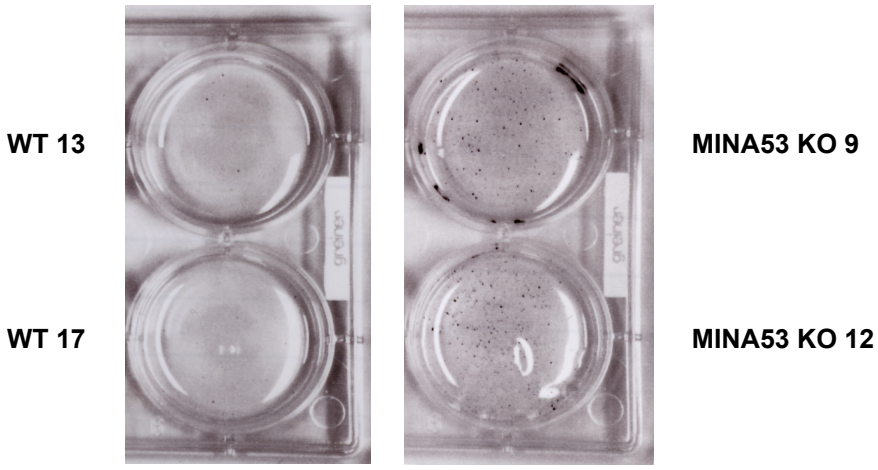

B

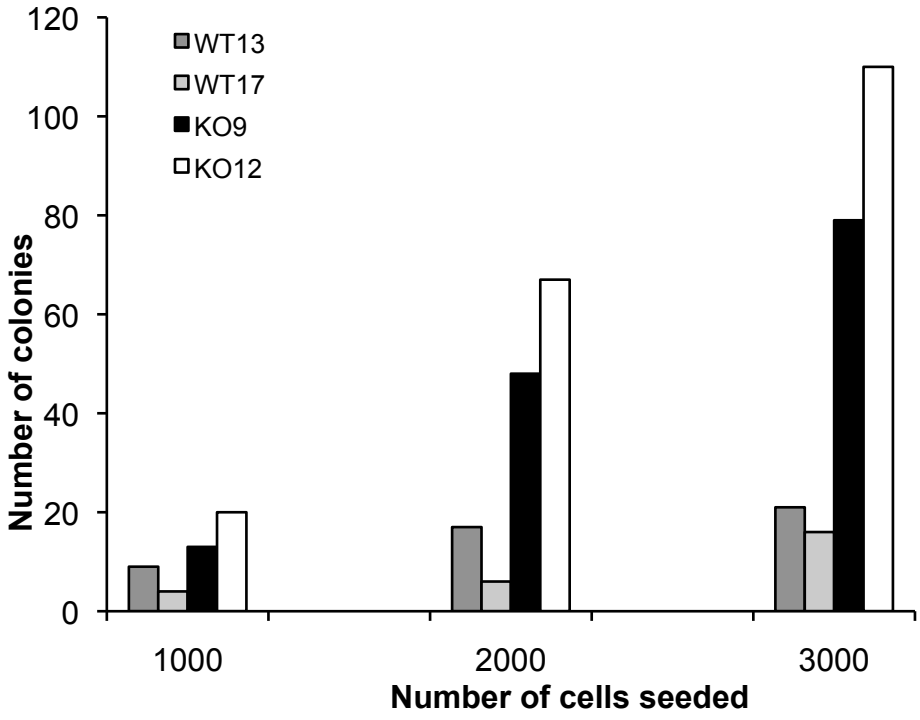

Figure 2.8. Effect of MINA53 on cell proliferation in K-Ras G12V transformed MEFs. A. K-Ras G12V transformed WT and MINA53 KO MEFs were seeded out at three different densities in 'soft agar', grown for 3 week where after formed colonies were stained with crystal violet and counted. B. Number of formed colonies in 'soft agar' after 3 weeks of growth.

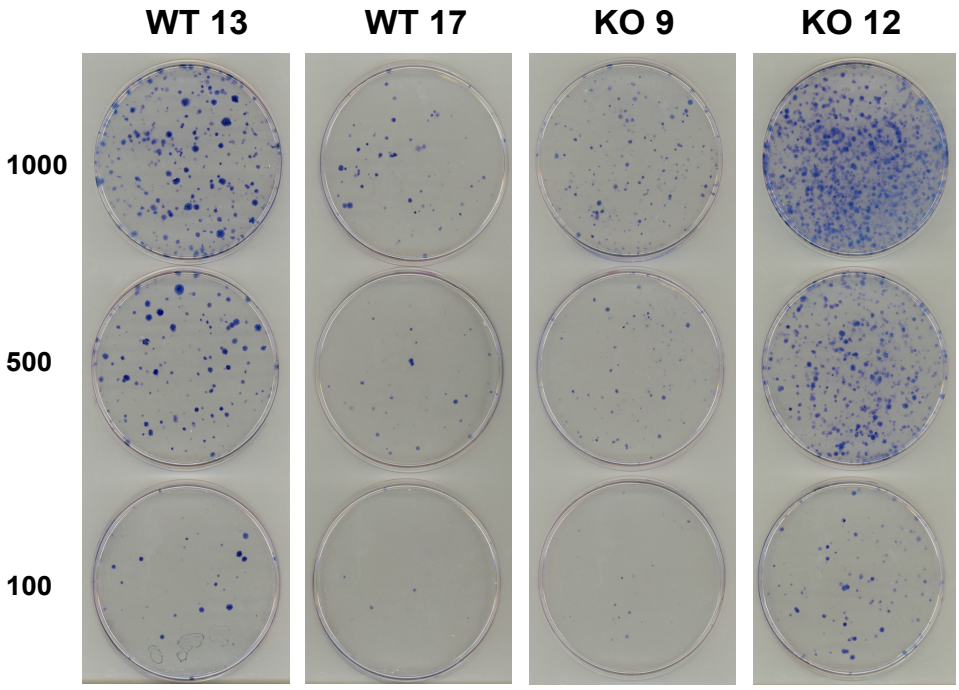

Figure 2.9. Effect of MINA53 on clonogenic survival in transformed MEFs. K-Ras G12V transformed WT and MINA53 KO MEFs were seeded out at three different densities, grown for 3 week where after formed colonies were stained with methylene blue.

2.4 Conclusion

In this chapter I have investigated the role of MINA53 in the growth of tumour cell lines and a transgenic MEF model. Others have reported that a reduction of MINA53 severely suppresses tumour cell proliferation. However, although several approaches and cell types were used I was unable to observe any significant effect of MINA53 inhibition on 2D proliferation. A possible explanation for the published observations may relate to the unusually high concentrations of oligonucleotide used in some studies (400nM; (Zhang et al., 2005) and 'off-target' effects of siRNA. Surprisingly the published siRNA sequence (MINA53 siRNA #2,) did not reduce MINA53 protein levels at a commonly used siRNA concentration (20 nM).

Interestingly, when I examined the role of MINA53 in 3D growth, I discovered a potential role for MINA53 in negatively regulating anchorage-independent growth of K-Ras-transformed MEFs. However, because only two cell lines were assayed per genotype there remains the possibility that these observations represent random variation between embryos, rather than a *bona fide* MINA53-dependent effect. Furthermore, the current MEF cell model does not allow the role of MINA53 enzyme activity in anchorage-independent growth and other cellular processes to be investigated. In Chapter 3 I address both these points by creating a cell model in which wildtype or enzyme-dead MINA53 are reconstituted into an isogenic KO MEF background.

Chapter 3

An isogenic MEF model for studying the enzymatic activity of MINA53

3.1 Introduction

MINA53 has been implicated in several important biological processes including proliferation, ribosome biogenesis, cytokine gene expression, chromatin modification and transformation (Tsuneoka et al., 2002), (Eilbracht et al., 2005), (Komiya et al., 2010a), (Komiya et al., 2010b), (Lu et al., 2009). Furthermore, in Chapter 2 I provide preliminary data implicating MINA53 in the suppression of anchorage-independent growth. However, the role of its potential enzymatic activity in these processes is not yet clear, despite the conservation of critical catalytic residues (see Chapter 1, figure 1.7). Therefore, I sought to establish a cellular model that could be used to dissect the roles of MINA53, and its enzyme activity, further.

3.2.1 MINA53 rescue MEFs for structure-function studies

To create a suitable model for studying the biological role(s) of MINA53 enzyme activity I decided to work in a single KO MEF cell line described in Chapter 2. This provided the complete absence of MINA53 and an 'isogenic' background in which to reconstitute expression. K-Ras-transformed MINA53 KO MEF cell line was reconstituted with empty vector control, wildtype or inactive (Fe(II) binding mutant H179A; see Chapter 1, figure 1.7) HA-tagged MINA53 (Fig 3.1). Retroviral delivery of the MINA53 cDNA's led to overexpression of MINA53 relative to WT MEFs (Figure 3.2A). Immunofluorescence staining confirmed the anticipated colocalisation of wildtype and mutant HA-MINA53 with the nucleolar marker, nucleolin (Figure 3.2B). Therefore, localisation of MINA53 to the nucleolus does not require its enzymatic activity. Reconstitution with either wildtype of H179A mutant MINA53 did not significantly affect the transformed morphology of KO

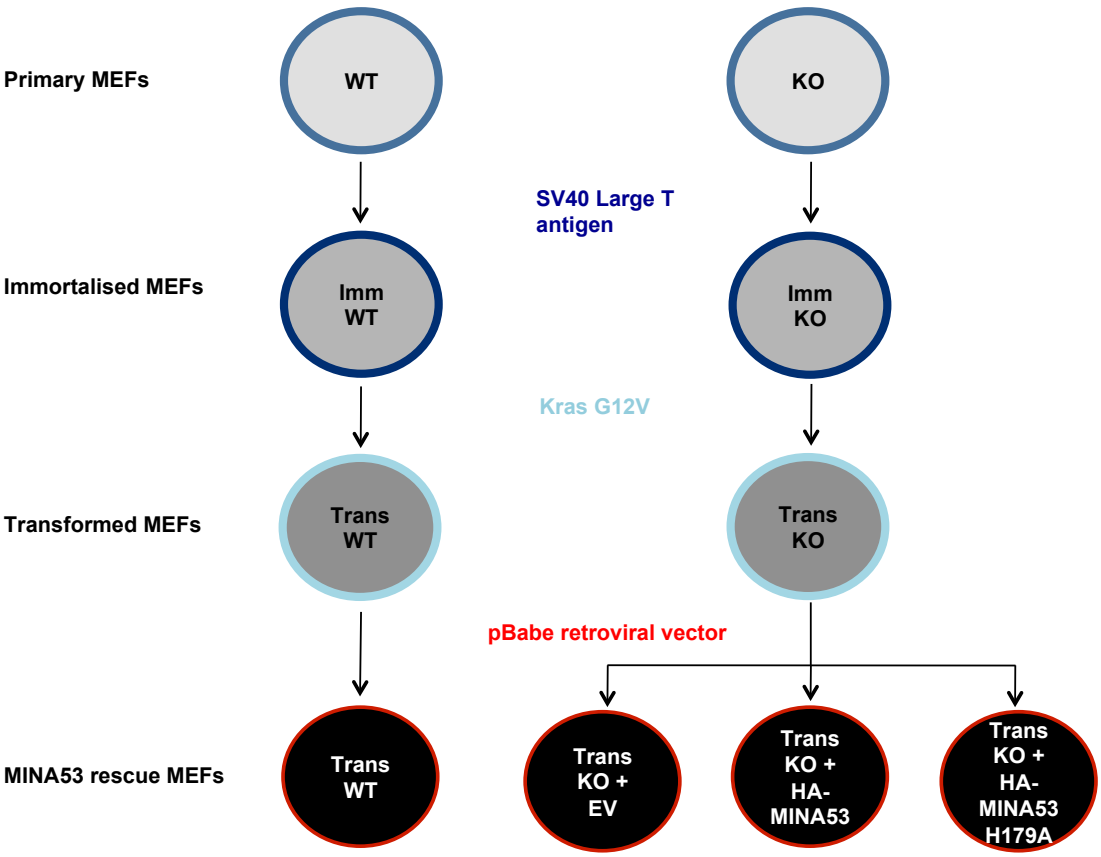

Figure 3.1. Generation of Kras-transformed WT and KO MINA53 MEFs. Schematic drawing outlining the procedure to generate Kras-transformed wild-type (WT), and MINA53 knockout (KO) mouse embryonic fibroblasts (MEFs) reconstituted with either empty-vector (EV), WT MINA53 or enzymatic inactive MINA53 (H179A). Primary MEFs derived from WT and MINA53 KO mouse embryos were immortalised using a retrovirus expressing SV40 Large T antigen and subsequently transformed by a retrovirus expressing oncogenic Kras G12V. In an isogenic background MINA53 KO MEFs were reconstituted with EV, WT MINA53 or enzyme inactive MINA53 (H179A).

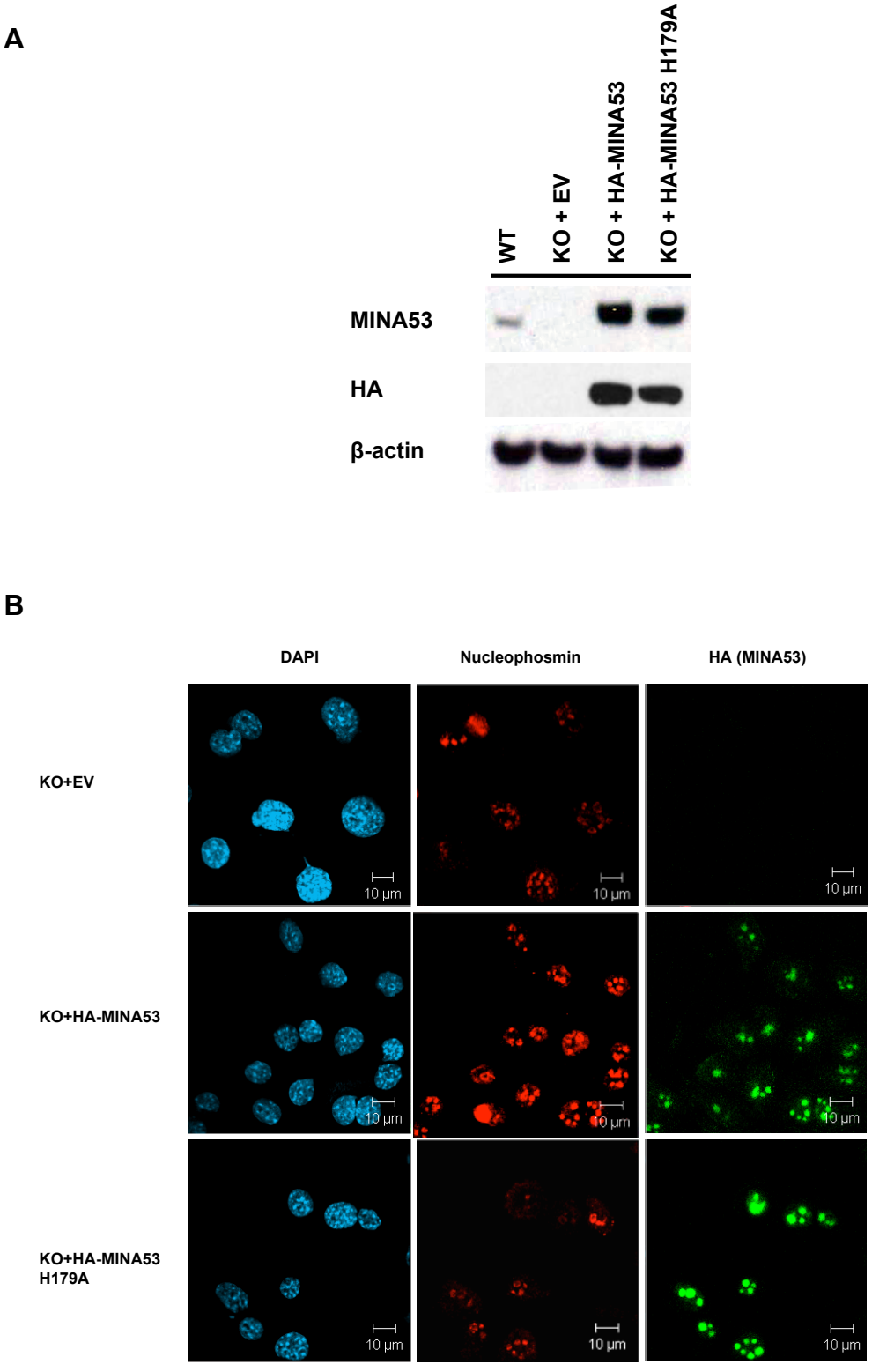

Figure 3.2. Kras-transformed WT and MINA53 KO MEFs reconstituted with MINA53. **A.** Western blot of MINA53 KO MEFs reconstituted with empty vector (EV), HA-tagged wild-type MINA53 or HA-tagged MINA53 iron binding mutant (H179A). **B.** Immunofluorescence of Wild-type MEF and HA-tagged knock-out (KO) rescue cell lines. Cells were stained with HA-FITC, nucleolar protein nucleophosmin and DAPI, and examined using a Zeiss 510 MetaHead confocal microscope.

MEFs (Figure 3.3A). Consistent with my previous findings, reconstitution of KO MEFs with WT or inactive MINA53 did not affect 2D proliferation (Figure 3.3B).

3.2.2 Effect of MINA53 reconstitution on the anchorage-independent growth of transformed KO MEFs

In an attempt to validate the MEF model for use in dissecting activity-dependent and in-dependent roles of MINA53 I next assessed the anchorage-independent growth capacity of the reconstituted MEFs. I previously observed that the presence of MINA53 suppressed the anchorage-independent growth of two independent K-Ras-transformed MINA53 MEF lines (2.3.4). Consistent with this, reconstitution of HA-MINA53 into one of these lines restored colony formation to normal levels (Figure 3.4). Importantly, reconstitution with the same level of HA-MINA53 H179A did not restore colony growth to wildtype MEF levels. Together these data indicate that regulation of anchorage-independent growth in transformed MEFs is both MINA53- and activity-dependent, and suggests the existence of one or more MINA53 substrates. Overexpression of reconstituted HA-MINA53 did not enhance the suppression of colony formation (relative to wildtype MEFs) (Figure 3.4), perhaps consistent with complete modification of the substrate(s) by endogenous levels of the enzyme (see Chapter 4).

3.2.3 Effect of MINA53 on clonogenic survival

Consistent with the data presented in 2.3.5, no effect of MINA53 or its activity was noted on the clonogenic survival of wildtype or MINA53 reconstituted MEFs (Figure 3.5).

A

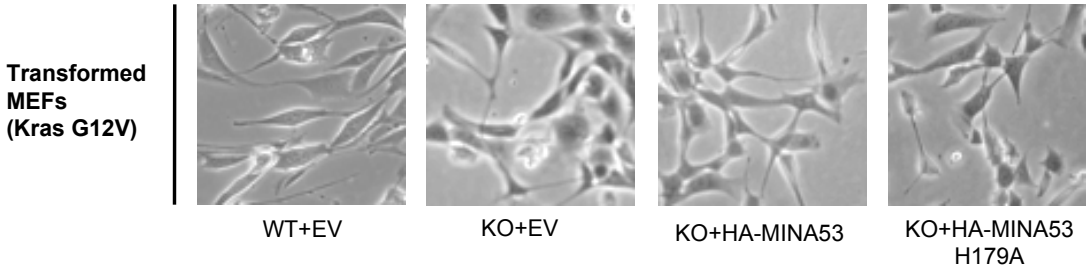

B

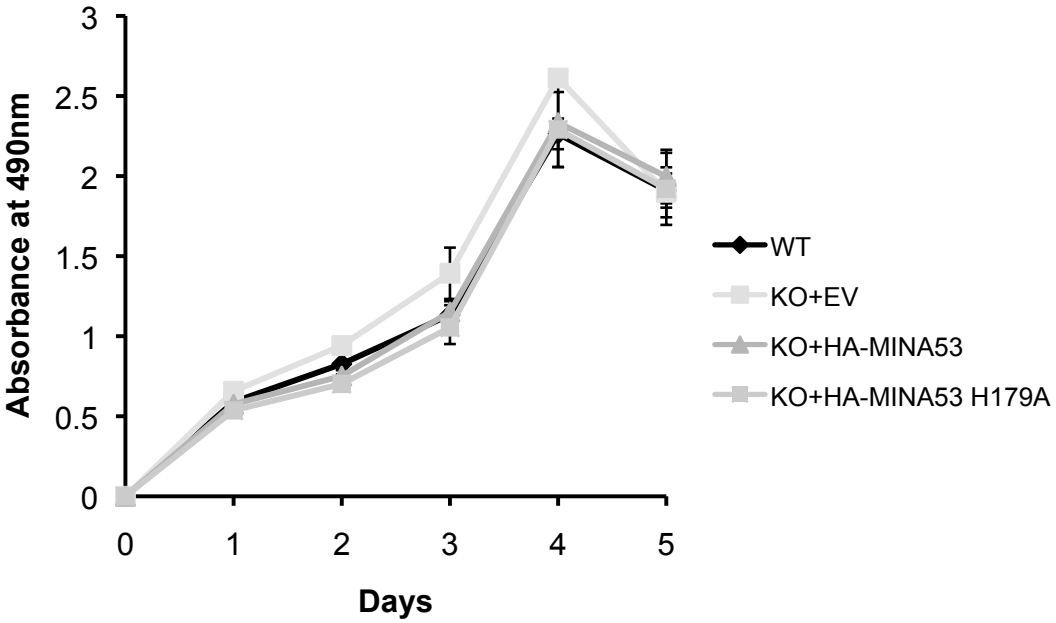

Figure 3.3. Kras-transformed WT and MINA53 KO MEFs reconstituted with MINA53. **A**. Phase contrast images of transformed WT and MINA53 KO MEFs. **B.** Cell growth of transformed WT and MINA53 KO MEFs reconstituted with either EV, WT or enzymatic inactive (H179A) MINA53, evaluated using a MTS assay.

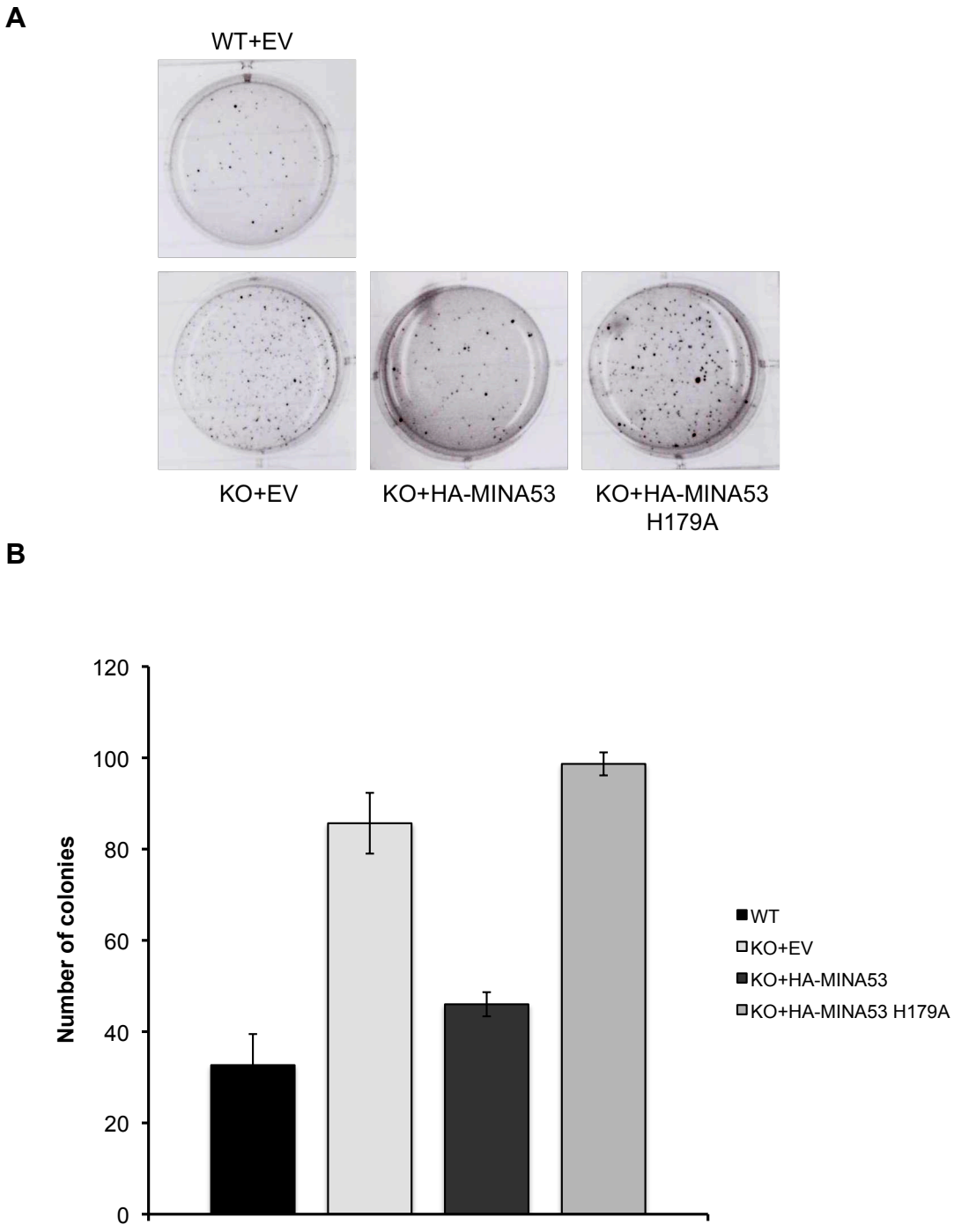

Figure 3.4. Effect of MINA53 on anchorage independent growth in transformed MEFs. A. K-Ras G12V transformed WT and MINA53 KO MEFs reconstituted with either empty vector, wildtype MINA53 or enzyamtic inactive MINA53 (H179A) were seeded out in semi-solid Noble agar medium and allowed to grow for 4 weeks after which the soft-agar colonies were stained with crystal violett and manually counted. **B**. Number of stained and counted soft-agar colonies (± SD) after 4 weeks of growth.

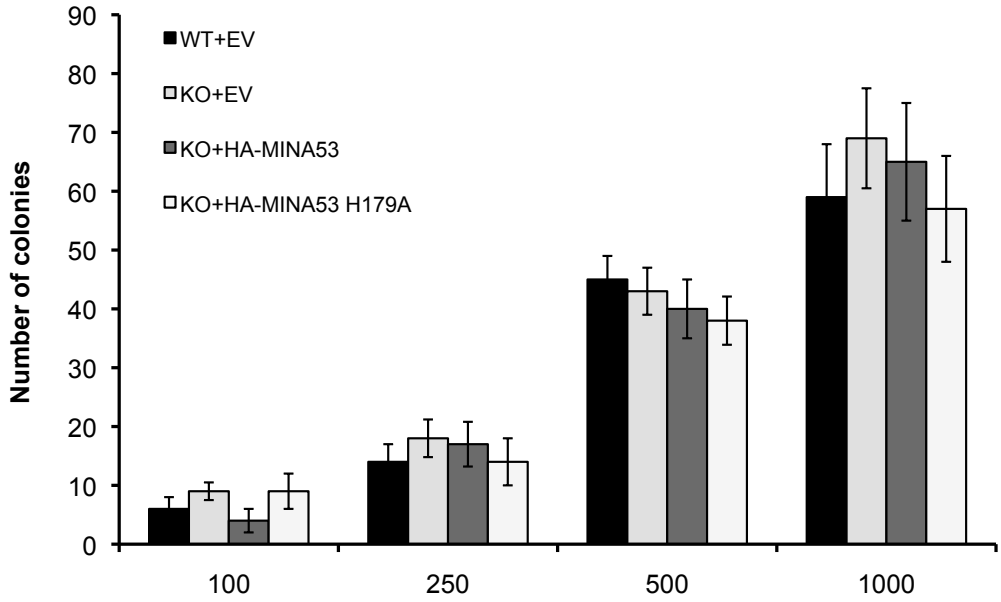

Figure 3.5. Effect of MINA53 on clonogenic survival in transformed MEFs. K-Ras G12V transformed WT and MINA53 MEFs reconstituted with EV, HA-MINA53 or enzyme inactive MINA53 (H179A) were seeded out at four different densities, grown for 3 weeks after the formed colonies were stained with crystal violet and counted.

3.3.1 Effect of MINA53 on *in vivo* tumour growth – pilot xenograft assay

Anchorage-independent growth assays such as the soft agar assay used above are considered to be a relatively reliable predictor of tumourigenic potential. Therefore, we considered the possibility that MINA53 and its enzyme activity would regulate the ability of K-Ras-transformed MEFs to grow as tumours in a xenograft transplantation assay (in collaboration with Professor Adrian Harris, WIMM, Oxford). This is a well-established model for examination of *in vivo* tumour growth, where tumour cells are injected into immuno-compromised mice in order to prevent rejection. Tumours typically develop over 1–8 weeks (depending on the number of cells injected), allowing the response to gene intervention or drug treatment on tumour growth to be monitored over time (Richmond and Su, 2008).

We first performed a small-scale pilot xenograft experiment using only the isogenic MINA53 KO and WT reconstituted K-Ras-transformed MEFs. This allowed an initial assessment of tumour growth rate and variability in order that we could determine appropriate sample sizes for subsequent experiments. The transformed MEF cell lines were injected subcutaneously into the flanks of BALB/c nude mice (n = 7, two injections per mice, one from each cell line). Tumour growth was measured three times a week for 3 weeks when the experiment was terminated to prevent unnecessary suffering. Tumour volume was calculated using a formula for ellipsoid volumes: length x width x height x $\pi/6$ (Tomayko and Reynolds, 1989).

Interestingly, and in agreement with our observations from soft agar growth assays, the presence of reconstituted HA-MINA53 suppressed xenograft tumour growth compared to KO transformed MEFs. At around day 12 after injection the

first significant signs of tumour growth were seen, from which point control KO MEFs exhibited significantly enhanced tumour growth compared to HA-MINA53 reconstituted MEFs (Figure 3.6A). At the end of the experiments tumours were excised, weighed and dissected: The weight of control MINA53 MEF KO tumours was around three times heavier than tumours formed from reconstituted HA-MINA53 MEFs (Figure 3.6B). The morphology of the control KO MEFs was reddish, cauliflower-like and soft, while the HA-MINA53 tumours were more pale, hardish (marble-like), with a clear separation from adjacent normal tissue, and, with a clear central necrosis (liquid) (data not shown). The morphology of the tumours suggests that the control KO cells were more proliferative and invasive than the HA-MINA53 MEFs, at least under the specific time frame and conditions used in this xenograft assay.

3.3.2 Effect of MINA53 activity on xenograft tumour growth

In order to examine if the enzymatic activity of MINA53 was required for the tumour growth differences observed above, we performed a new xenograft experiment including the MINA53 H179A reconstituted KO MEFs. For comparison we also included a wildtype MEF control line reconstituted with control empty vector. Seven BALC/c nude mice (n = 28 mice in total) were used per cell line and each mouse was injected twice, one subcutaneous injection into each flank. Each mouse was injected with the same cell line to prevent potential 'interference' between tumours from different MEFs. Tumour growth was measured three times a week for up to 8 weeks before termination of the experiment.

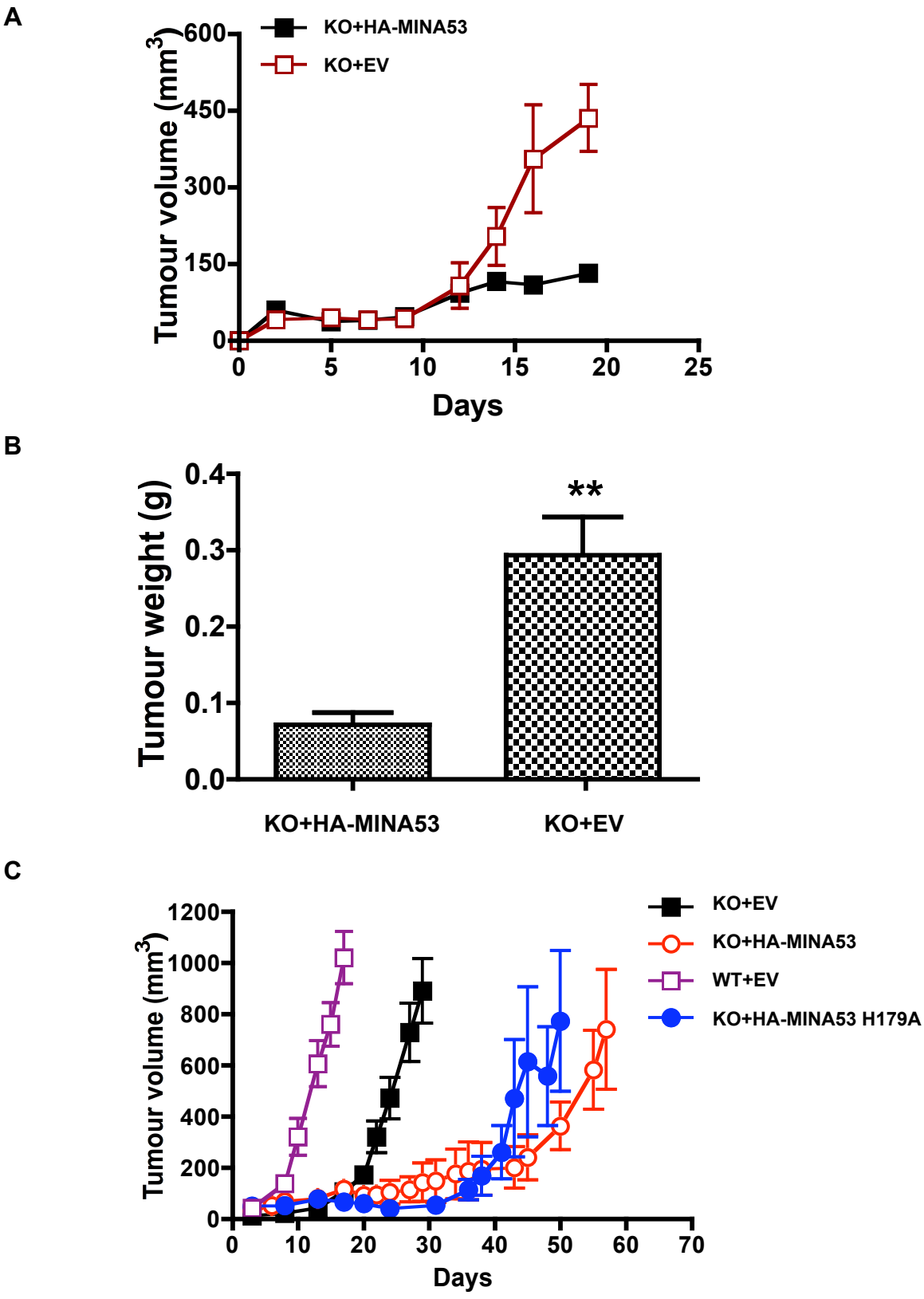

Figure 3.6. Effect of MINA53 on in vivo tumour growth. A. Tumour growth measurements (± SD) of K-Ras G12V transformed MINA53 KO MEFs reconstituted with either EV or HA-MINA53. Growth of seven tumours per cell line was monitored three times a week over a period of 19

days following injection into flanks of BALC/c nude mice. **B.** Weight of MINA53 KO+EV and KO+HA+MINA53 tumours (± SD) measured at termination of xenograft experiment. **C.** Tumour growth measurements (± SD) of K-Ras G12V transformed WT+EV, MINA53 KO MEFs reconstituted with EV, HA-MINA53 or enzyme inactive MINA53 (H179A). Growth of seven tumours per cell line was monitored three times a week over a period of 55 days following injection into flanks of BALC/c nude mice.

Consistent with the phenotypic variation that we have observed between non-isogenic MEF lines in other contexts (2.3.5, 3.4.1), tumours from wildtype transformed MEFs showed significantly faster growth rates compared to tumours derived from isogenic KO MEFs (Figure 3.6C). Therefore, the remaining analysis focuses on tumour growth data from the isogenic MINA53 KO and reconstituted MEF lines. Consistent with the pilot xenograft data described above, tumours from WT HA-MINA53 transformed MEFs grew significantly slower than their KO counterparts (Figure 3.6C). Interestingly, tumours derived from H179A HA-MINA53 transformed MEFs grew more similarly to WT HA-MINA53 tumours than KOs, suggesting that the suppressive role of MINA53 in this xenograft model is largely independent of enzyme activity. However, there was a trend for H179A HA-MINA53 tumours to grow marginally faster than WT HA-MINA53 tumours, perhaps consistent with a subtle requirement for MINA53 enzyme activity in tumour growth. It is unclear whether this phenomenon relates to the activity-dependent role of MINA53 in anchorage-independent growth described above (3.2.2).

3.4.1 Effect of MINA53 activity on gene expression

How do MINA53 expression and/or its enzyme activity suppress anchorage-independent growth and tumourigenesis? Since MINA53 has been shown to repress IL4 gene expression (Okamoto et al., 2009) and possibly to act as a histone demethylase (Lu et al., 2009). I next asked whether MINA53 regulates the gene expression profile of K-Ras-transformed MEFs in an enzyme- and activity-dependent manner. Therefore, I performed microarray analyses on duplicate cDNA samples generated from wildtype and isogenic reconstituted K-Ras-transformed

MEFs using Illumina MouseWG-6 v2 BeadChips (core facility, Wellcome Trust Centre for Human Genetics, Oxford).

As further evidence of the significant genetic variation between MEF lines derived from littermate embryos, the gene expression profile of the wildtype MEF line was so different from the isogenic set of MEFs that they could not be meaningfully included in the analyses (Figure 3.7). In contrast, the overall gene expression of the control MINA53 KO and reconstituted isogenic lines was very similar, suggesting that MINA53 expression and/or activity have subtle effects on gene expression in this model (Figure 3.7). Data analysis by GenePattern software identified 472 gene loci to be differentially regulated (>1.5-fold) in HA-MINA53 reconstituted MEFs compared to control KO and H179A HA-MINA53 reconstituted KO MEFs (Figure 3.7A and 3.7B). Therefore, MINA53 regulates gene expression in K-Ras-transformed MEFs in a largely enzyme activity-dependent manner (Figure 3.7C). Interestingly, most of the MINA53-regulated genes were found to be downregulated by its presence (Figure 3.7A, Table 3.1). A subset of MINA53-repressed genes was selected for validation by Q-PCR based on potential roles in anchorage-independent growth and tumourigenesis (see discussion). Consistent with the microarray data, Q-PCR of Fgf13, Gap43 and Pip5k1a from independent cDNA samples indicated activity-dependent repression of gene expression by reconstituted MINA53 (Figure 3.8). In contrast, the expression of very few genes was reproducibly increased by the activity of reconstituted MINA53 (Figure 3.9, Table 3.2). Validation of these by Q-PCR suggests a role for the activity of MINA53 in positive regulation of Igfbp5 and Cdkn1c (p57) expression (Figure 3.9), both of which also have potential roles in tumourigenesis (see discussion).

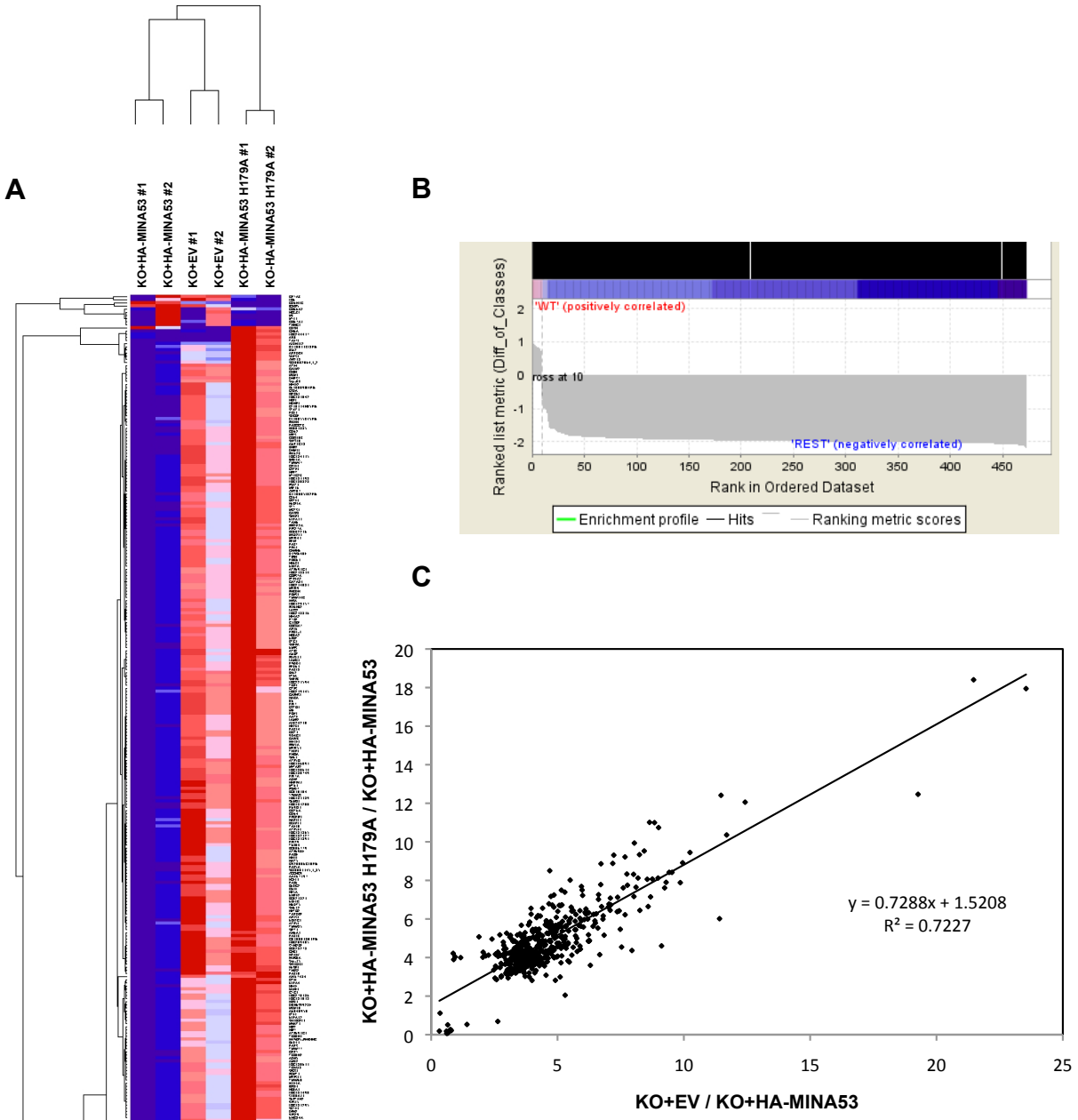

Figure 3.7. Heat map of hierarchical cluster analysis of cDNA microarray of transformed MINA53 KO MEFs reconstituted with wildtype MINA53, EV and enzymatic inactive MINA53 (H179A). A Heat map of K-Ras G12V MINA53 KO MEFs cell lines, showing 472 of the most dysregulated gene loci (>1.5-fold regulated). Each cell line done in duplicate. Analysis performed using GenePattern software. **B.** The proportion of 472 gene loci that are uniquely upregulated or downregulated in the wildtype MINA53 background. **C.** The 472 of the most dysregulated gene loci selected and plotted the fold regulation of KO+EV-MINA53 H179A (179) vs KO+HA-MINA53 (WT) against KO+EV (KO) vs KO+HAMINA53 (WT).

Table 3.1. Genes uniquely downregulated in the KO+HA-MINA53 MEF background.

Gene	Gene description	Fold regulation
PDE6D	phosphodiesterase 6D, cGMP-specific, rod, delta	-2.163
CAPN2	calpain 2, (m/II) large subunit	-2.115
UBE2E3	ubiquitin-conjugating enzyme E2E 3 (UBC4/5 homolog, yeast)	-2.107
RPL7A	ribosomal protein L7a	-2.09
ATP6AP2	ATPase, H+ transporting, lysosomal accessory protein 2	-2.083
BEX2	brain expressed X-linked 2	-2.08
PMM2	phosphomannomutase 2	-2.08
EPRS	glutamyl-prolyl-tRNA synthetase	-2.078
RAB10	RAB10, member RAS oncogene family	-2.077
TCP1	t-complex 1	-2.074
GNB1	guanine nucleotide binding protein (G protein), beta polypeptide 1	-2.068
ISGF3G	interferon-stimulated transcription factor 3, gamma 48kDa	-2.062
MRPS5	mitochondrial ribosomal protein S5	-2.06
GHR	growth hormone receptor	-2.058
METAP2	methionyl aminopeptidase 2	-2.057
RUVBL1	RuvB-like 1 (E. coli)	-2.057
BC028278		-2.057
IDH3G	isocitrate dehydrogenase 3 (NAD+) gamma	-2.056
PAPOLA	poly(A) polymerase alpha	-2.051
EIF5A	eukaryotic translation initiation factor 5A	-2.05
OBFC2A	oligonucleotide/oligosaccharide-binding fold containing 2A	-2.05
ATP5O	ATP synthase, H+ transporting, mitochondrial F1 complex, O subunit (oligomycin sensitivity conferring protein)	-2.049
YWHAQ	tyrosine 3-monooxygenase/tryptophan 5-monooxygenase activation protein, theta polypeptide	-2.048
LOC380749		-2.044
LOC223594		-2.044
LOC383189		-2.044
SNRPB	small nuclear ribonucleoprotein polypeptides B and B1	-2.043
SUCLG1	succinate-CoA ligase, GDP-forming, alpha subunit	-2.043
SH3GLB1	SH3-domain GRB2-like endophilin B1	-2.043
ETFA	electron-transfer-flavoprotein, alpha polypeptide (glutaric aciduria II)	-2.042
BC010304		-2.042
PPFIBP1	PTPRF interacting protein, binding protein 1 (liprin beta 1)	-2.041
HNRPA1	heterogeneous nuclear ribonucleoprotein A1	-2.041
LOC386091		-2.041
MYLC2B		-2.039
SUMO1	SMT3 suppressor of mif two 3 homolog 1 (S. cerevisiae)	-2.039
HNRPH1	heterogeneous nuclear ribonucleoprotein H1 (H)	-2.038
H2AFZ	H2A histone family, member Z	-2.038
C030003D03RIK		-2.038
LOC209405		-2.038
RAB5A	RAB5A, member RAS oncogene family	-2.037
MCM3	MCM3 minichromosome maintenance deficient 3 (S. cerevisiae)	-2.036
THBS2	thrombospondin 2	-2.035
PSMD7	proteasome (prosome, macropain) 26S subunit, non-ATPase, 7	-2.035
TES	testis derived transcript (3 LIM domains)	-2.034
ACADL	acyl-Coenzyme A dehydrogenase, long chain	-2.034
ADFP	adipose differentiation-related protein	-2.033
SCL0003876.1_26		-2.032
RBPMS2	RNA binding protein with multiple splicing 2	-2.032
PPP4R1	protein phosphatase 4, regulatory subunit 1	-2.031

Table 3.1. (*continued*)

Gene	Gene description	Fold regulation
LOC381200		-2.03
COPS7A	COP9 constitutive photomorphogenic homolog subunit 7A	-2.03
LOC380634		-2.029
LOC268569		-2.028
EIF4B	eukaryotic translation initiation factor 4B	-2.028
LOC434858		-2.027
LOC382127		-2.027
SYNJ2BP	synaptojanin 2 binding protein	-2.027
FUSIP1	FUS interacting protein (serine/arginine-rich) 1	-2.025
MTX1	metaxin 1	-2.024
TRAPPC6B	trafficking protein particle complex 6B	-2.022
RAET1B		-2.022
ATP5F1	ATP synthase, H+ transporting, mitochondrial F0 complex, subunit B1	-2.022
ATAD2	ATPase family, AAA domain containing 2	-2.02
MTCH2	mitochondrial carrier homolog 2 (C. elegans)	-2.02
PPP2R5C	protein phosphatase 2, regulatory subunit B (B56), gamma isoform	-2.02
PPM1A	protein phosphatase 1A (formerly 2C), magnesium-dependent, alpha	-2.02
LOC233908		-2.019
LOC380828		-2.019
RBM3	RNA binding motif (RNP1, RRM) protein 3	-2.019
FUT8	fucosyltransferase 8 (alpha (1,6) fucosyltransferase)	-2.019
H13		-2.019
PRDX3	peroxiredoxin 3	-2.018
RAB1B	RAB1B, member RAS oncogene family	-2.018
UBE1C	ubiquitin-activating enzyme E1C (UBA3 homolog, yeast)	-2.018
LOC381865		-2.018
SCL0003092.1_40		-2.018
RGS17	regulator of G-protein signalling 17	-2.017
MIR16		-2.017
CNIH	cornichon homolog (Drosophila)	-2.017
LOC381578		-2.016
ADSS	adenylosuccinate synthase	-2.016
RPL29	ribosomal protein L29	-2.015
EIF2S2	eukaryotic translation initiation factor 2, subunit 2 beta, 38kDa	-2.015
CYP20A1	cytochrome P450, family 20, subfamily A, polypeptide 1	-2.014
EEF2	eukaryotic translation elongation factor 2	-2.014
SUMO3	SMT3 suppressor of mif two 3 homolog 3 (S. cerevisiae)	-2.013
DSCR5		-2.013
SUMO2	SMT3 suppressor of mif two 3 homolog 2 (S. cerevisiae)	-2.013
ERGIC3	ERGIC and golgi 3	-2.012
DHRS7	dehydrogenase/reductase (SDR family) member 7	-2.012
CPSF6	cleavage and polyadenylation specific factor 6, 68kDa	-2.012
PHLDA3	pleckstrin homology-like domain, family A, member 3	-2.012
PSAT1	phosphoserine aminotransferase 1	-2.011
BC023823		-2.01
RAB6		-2.01
ZFP365		-2.01
UHRF2	ubiquitin-like, containing PHD and RING finger domains, 2	-2.009
PSMB7	proteasome (prosome, macropain) subunit, beta type, 7	-2.009
PPP1CA	protein phosphatase 1, catalytic subunit, alpha isoform	-2.009
FGF13	fibroblast growth factor 13	-2.008

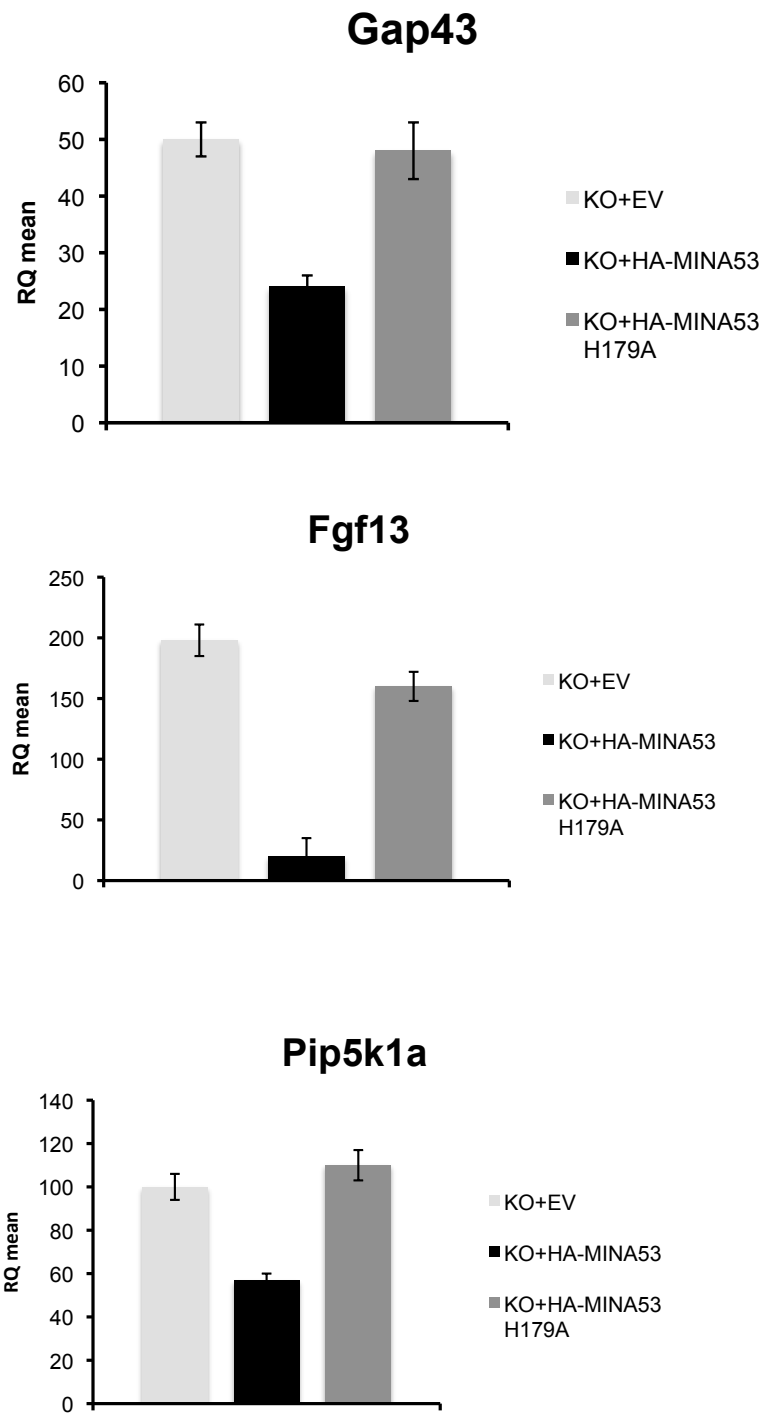

Figure 3.8. Validation of down-regulated genes from microarray using Q-PCR. cDNA reverse transcribed from total RNA from K-Ras transformed MINA53 KO MEFs reconstituted with EV, HA-MINA53 or enzyme inactive MINA53 (H179A) was subjected to Q-PCR analysis using specific DNA oligonucleotides. β-actin was used as an internal control.

Table 3.2. Genes uniquely upregulated in the KO+HA-MINA53 MEF background.

Gene	Gene description	Fold regulation
CDKN1C	cyclin-dependent kinase inhibitor 1C (p57, Kip2)	2.082
IGFBP5	insulin-like growth factor binding protein 5	1.557

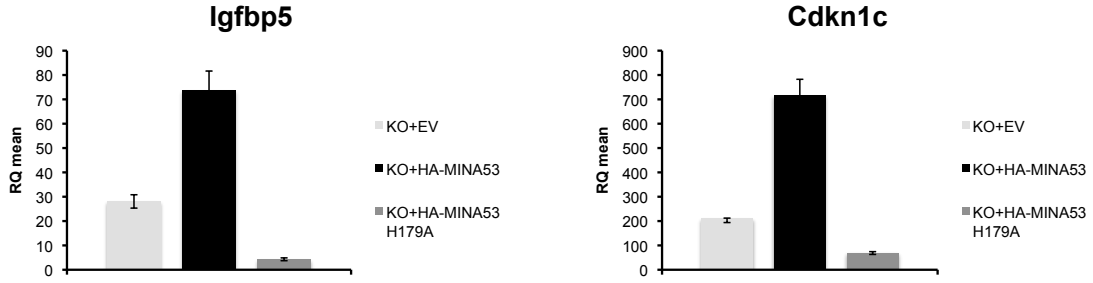

Figure 3.9. Validation of up-regulated genes from microarray using Q-PCR. cDNA reverse transcribed from total RNA from K-Ras transformed MINA53 KO MEFs reconstituted with EV, HA-MINA53 or enzyme inactive MINA53 (H179A) was subjected to Q-PCR analysis using specific DNA oligonucleotides. β-actin was used as an internal control.

Pathway analysis of the microarray data using Ingenuity software indicates that MINA53-regulated genes in transformed MEFs segregate into genes families involved in cell cycle regulation, protein translation and tight junction and integrin signalling (Figure 3.10). Several genes involved in well characterised signalling pathways that regulate cell proliferation and tumuourigenesis (e.g. PI3K, mTOR and MAPK pathways) were also identified.

3.5 Conclusion

In this Chapter I have described the generation of a K-Ras-transformed MEF model for investigating the role of MINA53 enzyme activity, and applied it to studies of anchorage-independent growth, clonogenic survival, xenograft tumour growth, and gene expression. I have shown that the suppressive effect of MINA53 on anchorage-independent growth observed in Chapter 2 is dependent on enzyme activity. Furthermore, this MEF model was used to show that MINA53 also suppresses tumourigenesis in a mouse xenograft assay. Although these effects were largely enzyme-independent, they were consistent with the anchorage-independent growth assay in demonstrating an anti- rather than a pro-tumourigenic role for MINA53 (at least in the context of MEFs). These results may be consistent with the observations of others: a recent study indicated that lung cancer patients with negative tumour MINA53 staining had a significantly worse prognosis than patients with positive staining (Komiya et al., 2010a). Furthermore, MINA53 shRNA increases the invasion of a squamous lung cancer cell line (H226B) and its overexpression in A549 induces apoptosis (Komiya et al., 2010a). Together this suggests that the role of MINA53 and its enzyme activity in cancer is complex, with cell and tissue specific factors likely determining whether MINA53 promotes

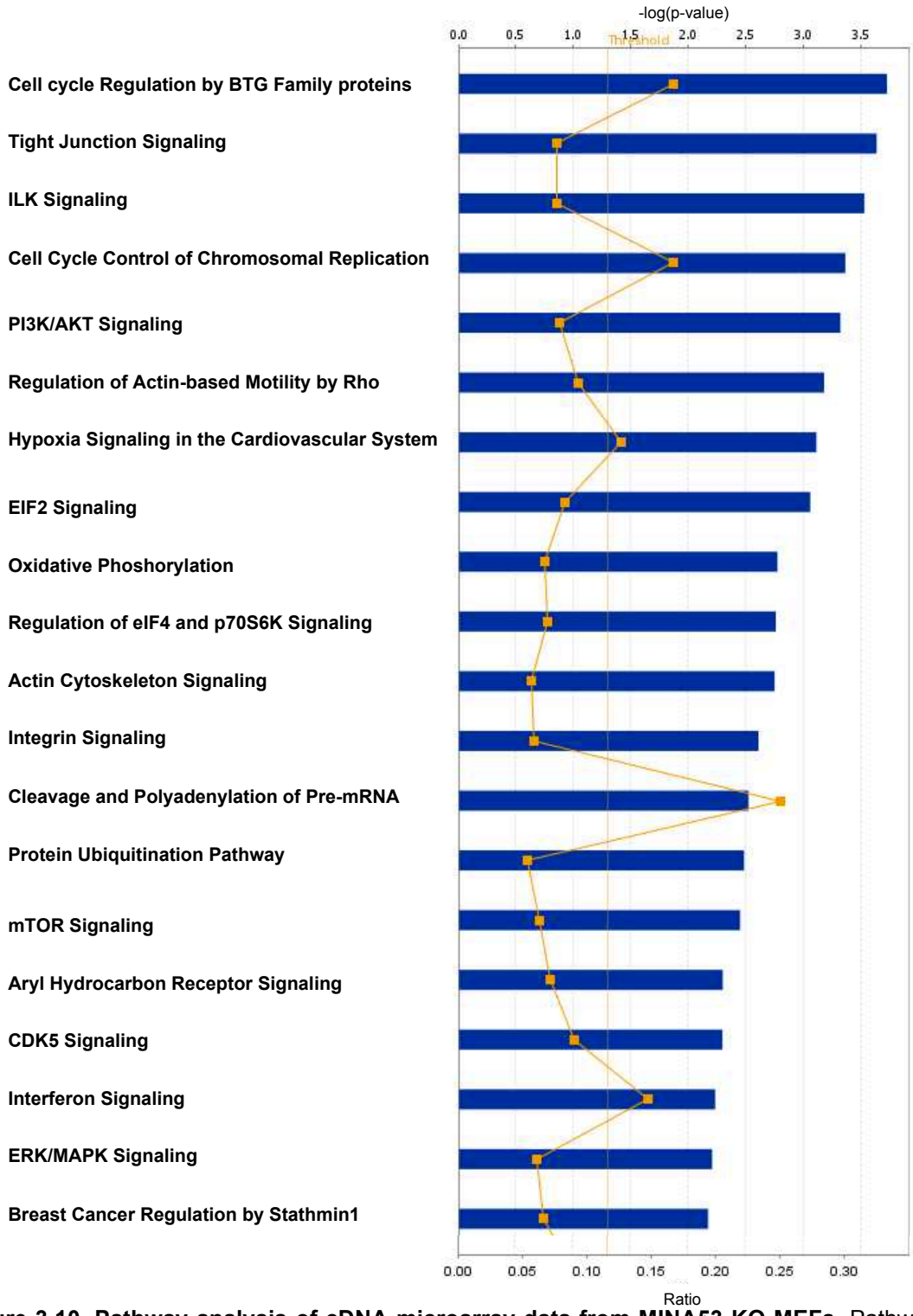

Figure 3.10. Pathway analysis of cDNA microarray data from MINA53 KO MEFs. Pathway analysis of cDNA microarray of K-Ras MINA53 KO MEFs reconstituted with wildtype MINA53, EV or enzymatic inactive MINA53 (H179A) showing the top 20 pathways regulated in a MINA53 enzyme dependent fashion. Analysis performed using Ingenuity pathway analysis software (IPA). The P values of each pathway reflect the significance of regulation of the pathway. Straight yellow line marks p-value threshold of 0.5. Yellow line with squares indicates proportion of genes in each family that are modified by MINA53.

or suppresses tumourigenesis. Further evidence for MINA53 as a negative regulator of tumourigenesis is presented in Chapter 6.

To identify genes and pathways that MINA53 might regulate in the context of transformation/tumourigenesis we performed microarray gene expression profiling on MINA53 KO and reconstituted transformed MEFs. Pathway analysis suggested that MINA53 regulates genes related to protein translation, ribosome biogenesis, cell cycle regulation and cell adhesion in an enzyme-dependent manner. Several of the downregulated genes, including the eIFs, are known to be overexpressed and promote growth in tumours (see discussion). Interestingly, one of the few upregulated genes in the wildtype MINA53 background was p57, thought to be a tumour suppressor, found reduced in many cancers through epigenetic modifications (Kavanagh and Joseph, 2011). The vast majority of genes differentially regulated by MINA53 were downregulated however, perhaps consistent with a general role for MINA53 as a transcriptional repressor. This may be consistent with a described role for MINA53 in repressing IL4 transcription (Okamoto et al., 2009).

The results from this Chapter suggest the existence one or more MINA53 substrates, and validate the isogenic MEF model as a useful system to further investigate the role of MINA53 and its enzyme activity in a variety of cellular process, such as tumourigenesis, gene expression, and ribosome biogenesis. In the following chapter we discuss our efforts to identify a substrate for MINA53.

Chapter 4

Ribosomal protein Rpl27a is a MINA53 substrate

4.1 Introduction

Despite the fact that MINA53 includes a well defined JmjC-domain and contains conserved catalytic residues required for the activity of other 2OG oxygenases, a viable substrate has yet to be identified. Substrate(s) are likely to exist however, as MINA53 2OG oxygenase activity has been confirmed using an 'uncoupled 2OG turnover assay' (decarboxylation of 2OG in the absence of prime substrate; Schofield laboratory, Oxford). The enzyme-dependent phenotypes described in Chapter 3 also suggest a role for one or more substrates in anchorage-independent growth and gene expression. The identification of these substrates would advance our understanding of the role of MINA53 in these processes and diseases such as cancer.

Others have previously reported that MINA53 functions as a histone demethylase (HDM), suppressing the formation of tri-methyl lysine 9 of histone H3 (Lu et al., 2009). However, substantial efforts in collaboration with the Schofield laboratory have so far failed to detect HDM activity *in vitro* or *in vivo*. This lack of HDM activity is in agreement with the relatively low sequence homology between JmjC-only 2OG enzymes and HDM's, and suggests that a new search for alternative MINA53 substrates would be worthwhile.

In this chapter we describe our efforts to identify a substrate for MINA53. In parallel with our observation of enzyme-dependent phenotypes in MEFs (Chapter 2), our collaborators were performing proteomic screens to identity substrates of 2OG oxygenases, including MINA53. Dr's Cockman and Granatino (Ratcliffe and Schofield laboratories, respectively) identified MINA53-interacting proteins as

candidate substrates: Enzymatic assay of overlapping peptides from these candidates was then undertaken in the presence of MINA53 (Dr Ge, Schofield laboratory). This peptide screening approach identified Rpl27a, a ribosomal large subunit protein, as a candidate MINA53 substrate.

This Chapter details my work aimed at validating Rpl27a as a *bona fide* endogenous cellular MINA53 substrate.

4.2.1 Identification of MINA53-interacting proteins by proteomic pulldown of FLAG-tagged MINA53

In order to identify MINA53-interacting proteins and hence potential substrates Dr's Cockman and Granatino performed a proteomic screen using U2OS cells expressing doxycyline-inducible FLAG-tagged MINA53. Anti-FLAG pulldowns from MINA53 or empty vector control cells were followed by in-solution tryptic digest of purified immunocomplexes and identification of associated proteins by mass spectrometry (MS).

Consistent with the work of others (Eilbracht et al., 2005), and the subcellular localization of MINA53 (Chapter 3, figure 3.2B), (Tsuneoka et al., 2002), most of the MINA53 interactors were nucleolar and ribosomal proteins (Figure 4.1).

4.2.2 MINA53 hydroxylates an Rpl27a peptide *in vitro*

To screen the MINA53 interactors for potential MINA53 substrates, Dr Ge performed enzymatic assays across an array of peptides that spanned several of the highest affinity interactors. Overlapping 19-20mer peptides were incubated

MINA53 Interactor	Accession	Protein Score	Peptide Detected	Peptide Score
Nucleophosmin	P06748	316	MTDQEAIQDLWQWR TVSLGAGAKDELHIVEAEAMNYEGSPIK	101.99 81.34
60S ribosomal protein L27a	P46776	159	NQSFCPTVNLDKLWTLVSEQTR	158.55
Polyadenylate-binding protein 1	P11940	133	ALYDTFSAFGNILSCK	132.86
60S ribosomal protein L3	P39023	121	SINPLGGFVHYGEVTNDFVMLK	55.91
60S acidic ribosomal protein P0	P05388	96	TSFFQALGITTK	59.37
60S ribosomal protein L21	P46778	91	VYNVTQHAVGIVVNK	64.71
60S ribosomal protein L4	P36578	90	YAICSALAASALPALVMSK	65.37

Figure 4.1. MINA53 interacting proteins. To identify potential substrates of MINA53 a proteomic pulldown of FLAG-tagged MINA53 or empty vector control from constitutively expressing U2OS cells was performed followed by tryptic digest of the immunecomplexes and identification by liquid chromatography tandem mass spectrometry (LC-MS/MS).

with recombinant His-tagged MINA53 together with cofactors (2OG, Fe(II) + ascorbate) followed by tryptic digest and MALDI-TOF MS analysis. Interestingly, a single peptide from the ribosomal protein Rpl27a (GNAGGLHHHR) exhibited a +16Da mass shift indicative of hydroxylation under these conditions (Figure 4.2; m/z shift of the doubly-charged ion from 528.2 to 536.2). A second less abundant species was also observed following incubation with MINA53, which showed a mass shift of -2Da, indicative of dehydration (-18Da) of the hydroxylated product (m/z shift of the doubly-charged hydroxylated ion from 536.2 to 527.2). This dehydration event is likely to represent an MS artifact as it was not observed in NMR or whole protein MS studies (see below, and data not shown). Dr Ge subsequently identified the site of MINA53 on the Rpl27a peptide as His-39 (GRGNAGGLHHHRINFDKYKP) by a combination of MS/MS fragmentation sequencing and alanine scanning. Sequence alignment of Rpl27a across various species indicates that the putative hydroxylation site is highly conserved (Figure 4.3). To verify whether endogenous cellular Rpl27a is a *bona fide* MINA53 substrate I then studied its interaction with, and hydroxylation by, MINA53 *in vivo*.

4.2.3 MINA543 interacts with Rpl27a *in vivo*

To validate the proteomic data suggesting an interaction between MINA53 and endogenous Rpl27a in U2OS cells, doxycyline-induced MINA53 and empty vector control complexes were anti-FLAG precipitated and analysed by western blot (Figure 4.4A). Rpl27a was specifically detected in the FLAG-MINA53 pulldown, confirming that MINA53 interacts with Rpl27a *in vivo*. I reasoned that if Rpl27a is a MINA53 substrate it should interact with the enzyme in an activity-dependent manner. To test this hypothesis, I repeated the interaction analysis using the

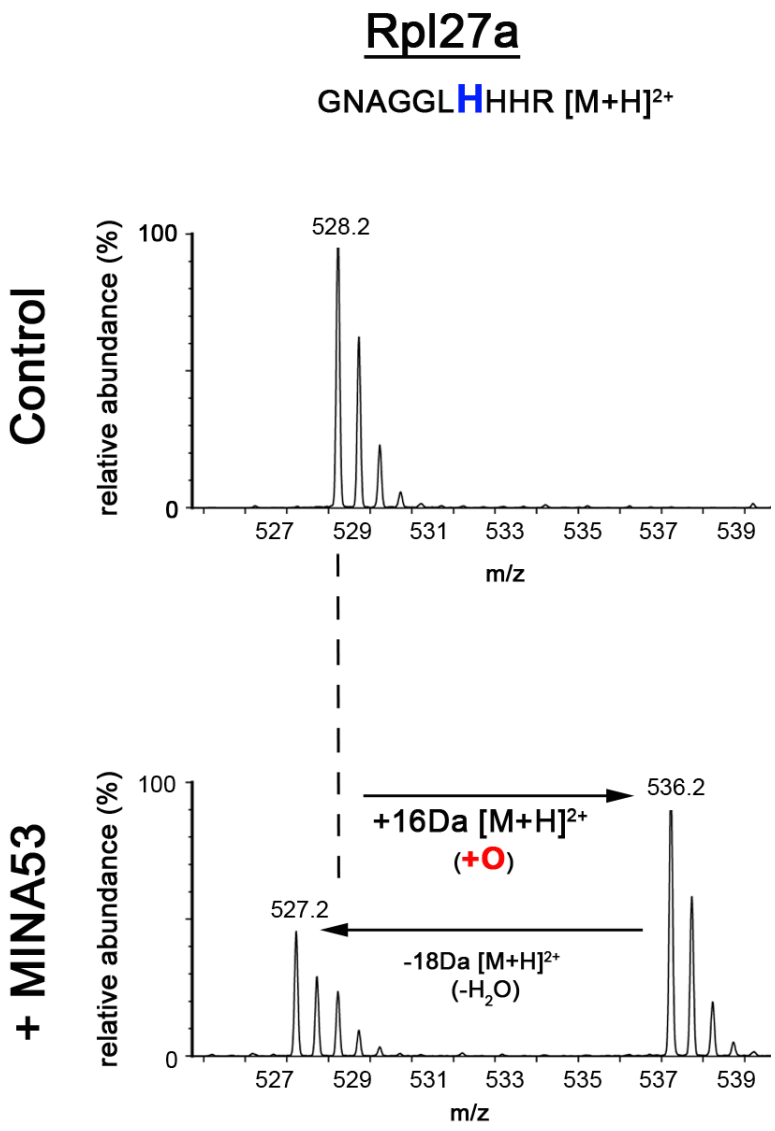

Figure 4.2. MINA53 hydroxylates Rpl27a *in vitro*. Rpl27a peptide (CGRGNAGG-LHHHRINFDKYHP) was incubated in the presence or absence of recombinant MINA53 enzyme, together with the cofactors 2-oxoglutarate (2OG), Fe (II) and ascorbate, followed by tryptic digest and analysis by MALDI-TOF MS. In the absence of MINA53 the doubly-charged Rpl27a peptide showed its predicted mass (m/z 528.2). In the presence of MINA53 with its cofactors, Fe (II), 2OG, and ascorbate the Rpl27a peptide exhibited a mass of m/z 527.2, indicative of hydroxylation and subsequent dehydration (data from Dr Wei Ge).

Figure 4.3. Hydroxylation site of Rpl27a is highly conserved. Sequence alignment of Rpl27a across various species. * indicate hydroxylation site (histidine 39). Sequence aligned using ClustalW and shaded using BoxShade.

reconstituted MINA53 MEFs described in chapter 3. Consistent with Rpl27a being a substrate for MINA53 it was only detected in immunocomplexes of wildtype, and not inactive H179A, MINA53 (Figure 4.4B). Together these results validate the proteomic screen and suggest detailed investigation of endogenous Rpl27a hydroxylation is warranted.

4.2.4 Purification of endogenous Rpl27a

In order to study endogenous Rpl27a hydroxylation it was first necessary to develop an assay for its biochemical purification. In collaboration with Dr Cockman we developed a technique to purify ribosomal proteins from cell extracts for subsequent MS analysis based on published protocols (Louie et al., 1996), (and Figure 4.5, 4.6 and 4.7). In brief, detergent-solubilised cell extracts are subject to sucrose cushion ultracentrifugation whereby organelles and ribosomes are separated according to their densities. A particle travels through the sucrose until its density matches the surrounding solution, with high-mass species such as ribosomes forming a pellet at the bottom of the centrifuge tube. This pellet is then dissolved in buffer containing magnesium, which is crucial for maintaining ribosome solubility and stability. Ribosomal RNA is subsequently denatured and removed from the purified ribosomes by acetic acid precipitation. Ribosomal proteins are then precipitated in acetone and dissolved in acetic acid/acetonitrile for further fractionation by liquid-chromatography (see below).

Using this technique I was able to show significant enrichment for ribosomal proteins by SDS-PAGE/coomassie staining (Figure 4.6A) and immunblotting: Ribosomal protein pellets contained large amounts of Rpl4, Rpl3 and the target

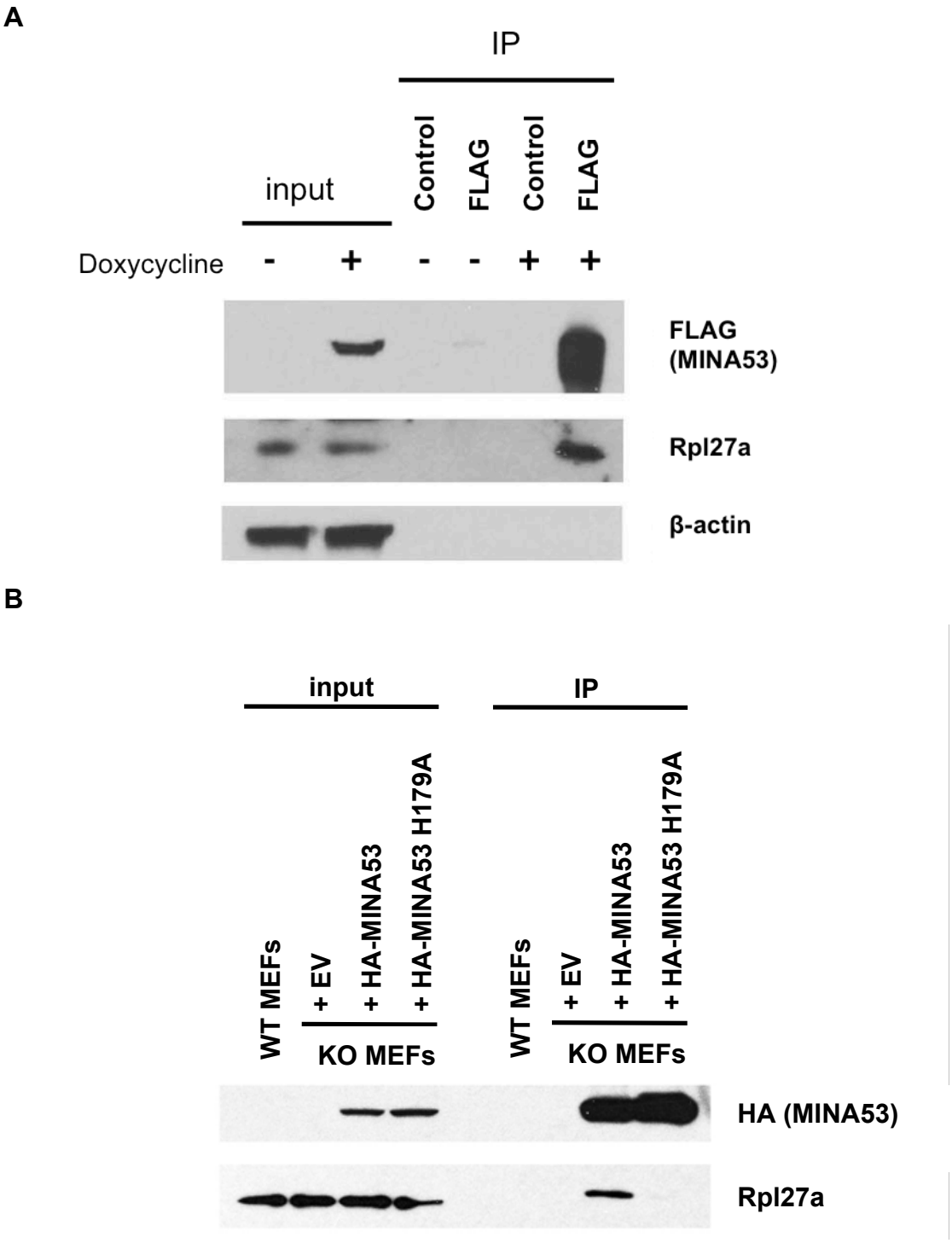

Figure 4.4. MINA53 interacts with Rpl27a. A. Anti-FLAG immunocomplexes were precipitated from either doxycycline-treated FLAG-tagged MINA53 or empty vector control (EV) U2OS inducible cells prior to western blot for the indicated proteins. The interaction was specific as Rpl27a was not detected in control pulldowns. **B.** Anti-HA immunocomplexes were precipitated from KO+EV, HA-tagged MINA53 and HA-tagged MINA53 H179A prior to western blot for indicated proteins.

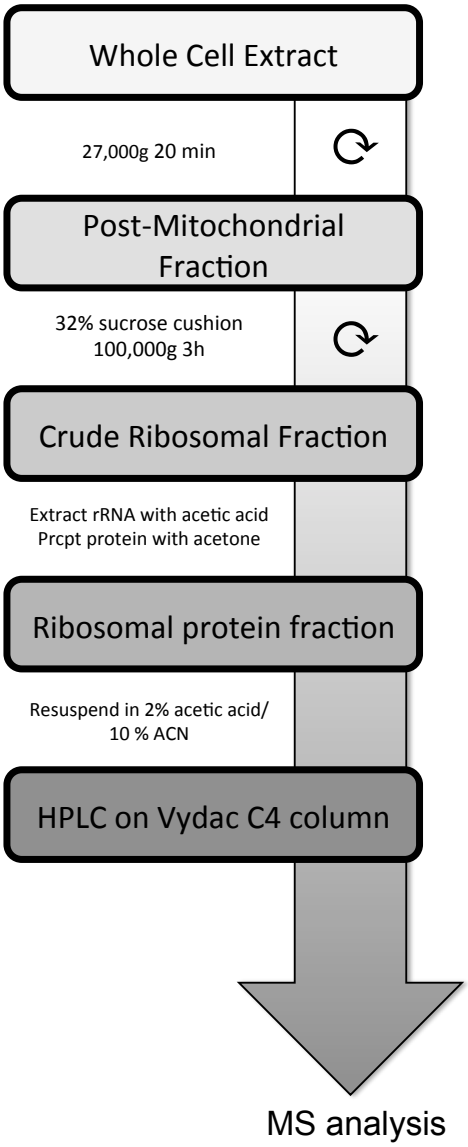

Figure 4.5. Purification of Rpl27a from cell extract. Schematic drawing outlining the procedure to purify ribosomal proteins from whole cell extract. Cells were lysed in a specific buffer (see material and methods) and subjected to a centrifugation at 27,000g for 20 min. The post-mitochondrial fraction was then layered on top of a 32 % sucrose cushion and ultracentrifugated at 100,000g for 3h. The ribosome pellet was treated with acetic acid to remove ribosomal RNA after which the ribosomal proteins were precipitated with acetone. Pellet was resuspended in 2% acetic acid/10% acetonitrile (ACN). The ribosomal protein solution was then subjected to reverse-phase high-performance liquid chromatography (RP-HPLC) to separated ribosomal proteins according to their hydrophobic properties. 250μg of ribosomal protein was loaded onto a VyCad214TP C4 250mmx4.6mm HPLC column (Grace discovery) and protein separated using an acetonitrile gradient. Proteins absorbance was measured at 214nm and fractions collected between 95 and 130 minutes to isolate Rpl27a before masspec analysis by LC-MS/MS or whole-protein MS.

protein Rpl27a, relative to the starting input material (Figure 4.6B). As expected of a nucleolar protein, MINA53 was not enriched in cytoplasmic ribosomes.

Next we sought to purify Rpl27a further by an established procedure involving reversed-phase high-performance liquid chromatography (HPLC) with a Vydac C4 column. Ribosomal proteins were bound to the column in 10% acetonitrile/0.08% TFA before elution in a discontinuous gradient of increasing acetonitrile concentration.

HPLC fractions were spotted onto Hybond-C pure nitrocellulose membrane and immunoblotted for Rpl27a to identify relevant fractions (Figure 4.7A). Samples from Rpl27a containing fractions were also subject to SDS-PAGE and coomassie staining to further confirm the presence of Rpl27a (Figure 4.7B). The Rpl27a fractions were then dried by vacuum centrifugation and subjected to trypsinolysis and MS analysis. This technique was then routinely used with success for a variety of other cell lines, tissues and tumour samples (see below).

4.2.5 Rpl27a is fully hydroxylated *in vivo*

To determine whether endogenous Rpl27a is hydroxylated *in vivo* we purified the protein from human embryonic kidney cells (HEK293T), as described above, followed by trypsinolysis and MS/MS sequencing using a Waters Nano-Acquity, QTOFpremier (Dr's Trudgian and Mackeen, Kessler and Schofield laboratories, Oxford Proteomics Facility). The MS analysis confirmed that endogenous Rpl27a is hydroxylated in HEK293T (Figure 4.8). The double-charged GNAGGLHHHR peptide exhibited a +16Da shift in the y-ion series from y4 onwards indicating hydroxyla-

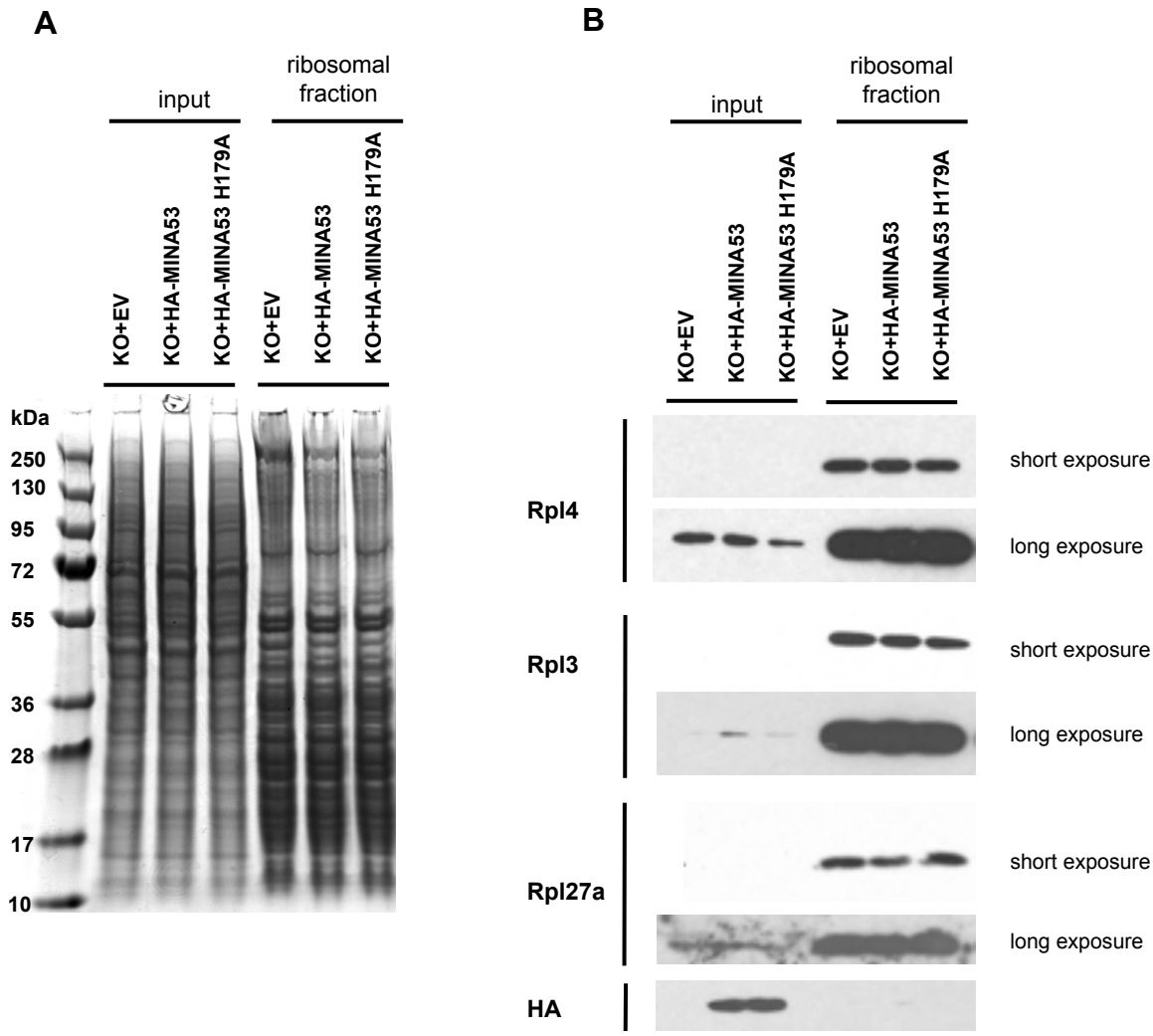

Figure 4.6. Purification of ribosomal proteins (1). A. Ribosomes were purified of MINA53 KO MEFs reconstituted with EV, HA-MINA53 or HA-MINA53 H179A by layering extracts on top of a 32% sucrose cushion and subjecting to ultracentrifugation at 100,000g for 3h (see Figure 5 and Material and Methods). Input and purified separated by SDS-PAGE and stained with coomassie. **B.** Western blot of input and purified ribosomes from transformed KO MEFS reconstituted with EV, HA-MINA53 or enzymatic inactive MINA53 (H179A).

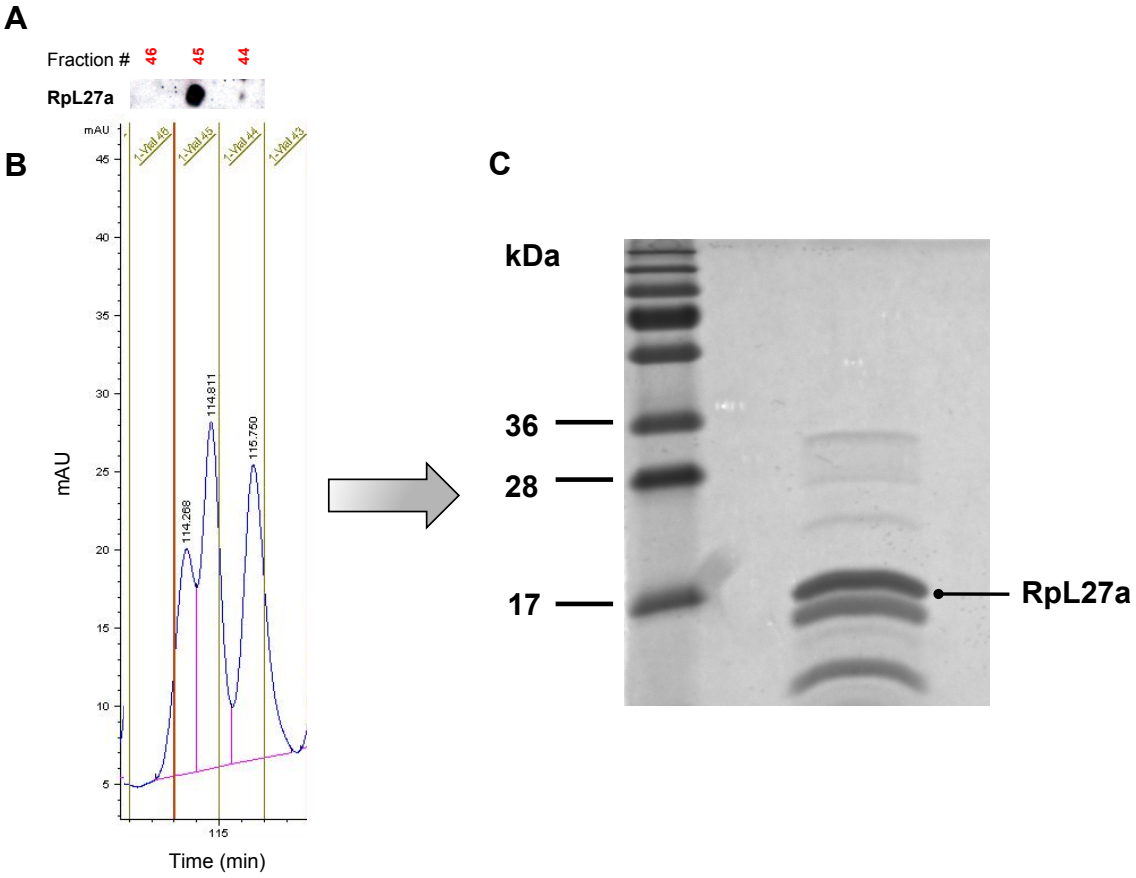

Figure 4.7. Purification of ribosomal proteins (2). A. Dot-blot of ribosomal protein fractions from RP-HPLC collected between 113 and 116 minutes. Note that Rpl27a is found predominantely in one single fraction (#45) in HEK293T **B.** RP-HPLC-trace from purified ribosomal proteins from HEK293T cells (mAU: milli-absorbance units). Protein absorbance was measured at 214nm and fractions collected between 113 and 116 minutes to isolate Rpl27a. **C.** SDS-PAGE stained with coomassie of Rpl27a fractions from RP-HPLC.

tion at His-39 (GNAGGLHHHR). The appearance of dehydrated y-ions from y4 and onwards further confirmed the hydroxylation site as His-39. The unhydroxylated peptide was not detected suggesting that Rpl27a is fully hydroxylated in HEK293T (Figure 4.8). I was unable to measure the extent of hydroxylation by classical LC-MS quantification because of the poor chromatographic properties of the tryptic peptide (no defined peak, likely due to the glycine/histidine rich nature of the peptide). Instead I relied on whole-protein mass detection and quantification (WP-MS) in collaboration with Rok Sekirnik (Schofield laboratory). Using this approach we detected a species with a mass of 16448.4Da. This corresponds to the expected mass of Rpl27a (16561Da) following removal of the initiating methionine (16430.19Da) and modification by hydroxylation (expected 16446.19Da, observed 16448.4Da; within the known error margin of the technique). Since the unhydroxylated mass was not detected, this confirmed that Rpl27a is abundantly hydroxylated in HEK293T cells (>95%).

I next aimed to determine whether Rpl27a His-39 hydroxylation is conserved in lower mammals, and whether the modification is also present in tissues. Therefore, I purified Rpl27a from several mouse organs following mechanical homogenization of fresh tissue samples in sucrose gradient fractionation buffer. MSMS sequencing following trypsinolysis of purified Rpl27a confirmed the presence of hydroxylation at His-39 in protein from mouse liver (Figure 4.9). WP-MS of ribosomal proteins purified from parallel samples detected a species corresponding to the mass of singly hydroxylated mouse Rpl27a (minus initiating methionine; expected 16490.27Da, observed 16490.1Da) (Figure 4.10A). Again, the unhydroxylated mass was not detected, suggesting that mouse liver Rpl27a is

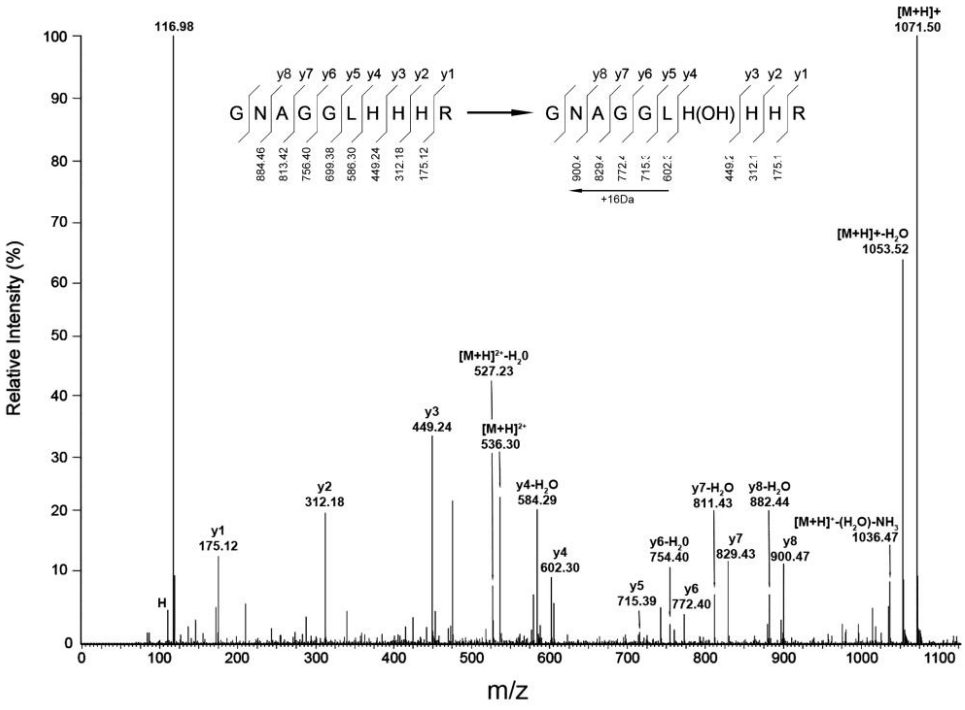

Figure 4.8. Rpl27a is fully hydroxylated in HEK293T cells. Endogenous Rpl27a was purified from HEK293T cells (see 4.2.4 and Material and methods) and subjected to trypsinolysis followed by MS/MS sequencing. From y4 the y-series exhibited a +16Da mass shift (compared to predicted peptide mass) indicative of hydroxylation at histidine 39. Note the presence of dehydration y-ions from y4 and onwards further supporting that Rpl27a is hydroxylated at H39. Unhydroxylated peptide was not detected indicating that Rpl27a is fully hydroxylated in HEK293T cells.

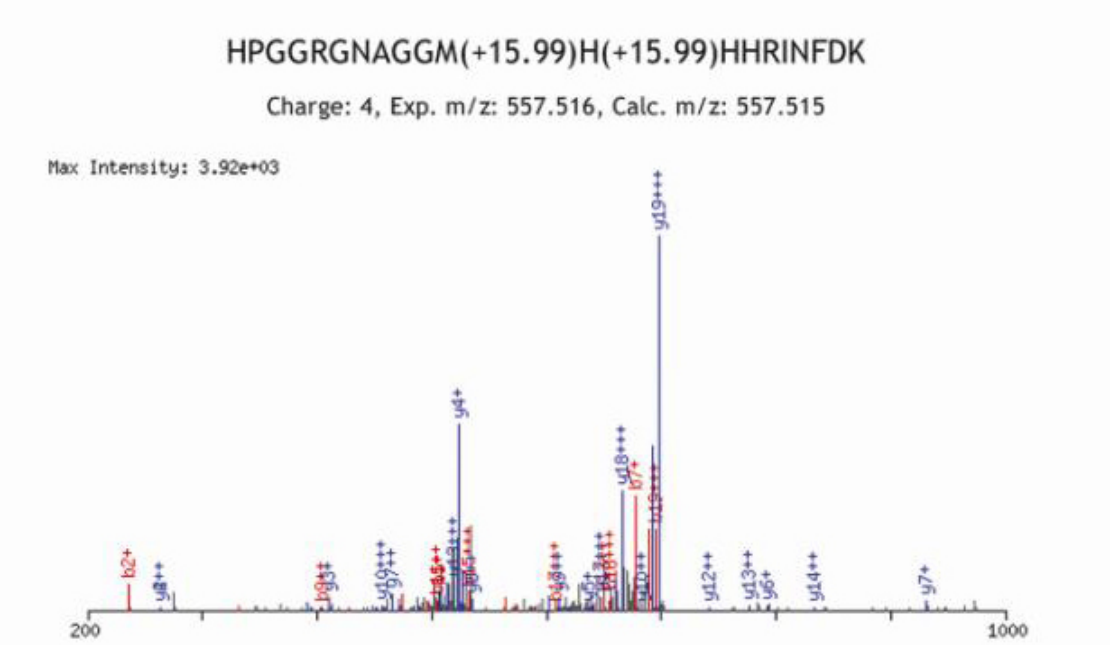

		b+	b++	b+++	y+	y++	y+++		
H	1	138.07	69.54	46.69				20	H
P	2	235.12	118.06	79.04	2089.98	1045.50	697.33	19	P
G	3	292.14	146.57	98.05	1992.93	996.97	664.98	18	G
G	4	349.16	175.08	117.06	1935.91	968.46	645.97	17	G
R	5	505.26	253.14	169.09	1878.89	939.95	626.97	16	R
G	6	562.28	281.65	188.10	1722.79	861.90	574.93	15	G
N	7	676.33	338.67	226.11	1665.77	833.39	555.93	14	N
A	8	747.36	374.19	249.79	1551.72	776.37	517.91	13	A
G	9	804.39	402.70	268.80	1480.69	740.85	494.23	12	G
G	10	861.41	431.21	287.81	1423.66	712.34	475.23	11	G
M	11	1008.44	504.73	336.82	1366.64	683.83	456.22	10	M
H	12	1161.50	581.25	387.84	1219.61	610.31	407.21	9	H
H	13	1298.56	649.78	433.52	1066.55	533.78	356.19	8	H
H	14	1435.61	718.31	479.21	929.50	465.25	310.50	7	H
R	15	1591.72	796.36	531.24	792.44	396.72	264.82	6	R
I	16	1704.80	852.90	568.94	636.34	318.67	212.78	5	I
N	17	1818.84	909.92	606.95	523.25	262.13	175.09	4	N
F	18	1965.91	983.46	655.98	409.21	205.11	137.07	3	F
D	19	2080.94	1040.97	694.32	262.14	131.57	88.05	2	D
K	20				147.11	74.06	49.71	1	K

+16Da $[M+H]^{2+}$

Figure 4.9. H39 hydroxylation of endogenous Rpl27a is hydroxylated in mouse liver. Endogenous Rpl27a was purified from mouse liver as described in methods prior to trypsinolysis and MS/MS. The tables summarise the ions detected from fragmented H39-hydroxylated Rpl27a tryptic peptide. Note the mass shift of 8 m/z in the doubly-charged y-ion (y^{++}) series from y9 onwards, indicating hydroxylation of H39.

abundantly hydroxylated (>95%). Similar analyses in other mouse tissues indicated that Rpl27a is ubiquitously and abundantly hydroxylation (>95% in all cases; Figure 4.10B). Since MINA53 has been implicated in cancer, we next sought to determine whether its substrate was also hydroxylated in tumours. Rok Sekirnik purified human Rpl27a from two independent samples from Non-Hodgkins lymphoma (obtained from the Oxford Centre for Histopathology Research) and demonstrated >95% Rpl27a hydroxylation in each case by WP-MS. Similar analysis of Rpl27a purified from normal tissue (placenta) also indicated >95% hydroxylation (Figure 4.10C). Together, these results suggest that Rpl27a is abundantly and ubiquitously hydroxylated at His-39 in both normal and pathological tissue samples.

4.2.6 Hydroxylation of Rpl27a is dependent on MINA53 *in vivo*

Although I have demonstrated endogenous hydroxylation of Rpl27a at the predicted MINA53 modification site, it is not possible to conclude from the data above that this modification is catalysed by MINA53. Since MINA53 is highly related to the 2OG oxygenase NO66 it is also important to demonstrate the contribution of each enzyme to the extent of Rpl27a His-39 hydroxylation *in vivo*. To address these issues we used shRNA-mediated knockdown of MINA53 and NO66 followed by WP-MS quantification of Rpl27a hydroxylation. WP-MS analyses were initially performed on Rpl27a purified from the control and MINA53 shRNA knockdown HEK293T and A549 cells presented in Chapter 2. Substantial knockdown of MINA53 protein expression in A549 cells shifted the mass of Rpl27a from 16446.1Da (singly hydroxylated) in control cells to 16431.5Da (expected 16430.19 for unmodified, within error) (Figure 4.11). Under these conditions the

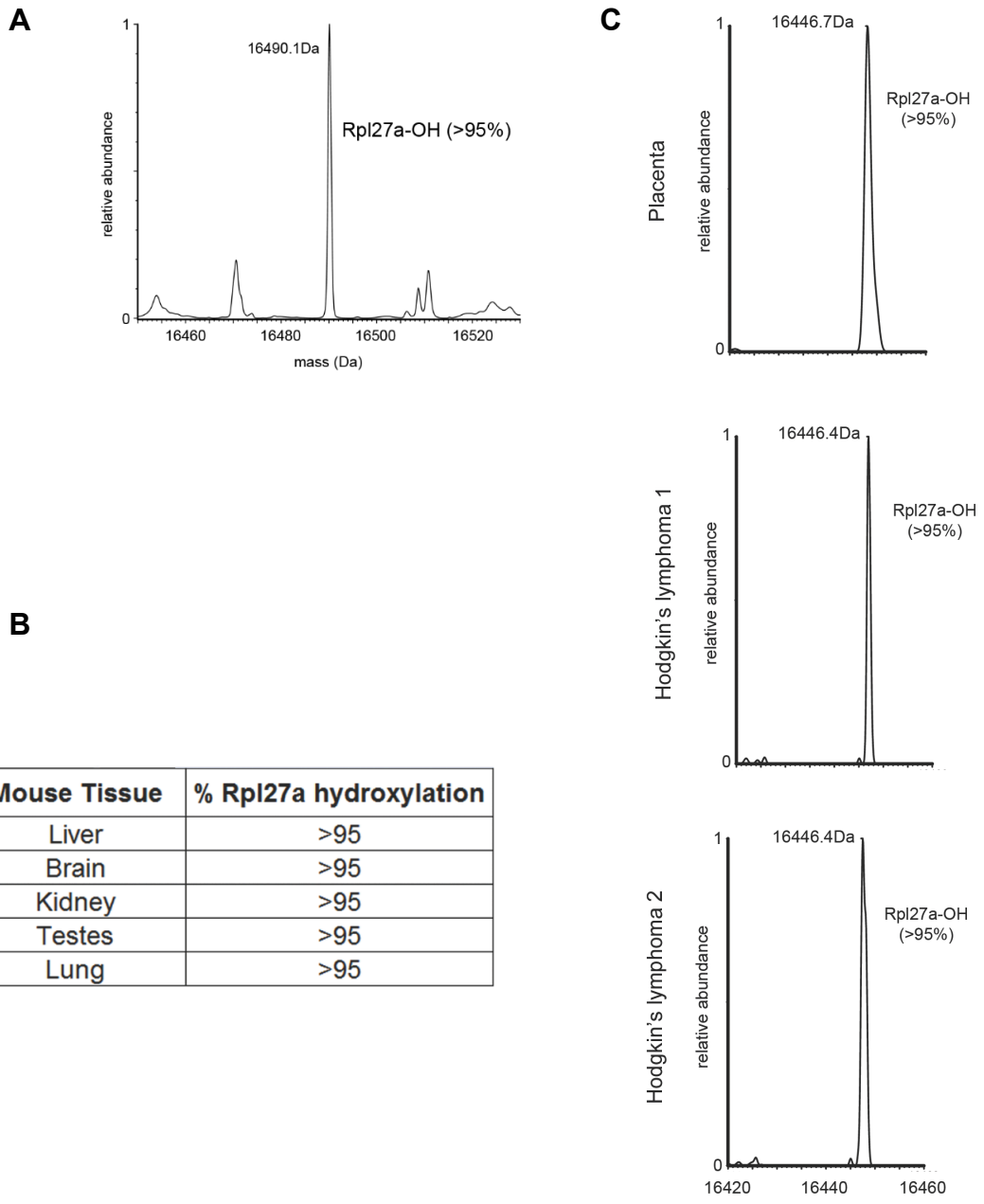

Mouse Tissue	% Rpl27a hydroxylation
Liver	>95
Brain	>95
Kidney	>95
Testes	>95
Lung	>95

Figure 4.10. MINA53 is fully hydroxylated in mouse and Hodgkin's lymphoma. Endogenous Rpl27a was purified as described in 4.2.4 and Figure 4.5, and then subjected to analysis by Whole-protein MS. **A.** Endogenous Rpl27a from mouse liver is completely hydroxylated since only the predicted protein mass with a +16Da mass shift (16490.1Da) was detected. **B.** Rpl27a is fully hydroxylated in all mouse tissues tested. **C.** Human placenta and two independent Hodgkin's lymphoma tumours exhibited fully hydroxylated Rpl27a (16446.4Da) (Rok Sekirnik, Department of Chemistry, Oxford).

hydroxylated Rpl27a species was not detected indicating that Rpl27a hydroxylation is completely dependent on MINA53 and is unlikely to be modified by a related 2OG oxygenase (including NO66). Consistent with no role for NO66 in Rpl27a His-39 hydroxylation, its knockdown by ShRNA did not affect its whole protein mass in A549 cells (Personal Communication, Penny Feng, Ratcliffe laboratory). Partial knockdown of MINA53 in HEK293T cells moderately suppressed the hydroxylation of Rpl27a relative to control ShRNA cells (Figure 4.12), with hydroxylated and unhydroxylated species detected at approximately 1:1 ratio. In both ShRNA models, Rpl27a protein levels were unaffected by MINA53 knockdown. Together these results demonstrate that endogenous Rpl27a His-39 hydroxylation is non-redundant and is dependent only on MINA53.

4.2.7 Hydroxylation of Rpl27a *in vivo* is dependent on the enzymatic activity of MINA53

To demonstrate that the hydroxylation of endogenous Rpl27a hydroxylation is dependent on MINA53 enzymatic activity I next studied the MEF model presented in Chapter 3. Rpl27a was purified from WT and MINA53 KO MEFs reconstituted with either empty vector (EV), HA-MINA53 or enzymatic inactive MINA53 (H179A). Western blot of Rpl27a suggested that its expression was subtly reduced by the presence of MINA53 (Figure 4.13), although the significance of this is not clear at present. WP-MS indicated that Rpl27a is fully hydroxylated in both wildtype and MINA53 KO MEFs reconstituted with HA-MINA53. Importantly, Rpl27a was completely unhydroxylated in the EV KO control or enzyme inactive MINA53 background (Figure 4.14). This data therefore confirms that the hydroxylation of Rpl27a is dependent on the enzymatic activity of MINA53 *in vivo*.

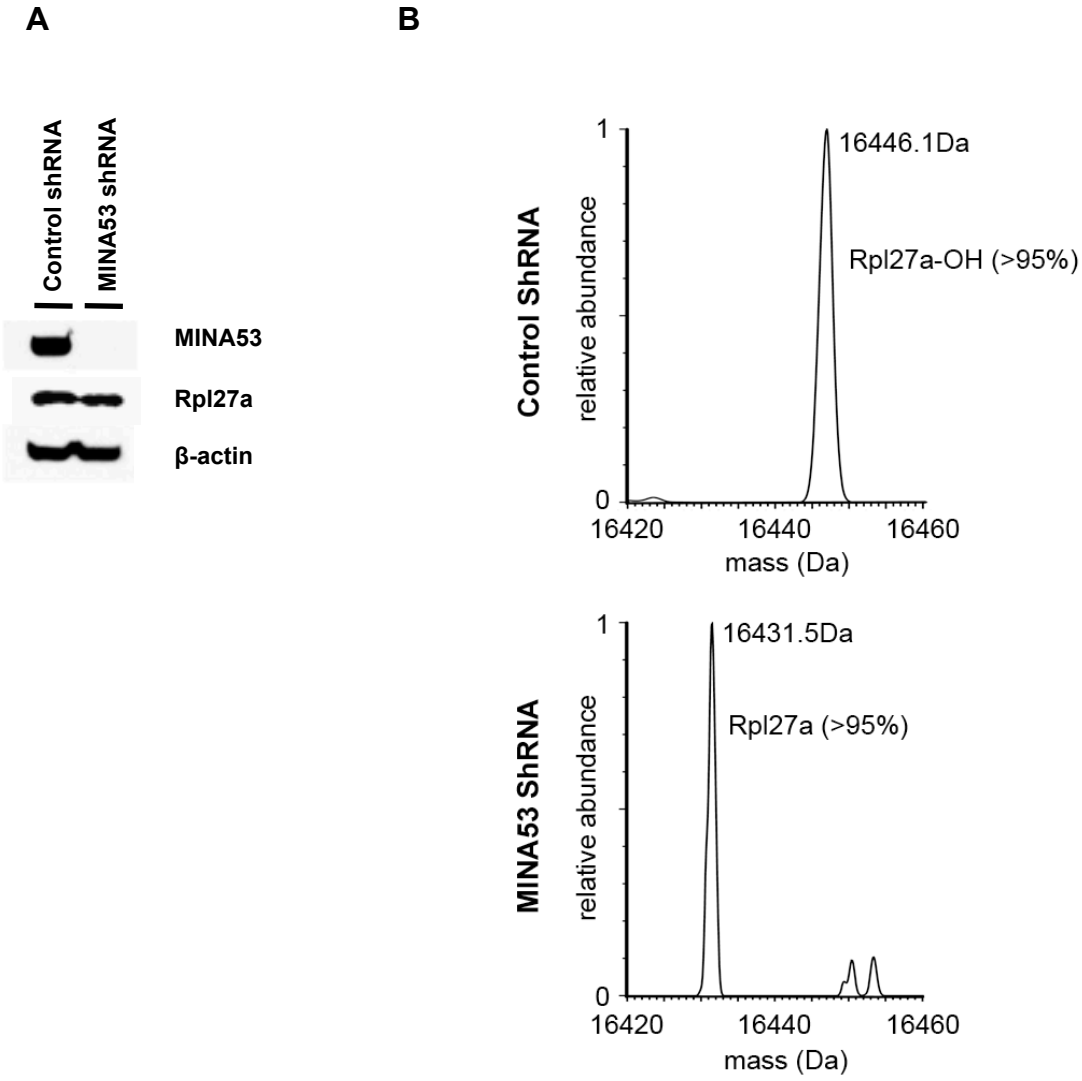

Figure 4.11. Hydroxylation of Rpl27a in A549 cells is dependent on MINA53. A. Western blot of constitutively expressing control and MINA53 shRNA A549 cells. **B.** Endogenous human Rpl27a purified from control and MINA53 shRNA expressing A549 cells were subjected to analysis by Whole-protein MS. Rpl27a from control cells was fully hydroxylated with predicted protein mass containing a +16Da mass shift (16446.1Da). MINA53 shRNA cells exhibited predicted mass of Rpl27a (16431.1Da) indicating that the protein is completely unhydroxylated in these cells.

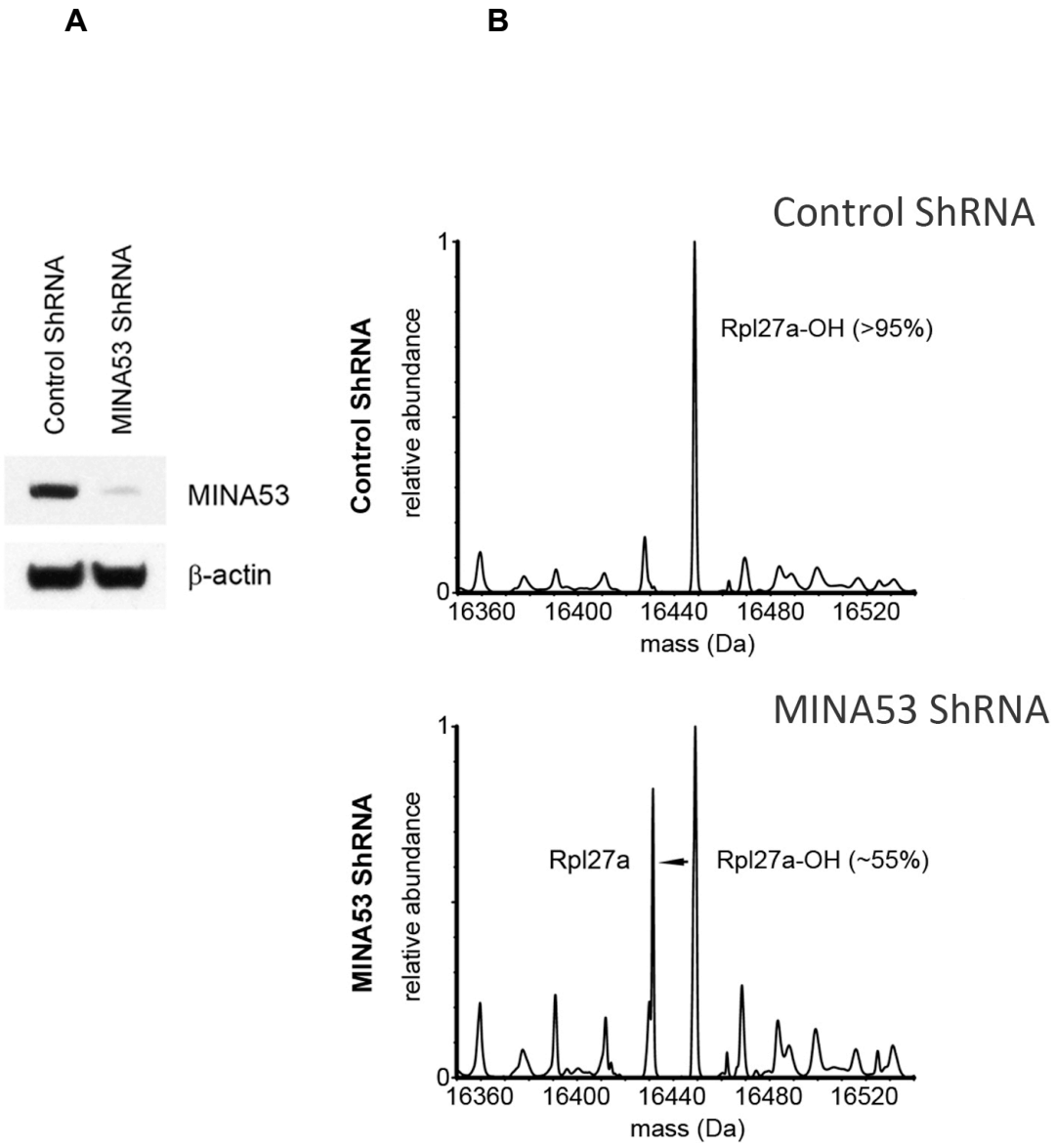

Figure 4.12. Hydroxylation of Rpl27a in HEK293T cell is dependent on MINA53. A. Western blot of stably expressing control and MINA53 shRNA HEK293T cell lines. **B**. Endogenous Rpl27a was purified (see 4.2.4) and subsequently analysed by Whole-protein MS. Human Rpl27a is completely hydroxylated in control cells as only protein mass containing a +16Da mass shift (16448.2Da) was detected. In MINA53 shRNA cells a peak corresponding to unhydroxylated Rpl27a (16431.5Da) together with the hydroxylated peak (16449.1 Da) was detected, indicating a suppression of hydroxylation when MINA53 is reduced by shRNA.

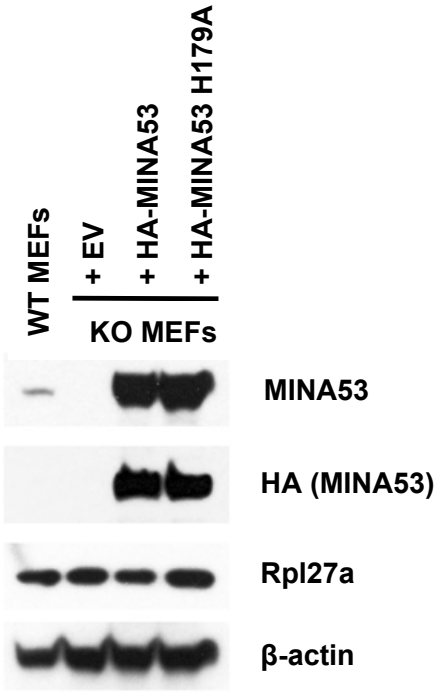

Figure 4.13. Western blot of Rpl27a in K-Ras transformed WT and MINA53 KO MEFs. Western blot of K-Ras G12V transformed WT and MINA53 KO MEFs reconstituted with EV, HA-MINA53 or HA-MINA53 H179A.

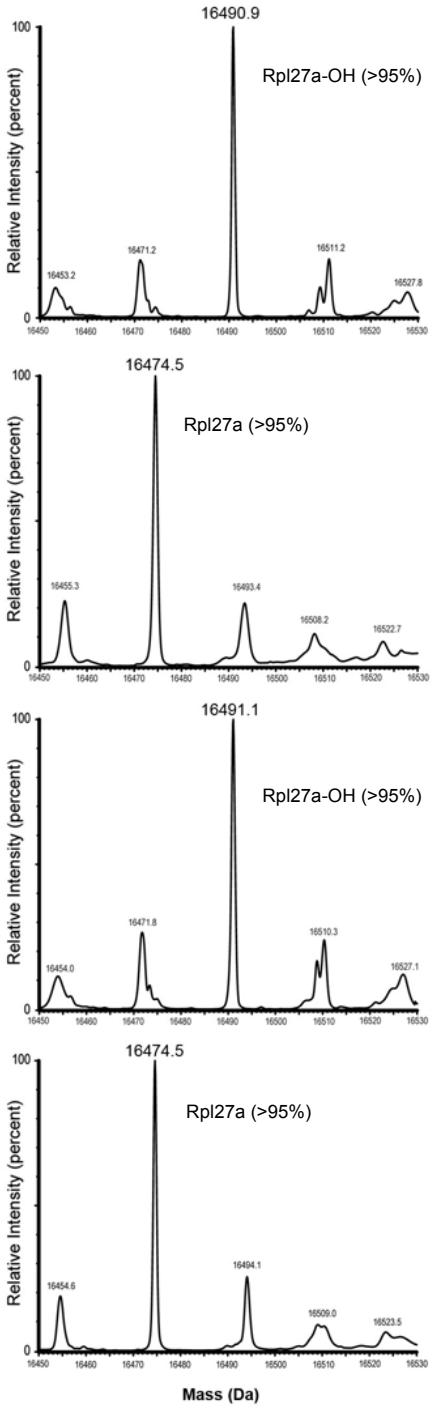

Figure 4.14. Hydroxylation of Rpl27a is dependent on the enzymatic activity of MINA53. Endogenous Rpl27a was purified from K-Ras transformed WT and MINA53 KO MEFs reconstituted with EV, HA-MINA53 or enzyme inactive MINA53 (H179A), and subjected to analysis by Whole-protein MS. MINA53 KO MEFs reconstituted with EV or enzyme inactive MINA53 exhibited the predicted protein mass of mouse Rpl27a (16474.5). WT and MINA53 KO MEFs reconstituted with HA-MINA53 contained mouse Rpl27a with a mass of 16491, indicative of fully hydroxylated Rpl27a.

4.2.8 Effect of hypoxia on hydroxylation of Rpl27a

Rpl27a was consistently found fully hydroxylated in all samples examined unless we artificially reduced the levels of MINA53. Since 2OG enzymes are oxygen dependent we next sought to examine if severe prolonged hypoxia (0.1 % O_2) could suppress the MINA53-dependent hydroxylation of Rpl27a. Transformed wildtype MEFs were incubated in a Invivo$_2$ Hypoxic Workstation (Ruskinn life sciences) hypoxia chamber for 72h at 0.1 % O_2, 37°C and 5% CO_2. Under these conditions, WP-MS indicated a modest decrease in Rpl27a hydroxylation (20%) (Figure 4.15). This suggests that MINA53 likely has a high affinity for O_2, similar to other 2OG enzymes such as FIH that operates efficiently under lower O_2 levels (Koivunen et al., 2004), (Stolze et al., 2004). Lower O_2 levels or anoxia may be required to suppress hydroxylation of Rpl27a. Furthermore, more sensitive methods of quantifying hydroxylation of newly-synthesised Rpl27a may be necessary to detect modest affects on hydroxylation. However, methods such as stable isotope labeling by amino acids (SILAC) are unsuitable in this case as they are not compatible with WP-MS.

4.3 Conclusion

In this chapter I describe my work to characterize a novel MINA53 substrate, the 60S ribosomal protein Rpl27a. I have shown that endogenous Rpl27a is hydroxylated at the predicted residue (His-39) and that this modification is essentially complete (>95%), ubiquitous and conserved. Furthermore, I have demonstrated that Rpl27a hydroxylation is non-redundant and entirely dependent on MINA53 and its enzymatic activity. Lastly, I provided preliminary data that the modification is relatively unaffected by low oxygen levels, perhaps consistent with

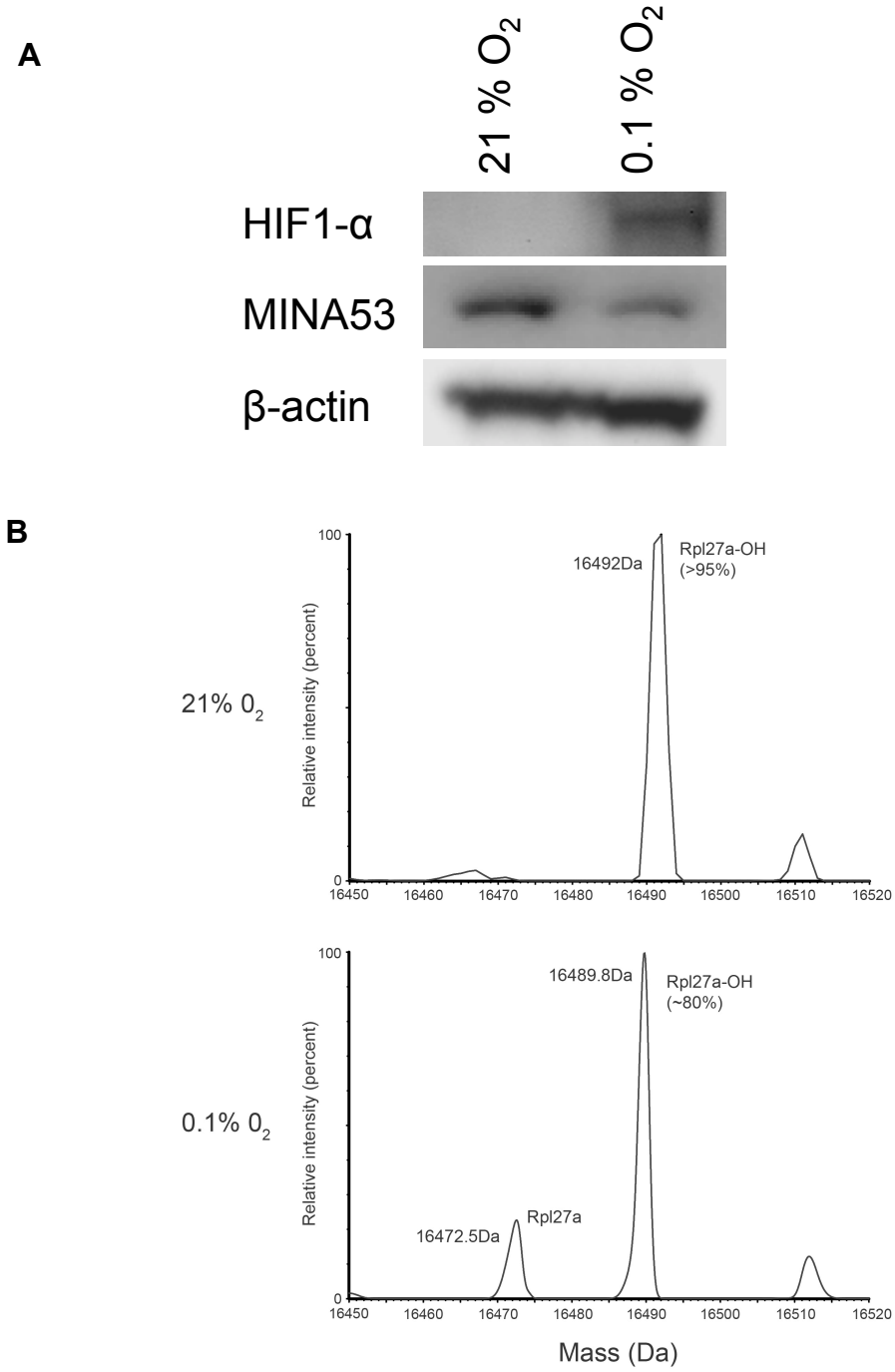

Figure 4.15. Effect of hypoxia on Rpl27a hydroxylation. WT MEFs were subjected to 72h of hypoxia at 0.1 % O_2. **A** Western blot of protein extracts from WT MEFs incubated at normoxia or hypoxia confirming effective hypoxia as judged by HIF1α induction. Note that MINA53 protein levels were partially suppressed under hypoxia. Therefore, the modest decrease in Rpl27a hydroxylation under these conditions could be due to reduced enzyme level, rather than oxygen availability. **B**. Whole-protein MS of endogenous Rpl27a purified from normoxic (top) or hypoxic (bottom) WT MEFs indicated a subtle decrease in Rpl27a hydroxylation in response to oxygen deprivation.

the persistence of abundant Rpl27a hydroxylation in hypoxic human tumour samples.

Although Rpl27a is a highly conserved ribosomal component, its function in the ribosome is not fully understood. Therefore, it is unclear whether and how Rpl27a hydroxylation may contribute to proposed MINA53-dependent functions such as tumourigenesis and ribosome biogenesis or gene expression and anchorage-independent growth (Chapter 3). However, since ribosomal proteins and the protein synthesis apparatus are widely implicated in cancer, the findings presented in this Chapter may provide an opportunity to further dissect the role(s) of MINA53 in tumourigenesis.

The function of Rpl27a and its hydroxylation in protein synthesis, tumourigenesis and other phenotypes described in Chapter 5, will be discussed in detail in Chapter 7.

Chapter 5

MINA53 regulates autophagy in an activity-dependent manner

5.1 Introduction

I have shown in Chapter 4 that MINA53 hydroxylates the 60S ribosomal subunit Rpl27a at H39. Although the exact function of Rpl27a and H39 within the ribosome is unclear, it has been proposed that Rpl27a is one of the first ribosomal proteins loaded on to rRNA during 60S biogenesis. Furthermore, Rpl27a H39 is located on a disordered loop that extends deep into the ribosome and proximal to a functional centre where the E-site tRNA binds. Therefore, I sought to test the hypothesis that MINA53 activity may regulate ribosome biogenesis and/or protein translation.

5.2.1 Polyribosome profiling

A well established method to study ribosome biogenesis and protein translation involves 'polyribosomal profiling'. Sucrose density gradients (7-47%) separate the small (40S) and large ribosomal subunits (60S), monosomes (80S), and polysomes according to their densities by ultracentrifugation of cell lysates. The abundance of each ribosomal species is then measured by UV absorbance (OD_{254}) of the RNA content following displacement from the gradient. A change in the ratio of polysomes to monosome can be indicative of a translational disturbance while difference in 40S/60S ratio may suggest problems in ribosome biogenesis (Esposito et al., 2010). In order to investigate whether loss of MINA53 activity (and Rpl27a hydroxylation) alters the ribosomal and translational status of cells, I analysed polyribosome profiles of the K-Ras transformed WT and MINA53 KO MEFS reconstituted with EV, HA-MINA53 or enzyme inactive MINA53 (H179A). Similar to previous analyses using this model, wildtype MEFs showed a different ribosome profile to the MINA53 KO MEFs (Figure 5.1). Interestingly however, I

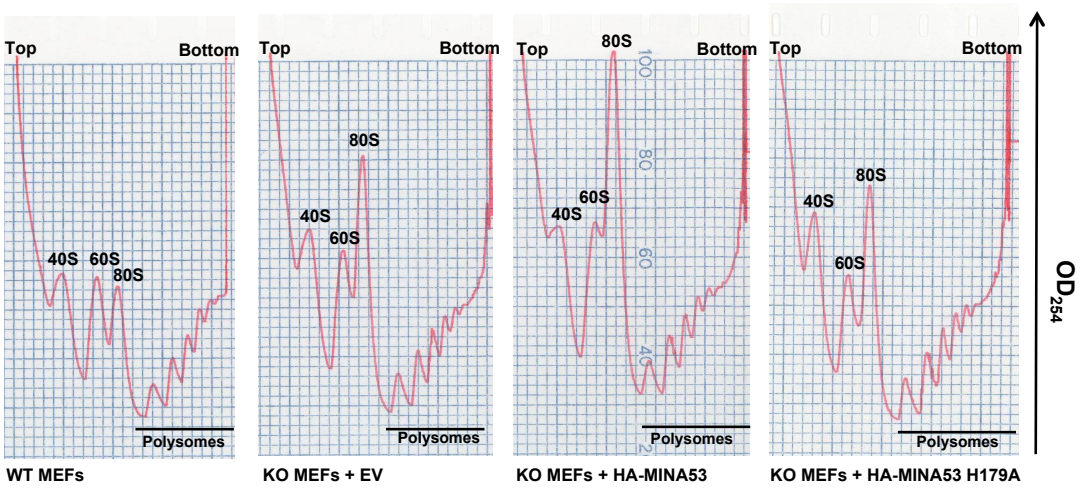

Figure 5.1. Polyribosome profiling. K-Ras transformed WT and MINA53 KO MEFs were seeded out and 48h later at around 90% confluency treated with 100ug/ml cyclohexamide for 15 min before harvest. Cells were layered on top of a 7-47% sucrose gradient and subjected to ultracentrifugation (100,000g for 4h) before analysis using polyribosome profiling.

observed a clear effect of MINA53 enzyme activity on the ribosome profile within the isogenic KO background. Whereas the peak corresponding to the 60S subunit was of equal intensity to the 40S subunit in WT-reconstituted KO MEFs, cells lacking MINA53 activity displayed a subtle decrease in 60S relative to 40S. Furthermore, these cells also displayed reduced levels of monosome relative to 40S, 60S and polysomes. Consistent with the similar growth kinetics of these cells (Chapter 3), there was no difference in the number or intensity of polysomes however, suggesting that the bulk translation rate is unaffected by MINA53. In conclusion, MINA53 activity modestly regulates 60S subunit and monosome abundance, but this effect is not sufficient to affect translation rate and cell growth.

5.2.2 Effect of ribosome biogenesis inhibitors on MINA53 MEFs

Next I considered the possibility that agents known to regulate ribosome biogenesis and/or protein translation could exaggerate the 60S/monosome defect in the MINA53 MEFs and elicit a 'synthetically lethal' interaction on growth/viability. I began by treating the MEF model with dose titrations of specific drugs that target early ribosome biogenesis before monitoring cell viability by MTS assay. LY294002 is an inhibitor of Phosphatidylinositol-3-kinase (PI3K), an important signaling enzyme involved in regulating protein translation *via* AKT and Mammalian target of Rapamycin (mTOR) (Gharbi et al., 2007), (Willems et al., 2012). Interestingly, PI3K inhibition was slightly more effective in reducing the apparent viability of cells that lacked MINA53 activity (Figure 5.2A).

The intercalating drug Actinomycin-D, is an inhibitor of RNA polymerase I and/or polymerase II, which are involved in transcription of ribosomal RNA and ribosomal

proteins, respectively. Low concentrations of this drug (0.04 ug/ml) are known inhibit RNA polymerase I specifically, while higher doses (5 ug/ml) inhibit both RNA polymerase I and II (Eilbracht et al., 2005). Compared to LY294002, Actinomycin D did not seem that have a significant enzyme dependent effect on cell viability (Figure 5.2B).

The antimetabolic drug 5-Fluorouracil (5-FU) is an inhibitor of thymidylate synthase, an enzyme involved in the production of thymidine. Inhibition leads to depletion of the dTTP pool followed by misincorporation of deoxyuridine into newly synthesised DNA and its irreversible damage (Longley et al., 2003). 5-FU is also thought to inhibit late processing stages of ribosome biogenesis in the nucleolus in several different ways; incorporation of 5-FU into RNA leads to inhibition of rRNA processing, post-transcriptional modification of tRNA, rRNA and snRNA as well as mRNA splicing. Furthermore, 5-FU prevents pseudouridylation, an important modification of rRNA in ribosome biogenesis (Burger et al., 2010). 5-FU was of also special interest because it targets late stages of ribosomal assembly that occur in the 'granular compartment' (Boisvert et al., 2007), the region of the nucleolus where MINA53 is enriched (Eilbracht et al., 2005). I therefore examined if 5-FU would induce a MINA53-dependent phenotype by treating the MEF model with a dose titration of this drug. However, although the 5-FU exhibited significant dose-dependent toxicity, this was identical in each of the four MEF lines (Figure 5.2C). In conclusion, although MINA53 activity modestly affected sensitivity to PI3K and RNA Polymerase I inhibition, none of the agents induced a dramatic loss of cell viability in a MINA53-dependent manner.

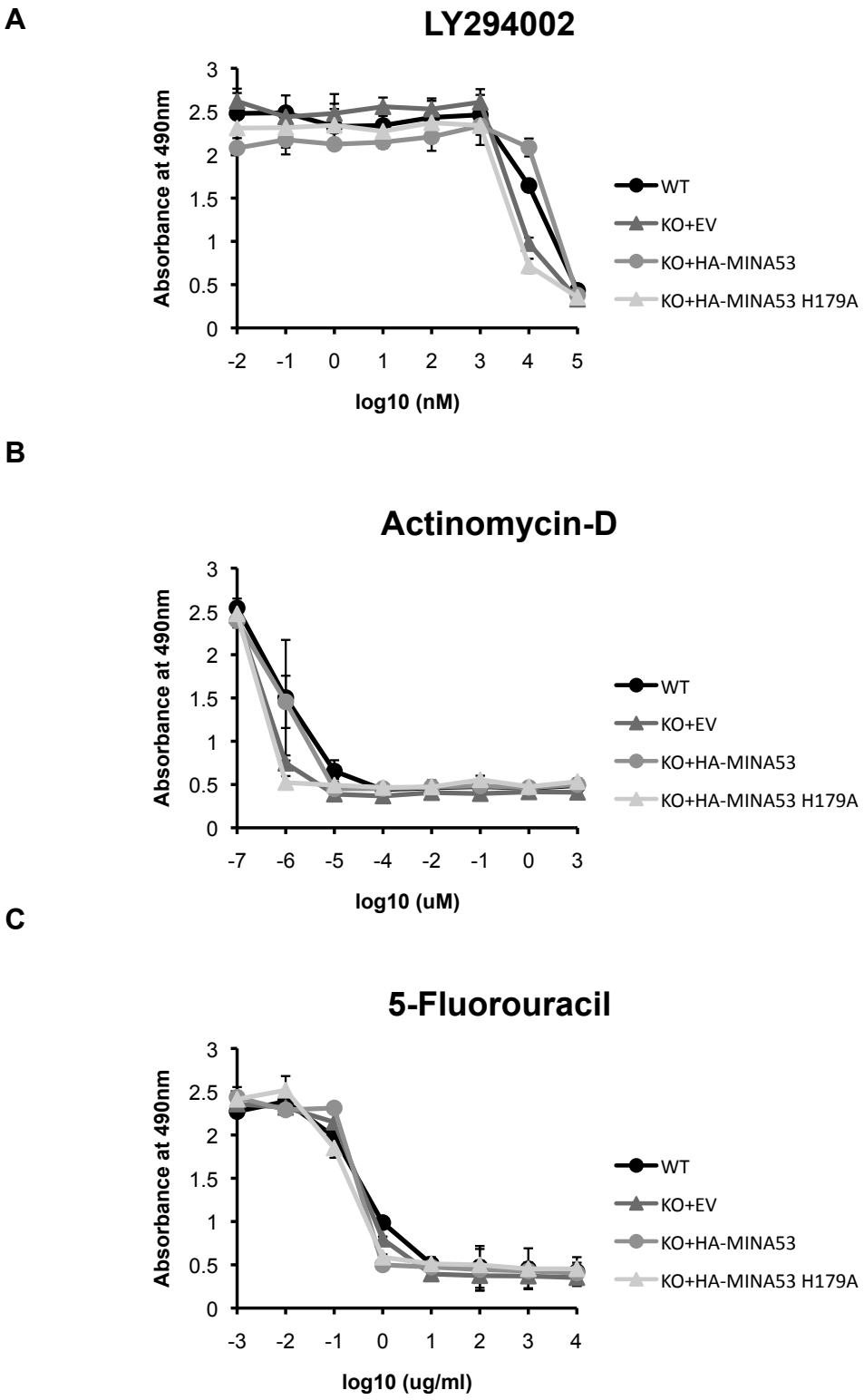

Figure 5.2. Dose-dependent inhibition of MTS signal by agents acting on ribosome biogenesis. K-Ras transformed WT and MINA53 KO MEFs reconstituted with EV, HA-MINA53 or HA-MINA53 H179A were incubated with varying doses of each drug for 48h before being assayed for cell viability using an MTS assay. **A.** LY294002 (PI3K inhibitor). **B.** Actinomycin-D (RNA polymeras I and/or II inhibitor). **C.** 5-Fluorouracil (thymidylate synthase inhibitor).

5.2.3 Effect of translational inhibitors on MINA53 MEFs

Next I wanted to explore if translational inhibitors known to target the large ribosomal subunit (60S) would aggravate a MINA53-dependent viability phenotype. Therefore, I performed dose-response experiments as above using the antibiotics anisomycin, sparsomycin and cycloheximide. Anisomycin suppress the peptidyltransferase activity of the ribosome while sparsomycin is thought to inhibit translation by stabilizing P site tRNA interactions within the ribosome and preventing substrate binding to the A site. Cyclohexamide prevents the translocation step of the elongation (Schneider-Poetsch et al., 2010). Interestingly, a yeast genetic screen recently identified a mutation at the residue adjacent to the MINA53 hydroxylation site (M38) that conferred resistance to cycloheximide (Schneider-Poetsch et al., 2010). However, no difference in cell viability was observed between the MINA53 MEF lines upon dose titration of cycloheximide or the other drugs described above (Figure 5.3A, B, C).

5.2.4 Effect of mTOR inhibitors on MINA53 MEFs

The serine/threonine kinase protein kinase mTOR is a central regulator of cell growth and has important roles in ribosome biogenesis and translation. mTOR is known to regulate ribosome biogenesis in at least two major ways. Firstly, it promotes translation of mRNA encoding all ribosomal proteins, through regulation via the 5'-terminal oligopyrimidine tract (5'TOP) sequence. Secondly, mTOR promotes transcription of ribosomal RNA through activation of RNA polymerase I (28S, 18S, 5.8 rRNA) and III (5S rRNA) (Mayer and Grummt, 2006), (Laplante and Sabatini, 2012). mTOR stimulates RNA polymerase I by activation of the regulatory element tripartite motif-containing protein (TIF-1A) (Mayer et al., 2004). It is

A

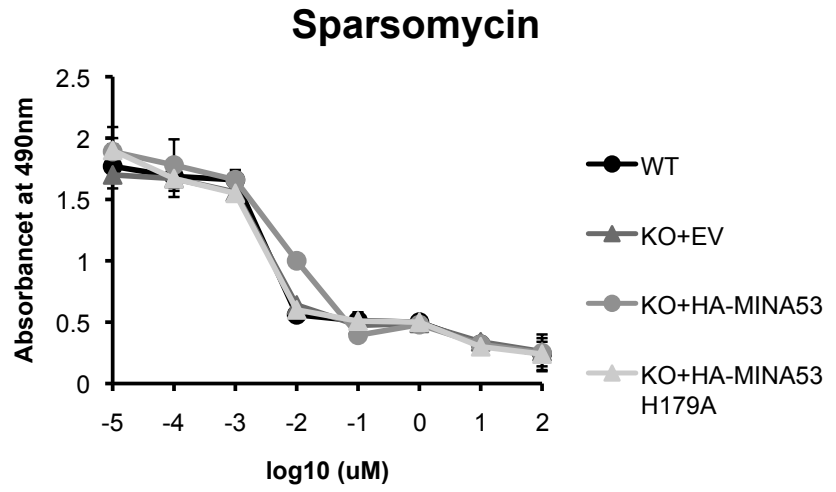

B

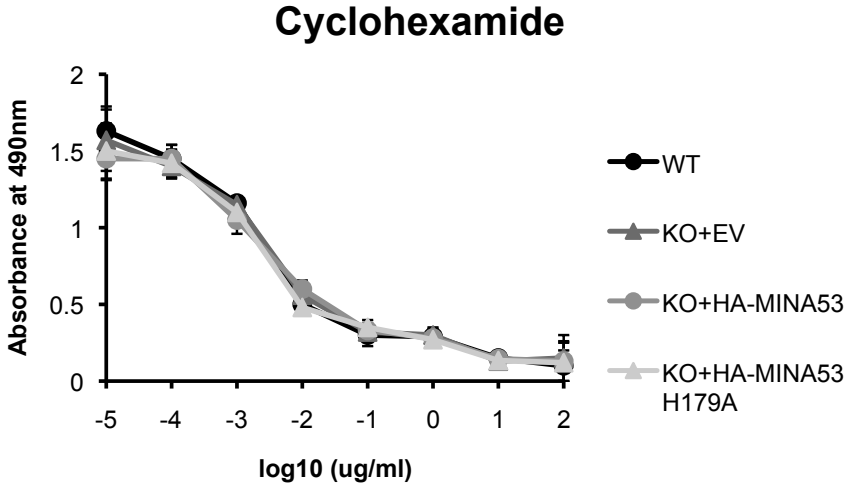

C

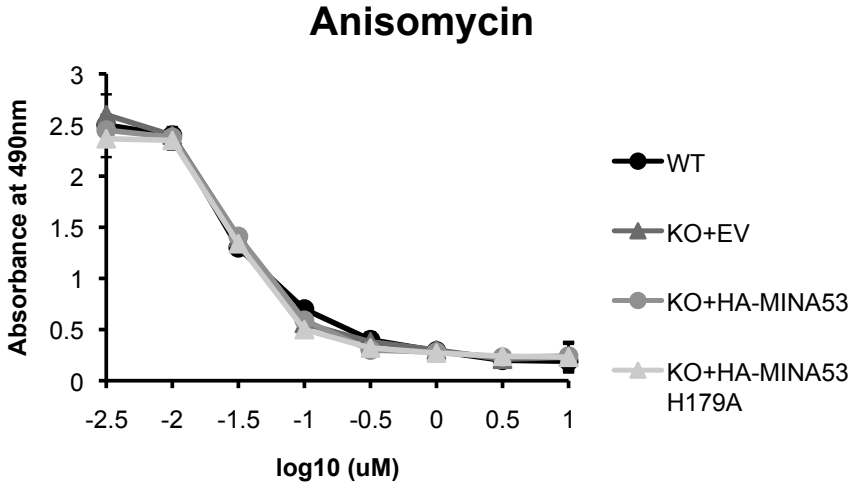

Figure 5.3. Dose-dependent inhibition of MTS signal by translational inhibitors. K-Ras transformed WT and MINA53 KO MEFS reconstituted with EV, HA-MINA53 or enzyme inactive MINA53 were treated with a range of doses of indicated drugs for 48h before analysis using an MTS assay. **A.** Sparsomycin. **B.** Cyclohexamide **C.** Anisomycin.

thought that mTOR stimulates RNA polymerase III (Pol III) activity by phosphorylation and inhibition of the Pol III repressor Maf1 (Laplante and Sabatini, 2012). Furthermore, mTOR promotes translation through phoshorylation of eukaryotic translation initiation factor 4E-binding protein 1 (4E-BP1) and preventing its inhibition of eukaryotic translation initiation factor, eIF4E (Mayer and Grummt, 2006), (Iadevaia et al., 2012). The mTOR dependent activation of S6K1 promotes translation initiation and elongation, and mRNA biogenesis. It was previously thought that S6K1 via phosprorylation of its substrate, the ribosomal protein S6, was involved in regulation of the 5'TOP mRNA, however that has been disproven (Laplante and Sabatini, 2012), (Tang et al., 2001).

The macrolide Rapamycin is a well known inhibitor of mTOR and is clinically used in treatment of certain cancers (Huang and Houghton, 2003), (Huang et al., 2003), (Ballou and Lin, 2008). Rapamycin-dependent inhibition of mTOR is associated with suppression of ribosomal RNA gene transcription and translational inhibition (Iadevaia et al., 2012), (Mayer and Grummt, 2006). Because of the critical involvement of mTOR in ribosome biogenesis I therefore decided to investigate the effect of MINA53 activity on loss of viability following mTOR inhibition. Interestingly, MEFs treated with increasing doses of Rapamycin (Figure 5.4A), or the rapalogue Everolimus (Figure 5.4B), displayed reduced viability that was striking exacerbated by loss of MINA53 activity. Western blot of Rapamycin-treated cells confirmed comparable mTOR inhibition in each of the cell lines (Figure 5.5). Surprisingly, we observed that despite reduced MTS signal in

A

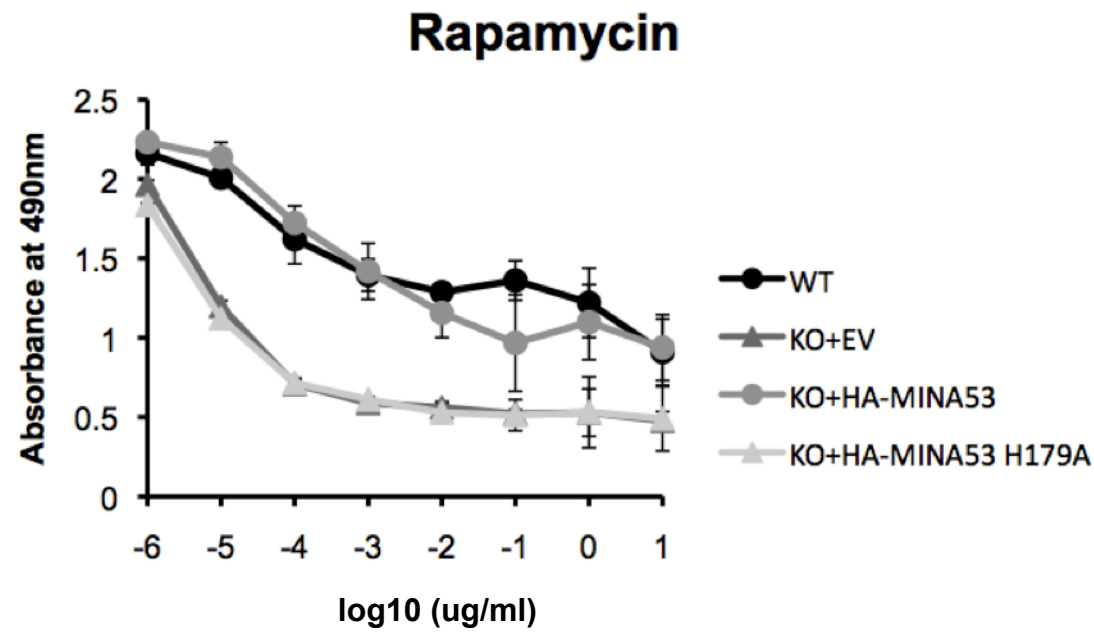

B

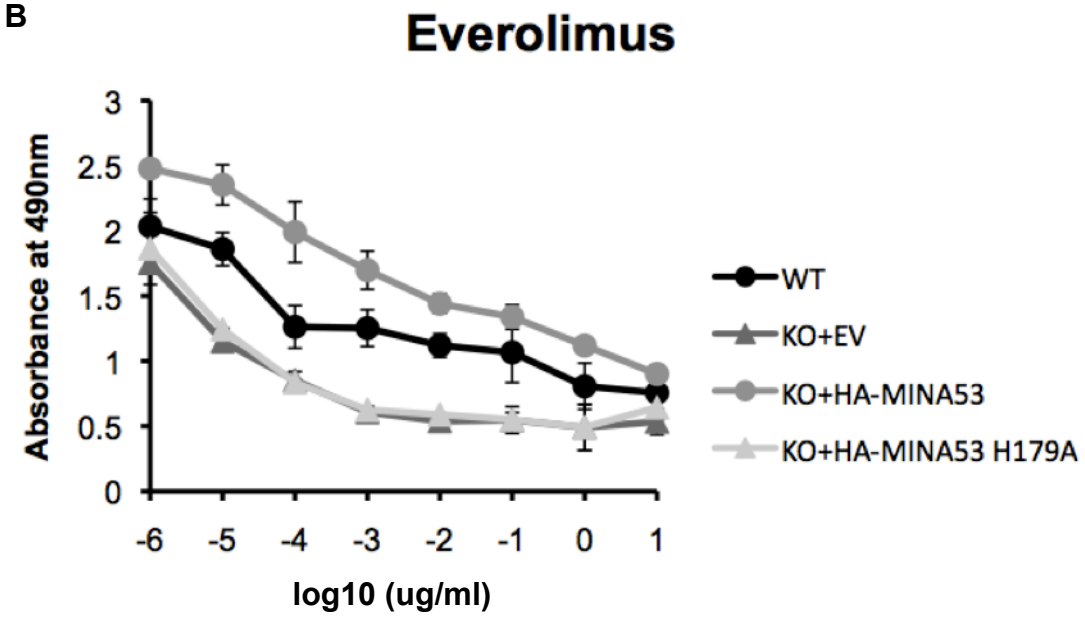

Figure 5.4. Dose-dependent inhibition of MTS signal by mTOR inhibitors. K-Ras transformed WT and MINA53 KO MEFS reconstituted with EV, HA-MINA53 or enzyme inactive MINA53 were treated with a range of doses of Rapamycin **(A)** and Everolimus **(B)** for 48h before analysis using an MTS assay.

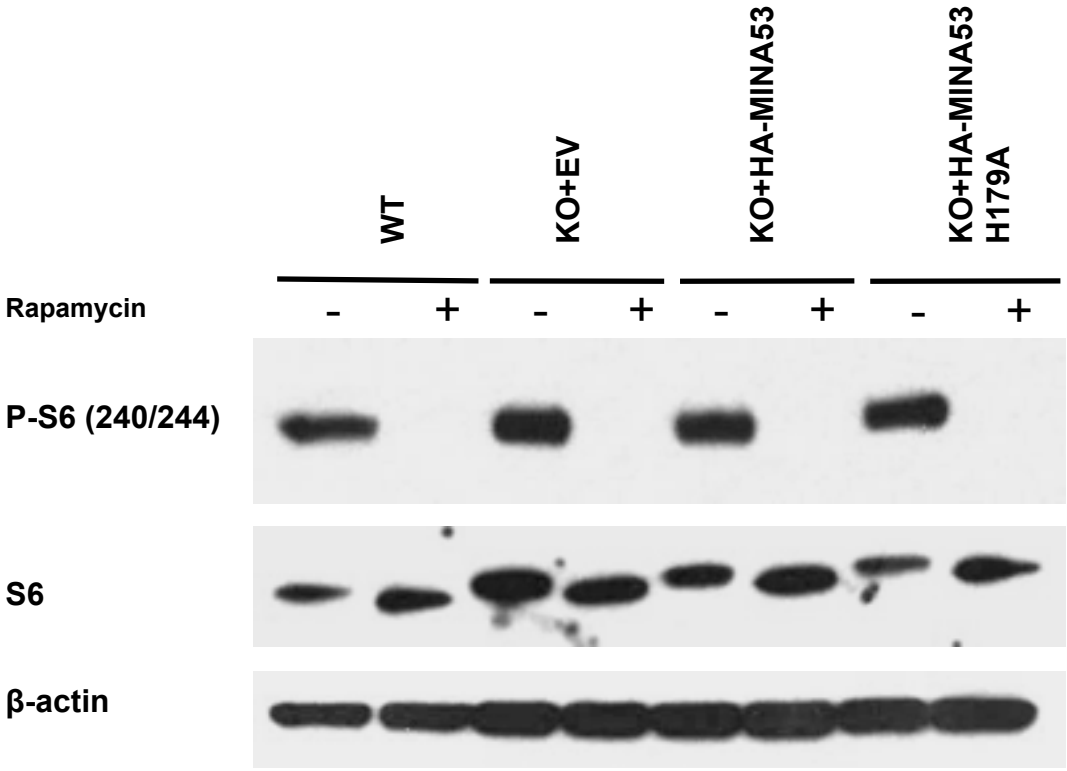

Figure 5.5. Confirmation of mTOR inhibition following Rapamycin treatment. K-Ras transformed WT and MINA53 KO MEFS reconstituted with EV, HA-MINA53 or enzyme inactive MINA53 were treated with 1ng/ml of Rapamycin for 48h before harvest for protein and western blot for the p-S6 (240/244), a downstream marker of mTOR activity.

Rapamycin-treated cells that lack MINA53 activity there was no loss of cell viability (Figure 5.6). In fact there was a small trend towards *increased* viability following Rapamycin treatment in cells that lacked enzyme activity. Since the MTS assay relies on mitochondrial reductase enzymes, I next explored the possibility that MINA53 activity may be required for maintaining mitochondrial number and/or activity under conditions of mTOR inhibition.

5.2.5 MINA53 and mitochondria

I first sought to determine if a decrease in mitochondrial number could explain the Rapamycin results from the MTS assay. Cytochrome C oxidase (COX-4), a mitochondrial protein in the electron transport chain (Kadenbach et al., 2000), is a commonly used marker for mitochondria. Indeed, western blot of cell extracts following Rapamycin treatment showed a significant reduction in COX-4 levels in MEFs that lacked MINA53 activity (Figure 5.7). MEFs that retained MINA53 activity showed no such loss of this mitochondrial marker. To verify these results, I next undertook immunoflouresence staining of Rapamycin-treated MEFs using a fluorescent mitochondrial probe called Mitotracker. This cell-permeable probe contain a thiol-reactive choloromethyl moiety that permanently accumulates in active mitochondria (Chazotte, 2011). Interestingly, mitochondrial staining in untreated MEFs lacking MINA53 activity appeared more punctuate than MEFs with reconstituted MINA53 (Figure 5.8). Importantly, Mitotracker staining intensity decreased in MEFs lacking MINA53 activity following addition of Rapamycin, in contrast to MINA53-reconstituted MEFs that maintained their mitochondria. These results are consistent with the COX-4 western blots, which taken together indicate that decreased mitochondria number is likely to be responsible for the enhanced

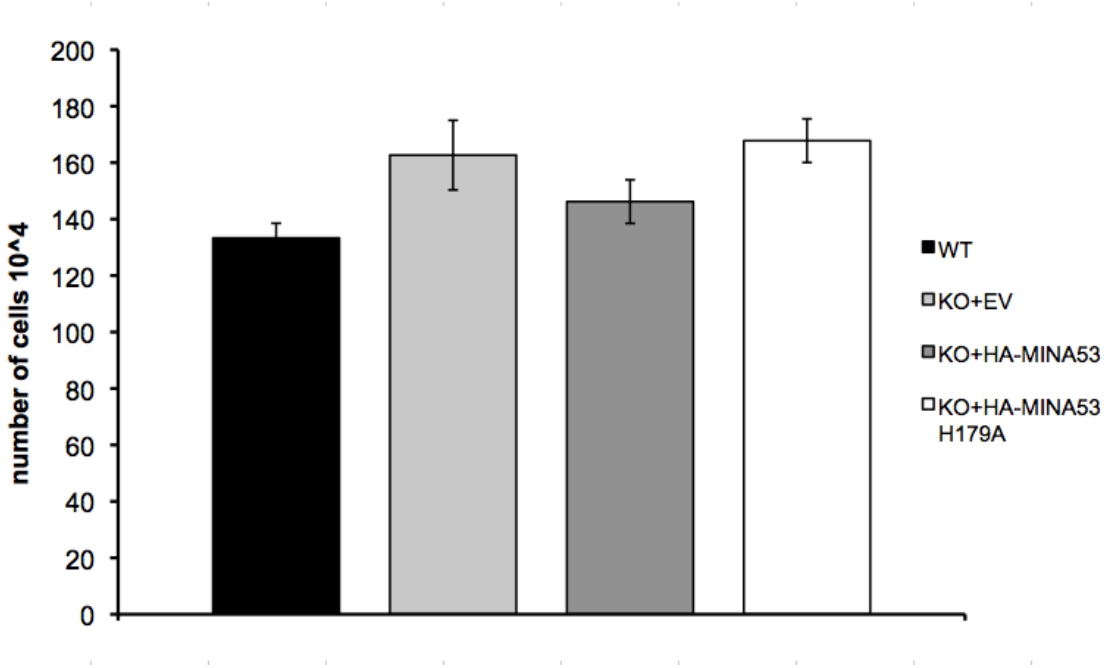

Figure 5.6. Number of cells following Rapamycin treatment. Number of K-Ras transformed WT and MINA53 KO MEFs reconstituted with EV, HA-MINA53 or enzyme inactive MEF cells after Rapamycin treatment (1ng/ml, 48h). Cells counted using a haemocytometer.

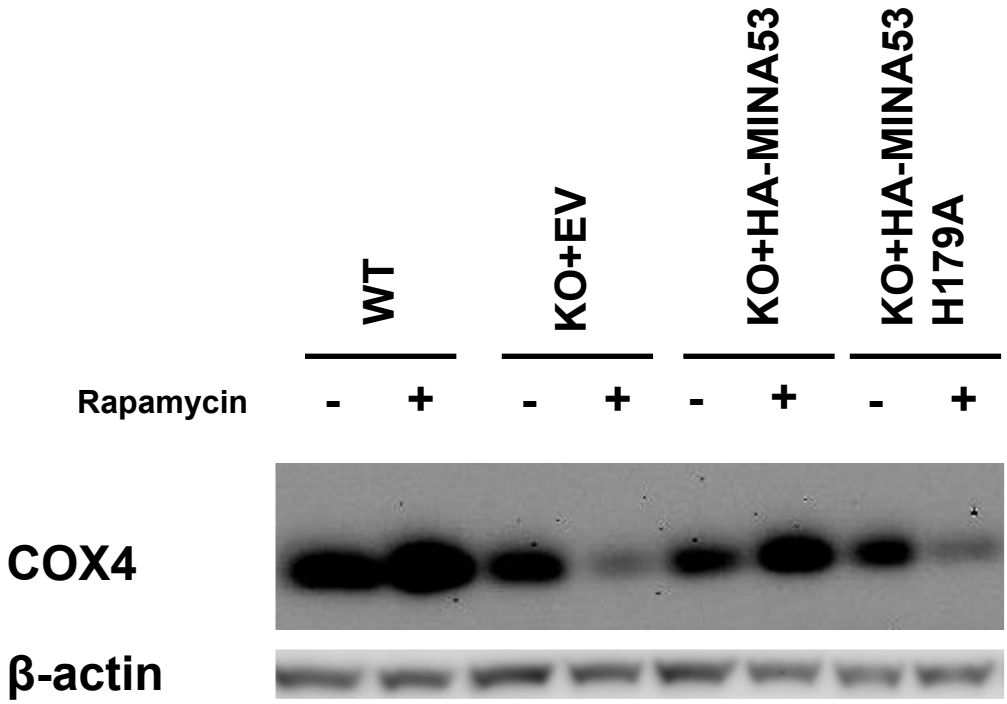

Figure 5.7. Effect of MINA53 activity with Rapamycin on mitochondrial marker COX4. K-Ras transformed WT and MINA53 KO MEFs reconstituted with EV, HA-MINA53 or enzyme inactive MINA53 (H179A) were treated with 1ng/ml Rapamycin for 48h after which cells were harvest and assayed for indicated proteins by western blot.

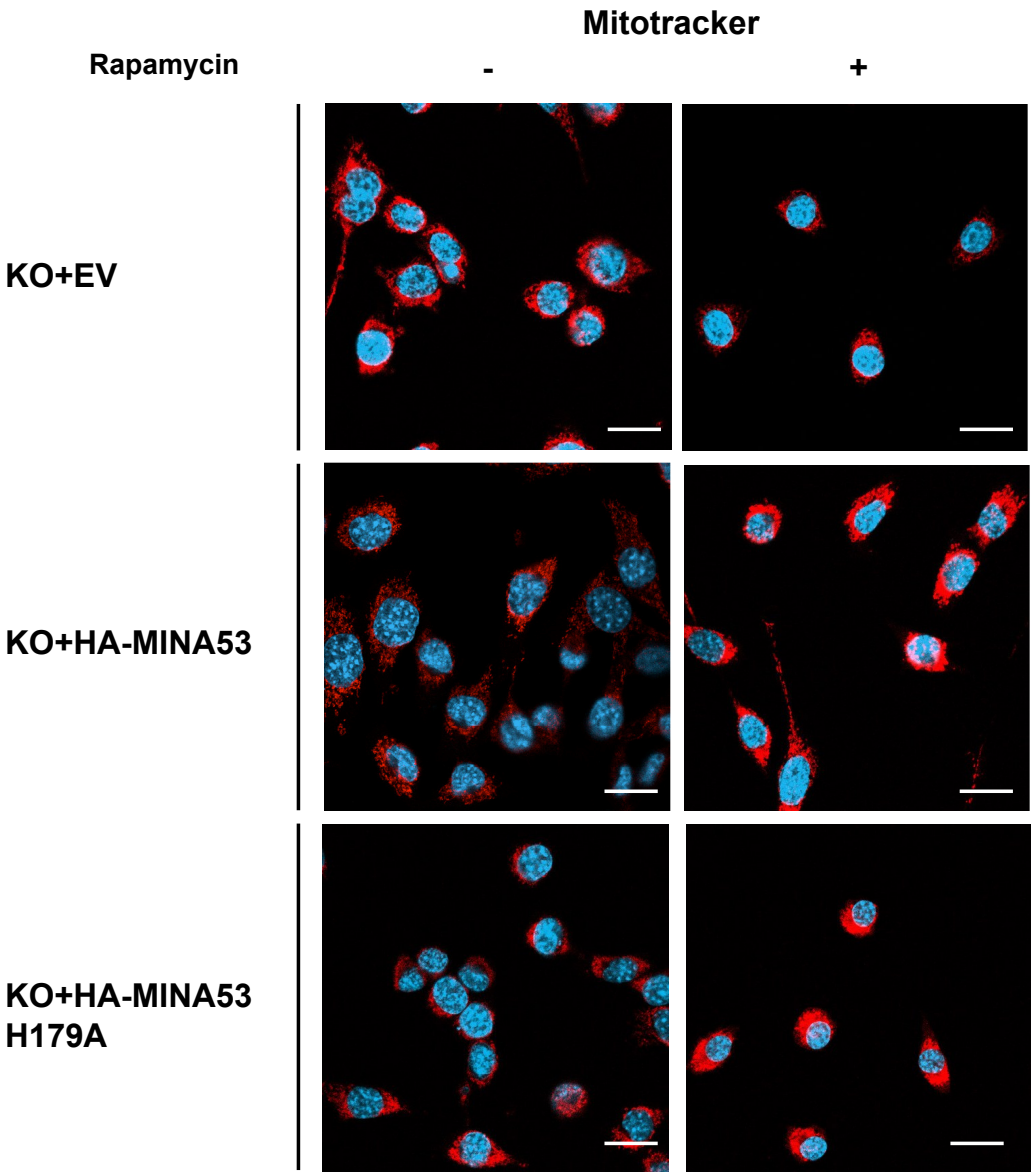

Figure 5.8. Decreased mitochondrial staining in MINA53 inactive MEFs. K-Ras transformed WT and MINA53 KO MEFs reconstituted with EV, HA-MINA53 or enzyme inactive MINA53 were treated with 1ng/ml Rapamycin for 48h after which cells were stained with Mitotracker and DAPI. Examined using a Zeiss 510 confocal microscope. Left hand column indicates reduced mitochondrial staining in cells lacking MINA53 activity. Right hand column (+Rapamycin) indicates induced mitochondrial loss, (protected in WT). White bar represent 10 μm.

loss of MTS signal following Rapamycin treatment of MINA53 KO and H179A reconstituted MEFs.

5.2.6 MINA53 enzyme activity regulates autophagy

Inhibition of mTOR is a well described stimuli of autophagy (Jung et al., 2010), (Kim et al., 2011a), a catabolic process involved in degradation of cellular components, including proteins, cell membranes and organelles, that serves to protect cells under conditions of stress and nutrient deprivation (Kundu and Thompson, 2008), (Kraft and Martens, 2012), (see Figure 5.9 and discussion). mTOR is a negative regulator of autophagy through phosphorylation of autophagy proteins ULK1/2 and Atg13 (Ganley et al., 2009), (Hosokawa et al., 2009), (Jung et al., 2009). Since autophagy can involve the destruction of mitochondria (mitophagy) (Ding and Yin, 2012), (Youle and Narendra, 2011) I therefore explored the possibility that the MINA53-dependent loss of mitochondria in response to Rapamycin was due to an autophagy defect in these cells. To begin testing this hypothesis I first measured Microtubule-associated protein 1A/1B-light chain 3 (LC3) II, a commonly used marker for autophagy. Upon induction of autophagy LC3 II binds to phoshatidylethanolamine in order to form the autophagosome (Tanida et al., 2008), and so an increase in LC3 II levels are indicative of autophagy (Figure 5.9). Consistently, each of the MEF lines showed increased LC3 II levels (and therefore autophagy) following Rapamycin treatment (Figure 5.10). Importantly, the basal levels of LC3 II were significantly elevated in untreated cells that lacked MINA53 activity, and this level was further augmented by Rapamycin treatment. Likewise, immunofluorescence staining using the

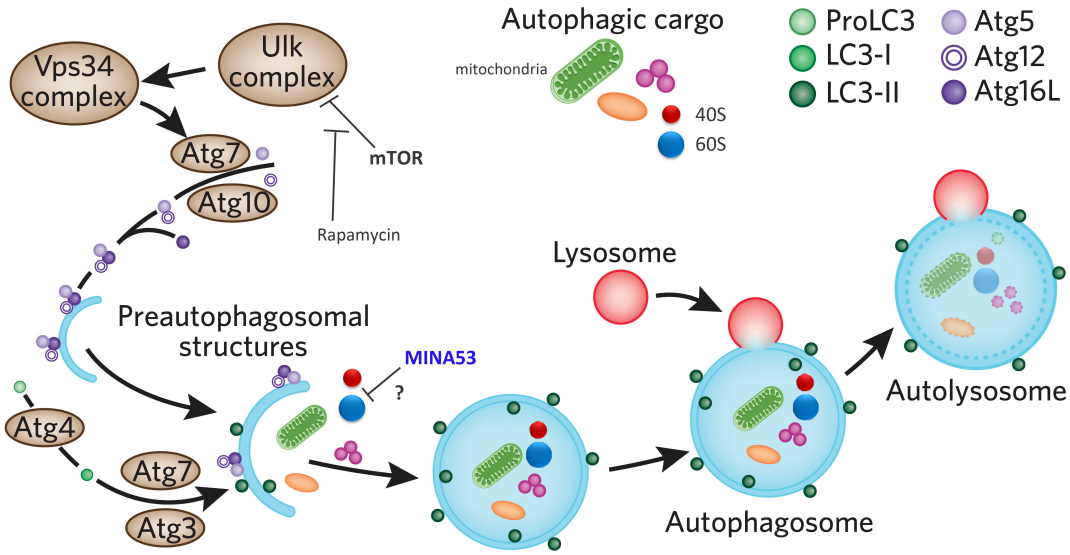

Figure 5.9. The autophagy pathway. Autophagy is initiated by the ULK complex in response to a variety of signals, including inhibition of mTOR associated with nutrient deprivation or rapamycin treatment. Double-layered membranes required for autophagosome formation are created by the Vps34 complex and Atg7/10. Two conjugation systems then add the Atg12–Atg5–Atg16L complex and LC3-II to the membrane, which folds around the target cargo, to form the autophagosome. Destruction of the contents is mediated by lysosomal fusion. The figure also depicts possible 40S and 60S 'ribophagy', a possible link to MINA53 and Rpl27a hydroxylation. This figure was adapted from (Fleming et al., 2011). Reprinted by permission from Nature Publishing Group, copyright 2010.

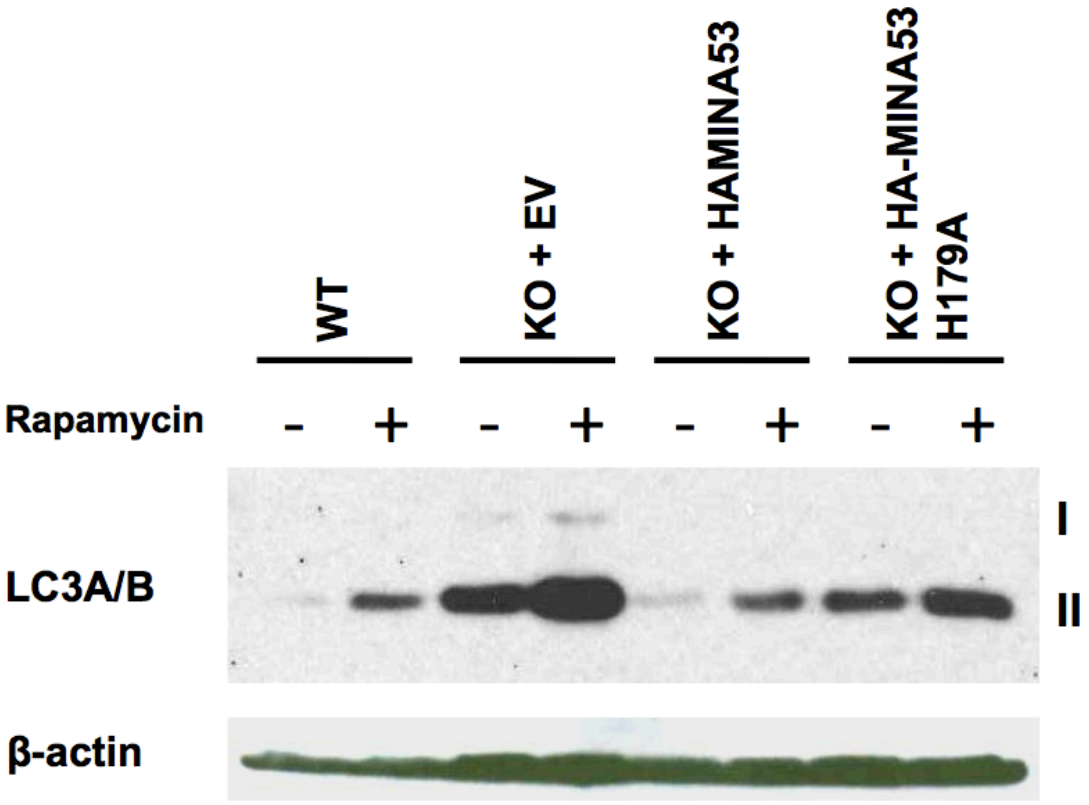

Figure 5.10. Increased autophagymarker LC3 A/B II in cells that lack MINA53 activity. Western blot of K-Ras transformed WT and MINA53 KO MEFs reconstituted with EV, HA-MINA53 or HA-MINA53 H179A. Cells were treated with 1ng/ml of Rapamycin for 72h before harvest.

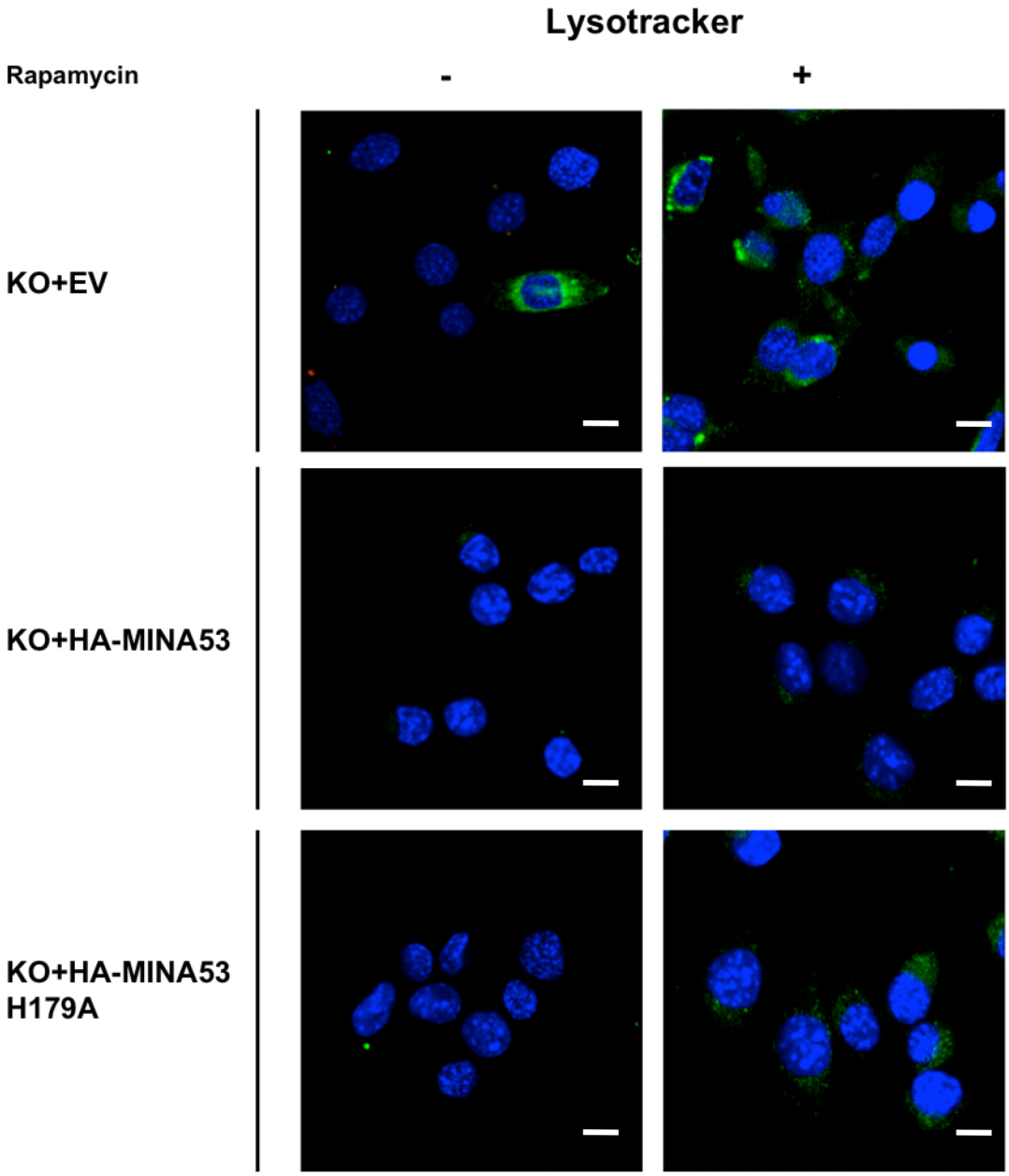

Figure 5.11. Increased autophagy in cells that lack MINA53 activity, in response to Rapamycin as indicated by Lysotracker staining. K-Ras transformed WT and MINA53 KO MEFs reconstituted with EV, HA-MINA53 or enzyme inactive MINA53 were treated with 1ng/ml Rapamycin for 48h after which cells were stained with lysotracker and DAPI. Examined using a Zeiss 510 confocal microscope. White bar represent 10 μm.

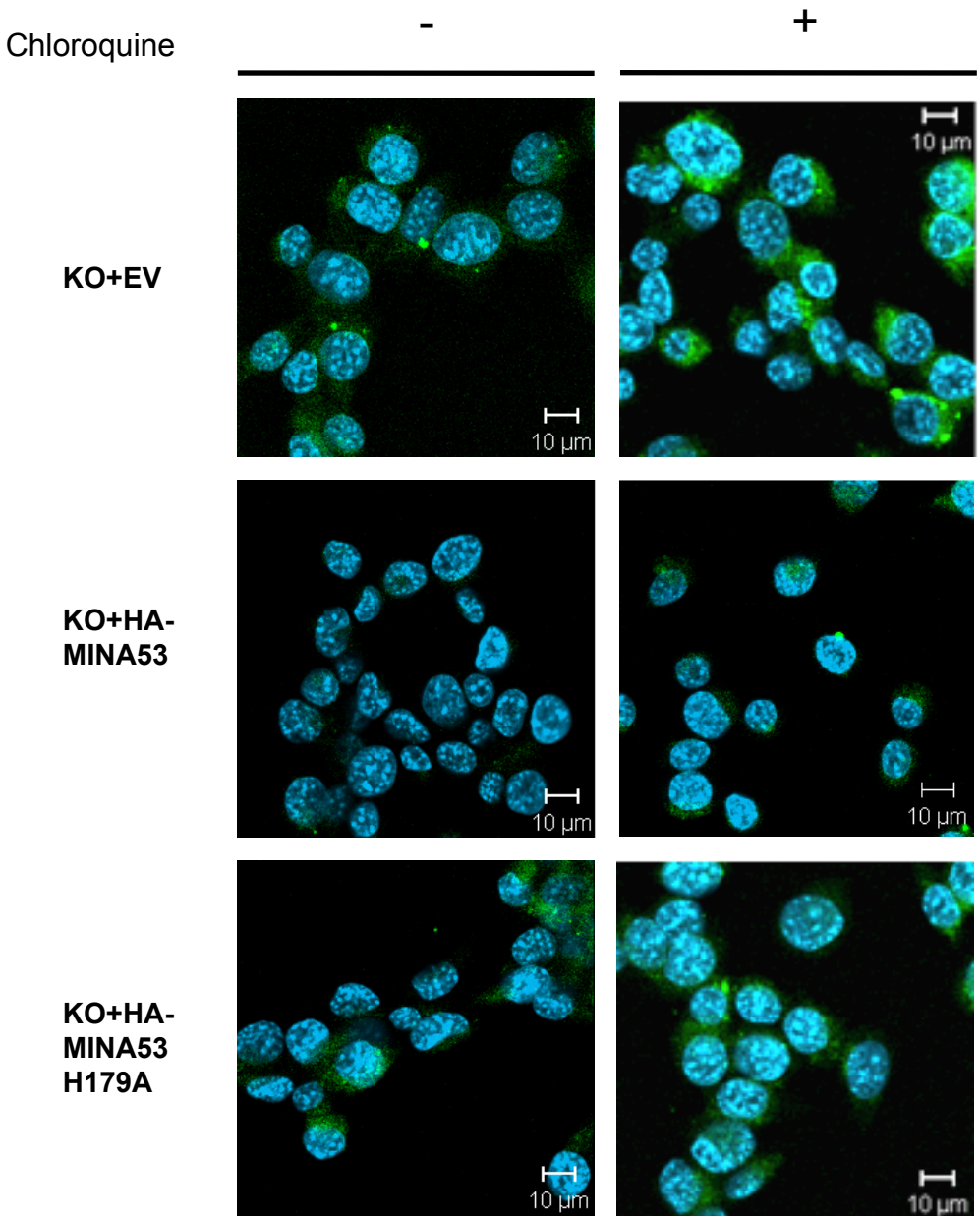

Figure 5.12. Increased autophagy in cells that lack MINA53 activity, in response to Chloroquine as indicated by Lysotracker staining. K-Ras transformed WT and MINA53 KO MEFs reconstituted with EV, HA-MINA53 or enzyme inactive MINA53 were treated with 100ug/ml Chloroquine for 4h after which cells were stained with lysotracker and DAPI. Examined using a Zeiss 510 confocal microscope.

lysosomal probe Lysotracker indicated increased Rapamycin-induced autophagy in the absence of MINA53 activity (Figure 5.11). Furthermore, cells treated with Chloroquine, an inhibitor of lysosomal acidification (Steinman et al., 1983), (thereby inducing accumulation of autophagosomes), resulted in a similar phenotype (Figure 5.12). Together, these data suggest that loss of MINA53 activity promotes basal and induced levels of autophagy.

5.3 Conclusion

In this chapter I have examined activity-dependent roles of MINA53 in ribosome biogenesis, translation and autophagy. Polyribosome profiling suggested that loss of MINA53 activity leads to a modest reduction of 60S ribosomal subunits and monosomes without any major consequences to overall protein translation. Although attempts to augment the biogenesis defect using a range of inhibitors did not elicit a significant loss of viability in KO MEFs, they did unexpectedly uncover a role for MINA53 activity in autophagy. How and whether MINA53 activity, substrate hydroxylation, 60S biogenesis, and autophagy may be related, and whether these observations also explain the phenotypes described in Chapter 4 will be discussed in detail in Chapter 7.

Chapter 6

Characterisation of two cancer mutations in MINA53

6.1 Introduction

The data presented in Chapter 3 support a role for MINA53 activity in negatively regulating anchorage-independent growth and transformation, which is at odds with reports demonstrating MINA53 overexpression in several cancers and its positive regulation of transformation in some cell types (Ogasawara et al., 2010), (Teye et al., 2007), (Ishizaki et al., 2007), (Tsuneoka et al., 2002), (Lu et al., 2009). Therefore, I searched available cancer databases to determine whether any other evidence exists to support my proposal that MINA53 may be deleterious to tumourigenesis. In this Chapter I present data that supports this hypothesis by characterising two cancer-associated mutations that inactivate MINA53 activity and fail to correct the autophagy defect or anchorange-independent growth of KO MEFs.

6.1.1 MINA53 is differentially expressed in human cancers

Initially I searched a publically available gene expression database for examples of differential MINA53 gene expression in normal versus tumour samples. Oncomine is a cancer microarray database created to facilitate investigation of data from genome wide expression analysis (Rhodes et al., 2004). In several cancer types, including prostate, lymphoma and leukemia, MINA53 was consistently upregulated compared to normal tissues (Figure 6.1). However, several other cancer types also exhibited significant downregulation of MINA53 mRNA, including; breast, head and neck, lung and pancreatic cancers (Figure 6.2, 3). The results suggest that the expression level of MINA53 differs depending on type of cancer and tissue type, and clearly shows that MINA53 is not always upregulated in tumours (Zhang et al., 2008), (Ishizaki et al., 2007), (Tsuneoka et al., 2004). The suppression of MINA53

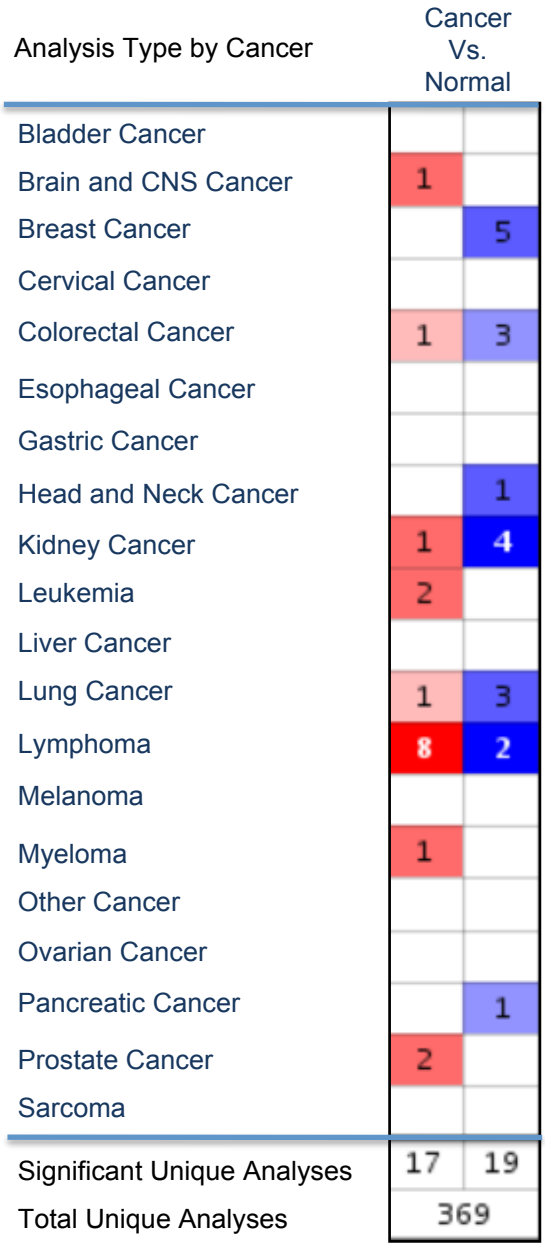

Figure 6.1. MINA53 is differentially expressed in human cancers. Data obtained from Oncomine, a human cancer microarray database. Upregulated MINA53 showed in red and downregulated MINA53 in blue. Number denotes unique microarray analyses for each cancer type. The threshold P-value is 0.01. MINA53 is differentially regulated by > 2-fold.

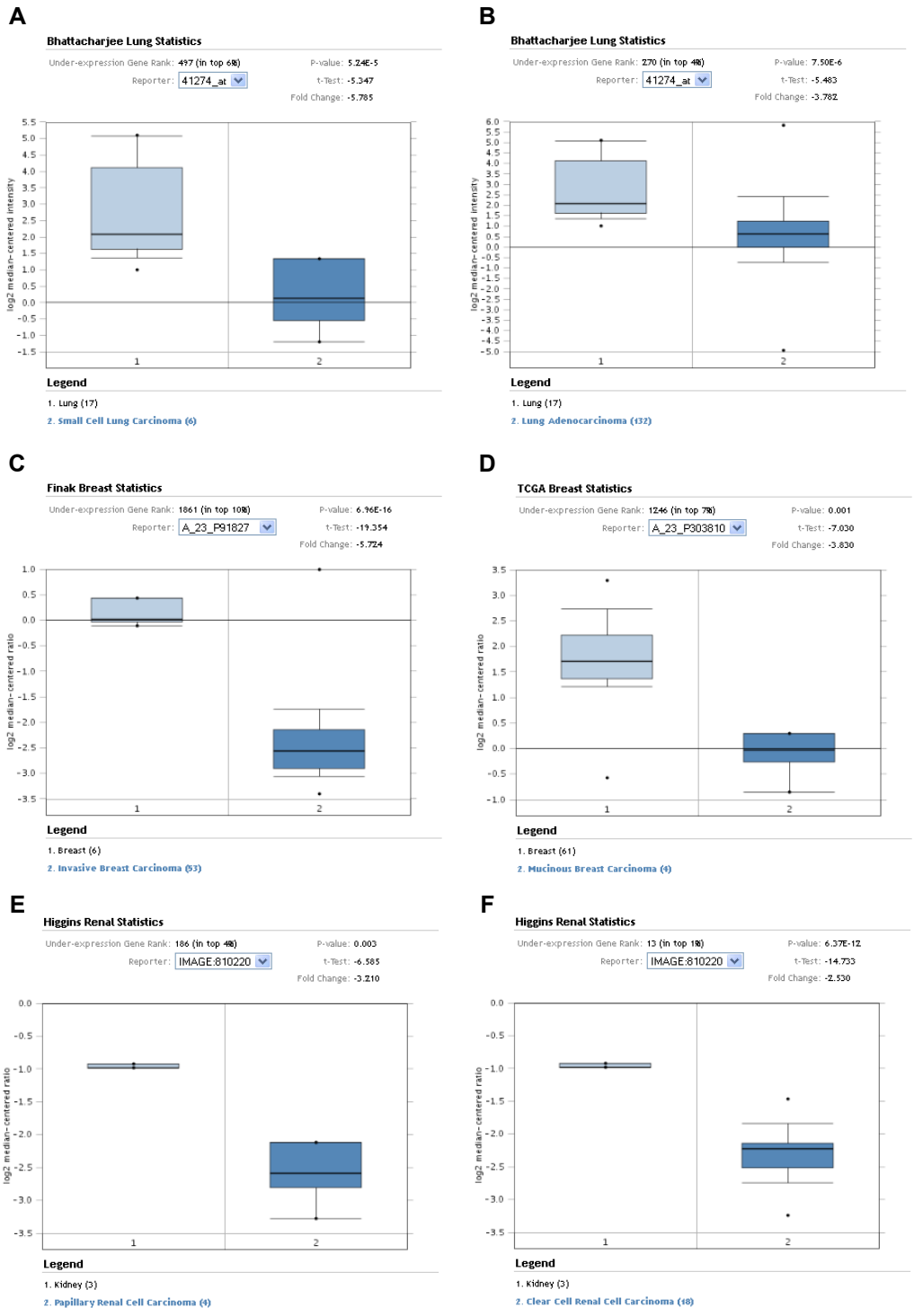

Figure 6.2. MINA53 is downregulated in several cancer types (I). MINA53 is downregulated in lung, breast and renal cancers (dark blue) as compared to normal tissues (light blue). Microarray data obtained from Oncomine database. **A.** Small Cell Lung Carcinoma. **B.** Lung Adenocarcinoma. **C.** Invasive Breast Carcinoma. **D.** Mucinous Breast Carcinoma. **E.** Papillary Renal Cell Carcinoma. **F.** Clear Cell Renal Cell Carcinoma.

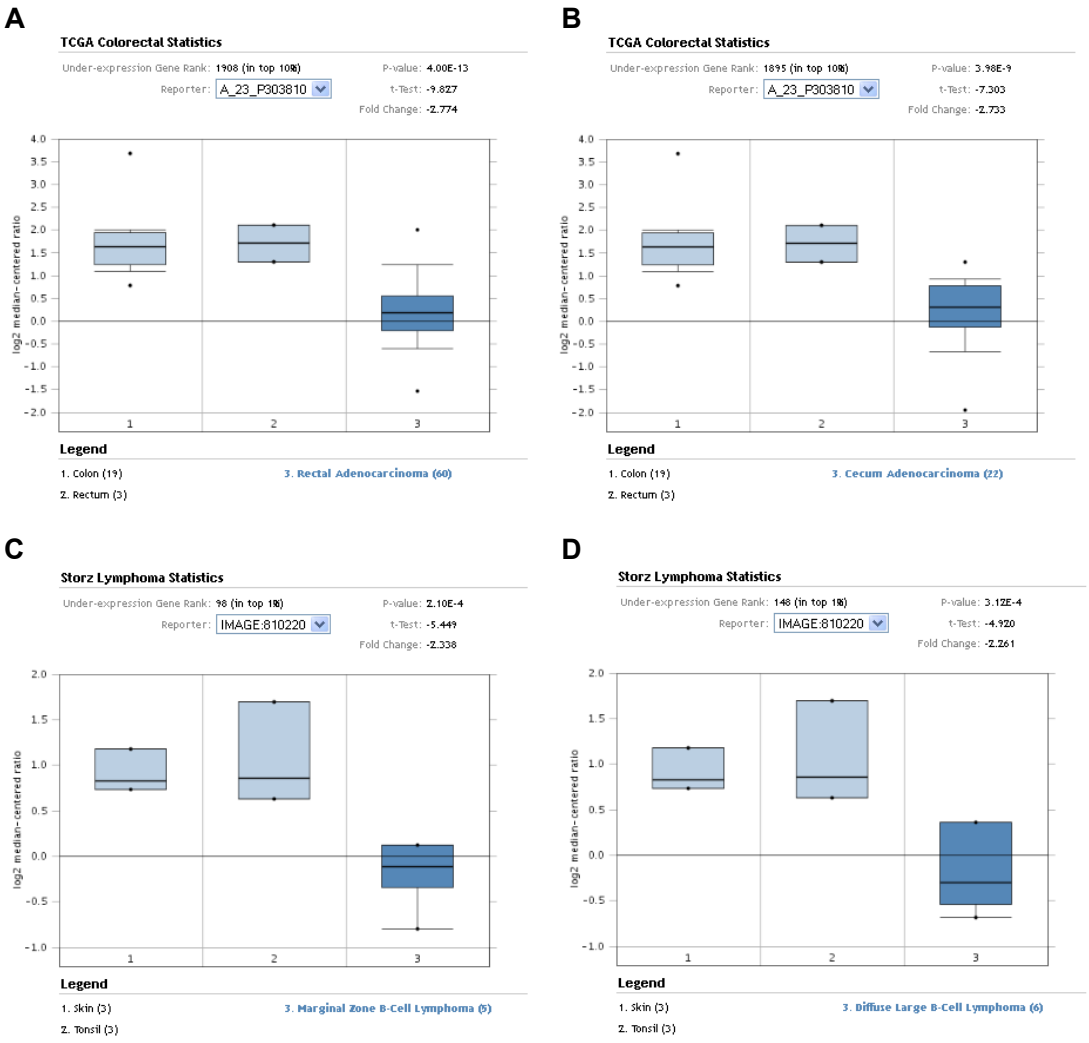

Figure 6.3. MINA53 is downregulated in several cancer types (II). MINA53 is downregulated in colorectal cancers and lymphoma (dark blue) as compared to normal tissues (light blue). Microarray data obtained from Oncomine databas **A.** Rectal adenocarcinoma. **B.** Cecum Adenocarcinoma. **C.** Marginal Zone B-cell lymphoma. **D.** Diffuse Large B-cell Lymphoma.

mRNA in some tumours suggests that the enzyme may have anti-tumourigenic properties in some tissues.

6.1.2 MINA53 is mutated in breast and ovarian cancer

To further extend these observations I next searched the Wellcome Trust Sanger Institutes COSMIC database, which contains a plethora of data on sequenced cancer genomes. Interestingly, two somatic mutations in MINA53 were described, one in breast (G175R) and the other in ovarian cancer (P341R).

6.1.3 MINA53 P341R

The P341R cancer mutation was found in an ovarian tumour. The mutation was heterozygous and the tumour histologically classified as a serous carcinoma. This tumour type arises from serum-producing epithelial cell lining the ovaries. Most low-grade serous ovarian tumours are mutated in K-Ras but lack mutations in P53 while high-grade ovarian tumours are frequently mutated in P53 (80%) but rarely in K-Ras (Vang et al., 2009). Patients diagnosed with high-grade serous carcinoma have a very poor prognosis (Li et al., 2012). In the P341R tumour sample no mutations was found for K-Ras but a homozygous mutation for P53 was identified (V157F) suggesting that the tumour might be a high-grade tumour type.

6.1.4 MINA53 G175R

In one tumour sample from a breast carcinoma a mutation at glycine 175 in MINA53 was identified, this residue was found to be mutated to arginine (G175R). Numerous coding mutations for other proteins were identified including mutations to ADAMTS-16 (R820W), and ATR (K704*). ADAMTS-16 (a disintegrin and

metalloproteinase domain with thrombospondin motifs) has no known functions but stable overexpression in chondrosarcoma cells correlated with suppression of cellular proliferation and migration (Surridge et al., 2009). ATR (ataxia telangiectasia mutated – and Rad3-related) is a critical regulator of DNA-damage response and mutations have been associated with decreased survival in certain cancers (Nam and Cortez, 2011). No further information regarding the tumour was available from the database.

6.2.1 Structural characterisation of G175R and P341R mutants

Bioinformatic sequence alignment indicates that G175 and P341 are highly conserved and therefore likely to be functionally important (see Chapter 1, figure 1.7). To attempt to determine the structural consequence of their mutation I modelled them onto an existing MINA53 structure (PDB:2XDV; Figure 6.4A). Interestingly, this analysis suggests that the G175R mutant is highly likely to be inactivating; The mutation likely interferes with the interaction of 2OG with K194 and the backbone amide nitrogen of G175 itself (Figure 6.4B). Since P341 resides outside the JmjC domain it is harder to predict the consequence of its mutation on activity/function. However, P341 does locate between the interface of the dimerisation domain and the C-terminal domain in a hydrophobic pocket that could serve to stabilise the interaction between these two regions of the enzyme (Figure 6.4C).

6.2.2 Rpl27a is not hydroxylated in HA-MINA53 G175R MEFs

I next sought to examine the effect of the cancer mutations on the enzyme activity of MINA53 by measuring Rpl27a in KO MEFs reconstituted with these mutants.

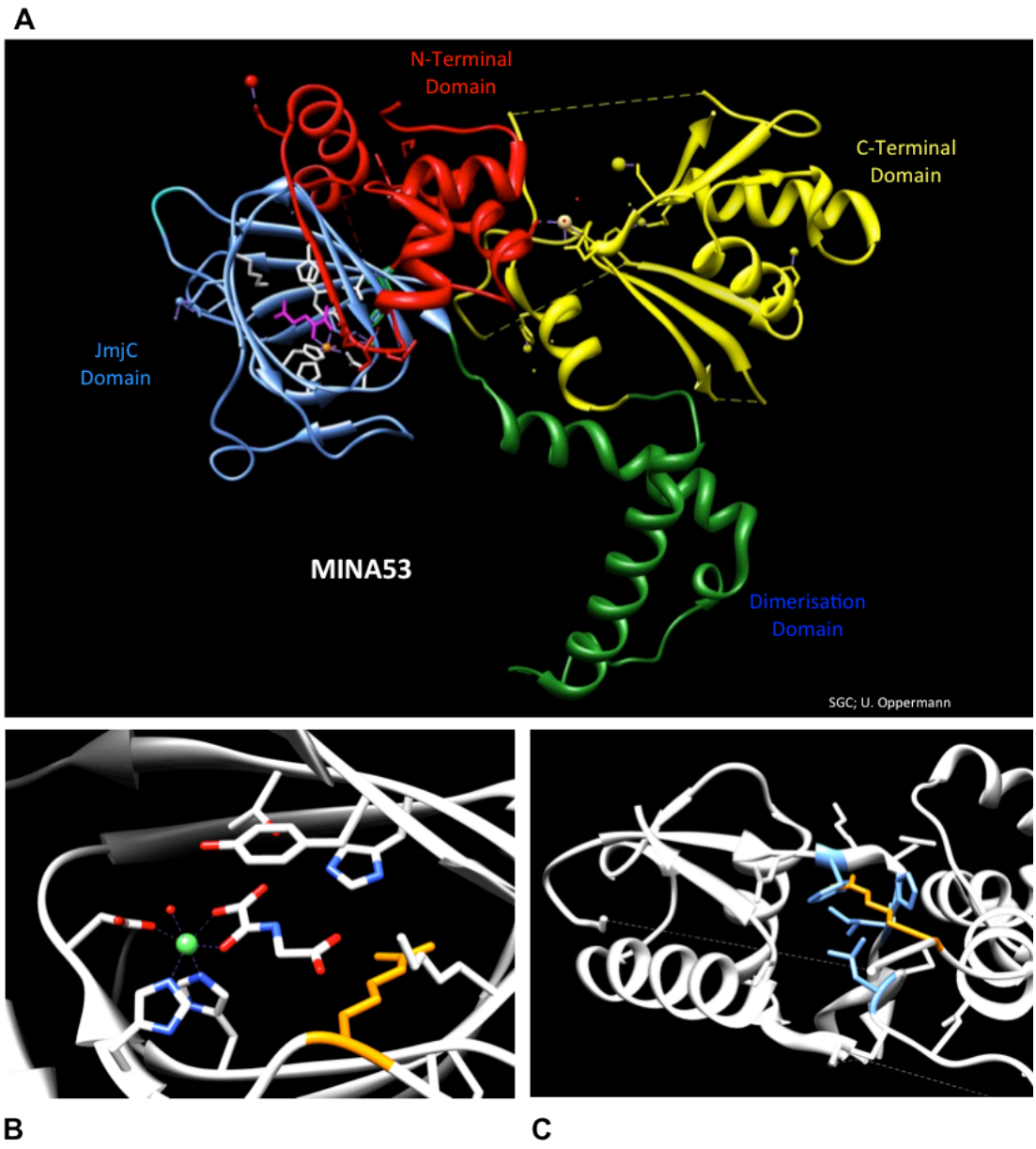

Figure 6.4. Structural model of MINA53. **A.** MINA53 with catalytic JmjC-domain in purple, N-terminal domain in red, C-terminal domain in yellow, Dimerisation domain in green. **B.** A three-dimensional view of the catalytic site of MINA53 showing the Fe(II) ion (green), stabilised by two histidine and a aspartate residue together with its cosubstrate, 2-oxoglutarate. G175 is shown mutated to arginine (marked in yellow), demonstrated potential for interference of K194A binding to 2OG. **C.** Position of P341R mutation (yellow) on structure of MINA53. Hydrophobic residues are highlighted in blue. Yellow highlights the mutated P341 to arginine.

Retroviral delivery of plasmids expressing HA-MINA53 G175R or P341R into K-Ras transformed MINA53 KO MEFs led to a level of overexpression similar to other MINA53 reconstituted cell lines (Figure 6.5). Unfortunately, initial attempts to purify endogenous Rpl27a from cells expressing the P341R mutant failed due to technical problems. However, WP-MS of Rpl27a purified from G175R MINA53 reconstituted cells was successful and indicated a complete loss of activity of this cancer mutant (Figure 6.6).

6.2.3 Anchorage-independent growth

In chapter 3 I observed a clear enzyme-dependent role of MINA53 in the suppression of anchorage-independent growth. I therefore next sought to determine if the two cancer mutations would mimic the KO and H179A-reconstituted MEFs in this respect. Interestingly, I found that the K-Ras transformed MINA53 KO MEFs reconstituted with either G175R and P341R formed significantly more colonies in 'soft-agar' compared to MEFs harbouring MINA53 activity (Figure 6.7); The number of colonies was similar to that formed by KO and H179A-reconstituted MEFs.

6.2.4 Autophagy

In Chapter 6 I describe a role for MINA53 activity in the regulation of basal and induced autophagy. In order to examine if the cancer mutants would also fail to restore normal autophagy regulation to KO MEFs I began by treating the reconstituted MEFs with a dose-titration of Rapamycin. Under these conditions

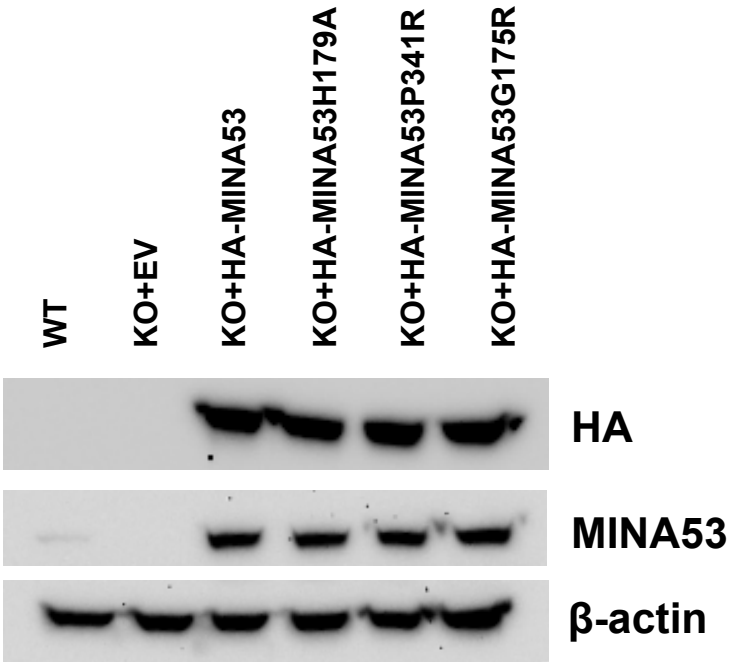

Figure 6.5. K-Ras-transformed WT and MINA53 KO MEFs reconstituted with MINA53 cancer mutations. Western blot of K-Ras transformed WT and MINA53 KO MEFs reconstituted with EV, HA-tagged wildtype MINA53, H179A, P341R and G175R.

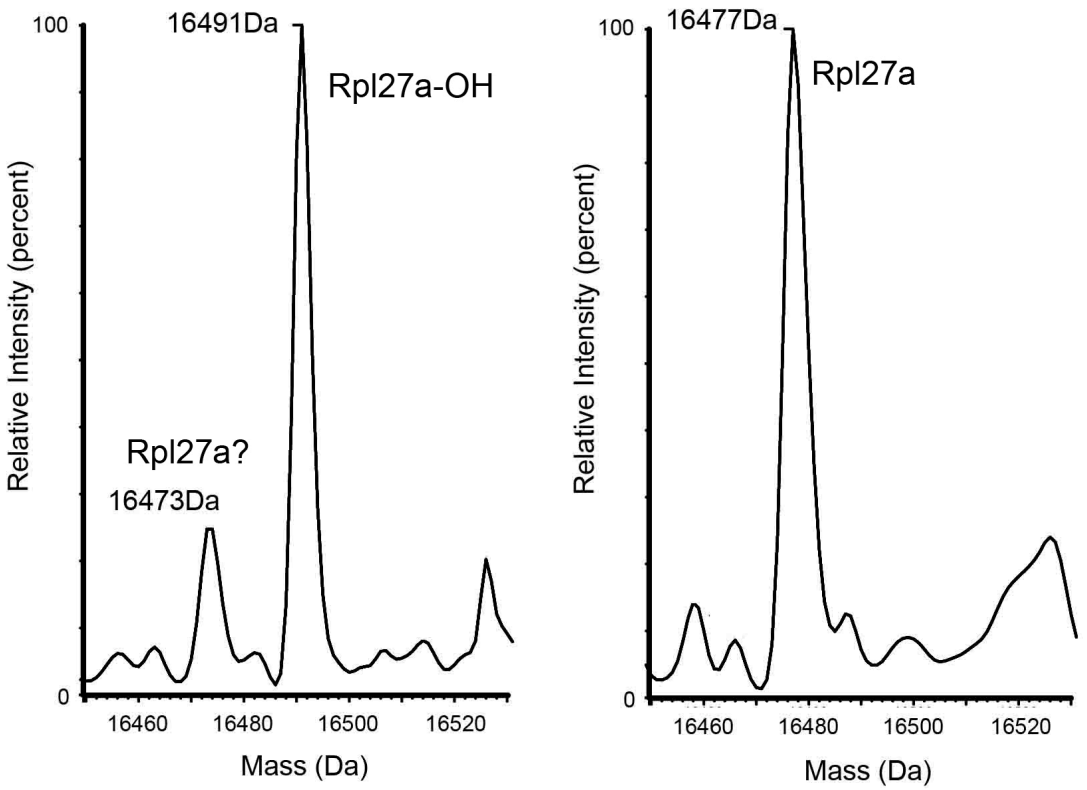

Figure 6.6. MINA53 G175R mutation leads to loss of enzymatic activity in MEFs. Endogenous Rpl27a was purified from K-Ras transformed WT (left) and MINA53 KO MEFs reconstituted with HA-MINA53 G175R (right), and subjected to analysis by whole-protein MS. WT MEFs exhibited the predicted mass of mouse Rpl27a with a +16Da mass shift (16491Da), while KO MEFs +HA-MINA53 G175R exhibited a mass of 16477Da, which likely represent unhydroxylated Rpl27a. The predicted mass for unhydroxylated Rpl27a, minus the initiating methionine, is 16474Da; the discrepancy reflects the error margin, which on this occasion was larger than normal due to technical limitations. The peak at 16473Da in WT MEFs is assigned as Rpl27a because it is the correct mass. However, this would give ~80% hydroxylation in normoxia and in the presence of MINA53 activity, which is at odds with all other analyses. It is possible therefore that this peak represents an independent protein.

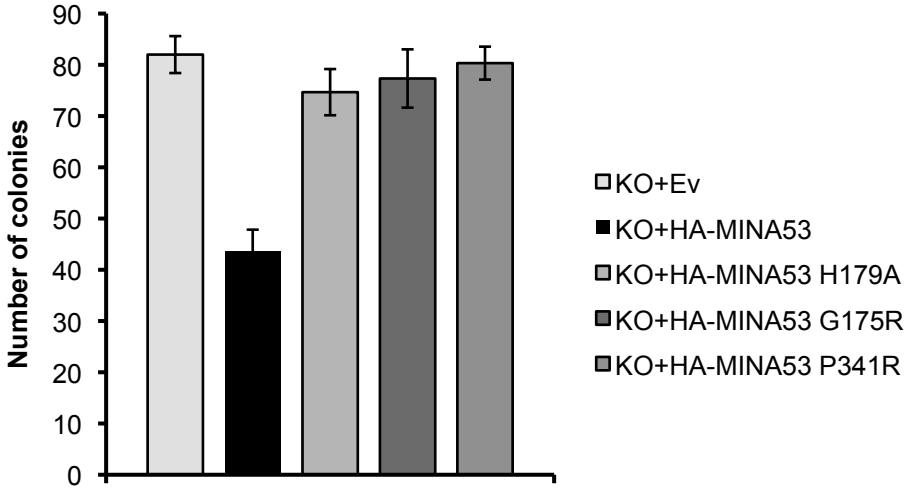

Figure 6.7. Effect of MINA53 cancer mutations on anchorage-independent growth. K-Ras transformed MINA53 KO MEFs reconstituted with EV, HA-MINA53, H179A, G175R and P341R were seeded in semi-solid Noble agar medium and allowed to grow for 4 weeks after which the soft-agar colonies were stained with crystal violet and manually counted. Graph shows number of stained and counted soft-agar colonies (± SD) after 4 weeks of growth.

both cancer mutations showed an enhanced reduction in MTS signal in response to Rapamycin that was identical to KO cells (Figure 6.8). Furthermore, both cancer mutants failed to prevent a loss of Mitotracker staining, or induction of Lysotracker staining, upon Rapamycin treatment (Figure 6.9). Finally, both cancer mutations also demonstrated increased LC3 II levels following Rapamycin (Figure 6.10), indicative of increased autophagy. Therefore, despite our inability to assay Rpl27a-OH levels in P341R MEFs, these data strongly suggest that both cancer mutations are inactive.

6.3 Conclusion

In this chapter I have provided gene expression data and genetic data that supports a negative role for MINA53 in tumourigenesis, thereby validating the results present in Chapter 3. Importantly, the fact that two independent cancer mutations prevent the enzyme activity of MINA53 is strongly suggestive of a role for one or more MINA53 substrates in tumour suppression. Whether Rpl27a fulfils this role is unclear at present. Furthermore, whether breast and ovarian tumour growth is enhanced by increased autophagy and anchorage-independent growth due to MINA53 mutation/inactivation is of interest.

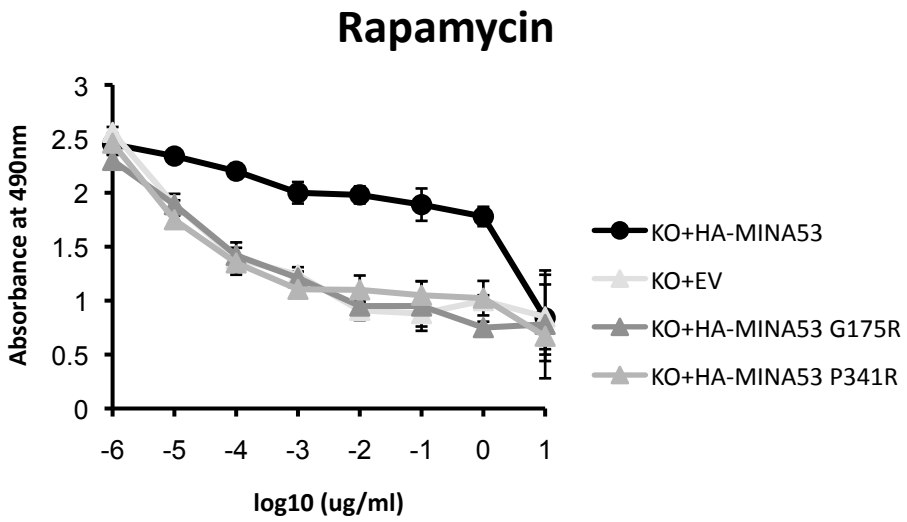

Figure 6.8. Dose-dependent inhibition of MTS signal using mTOR inhibitor Rapamycin. K-Ras transformed WT and MINA53 KO MEFS reconstituted with EV, HA-MINA53, G175R or P341R were treated with a range of doses of Rapamycin 48h before analysis using an MTS assay.

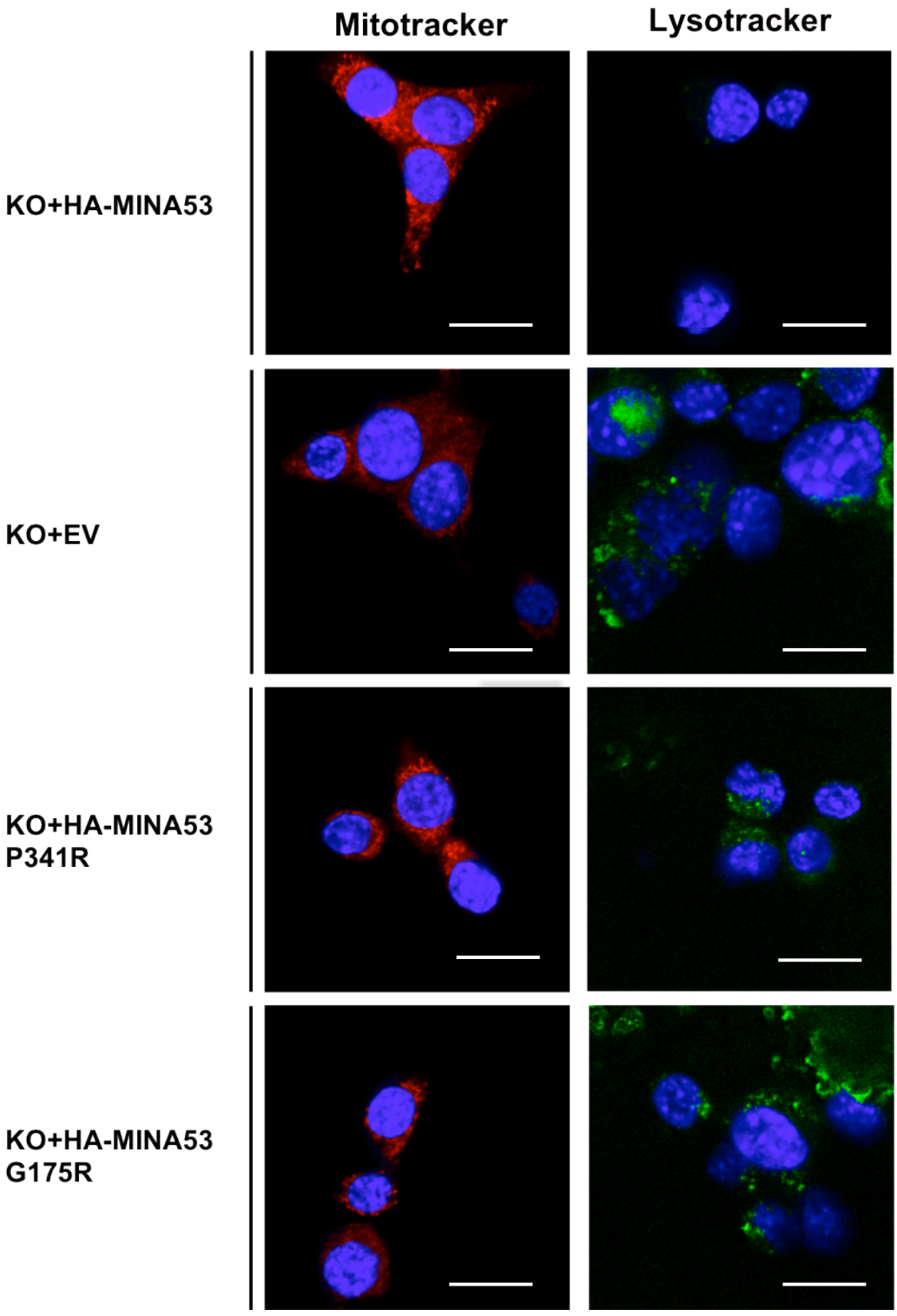

Figure 6.9. Effect of MINA53 cancer mutations on mitochondrial mass and autophagy. K-Ras transformed WT and MINA53 KO MEFS reconstituted with EV, HA-MINA53, G175R or P341R were treated with 1ng/ml Rapamycin for 48h before staining with Lysotracker (green) and Mitotracker (red) and DAPI (blue). Examined using a Zeiss 510 confocal microscope. White bar represent 10 μm.

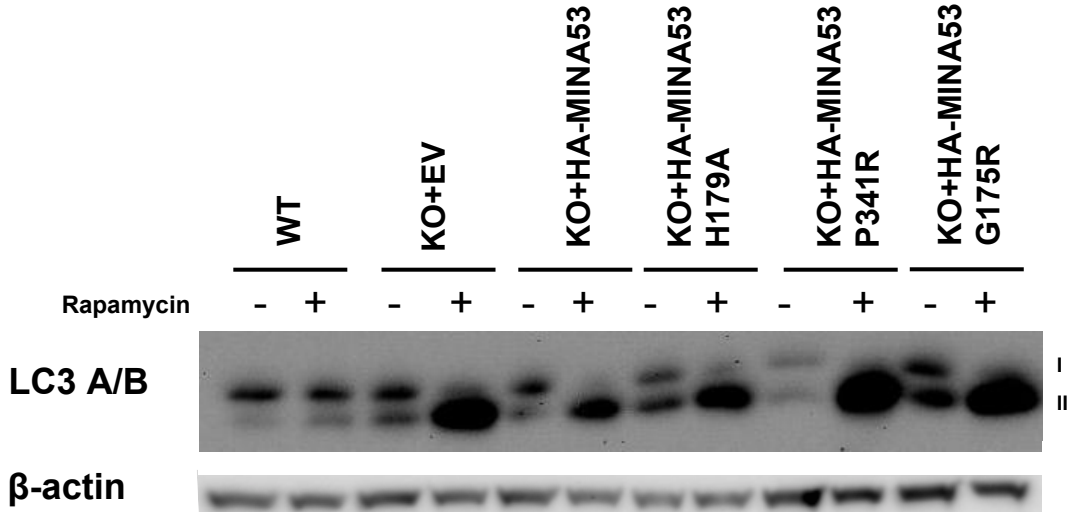

Figure 6.10. Effect of MINA53 cancer mutations on autophagy marker LC3A/B II. K-Ras transformed WT and MINA53 KO MEFS reconstituted with EV, HA-MINA53, P341R and G175R were treated with 1ng/ml Rapamycin for 48h before harvest for protein and analysed by western blot for the indicated proteins.

Chapter 7
Discussion

7.1 Overview

Initial studies aimed at replicating the published data implicating MINA53 in tumour cell proliferation led me to create an isogenic transformed MEF model for studying the role of MINA53 enzyme activity (Chapter 3). With this model I identified activity-dependent roles for MINA53 in anchorage-independent growth (Chapter 3), gene expression and 60S ribosomal abundance (Chapter 5). These phenotypes clearly demonstrated the presence of one or more MINA53 substrates, and were consistent with the discovery that MINA53 is a Histidinyl hydroxylase of the large 60S ribosomal subunit protein Rpl27a (Chapter 4). In this final chapter I discuss whether and how the MINA53 dependent hydroxylation of Rpl27a might be linked to 60S biogenesis, and in turn autophagy and tumourigenesis.

7.2 Ribosomal hydroxylation

In Chapter 4 I demonstrate that Rpl27a is hydroxylated at Histidine 39 in both human and mouse tissues, and that this modification is dependent on the enzyme activity of MINA53. Quantitative MS analysis indicated that Rpl27a was abundantly hydroxylated (>95%) in all cells and tissues studied suggesting that the modification is unlikely to fulfill a regulatory 'switch' role, such as that in the HIF system. In line with this, severe hypoxia (0.1% O_2, 72h) only modestly reduced the hydroxylation of Rpl27a (20% decrease). This suggests that MINA53 retains substantial activity under hypoxia, likely due to a high affinity for oxygen similar to other 2OG Oxygenases such as FIH (Koivunen et al., 2004), (Stolze et al., 2004). Therefore, MINA53 is unlikely to act as an oxygen sensor in the way that PHDs do in the HIF system.

As described in Chapter 1, NO66 is a 2OG oxygenase that is highly related to MINA53, both in primary sequence, subcellular localisation and regulation. Therefore, NO66 was also predicted to be a ribosomal histidinyl hydroxylase. Recent work has confirmed that NO66 targets H216 of the 60S ribosomal subunit Rpl8, and like MINA53, catalyses this modification extremely efficiently and in a manner that is relatively insensitive to hypoxia (Penny Feng, Ratcliffe laboratory, in collaboration with the Schofield laboratory). Whether other 2OG enzymes are involved in hydroxylation or demethylation of ribosomal proteins or rRNA (see below) is currently unknown, but would be of significant interest.

7.2.1 What is the *molecular* function of Rpl27a hydroxylation?

Protein hydroxylations generally serve to promote inter- and intra-molecular protein:protein interactions *via* hydrogen bonding. Therefore, it is possible that Rpl27a hydroxylation evolved to facilitate or stabilise rRNA:protein or protein:protein interactions within a ribosomal or preribosomal complex. High resolution crystal structures of mammalian ribosomes could aid in our understanding of ribosomal hydroxylation at the molecular level. However, existing structures have been obtained from lower organisms, and these lack MINA53 activity and Rpl27a hydroxylation. Although analyses of these structures places Histidine-39 in a disordered region of Rpl27a that extends deep into the ribosome, towards the tRNA exit site (data not shown), it is not immediately obvious what role modification of this residue might play. Understanding the exact molecular function of Rpl27a hydroxylation is made more challenging because the work presented in this thesis represents the first description of ribosomal

hydroxylation. This is in contrast to other modifications of the ribosome that have been more extensively studied and thus better understood.

Ribosomes are heavily modified organelles, both at the RNA and protein level. rRNA is post-transcriptionally modified by ~115 methyl groups and 95 pseudouridines in vertebrates (Maden and Hughes, 1997). Base methylation occurs in highly conserved rRNA sequences at the late stages of ribosome biogenesis (Bachellerie and Cavaille, 1997). Ribose methylation and pseudouridinylation are thought to alter the conformation and folding of rRNA (Fromont-Racine et al., 2003) preventing these modifications inhibits growth and decreases 40S abundance (Liang et al., 2009). Similar to rRNA, ribosomal proteins also show a variety of different post-translational modifications. For example, MS of 40S ribosomal proteins indicates extensive N-terminal demethionylation, acetylation and several other modifications that could not be assigned (Louie et al., 1996). Ribosomal proteins are also subject to post-translational methylation at lysine, and more predominantly arginine (Polevoda and Sherman, 2007). Preventing methylation of yeast Rpl42 at Lysine-55 causes increased cycloheximide sensitivity and abnormal growth during conditions of stress (Shirai et al., 2010). Likewise, deletion of the methyltransferase catalysing RpS2 arginine methylation in yeast causes an accumulation of 60S ribosomal subunits (Bachand et al., 2006). Arginine methylation of Rps10 is suggested to play a role in ribosome biogenesis, protein synthesis and cell growth (Ren et al., 2010). Taken together, these reports suggest that relatively subtle modifications such as methylation, and perhaps hydroxylation, could have important consequences to ribosome biosynthesis/function.

7.2.2 What is the *cellular* function of Rpl27a hydroxylation?

Rpl27a hydroxylation could play a role in either ribosome biogenesis or function. Interestingly, I have shown in Chapter 5 that cells lacking MINA53 activity show reduced 60S and monosome abundance, perhaps consistent with a role for Rpl27a hydroxylation in biogenesis of the 60S subunit. This possibility may also be consistent with observations that MINA53 is enriched in a nucleolar compartment dedicated to late stage processing of preribosomal particles (Eilbracht et al., 2005), and is associated with ribosomal proteins and RNA (Mathew Coleman, Personal Communication).

Ribosome biogenesis is a complex and energy consuming process involving almost 200 factors including RNA helicases, small nucleolar RNAs (snoRNPs), and endo- and exonucleases (Fromont-Racine et al., 2003), (Figure 7.1). Three forms of ribosomal RNA (18S, 5.8S, and 28S) are transcribed as a large pre-rRNA complex by RNA polymerase I from tandemly-repeated rDNA genes in the nucleolus. The fourth rRNA form (5S) is transcribed by RNA polymerase III in the nucleus and imported into the nucleolus. These transcripts are then cleaved, processed and subject to extensive methylation and pseudouridylation, as outlined above (Fromont-Racine et al., 2003), (Granneman and Baserga, 2004). Ribosomal proteins are added to the 40S RNA and 60S precursors at later stages in the nucleolus before the subunits are exported and further processed in the nucleus and cytoplasm (Fromont-Racine et al., 2003), (Granneman and Baserga, 2004). Considering that MINA53 is enriched in the nucleolar compartment responsible for these later stages of biogenesis (Eilbracht et al., 2005), it is interesting to speculate

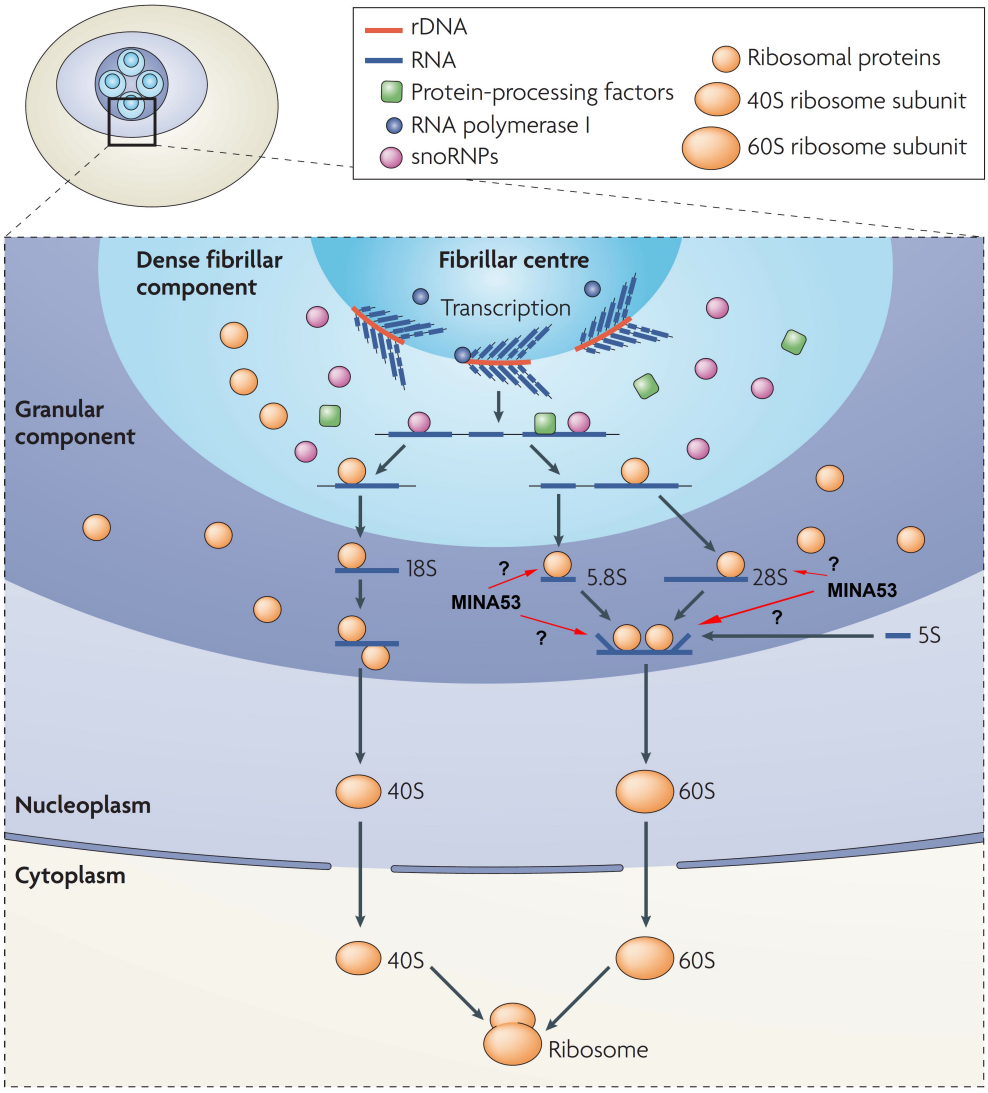

Figure 7.1. Ribosome biogenesis begins with the transcription of ribosomal DNA (rDNA) by RNA polymerase I at the border between the fibrillar centre (FC) and the dense fibrillar component (DFC). Full-length rRNA is then spliced and modified by small nucleolar ribonucleoproteins (snoRNPs) in the DFC. The pre-ribosomal complexes are assembled with ribosomal proteins in the granular component (GC), which is the region in which MINA53 is specifically enriched. The 5.8S and 28S rRNAs assemble with 5S rRNA to form the 60S subunit in the GC. This process could be regulated by MINA53 and Rpl27a hydroxylation (red arrows), although potential mechanisms are unknown (?). The mature 40S and 60S subunits are exported to the cytoplasm for mRNA translation. This figure was adapted from (Boisvert et al., 2007). Reprinted by permission from Nature Publishing Group, copyright 2007.

that hydroxylation could regulate the assembly of Rpl27a with rRNA and/or other ribosomal proteins. In this regard, it is of interest that Rpl27a is one of the first ribosomal proteins loaded onto rRNA during the 60S biogenesis pathway. Furthermore, the *S. cerevisiae* homologue of Rpl27a (Rpl28) was recently implicated in facilitating correct positioning of rRNA in the large ribosomal subunit (Poll et al., 2009).

7.3 MINA53 activity regulates autophagy

The modest reduction in 60S and monosome abundance in cells lacking MINA53 activity is not sufficient to reduce protein synthesis (as judged by polysome number and abundance) or growth in these cells. However, I considered that it may be possible to exacerbate the ribosomal subunit disturbance and precipitate a proliferative defect by treating MINA53 KO cells with drugs known to target pathways regulating translation and/or biogenesis. Whereas translational inhibitors such as anisomycin, sparsomycin and cycloheximide had no effect, Rapamycin and its analogue Everolimus showed a dramatic loss of MTS signal in cells lacking MINA53 activity. Surprisingly however, this was not associated with a reduction in cell viability (in fact, a slight increase in cell number was observed), but instead correlated with a loss of mitochondrial mass, likely due to increased autophagy and associated mitophagy in response to mTOR inhibition (Chapter 5). Interestingly, two of the other agents tested (LY294002 and Actinomycin-D) also showed a similar phenotype, although the difference was less apparent. Considering the Rapamycin results these agents should be re-visited to determine whether the differential loss of MTS signal in MEFS lacking MINA53 activity represents reduced cell viability or increased mitophagy/autophagy. Interestingly,

all the agents demonstrating this activity-dependent effect in the MTS assays could be considered to target the same pathway regulating ribosome biogenesis (PI3K-mTOR-RNA Polymerase I).

7.3.1 How does MINA53 activity regulate autophagy?

It is of interest that mTOR inhibition is thought to stimulate autophagy by mimicking nutrient deprivation (Altman and Rathmell, 2012). Is it possible that the decrease in 60S and monosome abundance in cells lacking MINA53 activity is interpreted as a response to nutrient deprivation? This could stimulate the basal levels of autophagy observed in MINA53 KO cells, which may in turn sensitise them to mTOR inhibition (Figure 2).

Recent work in yeast describes a specific autophagy pathway for degradation of ribosomes under nutrient starvation conditions, termed 'ribophagy' (Beau et al., 2008). Interestingly, ribophagy consists of independent pathways for the degradation of the small and large subunit. Therefore, it remains a possibility that the reduced 60S levels in cells lacking MINA53 activity are due to increased autophagy and 60S ribophagy, as opposed to decreased 60S biogenesis. In this scenario, autophagy/ribophagy would be causal with respect to reduced 60S abundance, rather than *vice versa* (Figure 7.2). If true, this would make it necessary to evoke an alternative hypothesis of autophagy regulation by MINA53 activity, such as specific gene regulation (see Section 7.5).

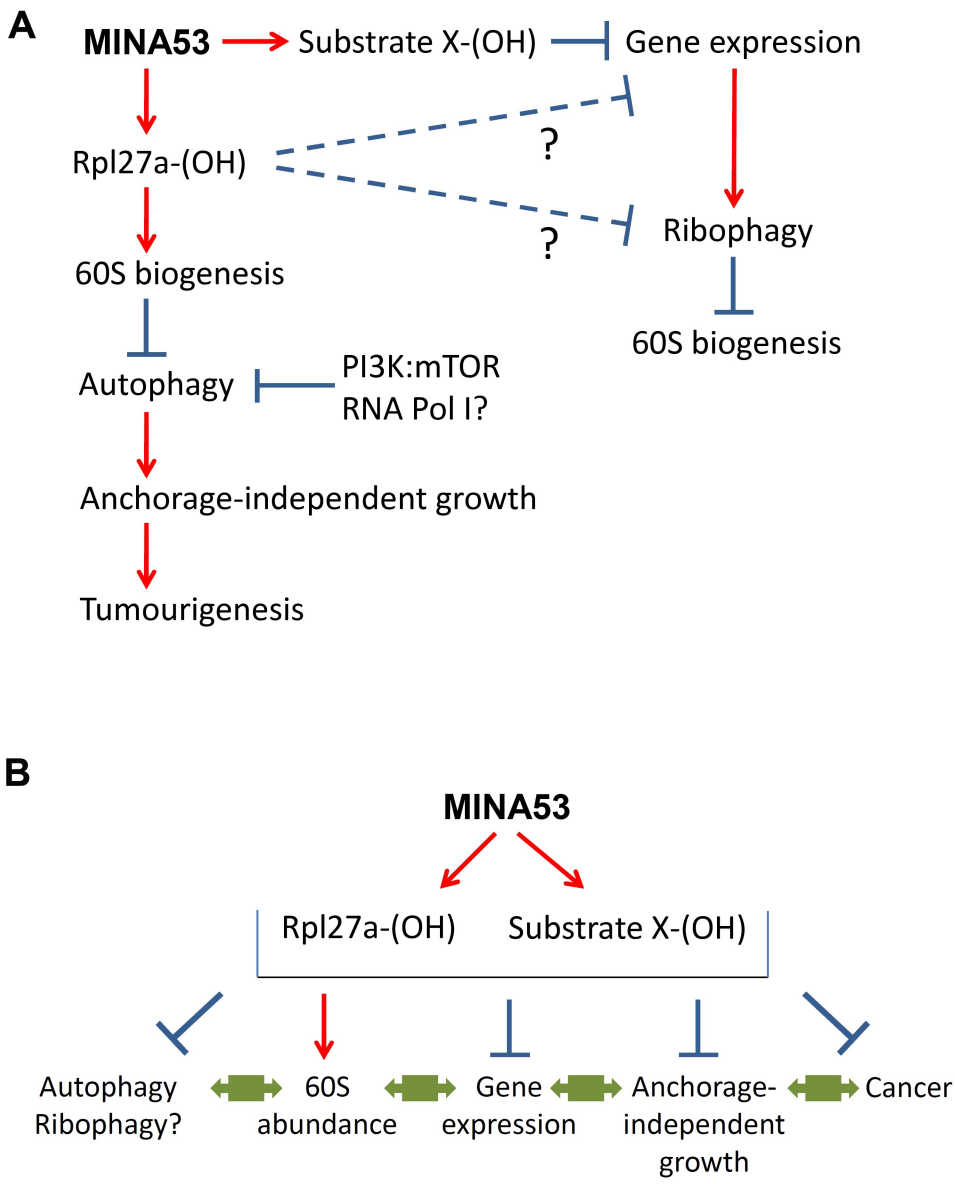

Figure 7.2. Models of regulation by MINA53 enzyme activity. Two models are presented highlighting possible links between the activity-dependent phenotypes described in this thesis. **A.** A more direct model by which Rpl27a hydroxylation regulates 60S biogenesis and in turn autophagy, anchorage-independent growth and tumourigenesis. The possibility that alternative substrates exist is highlighted, particularly their role in gene expression, but note that these substrates could play a role in any of the phenotypes observed. The possibility that MINA53 regulates 60S abundance *via* ribophagy is also shown, with possible regulatory links highlighted. **B.** A more indirect model by which substrates could regulate the observed activity-dependent MINA53 phenotypes, in which each of the processes has the potential to regulate any of the others.

7.4 Autophagy, anchorage-independent growth, and cancer

Whatever the mechanism by which MINA53 regulates autophagy, the enhanced autophagy levels in cells lacking MINA53 activity could explain their increased anchorage-independent growth; Autophagy has been implicated in stimulating K-Ras transformation. Overexpression of K-Ras induces Atg-5 and -7, and their suppression by shRNA inhibits anchorage-independent growth and xenograft tumourigenesis (Kim et al., 2011b), (Guo et al., 2011). It has been proposed that autophagy promotes K-Ras transformation by maintaining a healthy pool of organelles for cell proliferation and providing energy metabolites during periods of low nutrient availability (Brech et al., 2009). Autophagy also supports increased glucose uptake in Ras-transformed cells, suggesting one possible mechanism by which autophagy promotes transformation (Lock et al., 2011).

In the context of human cancer, autophagy is thought to have either an inhibitory or a stimulatory role, depending on the stage of tumourigenesis. Currently, it is thought that autophagy negatively affects tumour initiation but once the tumour is established it promotes cell survival and enhances adaptation to various stresses (Liu and Ryan, 2012). It is interesting to speculate that these opposing roles of autophagy could explain the observation that MINA53 is upregulated in some cancers, and downregulated or inactivated in others.

Our attempts to model the role of MINA53 enzyme activity in tumour growth were unsuccessful; whereas MINA53 regulates autophagy in an enzyme-dependent manner *in vitro*, xenograft growth was largely enzyme-independent. This suggests that MINA53-dependent regulation of autophagy (which is an activity-dependent

phenotype) is unlikely to play a significant role in xenograft tumour growth, at least in the cellular model described here. It would be useful to repeat an isogenic MINA53 rescue experiment in a human tumour cell line to explore this further; efforts are underway using an A549 ShRNA knockdown clone (Chapter 2), which showed complete loss of MINA53 activity (Chapter 4).

Why xenograft tumour growth was largely independent of enzyme activity when anchorage-independent growth was completely dependent is unclear but presumably relates to the more complex environment in which cells grow in a tumour.

7.5 MINA53 regulates gene expression

Chapter 3 describes a gene expression profiling experiment that was undertaken in order to identify candidate genes and signaling pathways that could play a role in the MINA53-dependent phenotypes observed early in this study. Overall, chronic loss of MINA53 activity only had modest effects on gene expression. Although these effects were both positive and negative, and activity-dependent and –independent, the largest group of regulated genes was that *repressed* by MINA53 *activity*. Pathway analysis indicates these genes are involved in translation, proliferation, cell growth, cell metabolism, cell signaling and ATP production. Interestingly, several of the most downregulated genes were elongation translation factors (eIFs), which are commonly upregulated in tumours, and correlate with increased survival and proliferation. For example, eIF4B which was downregulated uniquely in the MINA53 KO+HA-MINA53 MEF background, is required for tumour cell growth and survival (Shahbazian et al., 2010). It is

possible that activity-dependent repression of gene expression may contribute to the role of MINA53 in anchorage-independent growth, or in fact any of the other phenotypes described here (Figure 7.2B).

How does MINA53 activity regulate gene expression? The mechanism(s) involved could be direct, such as hydroxylation of a transcription factor or an extra-ribosomal function of Rpl27a (Figure 7.2A), or more indirect, downstream of effects on ribosomal function for example (Figure 7.2B). Interestingly, many ribosomal proteins are known to have extra-ribosomal functions; ribosomal protein S3 functions as a DNA repair endonuclease (Kim et al., 1995), ribosomal protein L13a interacts with the IFN-gamma activating inhibitor of translation (GAIT) complex to inhibiting translation of specific mRNAs (Mazumder et al., 2003), (Kapasi et al., 2007), and ribosomal protein L10 regulates c-Yes tyrosine kinase (Oh et al., 2002). Furthermore, under conditions of nucleolar stress specific ribosomal proteins can migrate from the nucleolus into the nucleus where they interact with and inhibit MDM2 E3 ligase activity leading to p53 activation (Chen et al., 2007), (Dai and Lu, 2004), (Jin et al., 2004), (Lohrum et al., 2003). Interestingly, it was recently suggested that Rpl27a might also be involved in a similar mechanism as Rpl27a mutation phenocopies models of elevated p53 in mice (Terzian et al., 2011). Taken together, these reports suggest that exploring the role of Rpl27a hydroxylation in regulating transcription factor activity would be of interest. However, since the described isogenic MEF model was immortalized with Large-T Antigen, these cells would not be suitable for studying any consequences on p53 activity.

Although MINA53 is *enriched* in the nucleolus, it is also found diffusely expressed through the nucleoplasm (Chapter 3, and (Eilbracht et al., 2005). This could be consistent with a direct role for MINA53 in regulating gene expression (Figure 7.2A), perhaps at the level of chromatin conformation (similar to a histone demethylase) or transcription factor activity (akin to FIH). Targeting of factors regulating gene expression could be consistent with the localisation of MINA53 to the IL4 promoter (ChIP analysis) (Okamoto et al., 2009) and the regulation of histone methylation marks (Lu et al., 2009) likely indirect as we have not detected any histone demethylase activity). Although existing proteomic data has not yet provided any good candidates for substrates in these pathways, it is interesting to note that the MINA53 hydroxylation motif in Rpl27a (G-[LM]-H-[HKR]-H-R) is present in several proteins, including transcriptional regulators (Figure 7.3). Interestingly, one of these, termed ZFHX3 (ATBF1), is a large transcriptional repressor protein consisting of 23 zinc-fingers, the last of which at the extreme C-terminus contains the putative MINA53 hydroxylation motif. Since ZFHX3/ATBF1 is a tumour suppressor gene that is mutated or deleted in several cancers (Cho et al., 2007), (Sun et al., 2007), (Kataoka et al., 2001) this protein warrants further investigation as a candidate MINA53 substrate that regulates gene expression.

7.6 MINA53 is mutated and inactivated in cancer

Despite the discrepancy between the effects of MINA53 activity in anchorage-independent growth *in vitro* versus xenograft growth *in vivo,* there is good genetic evidence for a negative role of MINA53 *activity* in some human tumours. Chapter 6 describes two MINA53 mutations detected in human tumours; G175R was sequenced from a breast carcinoma, and P341R from an ovarian serous carcinoma

Accession	Name	Description	Function
P46776	RPL27A	60S ribosomal protein L27a	Ribosomal function/assembly
Q15911	ZFHX3	Zinc finger homeobox protein 3	Transcriptional repressor
Q14929	ZN169	Zinc finger protein 169	Transcriptional regulation
Q96H40	ZN486	Zinc finger protein 486	Transcriptional regulation
Q01538	MYT1	Myelin transcription factor 1	Transcription factor
Q9NYV4	CDK12	Cyclin-dependent kinase 12	Transcriptional elongation/RNA splicing
P50748	KNTC1	Kinetochore-associated protein 1	Mitotic checkpoint
Q7L2E3-2	DHX30	ATP-dependent RNA helicase	RNA unfolding
Q96LT4-2	SAMD8	Sphingomyelin synthase-related protein 1	Lipid metabolism
O15169-2	AXIN1	Axin-1	Beta-catenin destruction
Q5KSL6	DGKK	Diacylglycerol kinase kappa	Generates phosphatidic acid
Q8N3F8	MILK1	MICAL-like protein 1	Cytoskeletal regulator
Q9NYC9	DYH9	Dynein heavy chain 9, axonemal	Force generating protein
Q8NEM7	FA48A	FAM48A	p38 MAPK Activation
Q01959	SC6A3	Sodium-dependent dopamine transporter	Amine transporter
Q99698-3	LYST	Lysosomal-trafficking regulator	Sorting of endosomal proteins
Q8IY33-4	MILK2	MICAL-like protein 2	Cytoskeletal regulator
Q13488	VPP3	V-type proton ATPase 116 kDa subunit a isoform 3	Proton channel

Figure 7.3. Candidate substrates for MINA53 identified *in silico*. The online Prosite tool was searched with the Rpl27a hydroxylation motif G-[LM]-H-[HKR]-H-R, with conservative substitutions allowed in regions identified as less critical for Rpl27a modification (Dr Wei Ge, Schofield Laboratory). This search returned 18 hits in humans, and included Rpl27a and 5 transcriptional regulators.

tumour. Reconstituting these mutants into the isogenic MINA53 KO model suggested they were likely inactive, since they failed to repress the anchorage-independent growth or autophagy phenotypes. Indeed, preliminary biochemical analysis of cells expressing G175R confirmed the complete absence of Rpl27a hydroxylation. This is consistent with the structural analysis indicating that this mutation is likely to strongly interfere with binding of 2OG.

During the course of writing this thesis a new mutation of MINA53 (K389N) was reported in a colon adenocarcinoma (Wellcome Trust Sanger Institutes COSMIC database). K389 resides on the edge of the C-terminal domain and points towards the dimerisation domain, perhaps playing a role in an interaction between these two domains that would be disrupted upon mutation to the shorter side chain of Asparagine (Figure 7.4). It will be interesting to reconstitute this new cancer mutant into our MINA53 KO model in order to assess its enzymatic activity.

Although relatively few cancer mutations have been sequenced thus far, the proportion of mutations overall is 3% (3 mutations in 94 examples), with 8% in breast and large intestine (1 out of 12 in each case), and 100% in ovarian cancer (1 out of 1). It is interesting to note that the cancer types in which mutations have been sequenced thus far correlate with those with reduced MINA3 mRNA expression (Chapter 6). Therefore, it is possible that inactivating mutations in MINA53 will be sequenced in other tumour types such as lymphoma, lung and kidney cancer in the future. Overall, these findings suggest the need for a focused effort to specifically sequence MINA53 in a large number of tumours, particularly those in which MINA53 mRNA is downregulated. In conclusion, inactivating

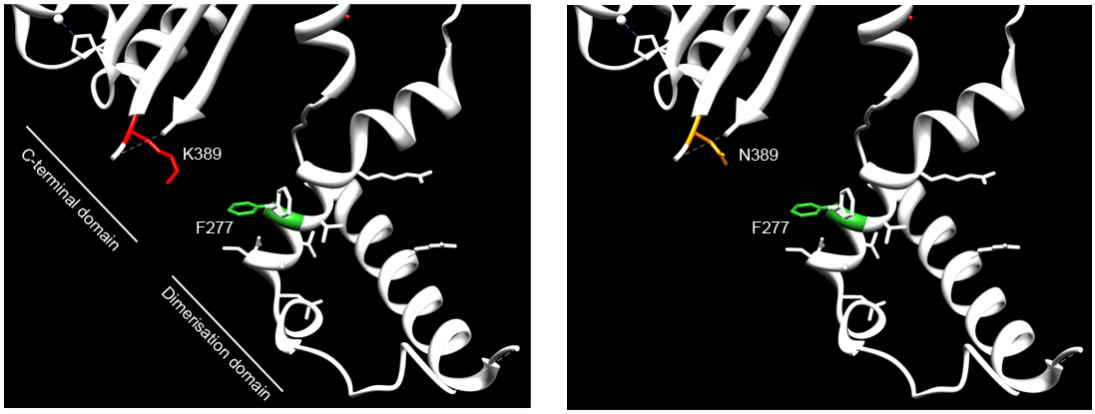

Figure 7.4. MINA53 K389N mutation in colon adenocarcinoma. K389 (red) is located on the edge of the C-terminal domain of MINA53 pointing towards residues (green) on the predicted dimerisation domain (left panel). The K389N mutation (orange) results in a shorter side chain that could disrupt any interaction between the two domains (right panel). Images were produced using Chimera software and data from the Oppermann laboratory (SGC, Oxford; PDB 2XDV).

mutations provide *strong* genetic evidence that MINA53 activity plays a role in suppressing tumour growth. How it does this is not clear, but considering the data I have presented on MINA53's role in regulating autophagy, correlating MINA53 status and autophagy in human tumours would be of interest.

7.7 2OG Oxygenases as cancer targets

As discussed above, I have shown that MINA53 is underexpressed or mutationally inactivated in specific tumour types, suggesting it is a tumour suppressor gene in some cells. Interestingly, other 2OG Oxygenases have also been implicated as tumour suppressor genes; UTX is a H3K27 histone demethylase that is mutated and inactivated in several cancers (van Haaften et al., 2009), and the H3K36me1/2 demethylase JHDM1B is a putative tumour suppressor that is mutated in lymphoma and underexpressed in glioblastoma multiforme (Cloos et al., 2008), (Frescas et al., 2007).

The majority of the available literature on MINA53 argues that it is generally overexpressed in tumours and therefore a good anti-cancer target. Other 2OG Oxygenases have also been reported as overexpressed in cancer and suggested as potential chemotherapeutic targets, including JMJD2C and JARID1, (Blair et al., 2011), (Ishimura et al., 2009; Italiano et al., 2006). The work in this thesis suggests that an essential aspect of any preclinical investigation into the candidacy of a 2OG Oxygenase as an anti-cancer target should include a survey of its expression and mutational status in a variety of tumour types.

Chapter 8
Materials and Methods

8.1 Reagents

8.1.2 Buffers

PBS

Phosphate-buffered saline (PBS) PBS was purchased in tablet form (Sigma-Aldrich) and prepared by dissolving 1 tablet in 200ml MilliQ-grade water.

PBST

0.1% (v/v) Tween-20 in PBS.

PBSTB

PBS with 0.5 % (v/v) Triton-X-100 and 1% (w/v) BSA.

Agarose gel loading buffer (5x)

50% (v/v) 10x TBE, 50% (v/v) glycerol, 0.05% (w/v) bromophenol blue.

SDS-PAGE resolving (lower) gel buffer (4x)

Tris-HCl pH 8.8 1.5 M, sodium dodecylsulphate (SDS) 0.4% (w/v).

SDS-PAGE stacking (upper) gel buffer (4x)

Tris-HCl pH 6.8 1.5 M, SDS 0.4% (w/v).

SDS-PAGE electrophoresis buffer (10x)

Tris(-hydroxymethyl)aminomethane (Tris) 0.25 M, glycine 1.9 M, SDS 1% (w/v). The 10x concentrate was diluted to 1x using MilliQ-grade water prior to use.

Protein transfer buffer (20x)

Tris 0.2 M, glycine 2 M. 20x transfer buffer was diluted to 1x using MilliQ-grade water plus 5% (v/v) methanol.

SDS-PAGE sample buffer (6x)

Upper gel buffer (4x) 7 ml, glycerol 30% (v/v), SDS 10% (w/v), DL-dithiothreitol (DTT) 0.6 M, bromophenol blue 0.05% (w/v); in a total volume of 10ml.

JIES protein extraction buffer

NaCl 100 mM, TrisHCl pH 7.4 20 mM, $MgCl_2$ 5 mM, Nonidet P-40 (NP40) 0.5% (v/v). Complete EDTA-free protease inhibitor cocktail (Roche Applied Science) was added immediately before use.

RIPA protein extraction buffer

Tris-HCl pH 7.4 50 mM, NP40, 1% (v/v), Sodium deoxycholate 0.5%, NaCl 150 mM, EGTA 1 mM, Na_3VO_4 1mM, NaF 1mM. Complete EDTA-free protease inhibitor cocktail was added immediately before use.

Urea-SDS buffer

Urea 6.87 M, glycerol 8.6% (v/v), sodium-dodecyl sulphate 0.9%, Tris-HCl pH 7.5 8.6 mM. Add 1 mM DTT before use and protease inhibitors if needed.

10% (w/v) Polyethylenimine (PEI)

10 ml of polyethylenimine plus 70 ml MilliQ-grade water. Titrate the solution to pH7.9 with concentrated HCl, and adjust the final volume to 100 ml with MilliQ-grade water. Filter-sterilised and stored at 4°C.

TFBI

Potassium acetate 30 mM, $RbCl_2$ 100 mM, $CaCl_2$ 10 mM, $MnCL_2$ 50 mM, glycerol 15% (v/v). Reagents were dissolved in 50 ml of MilliQ-grade water followed by addition of glycerol and pH adjusted to 5.8 using acetic acid 0.2 M. MilliQ-grade water was added to a final volume of 100 ml, filter-sterilised and stored at 4°C.

TFBII

3-(N-morpholino)propanesulfonic acid 10 mM, $CaCl_2$ 10 mM, $RbCl_2$ 10 mM were diluted in 5 ml of MilliQ-grade water before addition of glycerol 15% (v/v), and pH adjusted to 6.5 by NaOH 1M. MilliQ-grade water was added to a final volume of 100 ml, filter-sterilised and stored at 4°C.

A1 Buffer

Tris-HCl 20 mM pH7.8, NaCl 100 mM, KCl 20 mM, MgCl2 10 mM, 2-Mercaptoethanol 6 mM, sucrose 5% (w/v), Triton-X100 1%, 1x Complete protease inhibitor.

A2

Tris-HCl 20 mM pH7.8, NaCl 100 mM, KCl 20 mM, MgCl2 10 mM, 2-Mercaptoethanol 6 mM, sucrose 32% (w/v).

Buffer C

Tris pH7.5 50 mM, $MgCl_2$ 5 mM, KCl 25 mM.

Buffer A

Trifluoroacetic acid 0.1% (v/v), MilliQ-grade water (stored at 4°C, pre-warmed to room temperature before use).

Buffer B

Trifluoroacetic acid 0.08% (v/v), acetonitrile.

Protein extraction buffer for polyribosome profiling

HEPES-KOH 20 mM pH7.4, $MgCl_2$ 15 mM, KCl 200 mM, Triton X-100 1% (v/v), cycloheximide 100 μg/mL, DTT 2 mM, heparin 1 mg/mL. The last three components were added fresh.

Sucrose buffer for polyribosome profiling

7% and 47% (w/v) sucrose solutions were made up in NH_4Cl 50 mM, 50 mM Tris-Acetate pH 7.0, $MgCl_2$ 12 mM, and pH adjusted to 7.4 with 96% (v/v) Acetic acid.

8.2 Cell biology reagents

Actinomycin-D, LY294002, Cycloheximide, Sparsomycin, Anisomycin, Rapamycin, and Chloroquine were all purchased from Sigma.

8.3 Bacterial techniques

8.3.1 Solutions and media

All bacterial growth media were autoclaved at 121°C and 100kPa for 15 minutes before use.

YB

Yeast extract (Invitrogen) 0.5% (w/v), Tryptone (Invitrogen) 2% (w/v), $MgSO_4$ 0.5 % (w/v), pH adjusted to 7.6 by KOH 1M before autoclaving.

Luria-Bertani medium (LB)

Obtained in powder form (Invitrogen) and dissolving at 2 % (w/v) in MilliQ-grade water before autoclaving. For LB-agar plates, 1.5 % (w/v) agar was added prior to autoclaving.

SOC

SOC media was purchased from Invitrogen.

Ampicillin

Ampicillin selection was achieved using 100 ug/ml ampicillin added to liquid and solid culture media.

8.3.2 Bacterial strains

All cloning and site-directed mutagenesis procedures were carried out in XL10-Gold ultracompetent cells (Stratagene), Turbo competent cells (NEB) or Escherichia coli (E. coli) strain DH5alpha.

8.3.3 Generation of competent DH5alpha for transformation

A single colony was picked and inoculated in 5ml of YB and grown overnight at 220rpm and 37°C. The next morning the culture was back-diluted 100-fold into 400 ml YB media and cells grown to an OD_{550} of 0.5, cooled on ice and then

centrifugation at 3250g and 4°C for 5 minutes. The cell pellet was subsequently resuspended in 160ml ice-cold TFBI and incubated on ice for 5 minutes followed by centrifugation. The pellet was resuspended in 16ml of ice-cold TFBII and incubated on ice for 15 minutes before divided into 200 ul aliquots and storage at -80°C.

8.3.4 Transformation

50μl of competent bacteria were used per transformation together with 5μl of ligation reaction or 50 to 100ng of plasmid DNA. Bacteria were thawed on ice and incubated together with DNA for 30 minutes before heat-shocked at 42°C for 45 seconds. Cells were placed back on ice before addition of 0.5 ml of SOC media and incubation at 37°C with shaking at 220rpm for 1 hour. Cells were pelleted by centrifugation and then resuspended in 50μl of SOC medium before plating on ampicillin agar plates and incubation at 37°C overnight.

8.4 DNA techniques

8.4.1 Isolation and purification of plasmid DNA

Small-scale DNA plasmid purifications were commonly performed using a QIAprep spin miniprep kit from Qiagen. Alkyline lysis of the bacteria was followed by transfer of DNA onto a silica membrane under high-salt conditions and subsequent washes with a high-salt content. DNA was then eluted by a low-salt solution. Large-scale DNA preparations were done using a HiSpeed plasmid maxi kit from Qiagen. Alkaline lysis of cells was followed by binding of DNA onto an anion-exchange resin under conditions of low salt, medium-salt washing and then elution using a

high-salt solution. The eluted DNA was further concentrated by isopropanol precipitation. DNA was usually eluted in MilliQ-grade water.

8.4.1 Quantification of DNA

DNA was quantified using a NanoDrop ND-1000 spetrophotometer. MilliQ-grade water was used as a blank measurement. Usually 2μl of the DNA sample was used for each measurement. Absorbance was measured at 260 nm and purity determined by the 260 nm/280nm ratio. A DNA solution with a ratio around 1.9 was considered to be of sufficient quality.

8.4.2 Amplification of DNA by Polymerase Chain Reaction (PCR)

Usually 50 μl reactions were used containing 50 ng DNA template, 10 pmol of each oligonucleotide forward and reverse primer, 1x Cloned Pfu reaction buffer, and 0.2 mM dNTPs. Cloned Pfu Turbo DNA polymerase (2.5U, Stratagene) was added last. The reaction mixture was prepared on ice. PCR reactions were carried out using a PTC-200 Peltier thermal cycler (MJ Research), using the 25-30 cycles of the following conditions, or similar; 96°C 45s, 60°C 60s, 72°C 120s (per Kb).

8.4.3 Site-directed mutagenesis (SDM)

Specific primers were designed for each MINA53 mutation and mutants made in the pCMV SPORT6 MINA53 IMAGE clone background by PCR. A standard SDM included; 50 ng template, 20 pmol each primer, 1x Cloned Pfu reaction buffer, dNTP 1 mM, and 2.5U cloned Pfu DNA polymerase in a total reaction volume of 50μl. SDM PCR was carried out with 20 cycles of the following, or similar; 95°C 30s, 55 or 58°C 1 min, 68°C 12 min. Samples were treated with DpnI for 1h at 37°C for

the digestion of parental DNA and then transformed into XL-10 gold ultracompetent cells for antibiotic selection.

8.4.4 Construction of plasmids

The pBabe_PURO SV40 Large T construct was provided by P. Jat and used for retroviral infection and immortalisation of MEFs. Mouse MINA53 mutants were created by SDM as above; each construct was then amplified by PCR using oligonucleotides to encode a HA-epitope tag at the N-terminus, and subsequently cloned into pEF6 and pBabe-Neo (Addgene) by restriction enzyme digestion and ligation. Mouse K-Ras G12V was amplified by PCR from template DNA (Addgene) and cloned into pWZL-hygro vector (Addgene). In a standard subclone PCR reaction 50ng plasmid DNA was used, together with 20 pmol of each primer 2.5U Pfu DNA polymerase, 0.2 mM dNTP, and 1x Cloned Pfu reaction buffer in a total volume of 50µl. Subclone PCR was carried out as follows: 95°C 30s, 55 or 58°C 1 min, 72°C 3 min with 35 cycles. Samples were separated on a 1% (w/v) agarose electrophoresis gel (agarose dissolved in 1x Tris/Borate/EDTA buffer (Sigma-Aldrich, USA) with ethidium bromide 2 ug/ml (Sigma-Aldrich, USA)). PCR products of the correct size were excised using a scalpel and UV light source before purifing inserts using a Illustra GFX PCR DNA and gel band purification kit (GE Healthcare, USA). Inserts and plasmids were then digested using restriction enzymes and buffers from New England Biolabs according to manufacturer's protocol. In general, 1 µg of plasmid or 14 µl of PCR fragment were digested with 10U of each enzyme and 1 µl of appropriate restriction buffer, supplemented with Bovine Albumin serum (Sigma-Aldrich, USA) where required, in a total volume of 10 µl. Digestion was carried out for 4h or overnight at 37°C. Following digestion, vector

DNA was incubated for 15 min at 37°C with calf intestinal alkaline phosphatase (New England Biolabs, USA) to remove 5' phosphate groups. Digested vectors were separated on a 1% (w/v) agarose gel, excised and purified as above, while inserts were purified from solution using the same kit. All ligation reactions were performed using 20U T4 DNA ligase and 1 x T4 buffer (New England Biolabs, USA) in a total volume of 10 µl. Ligation was performed overnight at 16°C with a molar ratio of 3:1 insert to vector.

8.4.5 DNA sequencing

All plasmid inserts were sequence verified using specific primers by Source BioScience plc, Oxford.

8.4.6 Plasmids for protein expression in mammalian cells

pBabe_PURO_SV40_LargeT_antigen

pWZL_Hygro_K-Ras_G12V

pBabe_NEO_EV

pBabe_NEO_HA-MINA53

pBabe_NEO_HA_MINA53 H179A

pBabe_NEO_HA-MINA53 P341R

pBabe_NEO_HA-MINA53 G175R

8.5 Mammalian cell biology techniques

8.5.1 Cell culture

All cells were maintained in Dulbecco's Modified Eagle's Medium (DMEM) supplemented with foetal bovine serum (FBS) 10%, L-glutamine 2 mM, penicillin

50 IU/ml and streptomycin 50 μg/ml. Most cell lines were maintained under specific antibiotic selection (see below). Cells were maintained in a humidified atmosphere with 5% CO_2 at 37°C.

8.5.2 Plasmid transfection

Plasmids were transfected into cells using either PEI or Fugene6 (Promega) according to the manufacturers protocol. For a 6-well dish 1 μg of DNA was transfected into cells at 50% confluency. Plasmid DNA was first added to Optimem (Invitrogen) and vortexed before addition of 3 μl of Fugene-6. Samples were vortexed and incubated at room temperature for 30 min. Transfection mixtures were then added dropwise to cells and results analysed 48 to 72h post-transfection.

8.5.3 siRNA transfection

Cells were seeded in 6-well plates at $1x10^5$ cells/well, and the following day transfected with 20 nM MINA53 siRNA (MINA #10 (#1) or MINA 4563 (#2), Dharmacon) or 20 nM control siRNA (dHIF, Dharmacon) using Oligofectamine according to the manufacturer's protocol (Invitrogen). Results were analysed by western blot 48h after transfection.

8.5.4 Mammalian cell lysate preparation

Before cell lysis, culture media was removed cells washed twice in ice-cold PBS. For immunoprecipitation cells were lysed in either JIES buffer (U2OS-MINA53 inducible cells) or in RIPA buffer (MEFs). For western blot cells were lysed in JIES

buffer or Urea-SDS buffer containing 1x Complete EDTA-free protease inhibitor cocktail (Roche). Protein extracts were quantified using a DC protein assay (Bio-Rad).

8.5.5 Immunoprecipitation

Cells were lysed as above and HA-tagged MINA53 immunoprecipitated with anti-HA-antibody coupled agarose resin (Sigma) overnight at 4°C. Beads were then sedimented at 2000 rpm for 1 min followed by six washes with 1ml JIES buffer. Complexes were eluted by resuspening beads in 2xSDS-PAGE sample buffer.

8.5.6 Western blot

Proteins were resolved in 7.5%, 10% or 15% SDS-polyacrylamide gels run at 180V for 1h, or on 8-16% NuSep gradient gels (Generon) run at 200V for 40 min, before transfering to Immobilon P membrane (Millipore) for 1h at 100V. Membranes were blocked for 1h in PBST with 5% (w/v) skim-milk powder. Membranes were then incubated in primary-antibody in the same buffer, overnight at 4°C. The following day membranes were washed in PBST and incubated with a secondary antibody for 1h before final washing. Signals were visualized by chemiluminescence (Pierce, Thermo Scientific). The following antibodies and dilutions were used: anti-MINA53 (anti-rabbit-Ab, 1:1000, Invitrogen), anti-MINA53 (anti-mouse-Ab, 1:1000, Invitrogen), HA-HRP (1:4000, Roche Applied Science), anti-Rpl27a (1:1000, Abcam), anti-Rpl3 (1:1000, Proteintech), anti-Rpl4 (1:1000, Proteintech,), anti-S6 (1:1000, Cell signaling), anti-p-S6 (240/244) (1:1000, Cell signaling), anti-LC3 A/B (1:1000, Cell signaling), anti-COX-4 (1:1000, Cell signaling), anti-FLAG-HRP (Sigma) and anti-β-actin-HRP (1:2000, Abcam).

8.5.7 MTT assay

Cells were seeded at 2000 cells/well in a 96-well plate. The following day cells were incubated in 10 µl of 3-[4,5-dimethylthiazol-2-yl]-2,5-diphenyl-tetrazoliumbromide salt (MTT, Roche) solution for 4h, followed by solubilisation with 200 µl of solubilisation solution (Roche) overnight. The cells were then quantified for formazan product using a spectrophotometer at 590 nm.

8.5.8 MTS assay

Cells were seeded out at 2000 cells/well in a 96-well plate and incubated with 20ul of MTS reagent (CellTiter 96R Aqueous One solution Cell proliferation assay, Promega) for 1h at 37°C before analysis for the formazan product using a spectrophotomer at 490 nm.

8.5.9 Construction of MINA53 shRNA A549 stable cell lines

Five different shRNA constructs (MISSION, Sigma-Aldrich) were transfected into HEK293T cells using Fugene-6 as above, to screen for the hairpin giving the most efficient knockdown. One MINAS53 shRNA construct (TRCN0000130530 NM_032778.3-1528s1c2 TRC 1) showed the most efficient knock-down by western blot, as compared to the control shRNA. Control and MINA53 shRNA plasmids were subsequently transfected into A549 cells using Fugene-6 and selected the following day using puromycin (1 µg/ml). Cells were subsequently seeded in 15cm dishes and cultured for three weeks before picking clones to screen for MINA53 knockdown. Three independent clones were established for the control shRNA and for MINA53 shRNA and kept under continuous puromycin (1 µg/ml) selection.

8.5.10 Construction of MINA53 shRNA 293T stable cell lines

HEK293T cells were transfected with the same control and MINA53 shRNA constructs described above using Fugene-6. Transfected cells were kept under continous puromycin (1 μg/ml) selection.

8.5.11 Generation of primary MEFs from mice

Mice were culled by cervical dislocation and embryos extracted, before the removing the head, and one limb for genotyping. After removal of the liver, the embryo was macerated using scalpels and forceps (performed by Dr Mathew Coleman). Macerated tissue was then incubated for 5 min at 37°C in 3 ml trypsin. Samples were then dispersed using a pipette and re-incubated for 5 min at 37°C. DMEM medium was then added to stop trypsinisation and the cells centrifuged at 1000 rpm for 5 min. The supernatant was removed, cells were resuspended in fresh culture media and then seeded in 10 cm dishes and incubated at 37°C overnight. The media was replaced the following day and after 1 week mouse embryonic fibroblasts (MEFs) had grown out.

8.5.12 Establishment of immortalized MEFs

Phoenix retroviral packaging cells were used to generate the pBabe-puro SV40 Large T antigen for MEF immortalisation. Phoenix cells were seeded by adding $1/6^{th}$ of a confluent T175 flask into a 15cm dish. The following day 25 μg of plasmid was resuspended in 5 ml of Optimem plus 100 μl PEI. After incubating at room termpature for 30 min, samples were added dropwise to the Phoenix cells. Fresh culture media was added the following day and retroviral-containing media harvested 3 days subsequently. The retroviral media was sedimented at 1000 rpm

for 5 min to remove contaminating Phoenix cells and then filtered through a 0.45 μm sterile filter. The purified retroviral supernatant was then diluted with 5 ml DMEM and Polybrene added to 5 μg/ml (which improves infection efficiency by neutralizing charge repulsion between the virus and the cell surface). This retroviral media was then added to wild-type, heterozygous and MINA53 knockout MEFs cells that had been seeded the previous day at $1x10^5$ cells/well in a 6-well plate. Infections were incubated at 37°C for 8h before adding 20 ml culture media. Immortalised MEF cells were subsequently selected for using 1 μg/ml puromycin.

8.5.13 Establishment of K-Ras transformed MEF cell lines

Transformed cells were created by infection with a retrovirus expressing oncogenic K-Ras, essentially as described above. In short, Phoenix cells were seeded in 15 cm dishes and the following day transfected with pWZL-hygro K-Ras G12V. Three days after tranfection, retroviral media were harvested and filtered before infecting wild-type and knock-out MEFs. K-Ras expressing cells were selected 48h post-infection using 200 μg/ml hygromycin (Roche Applied Science).

8.5.14 Establishment of MINA53 KO MEFs reconstituted with empty vector (EV), HA-MINA53 and HA-MINA53 H179A

MINA53-reconstituted cells were created by infection with either a control empty retroviral vector, or the same vector expressing wildtype HA-MINA53 or various mutants, as described above. Transformed and reconstituted MEFs were selected using 200 μg/ml G418 and 200 μg/ml Hygromycin. For passage 50 μg/ml G418 was used.

8.5.15 Doxycycline-inducible 3X-FLAG-tagged MINA53

Doxycycline-inducible 3X-FLAG-tagged MINA53 expressing cells were created by Dr Nicholas Granatino by transfecting U2OS cells with pUHD10-3X-FLAG-MINA53 and selection in 400 μg/ml G418 and 200 μg/ml hygromycin B. MINA53 expression was induced by treating the cells with 0.5 μg/ml doxycycline every 24 hours. The cells were maintained in DMEM supplemented with 10% Tet-approved fetal calf serum (Takara), plus penicillin and streptomycin under standard conditions.

8.5.16 Clonogenic survival assay

Cells were seeded at the indicated concentrations in 6-well or 10 cm plates and grown for 3-4 weeks. Media was removed, and cells carefully washed in PBS before staining with methylene blue (50% (v/v) ethanol, 0.25% (w/v) 1,9-dimethyl-methylene blue (Sigma-Aldrich)) for 30 min. Staining media was removed, plates washed in PBS and the plates left to dry. The following day the number of stained colonies were manually counted.

8.5.17 Soft-agar growth assay

A 2% (w/v) stock solution of Noble agar (Sigma-Aldrich) was diluted to 0.6% in DMEM containing 20% (v/v) FBS. 2ml was aliquoted per well of a 6-well plate and allowed to solidify. Cells were then resuspended in 0.3% Noble agar solution in 20% FBS medium and added onto the solidified layer. Plates were incubated overnight at 37°C before adding 200 μl of DMEM containing 10% FBS to each well. This was repeated twice a week for 2-3 weeks until the clones were easily detected by eye. Tetrazolium salt (Sigma-Aldrich) was used to stain the clones; 500 μl of a 1

mg/ml stock was added per well and incubated overnight before visualizing and colony counting the following day.

8.5.18 Tumourgenicity of reconstituted MINA53 MEFs in nude mice

K-Ras transformed MEF cells (1 x 10^7) were resuspended to 100 μl before mixing with an equal volume of Matrigel (BD Science) and injection into the flank of a 6-8 week old female BALC/c nude mice. Tumour growth was measured three times a week and tumour volume calculated (length x width x height x π/6, Tomayko et al, 1989). For the pilot xenograft experiment, K-Ras transformed MINA53 KO+EV and MINA KO+HA-MINA53 cells were used (n = 7, two injections per mice, one from each cell line). Tumour growth was followed for 19 days. In the main study, four cell lines were used (K-Ras transformed wildtype MEFs, MINA53 KO+EV, MINA53 KO+HA-MINA53 and MINA53 KO+HA-MINA53 H179A MEFs) with seven BALC/c nude mice per cell line (28 mice in total, each mouse injected once). Tumour growth was followed for 55 days before termination. All procedures were carried out under Home Office regulations. Cell injections and tumour growth measurements were performed by Ji-Liang Li and Esther Bridges (Harris laboratory, WIMM, University of Oxford.

8.5.19 Immunofluorescence

HA and nucleolin staining

Cells were seeded in tissue culture slides (BD Bioscience) and fixed in 4 % (w/v) paraformaldehyde for 15 minutes at room temperature followed by PBS washes. Cells were then permeabilised in PBST for 10 minutes before washing twice in PBSTB. Samples were incubated for 1h with anti-nucleophosmin antibody (1:100,

Santa Cruz Biotechnology, USA) diluted in PBSTB. After PBSTB washes, the cells were incubated with anti-HA-FITC (1:250, Sigma-Aldrich, USA) and anti-rabbit Alexa Flour-555® (1:1000, Invitrogen) antibodies for 1h, also diluted in PBSTB. After a final wash in PBS, cells were mounted in Vectashield with DAPI (Vector Laboratories) and the edges of the coverslip were sealed with DPX (Fisher Scientific) and allowed to set for 24h at room temperature in the dark. Images were acquired using a confocal microscope (Zeiss 510 MetaHead) and analysed using LSM 510 software v4.2 (Carl Zeiss GmbH).

Mitotracker staining

Prior to fixation, cells were labelled with 250 nm Mitotracker® Red CMXRos (Invitrogen) for 15 minutes at 37°C. Cells were then fixed in 4% (w/v) paraformaldehyde for 15 minutes at room temperature followed by PBS washes. Samples were mounted and images acquired as above.

Lysotracker staining

Cells were labeled with 50 μM Lysotracker (Molecular Probes) for 1h at 37°C before fixation in 4% (w/v) paraformaldehyde for 15 minutes at room temperature and then PBS washes. Samples were mounted and images acquired as above.

8.5.20 RNA extraction, cDNA preparation, and Q-PCR

RNA was extracted from cells using TRI solution (Sigma-Aldrich) and prepared according to the manufacturer's protocol. In short, 200 μl of Chloroform (Sigma-Aldrich) was added to 1 ml of the TRI solution containing the RNA and centrifuged

at 18,000xg for 15 minutes. The upper phase was retained and incubated with 500 µl Isopropanol before centrifugation at 18,000xg for 15 minutes. Pellets were washed with 75% (v/v) ethanol and dried before resuspending in 20 µl of RNAse-free DEPC-water (Ambion, USA). Samples were incubated at 60°C for 15 minutes and cDNA synthesised using a cDNA Reverse Transcriptase kit (Applied Biosystems) according to manufacturers protocol. Q-PCR was performed using SYBR green dye (Applied Biosystems), with oligonucleotide primers specifically designed for each target. Samples were prepared according to manufacturer's protocol (Applied Biosystems) and analysed using a StepOnePlus Q-PCR machine from Applied Biosystems.

8.5.21 Isolation of ribosomes

Cells were lysed in buffer A1 and centrifuged at 18,000xg for 20 min at 4°C. 10ml of the protein extract was then carefully layered onto 28 ml Buffer A2 in a polyallomer tube before centrifugation at 100,000xg for 3h at 4°C (SW28 rotor). Ribosomal pellets were either resolubilised in UREA/SDS for analysis by Coomassie blue (Imperial protein stain, Thermo Scientific) staining or western blotting, or were further processed for HPLC purification or whole-protein MS of Rpl27a (see below).

8.5.22 Polyribosomal profiling

Cells were seeded to be 80-90% confluent 48 hours later at the time of harvest. Sucrose gradients were prepared one day before use in order to form a continuous gradient (stored at 4°C), as follows. Five different sucrose solutions were made by mixing 7% (w/v) and 47% (w/v) sucrose buffers into the following: 7%, 17%

(7%,47% at 3:1 ratio), 27% (7%,47% at 1:1 ratio), 37% (7%:47% at 0.68:1 ratio), 47%. Ultracentrifuge tubes (Seton Scientific) were immersed in dry ice with ethanol. 7ml of 47% sucrose solution was added to each tube and allowed to freeze for 15min. This process was then repeated with the 37%, 27%, 17% and 7% sucrose solutions in turn, with each solution layered on top of the last. These discontinuous gradients were then left overnight at 4°C to diffuse into continuous gradients. At the day of the harvest cells were treated with cycloheximide (100 ug/ml) for 15 min and then harvested in 1ml of polyribosome lysis buffer, subjected to 20 strokes of a dounce homogeniser using a Type B pestle before centrifugation at 14,000 x g for 5 min at 4°C. The supernatant was retained and the RNA concentration determined by Nanodrop. Sample equivalent to 500 μg RNA was gently layered on top of the gradient before ultracentrifugation at 100,000g for 4h at 4°C. Approximately 1h before completion of the spin the gradient fractionator used for polyribosome analyses was flushed with MilliQ-grade water, followed by 70% (v/v) ethanol, a second wash with MilliQ-grade water before sample tube piercing and displacement with Fluorinert (Sigma). The combined system consisted of a; TRIS peristaltic pump (Teledyne Isco), tube piercer and fluid displacement unit (Brandel), Type II FlowCell optical unit (Teledyne Isco), UA-6 UV/VIS detector, and Retriever 500 sample collector (Teledyne Isco). Ribosomal subunits were displaced from the gradient at a flow rate of 5 ml/min and rRNA detected at 254nm.

8.5.23 Microarray analysis

Total RNA was purified using a mirVana kit (Ambion). The quantity and quality of the RNA was determined using the Agilent BioAnalyzer 2100 (Agilent

Technologies). Gene expression data were obtained from two biological replicates from each of four cell lines: WT MEFs, MINA53 KO+EV, MINA53 KO+HA-MINA53 and MINA53 KO+HA-MINA53 H179A. Samples were hybridized to Illumina MouseWG-6 v2 BeadChips and chips scanned with Illumina BeadArray Reader. GenomeStudioV2010.1 (Illumina Inc) was used for data extraction. Data was analysed using GenePattern software (Broad Institute) and IPA pathway analysis (Ingenuity Systems).

8.5.24 Hypoxia experiment

Hypoxia was performed at 0.1% O_2 in a humidified atmosphere containing 5% CO_2 at 37°C, for 72 hours using a Ruskinn hypoxia station. Cells were lysed in buffer A1 in the presence of the generic 2OG oxygenase inhibitor N-oxalylglycine (NOG; Santa Cruz Biotechnology) at 1mM. Endogenous Rpl27a was purified as described above.

8.5.25 Purification of endogenous Rpl27a

Ribosomal pellets prepared as above were resuspended in Tris pH8 10 mM, $Mg(CH_3COO)_2$ 70 mM and 70% (v/v) glacial acetic acid before rotating at 4°C for 1 hour to precipitate rRNA. Samples were centrifuged at 18,000x*g* for 10 minutes at 4°C before removing the supernatant and mixing with 4 volumes of ice cold acetone. Ribosomal proteins were precipitated at -20°C for 2 hours followed by centrifugation at 18,000x*g* for 10 minutes at 4°C. Pellets were washed once in acetone before vacuum drying and then resuspending in 2% (v/v) acetic acid/10% (v/v) acetonitrile. 250μg ribosomal protein were then loaded onto a Vydac214TP C4 (250mmx4.6mm) HPLC column (GRACE discovery) prequilibriated in 10%

Buffer C (C_2H_3N/0.08% (v/v) TFA) and 90% Buffer D (0.1% (v/v) TFA) and separated with the following gradient at a flow rate of 1ml/minute: 10 min 10% Buffer C, 10-25 min 10-20 % Buffer C, 25-180 min 20-43 % Buffer C. Protein absorbance was measured at 214nm and fractions collected between 95 and 130 minutes. HPLC fractions were vacuum dried overnight and either resuspended in 6M Urea/100 mM Tris pH7.8 to identify fractions containing Rpl27a by dot-blot with anti-Rpl27a antibody, or subjected to in-solution trypsinolysis as described below.

8.6 Mass Spectrometry

8.6.1 In-solution trypsinolysis of Rpl27a

Dried HPLC fractions containing Rpl27a were resuspended in 100 μl 6M Urea/100 mM Tris pH7.8 prior to reduction with 5 μl 200 mM DTT for 1 hour, alkylation with 20μl 200 mM Iodoacetamide for 1 hour, and then quenching with 20 μl 200mM DTT for 1 hour. Samples were diluted with 775 μl MilliQ-H_2O then digested in-solution with 1 μg trypsin (Sigma-Aldrich) at 37°C overnight. Peptides from digested samples were then purified using C18 pipette tips according to the manufacturers protocol (Pierce), vacuum dried and resuspended in 20 μl of Buffer A (2% (v/v) acetonitrile, 0.1% (v/v) formic acid) prior to MS analysis. All MS was performed by the Kessler laboratory at the Oxford Proteomics Facility.

8.6.2 Mass Spectrometry analysis

Dried samples were resuspended in 20 μl of Buffer A and subjected to LC-MS/MS (Waters, Acquity, 75 μm x 250 mm, 1.7 μm particle size) analysis using a Thermo

LTQ Orbitrap Velos (Thermo Scientific) at a resolution of 30000. MS/MS spectra were acquired in CID mode, selecting up to 20 precursors. Peptides were separated by a linear gradient of 1-40% (v/v) Acetonitrile in 120 min at a flow rate of 250 nl/min. MS/MS spectra were extracted from raw files by ProteoWizard MSConvert (http://proteowizard.sourceforge.net/) using the 200 most intense peaks in each and converted into MGF files. The peaklists were searched against the IPI human database (v3.87, 91464 entries) using Mascot (http://www.matrixscience.com/) v2.3.01, allowing one missed cleavage and 20 ppm/0.5 Da mass deviations in MS/MSMS. Carbamidomethylation of cysteine was a fixed modification. Oxidation of methionine and histidine as well as deamidation of asparagine and glutamine were used as variable modifications. Annotation of oxidized methionines and histidines was performed manually and assisted with ModLS (http://cpfp.sourceforge.net/overview.html) as part of data analysis using the Central Proteomics Facilities Pipeline.

8.6.3 Whole-protein mass spectrometry UPLC system

Endogenous RPl27a was purified as described above and analysed by reversed phase ultra-performance liquid chromatography (RP-UPLC) and electrospray ionisation time-of-flight mass spectrometry (ESI-TOF MS) (all whole-protein was performed by Rok Sekirnik, Schofield laboratory, Oxford). The method used a Waters BEH C4 reversed phase column (2.1 x 150mm, 1.7 μm particle size, 300 Å pore size). A flow rate of 0.3 ml/min was used with the column held at 40°C using a Waters Acquity UPLC system connected directly to a Waters LCT ESI-TOF MS. The column was equilibrated with solvent A (0.1% (v/v) formic acid in water). 5 μL of ribosomal protein sample was injected onto the column and proteins eluted using

a stepped gradient from solvent A to solvent B (0.1% formic acid in acetonitrile). The following MS parameters were used: Polarity: ES+; Capillary voltage: 3,000V; Sample cone voltage: 35V; Extraction cone voltage: 2.5V; Desolvation temperature: 250°C; Cone gas flow rate: 10 L/hour; Desolvation gas flow (N_2): 500 L/hour. The mass spectra were acquired from 150 to 3200 *m/z* using MassLynx 4.1 software (Waters) and protein spectra deconvoluted using Maxent 1 with a range 3 to 30 kDa (0.1 Da resolution). Masses were confirmed using manual component analysis. Sodium formate was used to calibrate the instrument.

Chapter 9
Bibliography

Agger, K., Cloos, P.A., Christensen, J., Pasini, D., Rose, S., Rappsilber, J., Issaeva, I., Canaani, E., Salcini, A.E., and Helin, K. (2007). UTX and JMJD3 are histone H3K27 demethylases involved in HOX gene regulation and development. Nature *449*, 731-734.

Ahmad, W., Faiyaz ul Haque, M., Brancolini, V., Tsou, H.C., ul Haque, S., Lam, H., Aita, V.M., Owen, J., deBlaquiere, M., Frank, J.*, et al.* (1998). Alopecia universalis associated with a mutation in the human hairless gene. Science *279*, 720-724.

Altman, B.J., and Rathmell, J.C. (2012). Metabolic stress in autophagy and cell death pathways. Cold Spring Harb Perspect Biol *4*.

Annunen, P., Helaakoski, T., Myllyharju, J., Veijola, J., Pihlajaniemi, T., and Kivirikko, K.I. (1997). Cloning of the human prolyl 4-hydroxylase alpha subunit isoform alpha(II) and characterization of the type II enzyme tetramer. The alpha(I) and alpha(II) subunits do not form a mixed alpha(I)alpha(II)beta2 tetramer. J Biol Chem *272*, 17342-17348.

Asensio-Juan, E., Gallego, C., and Martinez-Balbas, M.A. (2012). The histone demethylase PHF8 is essential for cytoskeleton dynamics. Nucleic Acids Res.

Ayton, P.M., Chen, E.H., and Cleary, M.L. (2004). Binding to nonmethylated CpG DNA is essential for target recognition, transactivation, and myeloid transformation by an MLL oncoprotein. Mol Cell Biol *24*, 10470-10478.

Bachand, F., Lackner, D.H., Bahler, J., and Silver, P.A. (2006). Autoregulation of ribosome biosynthesis by a translational response in fission yeast. Mol Cell Biol *26*, 1731-1742.

Bachellerie, J.P., and Cavaille, J. (1997). Guiding ribose methylation of rRNA. Trends Biochem Sci *22*, 257-261.

Bai, C., Sen, P., Hofmann, K., Ma, L., Goebl, M., Harper, J.W., and Elledge, S.J. (1996). SKP1 connects cell cycle regulators to the ubiquitin proteolysis machinery through a novel motif, the F-box. Cell *86*, 263-274.

Ballou, L.M., and Lin, R.Z. (2008). Rapamycin and mTOR kinase inhibitors. J Chem Biol *1*, 27-36.

Bannister, A.J., and Kouzarides, T. (2011). Regulation of chromatin by histone modifications. Cell Res *21*, 381-395.

Barrick, D., Ferreiro, D.U., and Komives, E.A. (2008). Folding landscapes of ankyrin repeat proteins: experiments meet theory. Curr Opin Struct Biol *18*, 27-34.

Beau, I., Esclatine, A., and Codogno, P. (2008). Lost to translation: when autophagy targets mature ribosomes. Trends Cell Biol *18*, 311-314.

Blair, L.P., Cao, J., Zou, M.R., Sayegh, J., and Yan, Q. (2011). Epigenetic Regulation by Lysine Demethylase 5 (KDM5) Enzymes in Cancer. Cancers (Basel) *3*, 1383-1404.

Bodmer, D., Schepens, M., Eleveld, M.J., Schoenmakers, E.F., and Geurts van Kessel, A. (2003). Disruption of a novel gene, DIRC3, and expression of DIRC3-HSPBAP1 fusion transcripts in a case of familial renal cell cancer and t(2;3)(q35;q21). Genes Chromosomes Cancer *38*, 107-116.

Boisvert, F.M., van Koningsbruggen, S., Navascues, J., and Lamond, A.I. (2007). The multifunctional nucleolus. Nat Rev Mol Cell Biol *8*, 574-585.

Bose, J., Gruber, A.D., Helming, L., Schiebe, S., Wegener, I., Hafner, M., Beales, M., Kontgen, F., and Lengeling, A. (2004). The phosphatidylserine receptor has essential functions during embryogenesis but not in apoptotic cell removal. J Biol *3*, 15.

Brech, A., Ahlquist, T., Lothe, R.A., and Stenmark, H. (2009). Autophagy in tumour suppression and promotion. Mol Oncol *3*, 366-375.

Burger, K., Muhl, B., Harasim, T., Rohrmoser, M., Malamoussi, A., Orban, M., Kellner, M., Gruber-Eber, A., Kremmer, E., Holzel, M*., et al.* (2010). Chemotherapeutic drugs inhibit ribosome biogenesis at various levels. J Biol Chem *285*, 12416-12425.

Carpenter, G., and Cohen, S. (1990). Epidermal growth factor. J Biol Chem *265*, 7709-7712.

Chang, B., Chen, Y., Zhao, Y., and Bruick, R.K. (2007). JMJD6 is a histone arginine demethylase. Science *318*, 444-447.

Chazotte, B. (2011). Labeling mitochondria with MitoTracker dyes. Cold Spring Harb Protoc *2011*, 990-992.

Chen, D., Zhang, Z., Li, M., Wang, W., Li, Y., Rayburn, E.R., Hill, D.L., Wang, H., and Zhang, R. (2007). Ribosomal protein S7 as a novel modulator of p53-MDM2 interaction: binding to MDM2, stabilization of p53 protein, and activation of p53 function. Oncogene *26*, 5029-5037.

Cho, Y.G., Song, J.H., Kim, C.J., Lee, Y.S., Kim, S.Y., Nam, S.W., Lee, J.Y., and Park, W.S. (2007). Genetic alterations of the ATBF1 gene in gastric cancer. Clin Cancer Res *13*, 4355-4359.

Cloos, P.A., Christensen, J., Agger, K., and Helin, K. (2008). Erasing the methyl mark: histone demethylases at the center of cellular differentiation and disease. Genes Dev *22*, 1115-1140.

Cockman, M.E., Lancaster, D.E., Stolze, I.P., Hewitson, K.S., McDonough, M.A., Coleman, M.L., Coles, C.H., Yu, X., Hay, R.T., Ley, S.C*., et al.* (2006). Posttranslational hydroxylation of ankyrin repeats in IkappaB proteins by the hypoxia-inducible

factor (HIF) asparaginyl hydroxylase, factor inhibiting HIF (FIH). Proc Natl Acad Sci U S A *103*, 14767-14772.

Cockman, M.E., Webb, J.D., and Ratcliffe, P.J. (2009). FIH-dependent asparaginyl hydroxylation of ankyrin repeat domain-containing proteins. Ann N Y Acad Sci *1177*, 9-18.

Coleman, M.L., and Ratcliffe, P.J. (2007). Oxygen sensing and hypoxia-induced responses. Essays Biochem *43*, 1-15.

Cory, A.H., Owen, T.C., Barltrop, J.A., and Cory, J.G. (1991). Use of an aqueous soluble tetrazolium/formazan assay for cell growth assays in culture. Cancer Commun *3*, 207-212.

Crea, F., Sun, L., Mai, A., Chiang, Y.T., Farrar, W.L., Danesi, R., and Helgason, C.D. (2012). The emerging role of histone lysine demethylases in prostate cancer. Mol Cancer *11*, 52.

Dai, M.S., and Lu, H. (2004). Inhibition of MDM2-mediated p53 ubiquitination and degradation by ribosomal protein L5. J Biol Chem *279*, 44475-44482.

Dalgliesh, G.L., Furge, K., Greenman, C., Chen, L., Bignell, G., Butler, A., Davies, H., Edkins, S., Hardy, C., Latimer, C.*, et al.* (2010). Systematic sequencing of renal carcinoma reveals inactivation of histone modifying genes. Nature *463*, 360-363.

Del Rizzo, P.A., Krishnan, S., and Trievel, R.C. (2012). Crystal Structure and Functional Analysis of JMJD5 Indicate an Alternate Specificity and Function. Mol Cell Biol *32*, 4044-4052.

Dinchuk, J.E., Focht, R.J., Kelley, J.A., Henderson, N.L., Zolotarjova, N.I., Wynn, R., Neff, N.T., Link, J., Huber, R.M., Burn, T.C.*, et al.* (2002). Absence of post-translational aspartyl beta-hydroxylation of epidermal growth factor domains in mice leads to developmental defects and an increased incidence of intestinal neoplasia. J Biol Chem *277*, 12970-12977.

Ding, W.X., and Yin, X.M. (2012). Mitophagy: mechanisms, pathophysiological roles, and analysis. Biol Chem *393*, 547-564.

Eilbracht, J., Kneissel, S., Hofmann, A., and Schmidt-Zachmann, M.S. (2005). Protein NO52--a constitutive nucleolar component sharing high sequence homologies to protein NO66. Eur J Cell Biol *84*, 279-294.

Eilbracht, J., Reichenzeller, M., Hergt, M., Schnolzer, M., Heid, H., Stohr, M., Franke, W.W., and Schmidt-Zachmann, M.S. (2004). NO66, a highly conserved dual location protein in the nucleolus and in a special type of synchronously replicating chromatin. Mol Biol Cell *15*, 1816-1832.

Esposito, A.M., Mateyak, M., He, D., Lewis, M., Sasikumar, A.N., Hutton, J., Copeland, P.R., and Kinzy, T.G. (2010). Eukaryotic polyribosome profile analysis. J Vis Exp.

Fleming, A., Noda, T., Yoshimori, T., and Rubinsztein, D.C. (2011). Chemical modulators of autophagy as biological probes and potential therapeutics. Nat Chem Biol *7*, 9-17.

Fortschegger, K., and Shiekhattar, R. (2011). Plant homeodomain fingers form a helping hand for transcription. Epigenetics *6*, 4-8.

Frescas, D., Guardavaccaro, D., Bassermann, F., Koyama-Nasu, R., and Pagano, M. (2007). JHDM1B/FBXL10 is a nucleolar protein that represses transcription of ribosomal RNA genes. Nature *450*, 309-313.

Frisch, S.M., and Screaton, R.A. (2001). Anoikis mechanisms. Curr Opin Cell Biol *13*, 555-562.

Fromont-Racine, M., Senger, B., Saveanu, C., and Fasiolo, F. (2003). Ribosome assembly in eukaryotes. Gene *313*, 17-42.

Fukahori, S., Yano, H., Tsuneoka, M., Tanaka, Y., Yagi, M., Kuwano, M., Tajiri, T., Taguchi, T., Tsuneyoshi, M., and Kojiro, M. (2007). Immunohistochemical expressions of Cap43 and Mina53 proteins in neuroblastoma. J Pediatr Surg *42*, 1831-1840.

Ganley, I.G., Lam du, H., Wang, J., Ding, X., Chen, S., and Jiang, X. (2009). ULK1.ATG13.FIP200 complex mediates mTOR signaling and is essential for autophagy. J Biol Chem *284*, 12297-12305.

Gharbi, S.I., Zvelebil, M.J., Shuttleworth, S.J., Hancox, T., Saghir, N., Timms, J.F., and Waterfield, M.D. (2007). Exploring the specificity of the PI3K family inhibitor LY294002. Biochem J *404*, 15-21.

Gorres, K.L., and Raines, R.T. (2010). Prolyl 4-hydroxylase. Crit Rev Biochem Mol Biol *45*, 106-124.

Granneman, S., and Baserga, S.J. (2004). Ribosome biogenesis: of knobs and RNA processing. Exp Cell Res *296*, 43-50.

Gray, S.G., Iglesias, A.H., Lizcano, F., Villanueva, R., Camelo, S., Jingu, H., Teh, B.T., Koibuchi, N., Chin, W.W., Kokkotou, E.*, et al.* (2005). Functional characterization of JMJD2A, a histone deacetylase- and retinoblastoma-binding protein. J Biol Chem *280*, 28507-28518.

Guo, J.Y., Chen, H.Y., Mathew, R., Fan, J., Strohecker, A.M., Karsli-Uzunbas, G., Kamphorst, J.J., Chen, G., Lemons, J.M., Karantza, V.*, et al.* (2011). Activated Ras requires autophagy to maintain oxidative metabolism and tumorigenesis. Genes Dev *25*, 460-470.

Hahn, P., Wegener, I., Burrells, A., Bose, J., Wolf, A., Erck, C., Butler, D., Schofield, C.J., Bottger, A., and Lengeling, A. (2010). Analysis of Jmjd6 cellular localization and testing for its involvement in histone demethylation. PLoS One *5*, e13769.

Hamon, M.A., and Cossart, P. (2008). Histone modifications and chromatin remodeling during bacterial infections. Cell Host Microbe *4*, 100-109.

Hardy, A.P., Prokes, I., Kelly, L., Campbell, I.D., and Schofield, C.J. (2009). Asparaginyl beta-hydroxylation of proteins containing ankyrin repeat domains influences their stability and function. J Mol Biol *392*, 994-1006.

Hausinger, R.P. (2004). FeII/alpha-ketoglutarate-dependent hydroxylases and related enzymes. Crit Rev Biochem Mol Biol *39*, 21-68.

Hewitson, K.S., Granatino, N., Welford, R.W., McDonough, M.A., and Schofield, C.J. (2005). Oxidation by 2-oxoglutarate oxygenases: non-haem iron systems in catalysis and signalling. Philos Transact A Math Phys Eng Sci *363*, 807-828; discussion 1035-1040.

Hirsila, M., Koivunen, P., Gunzler, V., Kivirikko, K.I., and Myllyharju, J. (2003). Characterization of the human prolyl 4-hydroxylases that modify the hypoxia-inducible factor. J Biol Chem *278*, 30772-30780.

Hosokawa, N., Hara, T., Kaizuka, T., Kishi, C., Takamura, A., Miura, Y., Iemura, S., Natsume, T., Takehana, K., Yamada, N.*, et al.* (2009). Nutrient-dependent mTORC1 association with the ULK1-Atg13-FIP200 complex required for autophagy. Mol Biol Cell *20*, 1981-1991.

Hsia, D.A., Tepper, C.G., Pochampalli, M.R., Hsia, E.Y., Izumiya, C., Huerta, S.B., Wright, M.E., Chen, H.W., Kung, H.J., and Izumiya, Y. (2010). KDM8, a H3K36me2 histone demethylase that acts in the cyclin A1 coding region to regulate cancer cell proliferation. Proc Natl Acad Sci U S A *107*, 9671-9676.

Huang, S., Bjornsti, M.A., and Houghton, P.J. (2003). Rapamycins: mechanism of action and cellular resistance. Cancer Biol Ther *2*, 222-232.

Huang, S., and Houghton, P.J. (2003). Targeting mTOR signaling for cancer therapy. Curr Opin Pharmacol *3*, 371-377.

Hutton, J.J., Jr., Kaplan, A., and Udenfriend, S. (1967). Conversion of the amino acid sequence gly-pro-pro in protein to gly-pro-hyp by collagen proline hydroxylase. Arch Biochem Biophys *121*, 384-391.

Iadevaia, V., Huo, Y., Zhang, Z., Foster, L.J., and Proud, C.G. (2012). Roles of the mammalian target of rapamycin, mTOR, in controlling ribosome biogenesis and protein synthesis. Biochem Soc Trans *40*, 168-172.

Ishikawa, Y., Wirz, J., Vranka, J.A., Nagata, K., and Bachinger, H.P. (2009). Biochemical characterization of the prolyl 3-hydroxylase 1.cartilage-associated protein.cyclophilin B complex. J Biol Chem *284*, 17641-17647.

Ishimura, A., Terashima, M., Kimura, H., Akagi, K., Suzuki, Y., Sugano, S., and Suzuki, T. (2009). Jmjd2c histone demethylase enhances the expression of Mdm2 oncogene. Biochem Biophys Res Commun *389*, 366-371.

Ishizaki, H., Yano, H., Tsuneoka, M., Ogasawara, S., Akiba, J., Nishida, N., Kojiro, S., Fukahori, S., Moriya, F., Matsuoka, K.*, et al.* (2007). Overexpression of the myc target gene Mina53 in advanced renal cell carcinoma. Pathol Int *57*, 672-680.

Italiano, A., Attias, R., Aurias, A., Perot, G., Burel-Vandenbos, F., Otto, J., Venissac, N., and Pedeutour, F. (2006). Molecular cytogenetic characterization of a metastatic lung sarcomatoid carcinoma: 9p23 neocentromere and 9p23-p24 amplification including JAK2 and JMJD2C. Cancer Genet Cytogenet *167*, 122-130.

Jin, A., Itahana, K., O'Keefe, K., and Zhang, Y. (2004). Inhibition of HDM2 and activation of p53 by ribosomal protein L23. Mol Cell Biol *24*, 7669-7680.

Jung, C.H., Jun, C.B., Ro, S.H., Kim, Y.M., Otto, N.M., Cao, J., Kundu, M., and Kim, D.H. (2009). ULK-Atg13-FIP200 complexes mediate mTOR signaling to the autophagy machinery. Mol Biol Cell *20*, 1992-2003.

Jung, C.H., Ro, S.H., Cao, J., Otto, N.M., and Kim, D.H. (2010). mTOR regulation of autophagy. FEBS Lett *584*, 1287-1295.

Jung, J., Kim, T.G., Lyons, G.E., Kim, H.R., and Lee, Y. (2005). Jumonji regulates cardiomyocyte proliferation via interaction with retinoblastoma protein. J Biol Chem *280*, 30916-30923.

Kadenbach, B., Huttemann, M., Arnold, S., Lee, I., and Bender, E. (2000). Mitochondrial energy metabolism is regulated via nuclear-coded subunits of cytochrome c oxidase. Free Radic Biol Med *29*, 211-221.

Kapasi, P., Chaudhuri, S., Vyas, K., Baus, D., Komar, A.A., Fox, P.L., Merrick, W.C., and Mazumder, B. (2007). L13a blocks 48S assembly: role of a general initiation factor in mRNA-specific translational control. Mol Cell *25*, 113-126.

Kataoka, H., Miura, Y., Joh, T., Seno, K., Tada, T., Tamaoki, T., Nakabayashi, H., Kawaguchi, M., Asai, K., Kato, T.*, et al.* (2001). Alpha-fetoprotein producing gastric cancer lacks transcription factor ATBF1. Oncogene *20*, 869-873.

Kavanagh, E., and Joseph, B. (2011). The hallmarks of CDKN1C (p57, KIP2) in cancer. Biochim Biophys Acta *1816*, 50-56.

Kelly, L., McDonough, M.A., Coleman, M.L., Ratcliffe, P.J., and Schofield, C.J. (2009). Asparagine beta-hydroxylation stabilizes the ankyrin repeat domain fold. Mol Biosyst *5*, 52-58.

Khoshnoodi, J., Pedchenko, V., and Hudson, B.G. (2008). Mammalian collagen IV. Microsc Res Tech *71*, 357-370.

Kim, J., Chubatsu, L.S., Admon, A., Stahl, J., Fellous, R., and Linn, S. (1995). Implication of mammalian ribosomal protein S3 in the processing of DNA damage. J Biol Chem *270*, 13620-13629.

Kim, J., Kundu, M., Viollet, B., and Guan, K.L. (2011a). AMPK and mTOR regulate autophagy through direct phosphorylation of Ulk1. Nat Cell Biol *13*, 132-141.

Kim, M.J., Woo, S.J., Yoon, C.H., Lee, J.S., An, S., Choi, Y.H., Hwang, S.G., Yoon, G., and Lee, S.J. (2011b). Involvement of autophagy in oncogenic K-Ras-induced malignant cell transformation. J Biol Chem *286*, 12924-12932.

Kim, T.G., Jung, J., Mysliwiec, M.R., Kang, S., and Lee, Y. (2005). Jumonji represses alpha-cardiac myosin heavy chain expression via inhibiting MEF2 activity. Biochem Biophys Res Commun *329*, 544-553.

Klose, R.J., Kallin, E.M., and Zhang, Y. (2006). JmjC-domain-containing proteins and histone demethylation. Nat Rev Genet *7*, 715-727.

Koivunen, P., Hirsila, M., Gunzler, V., Kivirikko, K.I., and Myllyharju, J. (2004). Catalytic properties of the asparaginyl hydroxylase (FIH) in the oxygen sensing pathway are distinct from those of its prolyl 4-hydroxylases. J Biol Chem *279*, 9899-9904.

Komiya, K., Sueoka-Aragane, N., Sato, A., Hisatomi, T., Sakuragi, T., Mitsuoka, M., Sato, T., Hayashi, S., Izumi, H., Tsuneoka, M.*, et al.* (2010a). Expression of Mina53, a novel c-Myc target gene, is a favorable prognostic marker in early stage lung cancer. Lung Cancer *69*, 232-238.

Komiya, K., Sueoka-Aragane, N., Sato, A., Hisatomi, T., Sakuragi, T., Mitsuoka, M., Sato, T., Hayashi, S., Izumi, H., Tsuneoka, M.*, et al.* (2010b). Mina53, a novel c-Myc target gene, is frequently expressed in lung cancers and exerts oncogenic property in NIH/3T3 cells. J Cancer Res Clin Oncol *136*, 465-473.

Kouzarides, T. (2007). Chromatin modifications and their function. Cell *128*, 693-705.

Kraft, C., and Martens, S. (2012). Mechanisms and regulation of autophagosome formation. Curr Opin Cell Biol *24*, 496-501.

Krebs, L.T., Bradley, C.K., Norton, C.R., Xu, J., Oram, K.F., Starling, C., Deftos, M.L., Bevan, M.J., and Gridley, T. (2012). The Notch-regulated ankyrin repeat protein is required for proper anterior-posterior somite patterning in mice. Genesis *50*, 366-374.

Kundu, M., and Thompson, C.B. (2008). Autophagy: basic principles and relevance to disease. Annu Rev Pathol *3*, 427-455.

Kuratomi, K., Yano, H., Tsuneoka, M., Sakamoto, K., Kusukawa, J., and Kojiro, M. (2006). Immunohistochemical expression of Mina53 and Ki67 proteins in human primary gingival squamous cell carcinoma. Kurume Med J *53*, 71-78.

Lando, D., Peet, D.J., Gorman, J.J., Whelan, D.A., Whitelaw, M.L., and Bruick, R.K. (2002). FIH-1 is an asparaginyl hydroxylase enzyme that regulates the transcriptional activity of hypoxia-inducible factor. Genes Dev *16*, 1466-1471.

Laplante, M., and Sabatini, D.M. (2012). mTOR signaling in growth control and disease. Cell *149*, 274-293.

Lavaissiere, L., Jia, S., Nishiyama, M., de la Monte, S., Stern, A.M., Wands, J.R., and Friedman, P.A. (1996). Overexpression of human aspartyl(asparaginyl)beta-hydroxylase in hepatocellular carcinoma and cholangiocarcinoma. J Clin Invest *98*, 1313-1323.

Lee, J.W., Bae, S.H., Jeong, J.W., Kim, S.H., and Kim, K.W. (2004). Hypoxia-inducible factor (HIF-1)alpha: its protein stability and biological functions. Exp Mol Med *36*, 1-12.

Lee, Y.F., Miller, L.D., Chan, X.B., Black, M.A., Pang, B., Ong, C.W., Salto-Tellez, M., Liu, E.T., and Desai, K.V. (2012). JMJD6 is a driver of cellular proliferation and motility and a marker of poor prognosis in breast cancer. Breast Cancer Res *14*, R85.

Li, J., Fadare, O., Xiang, L., Kong, B., and Zheng, W. (2012). Ovarian serous carcinoma: recent concepts on its origin and carcinogenesis. J Hematol Oncol *5*, 8.

Li, M.O., Sarkisian, M.R., Mehal, W.Z., Rakic, P., and Flavell, R.A. (2003). Phosphatidylserine receptor is required for clearance of apoptotic cells. Science *302*, 1560-1563.

Liang, X.H., Liu, Q., and Fournier, M.J. (2009). Loss of rRNA modifications in the decoding center of the ribosome impairs translation and strongly delays pre-rRNA processing. RNA *15*, 1716-1728.

Liu, C., Gilmont, R.R., Benndorf, R., and Welsh, M.J. (2000). Identification and characterization of a novel protein from Sertoli cells, PASS1, that associates with mammalian small stress protein hsp27. J Biol Chem *275*, 18724-18731.

Liu, E.Y., and Ryan, K.M. (2012). Autophagy and cancer--issues we need to digest. J Cell Sci *125*, 2349-2358.

Lock, R., Roy, S., Kenific, C.M., Su, J.S., Salas, E., Ronen, S.M., and Debnath, J. (2011). Autophagy facilitates glycolysis during Ras-mediated oncogenic transformation. Mol Biol Cell *22*, 165-178.

Loenarz, C., and Schofield, C.J. (2008). Expanding chemical biology of 2-oxoglutarate oxygenases. Nat Chem Biol *4*, 152-156.

Lohrum, M.A., Ludwig, R.L., Kubbutat, M.H., Hanlon, M., and Vousden, K.H. (2003). Regulation of HDM2 activity by the ribosomal protein L11. Cancer Cell *3*, 577-587.
Longley, D.B., Harkin, D.P., and Johnston, P.G. (2003). 5-fluorouracil: mechanisms of action and clinical strategies. Nat Rev Cancer *3*, 330-338.

Louie, D.F., Resing, K.A., Lewis, T.S., and Ahn, N.G. (1996). Mass spectrometric analysis of 40 S ribosomal proteins from Rat-1 fibroblasts. J Biol Chem *271*, 28189-28198.

Lu, Y., Chang, Q., Zhang, Y., Beezhold, K., Rojanasakul, Y., Zhao, H., Castranova, V., Shi, X., and Chen, F. (2009). Lung cancer-associated JmjC domain protein mdig suppresses formation of tri-methyl lysine 9 of histone H3. Cell Cycle *8*, 2101-2109.

Mabjeesh, N.J., and Amir, S. (2007). Hypoxia-inducible factor (HIF) in human tumorigenesis. Histol Histopathol *22*, 559-572.

Maden, B.E., and Hughes, J.M. (1997). Eukaryotic ribosomal RNA: the recent excitement in the nucleotide modification problem. Chromosoma *105*, 391-400.

Maeda, T., Sepe, P., Lahousse, S., Tamaki, S., Enjoji, M., Wands, J.R., and de la Monte, S.M. (2003). Antisense oligodeoxynucleotides directed against aspartyl (asparaginyl) beta-hydroxylase suppress migration of cholangiocarcinoma cells. J Hepatol *38*, 615-622.

Masson, N., and Ratcliffe, P.J. (2003). HIF prolyl and asparaginyl hydroxylases in the biological response to intracellular O(2) levels. J Cell Sci *116*, 3041-3049.

Mayer, C., and Grummt, I. (2006). Ribosome biogenesis and cell growth: mTOR coordinates transcription by all three classes of nuclear RNA polymerases. Oncogene *25*, 6384-6391.

Mazumder, B., Sampath, P., Seshadri, V., Maitra, R.K., DiCorleto, P.E., and Fox, P.L. (2003). Regulated release of L13a from the 60S ribosomal subunit as a mechanism of transcript-specific translational control. Cell *115*, 187-198.

McDonough, M.A., Loenarz, C., Chowdhury, R., Clifton, I.J., and Schofield, C.J. (2010). Structural studies on human 2-oxoglutarate dependent oxygenases. Curr Opin Struct Biol *20*, 659-672.

McMullen, B.A., Fujikawa, K., and Kisiel, W. (1983). The occurrence of beta-hydroxyaspartic acid in the vitamin K-dependent blood coagulation zymogens. Biochem Biophys Res Commun *115*, 8-14.

McNeill, L.A., Hewitson, K.S., Claridge, T.D., Seibel, J.F., Horsfall, L.E., and Schofield, C.J. (2002). Hypoxia-inducible factor asparaginyl hydroxylase (FIH-1) catalyses hydroxylation at the beta-carbon of asparagine-803. Biochem J *367*, 571-575.

Mosmann, T. (1983). Rapid colorimetric assay for cellular growth and survival: application to proliferation and cytotoxicity assays. J Immunol Methods *65*, 55-63.

Myllyharju, J. (2003). Prolyl 4-hydroxylases, the key enzymes of collagen biosynthesis. Matrix Biol *22*, 15-24.

Myllyharju, J. (2008). Prolyl 4-hydroxylases, key enzymes in the synthesis of collagens and regulation of the response to hypoxia, and their roles as treatment targets. Ann Med *40*, 402-417.

Myllyharju, J., and Kivirikko, K.I. (2004). Collagens, modifying enzymes and their mutations in humans, flies and worms. Trends Genet *20*, 33-43.

Myllyla, R., Wang, C., Heikkinen, J., Juffer, A., Lampela, O., Risteli, M., Ruotsalainen, H., Salo, A., and Sipila, L. (2007). Expanding the lysyl hydroxylase toolbox: new insights into the localization and activities of lysyl hydroxylase 3 (LH3). J Cell Physiol *212*, 323-329.

Nam, E.A., and Cortez, D. (2011). ATR signalling: more than meeting at the fork. Biochem J *436*, 527-536.

Nissi, R., Autio-Harmainen, H., Marttila, P., Sormunen, R., and Kivirikko, K.I. (2001). Prolyl 4-hydroxylase isoenzymes I and II have different expression patterns in several human tissues. J Histochem Cytochem *49*, 1143-1153.

Ogasawara, S., Komuta, M., Nakashima, O., Akiba, J., Tsuneoka, M., and Yano, H. (2010). Accelerated expression of a Myc target gene Mina53 in aggressive hepatocellular carcinoma. Hepatol Res *40*, 330-336.

Oh, H.S., Kwon, H., Sun, S.K., and Yang, C.H. (2002). QM, a putative tumor suppressor, regulates proto-oncogene c-yes. J Biol Chem *277*, 36489-36498.

Okamoto, M., Van Stry, M., Chung, L., Koyanagi, M., Sun, X., Suzuki, Y., Ohara, O., Kitamura, H., Hijikata, A., Kubo, M.*, et al.* (2009). Mina, an Il4 repressor, controls T helper type 2 bias. Nat Immunol *10*, 872-879.

Polevoda, B., and Sherman, F. (2007). Methylation of proteins involved in translation. Mol Microbiol *65*, 590-606.

Poll, G., Braun, T., Jakovljevic, J., Neueder, A., Jakob, S., Woolford, J.L., Jr., Tschochner, H., and Milkereit, P. (2009). rRNA maturation in yeast cells depleted of large ribosomal subunit proteins. PLoS One *4*, e8249.

Potter, G.B., Beaudoin, G.M., 3rd, DeRenzo, C.L., Zarach, J.M., Chen, S.H., and Thompson, C.C. (2001). The hairless gene mutated in congenital hair loss disorders encodes a novel nuclear receptor corepressor. Genes Dev *15*, 2687-2701.

Qi, H.H., Ongusaha, P.P., Myllyharju, J., Cheng, D., Pakkanen, O., Shi, Y., Lee, S.W., and Peng, J. (2008). Prolyl 4-hydroxylation regulates Argonaute 2 stability. Nature *455*, 421-424.

Ren, J., Wang, Y., Liang, Y., Zhang, Y., Bao, S., and Xu, Z. (2010). Methylation of ribosomal protein S10 by protein-arginine methyltransferase 5 regulates ribosome biogenesis. J Biol Chem *285*, 12695-12705.

Rhodes, D.R., Yu, J., Shanker, K., Deshpande, N., Varambally, R., Ghosh, D., Barrette, T., Pandey, A., and Chinnaiyan, A.M. (2004). ONCOMINE: a cancer microarray database and integrated data-mining platform. Neoplasia *6*, 1-6.

Richmond, A., and Su, Y. (2008). Mouse xenograft models vs GEM models for human cancer therapeutics. Dis Model Mech *1*, 78-82.

Risteli, J., Tryggvason, K., and Kivirikko, K.I. (1977). Prolyl 3-hydroxylase: partial characterization of the enzyme from rat kidney cortex. Eur J Biochem *73*, 485-492.

Schneider-Poetsch, T., Ju, J., Eyler, D.E., Dang, Y., Bhat, S., Merrick, W.C., Green, R., Shen, B., and Liu, J.O. (2010). Inhibition of eukaryotic translation elongation by cycloheximide and lactimidomycin. Nat Chem Biol *6*, 209-217.

Schofield, C.J., and Ratcliffe, P.J. (2004). Oxygen sensing by HIF hydroxylases. Nat Rev Mol Cell Biol *5*, 343-354.

Schofield, C.J., and Zhang, Z. (1999). Structural and mechanistic studies on 2-oxoglutarate-dependent oxygenases and related enzymes. Curr Opin Struct Biol *9*, 722-731.

Secombe, J., Li, L., Carlos, L., and Eisenman, R.N. (2007). The Trithorax group protein Lid is a trimethyl histone H3K4 demethylase required for dMyc-induced cell growth. Genes Dev *21*, 537-551.

Shahbazian, D., Parsyan, A., Petroulakis, E., Hershey, J., and Sonenberg, N. (2010). eIF4B controls survival and proliferation and is regulated by proto-oncogenic signaling pathways. Cell Cycle *9*, 4106-4109.

Shirai, A., Sadaie, M., Shinmyozu, K., and Nakayama, J. (2010). Methylation of ribosomal protein L42 regulates ribosomal function and stress-adapted cell growth. J Biol Chem *285*, 22448-22460.

Sinha, K.M., Yasuda, H., Coombes, M.M., Dent, S.Y., and de Crombrugghe, B. (2010). Regulation of the osteoblast-specific transcription factor Osterix by NO66, a Jumonji family histone demethylase. EMBO J *29*, 68-79.

Steinman, R.M., Mellman, I.S., Muller, W.A., and Cohn, Z.A. (1983). Endocytosis and the recycling of plasma membrane. J Cell Biol *96*, 1-27.

Stenflo, J., Holme, E., Lindstedt, S., Chandramouli, N., Huang, L.H., Tam, J.P., and Merrifield, R.B. (1989). Hydroxylation of aspartic acid in domains homologous to the epidermal growth factor precursor is catalyzed by a 2-oxoglutarate-dependent dioxygenase. Proc Natl Acad Sci U S A *86*, 444-447.

Stenflo, J., Lundwall, A., and Dahlback, B. (1987). beta-Hydroxyasparagine in domains homologous to the epidermal growth factor precursor in vitamin K-dependent protein S. Proc Natl Acad Sci U S A *84*, 368-372.

Stolze, I.P., Tian, Y.M., Appelhoff, R.J., Turley, H., Wykoff, C.C., Gleadle, J.M., and Ratcliffe, P.J. (2004). Genetic analysis of the role of the asparaginyl hydroxylase factor inhibiting hypoxia-inducible factor (FIH) in regulating hypoxia-inducible factor (HIF) transcriptional target genes [corrected]. J Biol Chem *279*, 42719-42725.

Sun, X., Zhou, Y., Otto, K.B., Wang, M., Chen, C., Zhou, W., Subramanian, K., Vertino, P.M., and Dong, J.T. (2007). Infrequent mutation of ATBF1 in human breast cancer. J Cancer Res Clin Oncol *133*, 103-105.

Surridge, A.K., Rodgers, U.R., Swingler, T.E., Davidson, R.K., Kevorkian, L., Norton, R., Waters, J.G., Goldring, M.B., Parker, A.E., and Clark, I.M. (2009). Characterization and regulation of ADAMTS-16. Matrix Biol *28*, 416-424.

Suzuki, C., Takahashi, K., Hayama, S., Ishikawa, N., Kato, T., Ito, T., Tsuchiya, E., Nakamura, Y., and Daigo, Y. (2007). Identification of Myc-associated protein with JmjC domain as a novel therapeutic target oncogene for lung cancer. Mol Cancer Ther *6*, 542-551.

Tachibana, M., Kiyokawa, E., Hara, S., Iemura, S., Natsume, T., Manabe, T., and Matsuda, M. (2009). Ankyrin repeat domain 28 (ANKRD28), a novel binding partner of DOCK180, promotes cell migration by regulating focal adhesion formation. Exp Cell Res *315*, 863-876.

Takeuchi, T., Kojima, M., Nakajima, K., and Kondo, S. (1999). jumonji gene is essential for the neurulation and cardiac development of mouse embryos with a C3H/He background. Mech Dev *86*, 29-38.

Tang, H., Hornstein, E., Stolovich, M., Levy, G., Livingstone, M., Templeton, D., Avruch, J., and Meyuhas, O. (2001). Amino acid-induced translation of TOP mRNAs is fully dependent on phosphatidylinositol 3-kinase-mediated signaling, is partially inhibited by rapamycin, and is independent of S6K1 and rpS6 phosphorylation. Mol Cell Biol *21*, 8671-8683.

Tanida, I., Ueno, T., and Kominami, E. (2008). LC3 and Autophagy. Methods Mol Biol *445*, 77-88.

Terzian, T., Dumble, M., Arbab, F., Thaller, C., Donehower, L.A., Lozano, G., Justice, M.J., Roop, D.R., and Box, N.F. (2011). Rpl27a mutation in the sooty foot ataxia mouse phenocopies high p53 mouse models. J Pathol *224*, 540-552.

Teye, K., Arima, N., Nakamura, Y., Sakamoto, K., Sueoka, E., Kimura, H., and Tsuneoka, M. (2007). Expression of Myc target gene mina53 in subtypes of human lymphoma. Oncol Rep *18*, 841-848.

Teye, K., Tsuneoka, M., Arima, N., Koda, Y., Nakamura, Y., Ueta, Y., Shirouzu, K., and Kimura, H. (2004). Increased expression of a Myc target gene Mina53 in human colon cancer. Am J Pathol *164*, 205-216.

Tomayko, M.M., and Reynolds, C.P. (1989). Determination of subcutaneous tumor size in athymic (nude) mice. Cancer Chemother Pharmacol *24*, 148-154.

Tryggvason, K., Risteli, J., and Kivirikko, K.I. (1976). Separation of prolyl 3-hydroxylase and 4-hydroxylase activities and the 4-hydroxyproline requirement for synthesis of 3-hydroxyproline. Biochem Biophys Res Commun *76*, 275-281.

Tsukada, Y., Fang, J., Erdjument-Bromage, H., Warren, M.E., Borchers, C.H., Tempst, P., and Zhang, Y. (2006). Histone demethylation by a family of JmjC domain-containing proteins. Nature *439*, 811-816.

Tsuneoka, M., Fujita, H., Arima, N., Teye, K., Okamura, T., Inutsuka, H., Koda, Y., Shirouzu, K., and Kimura, H. (2004). Mina53 as a potential prognostic factor for esophageal squamous cell carcinoma. Clin Cancer Res *10*, 7347-7356.

Tsuneoka, M., Koda, Y., Soejima, M., Teye, K., and Kimura, H. (2002). A novel myc target gene, mina53, that is involved in cell proliferation. J Biol Chem *277*, 35450-35459.

Valtavaara, M., Szpirer, C., Szpirer, J., and Myllyla, R. (1998). Primary structure, tissue distribution, and chromosomal localization of a novel isoform of lysyl hydroxylase (lysyl hydroxylase 3). J Biol Chem *273*, 12881-12886.

van der Rest, M., and Garrone, R. (1991). Collagen family of proteins. FASEB J *5*, 2814-2823.

van Haaften, G., Dalgliesh, G.L., Davies, H., Chen, L., Bignell, G., Greenman, C., Edkins, S., Hardy, C., O'Meara, S., Teague, J.*, et al.* (2009). Somatic mutations of the histone H3K27 demethylase gene UTX in human cancer. Nat Genet *41*, 521-523.

Vandamme, J., Lettier, G., Sidoli, S., Di Schiavi, E., Norregaard Jensen, O., and Salcini, A.E. (2012). The C. elegans H3K27 demethylase UTX-1 is essential for normal development, independent of its enzymatic activity. PLoS Genet *8*, e1002647.

Vang, R., Shih Ie, M., and Kurman, R.J. (2009). Ovarian low-grade and high-grade serous carcinoma: pathogenesis, clinicopathologic and molecular biologic features, and diagnostic problems. Adv Anat Pathol *16*, 267-282.

Vranka, J., Stadler, H.S., and Bachinger, H.P. (2009). Expression of prolyl 3-hydroxylase genes in embryonic and adult mouse tissues. Cell Struct Funct *34*, 97-104.

Vranka, J.A., Sakai, L.Y., and Bachinger, H.P. (2004). Prolyl 3-hydroxylase 1, enzyme characterization and identification of a novel family of enzymes. J Biol Chem *279*, 23615-23621.

Wang, C., Luosujarvi, H., Heikkinen, J., Risteli, M., Uitto, L., and Myllyla, R. (2002). The third activity for lysyl hydroxylase 3: galactosylation of hydroxylysyl residues in collagens in vitro. Matrix Biol *21*, 559-566.

Webby, C.J., Wolf, A., Gromak, N., Dreger, M., Kramer, H., Kessler, B., Nielsen, M.L., Schmitz, C., Butler, D.S., Yates, J.R., 3rd*, et al.* (2009). Jmjd6 catalyses lysyl-hydroxylation of U2AF65, a protein associated with RNA splicing. Science *325*, 90-93.

Whetstine, J.R., Nottke, A., Lan, F., Huarte, M., Smolikov, S., Chen, Z., Spooner, E., Li, E., Zhang, G., Colaiacovo, M.*, et al.* (2006). Reversal of histone lysine trimethylation by the JMJD2 family of histone demethylases. Cell *125*, 467-481.

Willems, L., Tamburini, J., Chapuis, N., Lacombe, C., Mayeux, P., and Bouscary, D. (2012). PI3K and mTOR signaling pathways in cancer: new data on targeted therapies. Curr Oncol Rep *14*, 129-138.

Xi, Z.Q., Sun, J.J., Wang, X.F., Li, M.W., Liu, X.Z., Wang, L.Y., Zhu, X., Xiao, F., Li, J.M., Gong, Y.*, et al.* (2007). HSPBAP1 is found extensively in the anterior temporal neocortex of patients with intractable epilepsy. Synapse *61*, 741-747.

Yamane, K., Toumazou, C., Tsukada, Y., Erdjument-Bromage, H., Tempst, P., Wong, J., and Zhang, Y. (2006). JHDM2A, a JmjC-containing H3K9 demethylase, facilitates transcription activation by androgen receptor. Cell *125*, 483-495.

Yang, M., Chowdhury, R., Ge, W., Hamed, R.B., McDonough, M.A., Claridge, T.D., Kessler, B.M., Cockman, M.E., Ratcliffe, P.J., and Schofield, C.J. (2011). Factor-inhibiting hypoxia-inducible factor (FIH) catalyses the post-translational hydroxylation of histidinyl residues within ankyrin repeat domains. FEBS J *278*, 1086-1097.

Yeowell, H.N., Ha, V., Clark, W.L., Marshall, M.K., and Pinnell, S.R. (1994). Sequence analysis of a cDNA for lysyl hydroxylase isolated from human skin fibroblasts from a normal donor: differences from human placental lysyl hydroxylase cDNA. J Invest Dermatol *102*, 382-384.

Yokoyama, A., Okuno, Y., Chikanishi, T., Hashiba, W., Sekine, H., Fujiki, R., and Kato, S. (2010). KIAA1718 is a histone demethylase that erases repressive histone methyl marks. Genes Cells *15*, 867-873.

Youle, R.J., and Narendra, D.P. (2011). Mechanisms of mitophagy. Nat Rev Mol Cell Biol *12*, 9-14.

Youn, M.Y., Yokoyama, A., Fujiyama-Nakamura, S., Ohtake, F., Minehata, K., Yasuda, H., Suzuki, T., Kato, S., and Imai, Y. (2012). JMJD5, a Jumonji C (JmjC) domain-containing protein, negatively regulates osteoclastogenesis by facilitating NFATc1 protein degradation. J Biol Chem *287*, 12994-13004.

Zhang, Q., Hu, C.M., Yuan, Y.S., He, C.H., Zhao, Q., and Liu, N.Z. (2008). Expression of Mina53 and its significance in gastric carcinoma. Int J Biol Markers *23*, 83-88.

Zhang, Y., Lu, Y., Yuan, B.Z., Castranova, V., Shi, X., Stauffer, J.L., Demers, L.M., and Chen, F. (2005). The Human mineral dust-induced gene, mdig, is a cell growth regulating gene associated with lung cancer. Oncogene *24*, 4873-4882.

Acknowledgements

I first like to thank my direct supervisor Mathew Coleman for all incredible advice, help and expertise over the last few years. Thanks for believing in me. Thanks also to Peter Ratcliffe for supervisory input and for giving me an opportunity to study for a D Phil in the Ratcliffe lab.

Thanks to all members of the Ratcliffe group for making the lab such a great place to work in. Especially: Atsushi, Penny, Rachelle, Nayia, Ming, Norma, Yamin, Tina, Julie, Paddy and Matt. Thanks to David Mole for all help with microarray analysis. Thanks to Adrian Harris, Ji-Liang and Esther Bridges for all help and advice regarding the xenograft experiment. Also, thanks to Rok Sekirnik for everything related to Wp-MS.

Finally, an immense gratitude to my family for all support, encouragement and for always being there for me. This thesis is dedicated to you.